

AD-A139 321

COORDINATED RESEARCH PROGRAM IN PULSED POWER PHYSICS  
(U) TEXAS TECH UNIV LUBBOCK DEPT OF ELECTRICAL  
ENGINEERING M KRISTIANSEN ET AL. 27 FEB 84

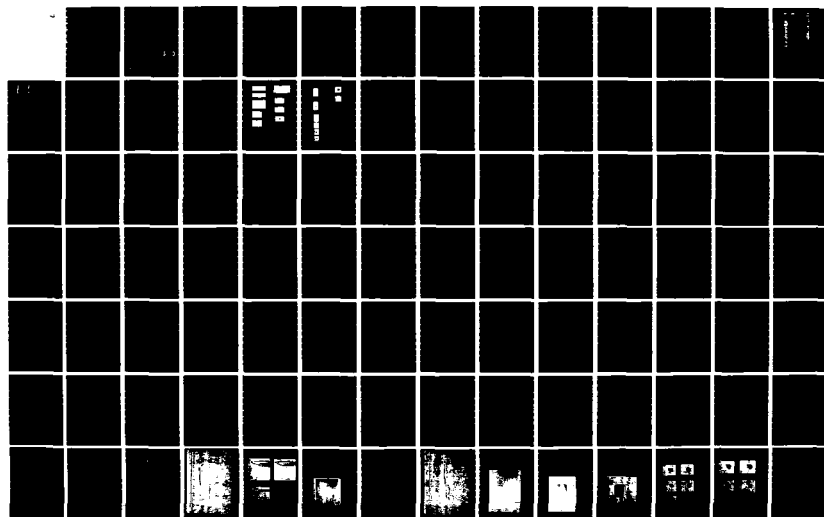
1/5

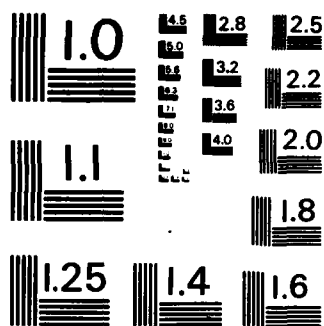
UNCLASSIFIED

AFOSR-TR-84-0174 F49620-79-C-0191

F/G 10/2

NL



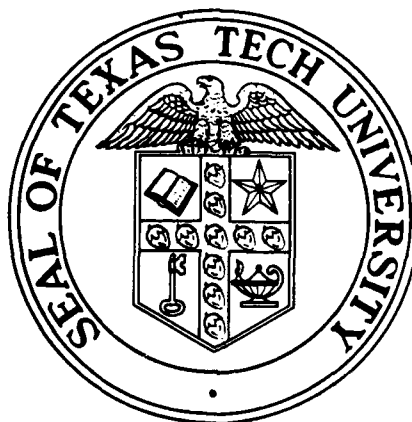


MICROCOPY RESOLUTION TEST CHART  
NATIONAL BUREAU OF STANDARDS-1963-A

on  
COORDINATED RESEARCH PROGRAM  
in  
PULSED POWER PHYSICS

February 27, 1984

AD A139321



Air Force Office of Scientific Research  
Contract No. F49620-79-C-0191

DTIC  
ELECTE  
MAR 23 1984  
S R A D

PLASMA AND SWITCHING LABORATORY  
LASER LABORATORY

Department of Electrical Engineering  
TEXAS TECH UNIVERSITY

Lubbock, Texas 79409

DTIC FILE COPY

Approved for public release;  
distribution unlimited.

84 03 22 117

Unclassified

SECURITY CLASSIFICATION OF THIS PAGE (When Data Entered)

REPORT DOCUMENTATION PAGE		READ INSTRUCTIONS BEFORE COMPLETING FORM
1. REPORT NUMBER <b>AFOSR-TR- 84-0174</b>	2. GOVT ACCESSION NO. <b>AD-A139 321</b>	3. RECIPIENT'S CATALOG NUMBER
4. TITLE (and Subtitle) <b>Coordinated Research Program in Pulsed Power Physics</b>		5. TYPE OF REPORT & PERIOD COVERED <b>Final Report July 1, 1979-December 31, 1983</b>
		6. PERFORMING ORG. REPORT NUMBER
7. AUTHOR(s) <b>M. Kristiansen L. Hatfield F. Williams M. Hagler G. Schaefer H. Krompholz J. Craig K. Schoenbach E. Kunhardt</b>		8. CONTRACT OR GRANT NUMBER(s) <b>F49620-79-C-0191 MI PR-16-81, 13-82, 10388</b>
9. PERFORMING ORGANIZATION NAME AND ADDRESS <b>Department of Electrical Engineering Texas Tech University, P.O. Box 4439 Lubbock, Texas 79409</b>		10. PROGRAM ELEMENT, PROJECT, TASK AREA & WORK UNIT NUMBERS <b>61102F 2301/A7</b>
11. CONTROLLING OFFICE NAME AND ADDRESS <b>Air Force Office of Scientific Research/NP Bldg. 410, Bolling AFB Washington, D.C. 20332</b>		12. REPORT DATE <b>February 27, 1984</b>
		13. NUMBER OF PAGES <b>389</b>
14. MONITORING AGENCY NAME & ADDRESS (if different from Controlling Office)		15. SECURITY CLASS. (of this report) <b>Unclassified</b>
		15a. DECLASSIFICATION/DOWNGRADING SCHEDULE
16. DISTRIBUTION STATEMENT (of this Report)  <b>Approved for public release; distribution unlimited.</b>		
17. DISTRIBUTION STATEMENT (of the abstract entered in Block 20, if different from Report)		
18. SUPPLEMENTARY NOTES		
19. KEY WORDS (Continue on reverse side if necessary and identify by block number) <b>Pulsed Power, Switching, Electromechanical Pulse Device, Laser Triggering, Electron Beam Triggering, Surface Physics, Electrode Erosion, Spark Gap, Discharge, Spectroscopy, Opening Switches</b>		
20. ABSTRACT (Continue on reverse side if necessary and identify by block number) <b>The work on eight program elements, related to pulsed power, research over the past four years is summarized. These program elements form a multi-disciplinary, coordinated program whose main emphasis is to gain improved understanding of high power, repetitive closing and opening switches. The main emphasis is concerned with triggering of discharges in gas filled spark gaps and the associated elec- trode erosion and insulator damage. Considerable efforts are also being made to understand the limitations and fundamental discharge phenomena in fast opening switches for inductive energy storage. A novel electromechanical pulse generator</b>		

DD FORM 1 JAN 73 1473

EDITION OF 1 NOV 65 IS OBSOLETE

Unclassified

SECURITY CLASSIFICATION OF THIS PAGE (When Data Entered)



Unclassified

SECURITY CLASSIFICATION OF THIS PAGE(When Data Entered)

20. Abstract (continued)

which promises to deliver fast, repetitive pulses has also been investigated. The major, overall, accomplishments in each program element are summarized and last year's work is described in some detail.

**UNCLASSIFIED**

SECURITY CLASSIFICATION OF THIS PAGE(When Data Entered)

Final Report  
on  
COORDINATED RESEARCH PROGRAM  
IN  
PULSED POWER PHYSICS

AFOSR Contract #F49620-79-C-0191

February 27, 1984

Program Director:	M. Kristiansen
Associate Program Director:	M. Hagler
Principal Investigators:	M. Hagler L. Hatfield M. Kristiansen H. Krompholz G. Schaefer K. Schoenbach F. Williams
Post Doctoral Fellow:	D. Pease
Associate Investigator:	J. Marx
Technician III:	K. Zinsmeyer
Secretary III:	M. Byrd J. Davis
Graduate Students:	R. Biesele R. Cooper R. Curry S. Dahli A. Donaldson R. Dougal H. Dunlap J. Gahl L. Gordon H. Harjes G. Hutcheson G. Jackson D. Johnson G. Leiker B. Maas R. Ness K. Pinegar D. Skaggs L. Thurmond C. Yeh*



Accession For	
NTIS GRA&I	<input checked="" type="checkbox"/>
DTIC TAB	<input type="checkbox"/>
Unannounced	<input type="checkbox"/>
Justification	
A-1	

\* Paid by the Republic of China (Taiwan)

AIR FORCE... (AFS)  
NOTICE  
This...  
appro...  
Distrib... unlimited.  
MATTHEW J. WILKINSON  
Chief, Technical Information Division

## TABLE OF CONTENTS

Summary of Research Objectives for 1982-83 . . . . .	1
Introduction . . . . .	3
Summary of Total Contract Work (1979-1983) . . . . .	4
Summary of Work During the Last Contract Period (1982-83). .	47
<b>Project Descriptions</b>	
Project No. 1: Electron Beam Initiated Breakdown (Completed in 1980)	
Project No. 2: Transient Processes in Laser- Triggered Breakdown . . . . .	49
Project No. 3: Spark Gap Discharge and Erosion Phenomena . . . . .	90
Project No. 4: Pulsed Power Surface Physics and Applications . . . . .	207
Project No. 5: Excited State Spectroscopy of Electrically Excited Gases . . . . .	238
Project No. 6: Exploratory Concepts . . . . .	256
Project No. 7: Electromechanical Pulse Device (Completed in 1982)	
Project No. 8: } Optically Controlled Discharges and	
Project No. 9: } Opening Switches . . . . .	282
Faculty Publications, 1979-83 . . . . .	362
Interactions, 1982-83 . . . . .	369
Advanced Degrees Awarded, 1980-83 . . . . .	380
Seminars, 1982-83 . . . . .	382
Guests, 1982-83 . . . . .	384

## SUMMARY OF RESEARCH OBJECTIVES

for

1982-83

Project No. 1: No work was planned for this year.

Project No. 2: The main goal was to obtain improved theoretical and experimental understanding of the initial breakdown processes in a laser triggered spark gap.

Project No. 3: The two main goals were:

- a) to gain improved understanding of the electrode erosion process in a spark gap, and
- b) to develop an experimentally verifiable model for the statistical breakdown distribution of a spark gap.

Project No. 4: The main effort was directed at understanding the materials synergism and the materials phenomena occurring in high power spark gaps, especially the dielectric surface phenomena.

Project No. 5: The emphasis here was on developing new diagnostic techniques for spark gaps and applying them to triggered breakdown phenomena.

Project No. 6: This project considered several small investigations, of a preliminary nature. The main ones among these were investigations of surface discharge phenomena (trigger optimization), measurements of the time dependent arc voltage in a spark gap, and investigations of novel electrostatic trigger concepts.

Project No. 7: No work was planned for this year.

Project No. 8: The main goals were to determine the V-I characteristics of self-sustained discharges and to investigate the optical control of diffuse discharges both experimentally and theoretically.

Project No. 9: This project, which is closely coordinated with Project No. 8 had as its main purpose to develop an experimental arrangement for rapid, burst mode operation of an e-beam controlled opening switch and to determine the switch characteristics, experimentally and theoretically, during the opening and closing phase.

## INTRODUCTION

The Coordinated Research Programs in Pulsed Power Physics is a multi-investigator program which currently involves seven Principal Investigators, one Associate Investigator, one Postdoctoral Fellow, and 14 graduate students from the departments of Electrical Engineering, Physics and Chemistry at Texas Tech University. Other Principal and Associate Investigators and graduate students from the departments of Electrical Engineering, Mechanical Engineering, and Physics have also participated in the program at various times. The program grew out of several, earlier, independent AFOSR-supported, research programs at Texas Tech University and is currently supported jointly by AFOSR and ARO. Substantial matching commitments were made by Texas Tech University in the form of extensive, modern laboratory space and matching funds. Most of the research is concerned with the physics of high power switches.

Since this is the Final Report on a 4-year project it has been organized somewhat different than the three previous, Annual Reports. There is first a general (historical) overview of each project and their overall achievements. This is followed by a summary of the results from the last contract period and then a detailed discussion of these results. The total number of journal article publications and conference proceedings papers resulting from this contract are listed at the end of the report but the Interactions section has been abbreviated and primarily limited to last year's interactions.

Summary of Total Contract Work  
(1979-1983)

Project No. 1

Electron Beam Initiated Triggering

(K. McDonald, M. Newton, T. Tzeng,  
E. Kunhardt, and M. Kristiansen)

This work was completed early in the program and the main results are summarized in the two attached publications (Appendices I and II). This program element successfully determined the most important parameter influences in electron beam triggered switching. It also demonstrated jitter of 100 ps or less for triggering high impedance (50  $\Omega$ ), high voltage (100-400 kV) systems.

# An Electron-Beam Triggered Spark Gap

K. McDONALD, M. NEWTON, E. E. KUNHARDT, MEMBER, IEEE, M. KRISTIANSSEN, FELLOW, IEEE,  
AND A. H. GUENTHER, FELLOW, IEEE

**Abstract**—The triggering of a high-voltage gas-insulated spark gap by an electron (*e*) beam has been investigated. Rise times of approximately 2.5 ns with subnanosecond jitter ( $\sim 0.2$  ns) have been obtained for 3-cm gaps charged at voltages as low as 50 percent of the self-breakdown voltage (varied up to 0.5 MV). The switch delay (including the *e*-beam diode) was 52 ns. The triggering *e*-beam pulse has a duration of 15 ns and a 0–50 percent rise time of 1.5 ns. The *e*-beam current is 0.5 kA, and the electron energy can be varied in the range from 80 to 145 keV. The working media were  $N_2$ , mixtures of  $N_2$  and Ar, and  $N_2$  and  $SF_6$  at pressures of 1–3 atm. Voltage, current, and jitter measurements have been made for a wide range of gap conditions and *e*-beam parameters. Variations in the character of the discharge have been inferred using streak and open shutter photography. The photographs show that the discharge has a broad cross section and that its character varies for differing polarities and voltages. The effects of varying the *e*-beam width and the beam energy are discussed.

## INTRODUCTION

THE DEVELOPMENT of reliable high-voltage low-jitter fast rise-time long-life switches is important to energy production (fusion reactors development, lasers for isotope separation), defense (simulators for nuclear weapons effects), and many other applications (industrial manufacturing processes). A research program is currently underway to improve the physical understanding of various breakdown processes for the subsequent development of a low-inductance fast rise-time low-jitter command-fired spark gap switch, with low prefire probability, and capable of operating at high voltages (MV). Two different spark gap trigger mechanisms, laser triggering (LTS) [1], [2] and electron (*e*)-beam triggering (EBTS) [3]–[7] have been found to produce excellent jitter characteristics. These two methods have certain similarities but differ in the basic processes involved. This paper describes an investigation of EBTS. The breakdown leads to the formation of a volume discharge (proportional in cross section to the cross-sectional area of the injected beam) which helps reduce electrode erosion and switch inductance. The switch is shown to exhibit subnanosecond jitter (with respect to the *e*-beam diode current) at voltages as low as 50 percent of the self-breakdown voltage  $V_{sb}$ .

Manuscript received February 4, 1980; revised April 18, 1980. This work was supported by AFOSR under Grant AFOSR 76-3124 and Contract F49620-79-C-0191.

K. McDonald was with the Department of Electrical Engineering, Texas Tech University, Lubbock, TX. He is now with Sandia Laboratories, Albuquerque, NM.

M. Newton was with the Department of Electrical Engineering, Texas Tech University, Lubbock, TX. He is now with Lawrence Livermore Laboratory, Livermore, CA.

E. E. Kunhardt and M. Kristiansen are with the Department of Electrical Engineering, Texas Tech University, Lubbock, TX 79409.

A. H. Guenther is with the Air Force Weapons Laboratory, Kirtland AFB, NM 87117.

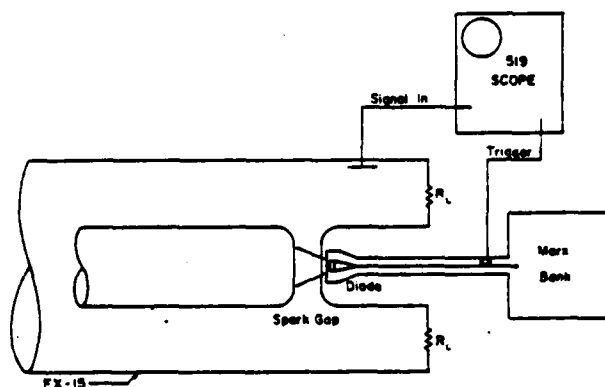


Fig. 1. Basic arrangement.

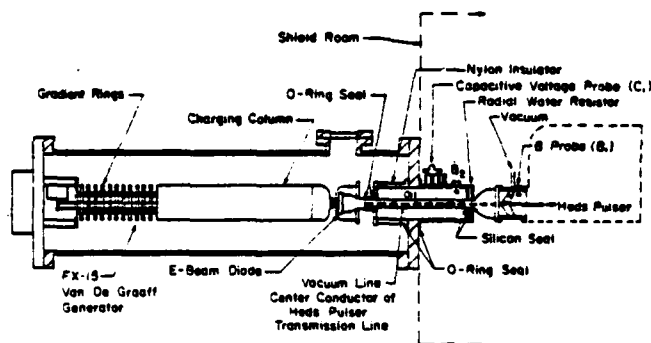


Fig. 2. Experimental arrangement.

## THE EXPERIMENTAL ARRANGEMENT

The experiment consists of an energy storage element, a gas insulated pressurized spark gap, and a source of energetic electrons (Fig. 1). The energy storage element and the spark gap are both contained within the high pressure vessel of a Van de Graaff charged coaxial line (Fig. 2). The line can be charged to approximately 1 MV and delivers a rectangular pulse of approximately 10-ns full width at half maximum (FWHM) duration. The spark gap is formed by an interruption in the center conductor of the line. The stainless steel electrodes have a Bruce profile [8] and a diameter of 21.5 cm. The high pressure insulating gas for the gap also serves as the dielectric for the coaxial line. The *e* beam is generated by a cold cathode field emission vacuum diode which is located behind the grounded electrode. It is placed inside the inner conductor of the output coaxial line, so as to introduce the *e* beam axially through a 2.5-cm diameter aperture in the center of the electrode. In order to maintain a uniform field distribution in the gap, and to protect the foil from the discharge, the aperture was covered with a stainless steel mesh (grid size: 0.127 cm).



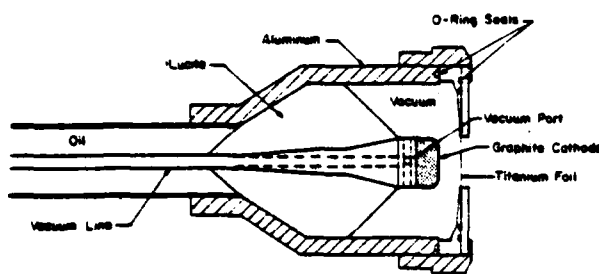


Fig. 3. The diode.

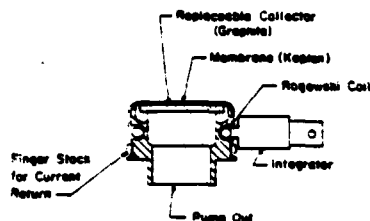


Fig. 4. Faraday cup collector.

The diode [9] (Fig. 3) utilizes a spiral grooved graphite cathode and a thin foil anode. Graphite was chosen because of its fast "turn on" properties [10]. The  $e$ -beam current was measured with a Faraday cup collector and a self-integrating Rogowski coil [11], as shown in Fig. 4. The Faraday cup was placed directly over the exit aperture of the  $e$  beam. Time integrated radial intensity profile measurements were made by recording the beam directly on film and then scanning the film with a densitometer. For these measurements the beam propagated in vacuum and was first attenuated by a thin graphite sheet to ensure film linearity. The diode emits, through a 2-mil titanium foil, a 0.5-kA 145-keV burst of electrons with a 0-50 percent rise time of 1.5 ns and a duration of 15 ns. The average (across the surface) beam current density was about 110 A/cm<sup>2</sup>. The diode was designed to have an impedance of 70  $\Omega$  to match the driving generator. This generator is a 25-stage modified Marx pulse forming network (Heds pulser) [12]. It combines the voltage multiplicative feature of the standard Marx circuit with the pulse shaping characteristics of a lumped parameter network. The sequence of events in the experiment is as follows: the coaxial line is charged to the desired voltage by the Van de Graaff generator. The modules in the Heds pulser are charged and a trigger signal initiates the Marx circuit erection. This produces an approximately trapezoidal 200-kV pulse of 50-ns FWHM duration with a 4-ns rise time. This pulse propagates down a 70- $\Omega$  oil-filled coaxial transmission line and appears across the anode-cathode gap of the diode. (The outer conductor of the Marx generator to diode transmission line also serves as the inner conductor for the FX-15 output transmission line.) The pulsed beam of electrons travels through 1.5 cm of the high pressure gas before it enters the spark gap region. The insulating gas in the high field gap region is then ionized, resulting in the subsequent formation of an ionized conduction path and the collapse of the voltage across the gap. The charged coaxial line and the resulting wave propagates down a 50- $\Omega$  oil-filled output transmission line, which is terminated in a matching AlCl<sub>3</sub> water resistor.

## EXPERIMENTAL APPROACH

The following characteristics of the spark gap breakdown were investigated: 1) the rise time of the resulting voltage, 2) the switch delay and jitter, and 3) the spatial character of the breakdown. The diagnostics used were open shutter and streak photography to record the character of the discharge, and a capacitive voltage divider probe ( $C_1$ ), located in the generator output transmission line (Fig. 1) to monitor the output voltage pulse when the gap breaks down.

The following experimental parameters were varied during the investigation: 1) *The gap polarity* (depending on how the Van de Graaff was charged, the target electrode was either positive or negative. When the electrode was charged positive the injected electrons were accelerated by the initial electric field in the gap, and when the electrode was negative the beam was decelerated.); 2) *the gap voltage  $V_g$*  ( $V_g$  was varied between 50 percent and 98 percent of the self-breakdown voltage  $V_{sb}$ , which ranged from 75 kV to over 400 kV); 3) *the gas pressure* (1-3 atm); 4) *the type of gas* ( $N_2$ , mixtures of  $N_2$  and A, and mixtures of  $N_2$  and  $SF_6$ ); 5) *the  $e$ -beam diameter* (1.25 cm and 2.50 cm); and 6) *the diode voltage* (10 kV to 220 kV, resulting in somewhat lower beam energy of 45 keV due to losses in the diode foil [13]).

## RESULTS

The pulse rise time was observed to vary slightly with the beam energy and ranged from 2.5 to 3 ns. The larger value was obtained for a diode voltage of 150 kV and a gap voltage  $V_g = 100$  kV at 50 percent of  $V_{sb}$ .

The rise time was also expected to vary with the beam, and hence discharge diameter but this was not observed. For a coaxial system the inductance varies as the natural logarithm of the ratio of the radii involved  $\sim \ln(b/a)$ . Since the beam diameter was varied by a factor of two, one might expect approximately a 20 percent variation in the inductance. At the present time we do not have enough information about the channel formation and the current profile to make an estimate about the total rise-time variation one may expect for a factor of two change in  $e$ -beam diameter (corresponding to an observed factor of two change in discharge diameter).

The jitter was found to be virtually identical for all our experimental parameter combinations. Fig. 5(a) is representative of all jitter measurements. There are 15 separate, superimposed traces of the voltage pulse, as monitored by the capacitive probe ( $C_1$ ), and displayed on a Tektronix 519 oscilloscope. The scope was triggered with the signal from the  $B$  probe ( $B_1$ ) located on the diode transmission line (Fig. 1). The sweep speed was 2 ns/div; thus the resolution is approximately 0.2 ns and the jitter can be seen to be no greater than this amount. These particular traces correspond to breakdown of a 3.2-cm gap in  $N_2$  at 3-atm pressure. The gap voltage was  $V_g = 235$  kV (94 percent of  $V_{sb}$ , the self-breakdown voltage being 250 kV). The traces in Fig. 5(b) are further examples of the excellent jitter characteristics. All parameters were identical to those given above except that in this case  $V_g \sim 0.52V_{sb}$ . This implies that  $e$ -beam triggering can afford very low jitter under low prefire probability conditions. These two experi-



Fig. 5. Jitter.

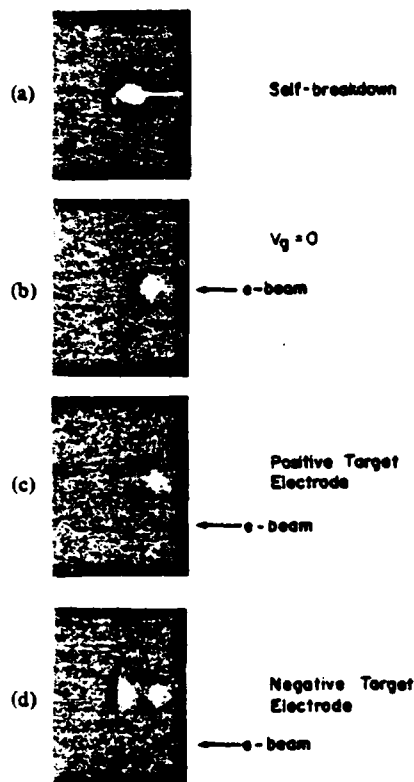
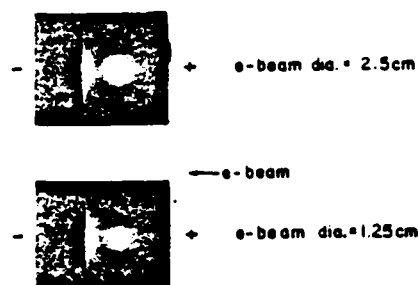
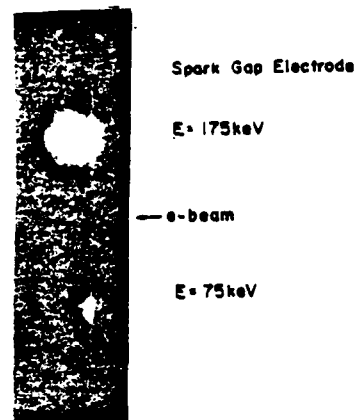
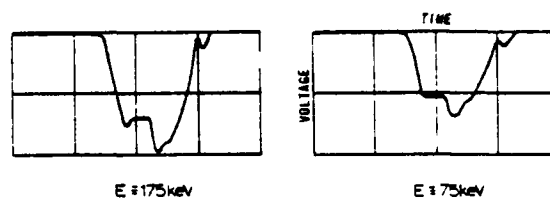


Fig. 6. Variation in the open shutter photographs of the discharge as a function of the polarity of the target electrode.

ments were conducted for both positive and negative gap polarities, yielding essentially identical results. The delay time was measured to be 52 ns in pure  $N_2$ , which is consistent with previous studies [6]. It was also found that for these relatively low voltages and pressures, the delay was invariant to both the pressure and the gap voltage. One should also note that these results were obtained with a dc-charged gap; one would expect no degradation in performance for a pulse-charged gap.

The general character of the gas discharge for  $e$ -beam initiated breakdown was studied from open shutter photographs. Fig. 6(a)–(d) shows open shutter photographs of the gas luminosity when the gap undergoes self-breakdown and when an  $e$  beam is injected for the cases when the gap is uncharged and when the electrode polarity is positive or negative, as indicated. These photographs are representative of the spatial character of the luminosity observed throughout the range of the investigations. For the same polarity, the light intensity varied in magnitude as the gas pressure and/or electrode voltage was varied. For different polarities, the character of the light emission are quite different, as shown in Fig. 6(c), (d), indicating

Fig. 7. Variation in the open shutter photographs of the discharge as a function of the  $e$ -beam cross-sectional area.Fig. 8. Variation in the open shutter photographs of the discharge for two different  $e$ -beam energies.Fig. 9. Pulse amplitude for two different  $e$ -beam energies.

that there is probably a difference in the breakdown processes. Note, however, that for both cases, the breakdown takes the form of a volume discharge. There was, however, some indication of localized spark channel formation at very high gap voltages when using some  $SF_6$  gas admixtures. The difference in discharge luminosity for the two electrode polarities, and the filamentary discharge that occurred at some high voltages ( $V_g > 2V_{diode}$ ) when  $SF_6$  was used, are still the subject of investigation and will be discussed in a later paper. Fig. 7 shows the discharge luminosity for two different  $e$ -beam diameters. The discharge cross section appears to be proportional to the cross-sectional area of the injected beam.

The light intensity of the discharge is seen to be significantly increased when a more energetic beam is introduced into the gap, as shown in Fig. 8. The amplitude of the output voltage pulse was also found to be a function of the beam energy, as shown in Fig. 9. These results indicate that the degree of ionization in the discharge plasma, hence the resistivity, varies with the beam energy. The voltage drop across the gap is, therefore, a function of the  $e$ -beam energy.

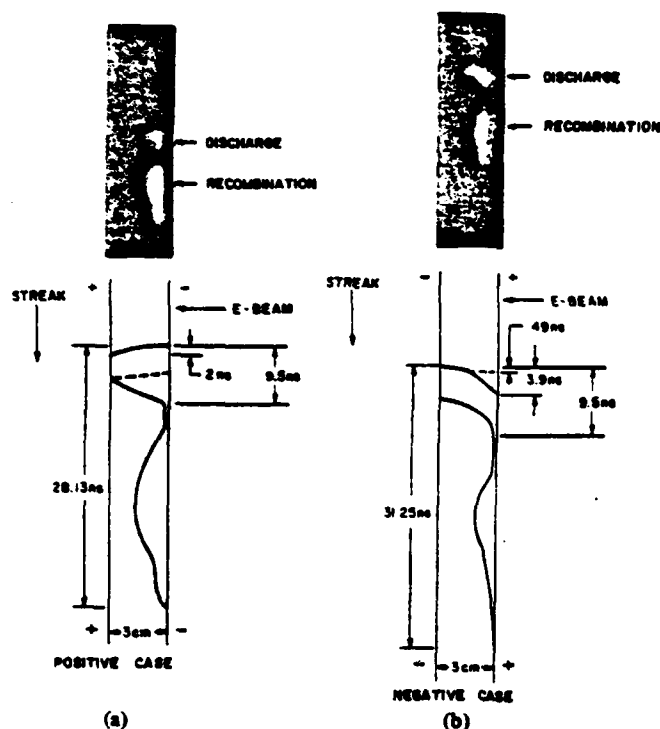


Fig. 10. Streak photographs of *e*-beam initiated breakdown and scale drawings of each for two different electrode polarities.

Streak photographs of the discharge are shown in Fig. 10. In one case the beam is fired from the cathode and in the other case from the anode. A mixture of 20 percent A and 80 percent  $N_2$  was used to increase the luminosity level so that streak photographs could be recorded. In both cases the gas pressure was  $3.1 \times 10^5$  Pa (30 psig) and the gap voltage was  $V_g \sim 250$  kV  $\sim 0.95 V_{sb}$ . The slit was parallel to the axis of the gap. Two distinct luminosity regions are apparent. The first (9.5 ns long) region is believed to be caused by the actual discharge while the second ( $\sim 20$  ns) region is probably due to recombination light in the afterglow. Note that the 9.5-ns duration of the first region corresponds closely to the FWHM length of the generator current pulse. In Fig. 10(a) (*e* beam fired from the cathode) the initial luminosity front appears to propagate from cathode to anode in 2 ns which corresponds to a velocity of  $1.5 \times 10^7$  m/s. For the opposite electrode polarity case (Fig. 10(b)) the discharge *also* propagates from cathode to anode but now with a velocity of  $3.0 \times 10^7$  m/s for the first half of the gap distance and then with a velocity of  $4.4 \times 10^6$  m/s the rest of the way. The streak camera is unable to resolve the early luminosity phenomena so the velocity quoted for the first part is probably too high. The detailed explanation of the observed phenomena is the subject of further research and also will be discussed in a later paper.

#### CONCLUSIONS

The results obtained in this series of experiments on EBTS are summarized as follows: 1) fast rise time (2.5 ns), 2) low jitter (less than 0.2 ns for  $V_g \geq 50$  percent  $V_{sb}$ ), and 3) volumetric or diffuse discharge. These characteristics make EBTS highly attractive for many applications.

The demonstrated low jitter, particularly when operated at voltages well below the self-breakdown voltages, is one of the most significant results of this work. Small jitter is crucial to the successful operation of any pulsed power system. However, it becomes extremely critical in any scheme that utilizes the simultaneous discharge of parallel pulse forming lines into a common load. The prefire probability, although not measured directly, should be low with this type of triggered switch since it works reliably and with low jitter at voltages down to at least  $0.5 V_{sb}$ .

The EBTS breakdown was observed to take the form of a volumetric discharge, proportional to the size of the injected beam. This large area breakdown offers several advantages over the narrow channel breakdown found in most switches. These are: 1) The EBTS can be scaled up to very large area electrodes and transmission lines while maintaining a low switch inductance (a particularly attractive concept is an annular *e*-beam geometry), whereas other switches cannot duplicate this, unless multiple current-sharing channels are formed. This, however, is not always easily accomplished. The broad discharge should result in a substantial lowering of the switch inductance, hence, faster rise times. 2) The diffuse discharge minimizes electrode erosion, thereby enhancing the switch lifetime and thus promoting the possibility of developing a reliable rep-rated EBTS. The recovery time should also be reduced, as contrasted to a narrow channel discharge case, because of the lower discharge temperature.

In this work the diode voltage was limited by equipment constraints to about 220 kV. This caused excessive energy deposition in the 2-mil titanium foil and hence shortened its lifetime (to  $\sim 1000$  shots). A thinner foil also did not last long because of the high gas pressure it had to withstand ( $\sim 3 \times 10^5$  Pa or  $\sim 3$  atm). Higher beam energies ( $\sim 300$  keV) would overcome this problem, and it is also speculated that higher beam energies may be needed to avoid filamentary discharges at high pressures of pure  $SF_6$  gas (i.e., at very high gap voltages).

At the present time the continued research is aimed at answering various unresolved questions and extending the technique to a greater range of parameter space.

#### REFERENCES

- [1] A. H. Guenther and J. R. Bettis, "The laser triggering of high voltage switches," *J. Phys. D.: Appl. Phys.*, vol. 11, pp. 1577-1613, Feb. 1978.
- [2] H. C. Harjes *et al.*, "Laser triggering through fiber optics of a low jitter spark gap," this issue, pp. 170-176.
- [3] B. M. Kovalchuk, V. V. Kremnew, and G. A. Mesyats, "Avalanche discharge in a gas and the generation of nanosecond and subnanosecond large current pulses," *Sov. Phys. Dokl.*, vol. 15, no. 3, pp. 267-269, Sept. 1970.
- [4] E. A. Abramyan, V. V. Borob'ev, A. A. Egorov, V. A. Elkin, and A. G. Ponomarenko, "Initiation of a discharge in a megavolt gas spark gap by an electron beam," *Prib. Tekh. Eksp.*, no. 1, pp. 117-118, Jan.-Feb. 1971.
- [5] Yu. D. Korolev and A. P. Khyzev, "Formation of a spark channel in a bulk discharge initiated by a fast-electron beam," *Teplofiz. Vys. Temp.*, vol. 13, no. 4, pp. 861-862, Jul-Aug. 1975.
- [6] A. S. El'Chaninov, V. G. Emel'yanov, B. M. Kovalchuk, G. A. Mesyats, and Yu. R. Potapitsyn, "Nanosecond-range triggering of megavolt switches," *Sov. Phys. Tech. Phys.*, vol. 20, no. 1, pp. 51-54, July 1975.

- [7] Yu. I. Bychkov, Yu. D. Korolev, G. A. Mesyats, V. V. Savin, and A. P. Khyzhev, "Dynamic atmospheric pressure discharge excited by an electron beam," *Sov. Phys.-Tech. Phys.*, vol. 20, no. 1, pp. 1502-1504, Nov. 1975.
- [8] F. M. Bruce, "Calibration of uniform-field spark-gaps for high-voltage measurements at power frequencies," *J. Inst. Elec. Eng.*, vol. 94, part I, no. 78, pp. 279-280, June 1947.
- [9] M. Newton, K. McDonald, E. E. Kunhardt, M. Kristiansen, and A. H. Guenther, "Applications of electron beams for precise switching of high voltages," in *3rd Int. Topical Conf. on High Power Electron and Ion Beam Res. and Tech.*, Inst. Nucl. Phys., Novosibirsk, USSR, July 1979.
- [10] R. K. Parker, "Explosive electron emission and the characteristics of high-current electron flow," Tech. Rep. AFWL-TR-73-92, Jan. 1973.
- [11] D. Pellinen and V. Staggs, "A technique to measure high-power beam currents," *Rev. Sci. Instr.*, vol. 44, no. 1, pp. 46-49, Jan. 1973.
- [12] J. K. Trolan, F. M. Charbonnier, F. M. Collins, and A. H. Guenther, "A versatile ultrafast pulse power system," in *Exploding Wires III*. New York: Plenum, 1964, pp. 361-389.
- [13] R. A. Fitch, "Salving diagnostics in the pulse-power environment," in *Proc. 1st IEEE Int. Pulsed Power Conf.*, Lubbock, TX, June 1976, pp. IIID5-1-IIID5-13.

# The Effect of Space Charge Induced by an Electron Beam on Spark Gap Operation

Y. H. TZENG, E. E. KUNHARDT, MEMBER, IEEE, M. KRISTIANSEN, FELLOW, IEEE,  
AND A. H. GUENTHER, FELLOW, IEEE

**Abstract**—An investigation in to the effect of electron-beam (*e*-beam) induced space charge on the insulating property of a gas in a spark gap is presented. The characteristics of the gas transition from insulator to conductor show strong dependence on the amount and location of the space charge introduced. Investigations of the delay time and the characteristics of the conducting channel have been made. The delay time from the injection of the *e*-beam to the collapse of the gap voltage ranges from  $10^{-9}$  to  $10^{-3}$  s. From open shutter photography, we observe that the character of the conducting channel is quite varied. Dark, diffuse, filamentary, or diffuse followed by filamentary (single or multiple) channels have been observed, depending on the space-charge conditions. The fundamental processes leading to the collapse of the insulating property of the gas for various experimental conditions are discussed.

## I. INTRODUCTION

THE DEVELOPMENT of high-power switches has recently received a great deal of attention as a common and crucial area of interest for scientists working on high-power lasers, fusion, high-current charged particle accelerators, and weapons-effect simulators. These switches must be capable of fast and repetitive transfer or interruption of high-voltage high current from an energy storage device to various transducers. To meet these requirements, a number of novel switches have been proposed [1]. In many of these approaches, switching is accomplished by causing a transition between insulating and conducting states of a gas. The various devices that operate in this fashion differ mainly in the way this transition is initiated and in the characteristics of the conducting stage, i.e., whether it be a diffuse or filamentary discharge.

The electron beam (*e*-beam) has been shown to be a powerful tool for initiating either a self-sustaining or a nonself-sustaining discharge in a high-pressure gas in a spark gap [2], [3]. This paper presents an investigation into the effects of the space charge induced by an *e*-beam on spark gap operation. These effects are fundamental to the understanding of the *e*-beam switching.

In Section II of this paper, the experimental setup and procedures are described. In Section III, the *e*-beam penetration depth is calculated theoretically for the discussions presented

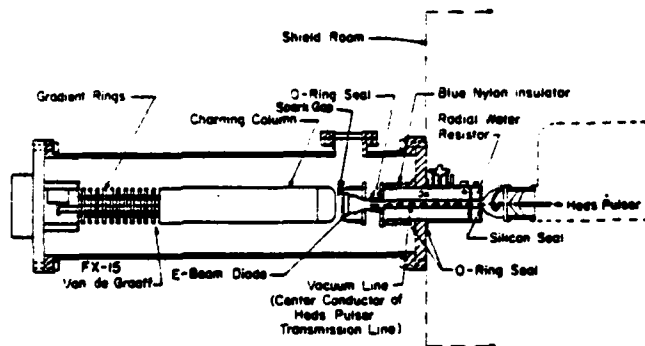


Fig. 1. Experimental arrangement.

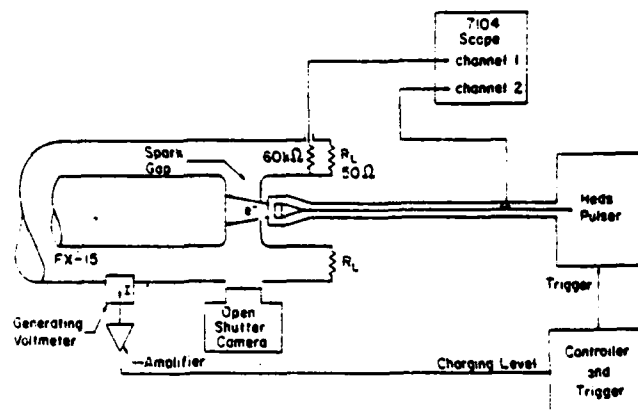


Fig. 2. Diagnostic setup.

in Section IV on the experimental results. These results significantly extend those presented in a previous paper [4]. We give further discussions of the physical processes occurring in *e*-beam switching. Recommendations for *e*-beam switching applications are given in Section V.

## II. EXPERIMENTAL ARRANGEMENT

Two diagrams of the apparatus used for these investigations are shown in Figs. 1 and 2. This setup has been described in detail in [4], [5]. Briefly, the experiment consists of an energy storage element, a gas insulated pressurized spark gap, and a source of energetic electrons. The energy storage element and the spark gap are contained within the high-pressure vessel of a Van de Graaff charged coaxial line. The line can be charged to approximately 1 MV and delivers a rectangular pulse of approximately 10 ns, full width at half-maximum duration. The *e*-beam is generated by a cold cathode field

Manuscript received April 20, 1982; revised July 2, 1982. This work was supported by Air Force Office of Scientific Research and Army Research Office.

Y. H. Tzeng and M. Kristiansen are with the Department of Electrical Engineering, Texas Technical University, Lubbock, TX 79409.

E. E. Kunhardt is with the Departments of Electrical Engineering and Physics, Texas Technical University, Lubbock, TX 79409.

A. H. Guenther is with the Air Force Weapons Laboratory, Kirtland Air Force Base, NM 87117.

emission vacuum diode which is located behind the electrode facing the Van de Graaff charged line. Modification to the diode described in [4] are discussed in [5]. A better characterization of the  $e$ -beam has also been made (see [5]).

The effects that we have studied include: 1) the characteristics of the resulting current pulse (i.e., amplitude, length, rise time, and waveform); 2) the switch delay time and jitter, and 3) the spatial character of the discharge channel.

The parameters varied during the course of these investigations are: 1) the gap polarity (depending on how the Van de Graaff is charged, the target electrode can be either positive or negative); 2) the gap voltage  $V_g$  (varied between 30–95 percent of the self-breakdown voltage, which ranges from 40 to 500 kV); 3) the gas pressure (3–7 atm); 4) the type of gas ( $N_2$  and mixtures of  $N_2$  and  $SF_6$ ); 5) the  $e$ -beam current (varied by putting a 1-mm thick aluminum mask with the desired area of uniformly distributed holes in front of the beam.) The current can be varied from about 4 A to 1 kA; 6) the average  $e$ -beam energy (35–180 keV); and 7) the  $e$ -beam pulse length (2–50 ns).

### III. CALCULATION OF THE $e$ -BEAM PENETRATION DEPTH

The energy loss of fast electrons in penetrating through a gas is given by [6]

$$\frac{1}{\rho} \frac{dW}{dx} = \frac{A}{r^2} (B - 1.4 + 21n(r/(1-r^2)^{1/2}) + 1n(1/(1-r^2)^{1/2} - 1) + 1 - r^2) \quad (1)$$

where

- $\rho$  is the density of gas ( $g/cm^3$ ),
- $W$  the energy of electron, including the rest energy (MeV),
- $r$  equal to the ratio of the electron velocity to the speed of light,
- $A$  0.0765 for  $N_2$ , and
- $B$  18.0 for  $N_2$ .

Let  $f(W)$  be  $dW/dx$ , then the penetration depth of electrons in  $N_2$  with or without external applied electric field is calculated by [7]

$$x(cm) = \int_{W_0}^{W_1} \frac{1}{f(W) - E} dW \quad (2)$$

where  $E$  is the external electric field,  $W_1$  is the energy of an electron, and  $W_0$  is the energy (including the rest energy) of an electron when it just penetrates the gas. The penetration depth of fast electrons in 3- and 7-atm  $N_2$  for different external applied electric fields are shown in Figs. 3 and 4. For positive external electrical field, the penetration depth is calculated to be the distance the electron penetrates so that the energy loss, i.e.,  $f(W)$ , is approximately equal to the energy gained from the field.

### IV. RESULTS AND DISCUSSIONS

Since the parameter space investigated is large, we have chosen the type of gas and the gap voltage polarity, in reference to the direction of the  $e$ -beam, to subdivide this space.

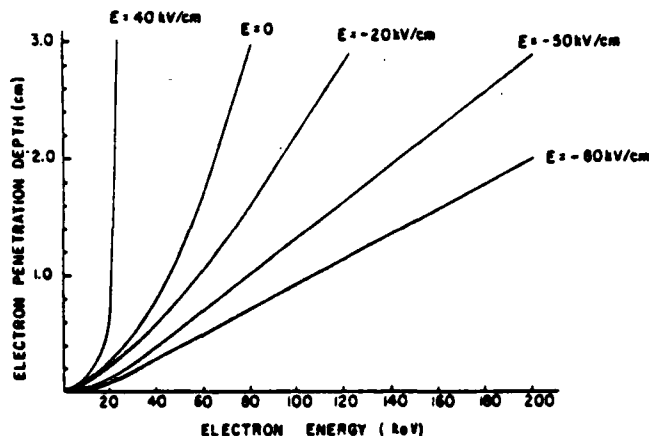


Fig. 3. Electron penetration depth in 3 atm  $N_2$ .

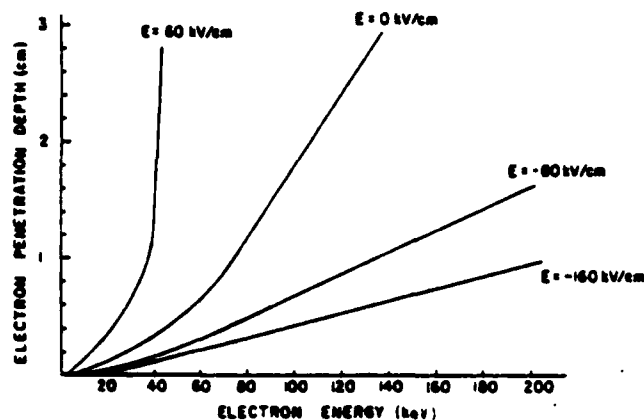


Fig. 4. Electron penetration depth in 7 atm  $N_2$ .

This choice is based on the similarities of the physical processes that occur in the regimes defined by these parameters. We shall first present the results obtained using pure nitrogen, followed by those obtained with mixtures of  $N_2$  and  $SF_6$ . Because  $SF_6$  is electronegative, the nature of the  $e$ -beam induced space charge is significantly different from that for pure  $N_2$ . This has a great influence on the subsequent evolution of the space charge in the gap, and ultimately on the characteristics of the pulse observed at the load.

In general, for pure  $N_2$  and negative gap voltage polarity (i.e., the  $e$ -beam is retarded by the external field) the discharge current characteristics and the conducting channel luminosity are strong functions of  $e$ -beam current amplitude and pulse length, and are relatively weak functions of average  $e$ -beam energy. This is also observed for positive gap polarity. Fig. 5 shows the discharge current pulses at the load as a function of  $e$ -beam current amplitude and pulse length for both gap voltage polarities. For both gap voltage polarities, no filamentary arc channels are observed when the amount of space charge introduced by the  $e$ -beam is large. All the  $e$ -beam initiated discharge current pulses shown in Fig. 5 correspond to diffuse discharge channels. Since the discharge current source is a charged transmission line with a two-way delay time of 10 ns and the load is matched to the line, the discharge current pulse is a square pulse with a duration of 10 ns only when the gap resistance is small compared to the characteristic

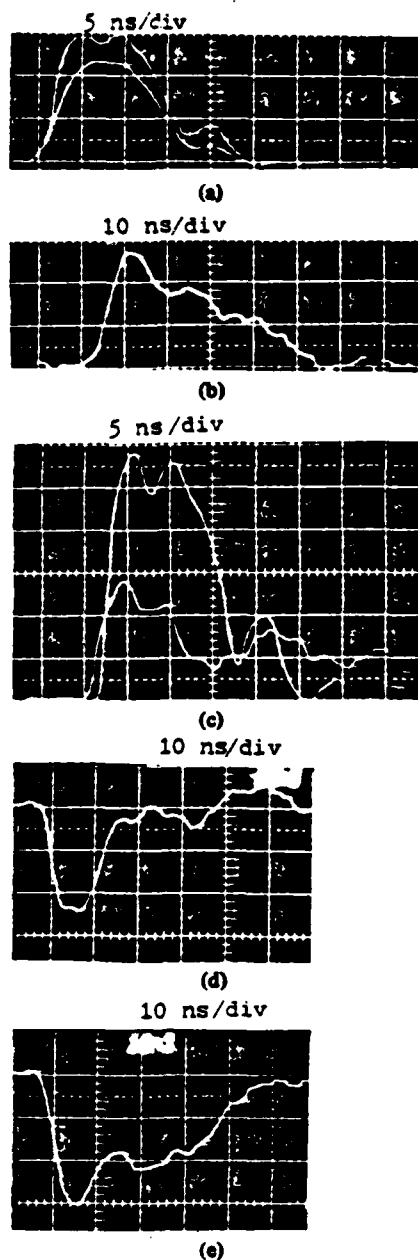


Fig. 5. Discharge current pulses. (a) Self-breakdown (top one,  $V_{sb} = 176$  kV),  $e$ -beam initiated (bottom one,  $V_g = 132$  kV,  $e$ -beam: 700 A, 60 keV, 40 ns). (b)  $e$ -beam initiated ( $V_g = 132$  kV,  $e$ -beam: 70 A, 60 keV, 40 ns). (c) Self-breakdown (top one,  $V_{sb} = 170$  kV),  $e$ -beam initiated (bottom one,  $V_g = 140$  kV;  $e$ -beam: 580 A, 70 keV, 2.5 ns). (d)  $e$ -beam initiated ( $e$ -beam: 700 A, 60 keV). (e)  $e$ -beam initiated ( $e$ -beam: 70 A, 60 keV).

impedance of the charged transmission line ( $50 \Omega$  in this experiment). When the gap resistance is high, the mismatching created will cause reflections, thus forming a current pulse longer than 10 ns with a smaller amplitude. Thus from Fig. 5, we note that for the same average  $e$ -beam energy, the discharge current pulse gets smaller in amplitude, has longer rise time, and becomes wider as the  $e$ -beam current is lowered or made shorter in duration. This implies that the gap resistance decreases when the  $e$ -beam current increases. Using the same arguments, we find that when the target electrode is charged negative and the gas pressure is increased from 5 to 7 atm, the gap resistance increases considerably. The variation of gap resistance due to a similar pressure change for the positive



Fig. 6. The delay and jitter measurements.

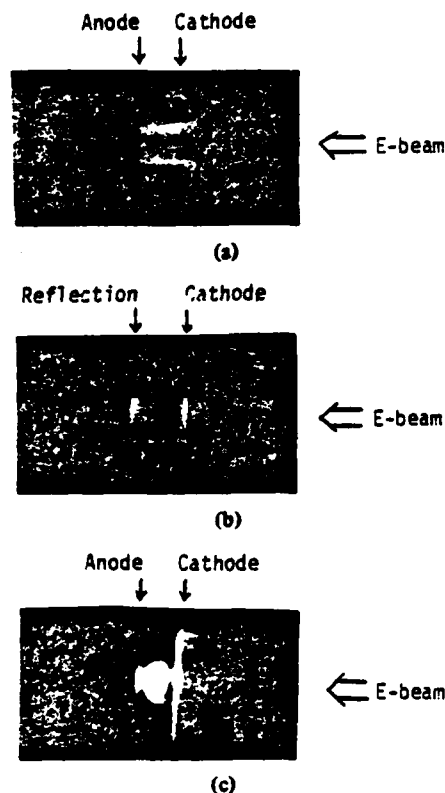


Fig. 7. Discharge channels when  $e$ -beam was injected from cathode. (a) Discharge channels initiated by a 4-A, 150-keV, 10-ns  $e$ -beam. (A 1-mm thick Al mask with 8 holes was put in front of the  $e$ -beam, and the gap voltage was below 95 percent of  $V_{sb}$ ). (b) Discharge channel initiated by a 500-A 35-keV 10-ns  $e$ -beam. (c) Discharge channel initiated by 2 500-A 35-keV 2.5-ns  $e$ -beams.

target case is not observed. A 700-A, 60-keV, and 35-ns  $e$ -beam is used for both of these gas pressure experiments. The discharge current pulse rise time was observed to range from 2.5 ns to more than 10 ns. The lower limit is the same as that for a self-breakdown pulse. In general, the smaller the  $e$ -beam current is, the longer the rise time is. From this kind of measurements, we conclude that the delay time measured from the injection of the  $e$ -beam to the appearance of a sharp rise in the discharge current is less than 1 ns (not including the delay time of the transmission line used for diagnostics). Similarly, the jitter is lower than the resolution of the experimental setup (sub-nanosecond). In general, the variation of delay time with respect to gap voltage polarity, gap voltage, gap pressure,  $e$ -beam energy, and current is not detectable. A superposition of 5 discharge current pulses is shown in Fig. 6.

The spatial characteristics of the  $e$ -beam initiated discharge channel are determined from open shutter photographs. Examples are shown in Fig. 7 for a positive target electrode and

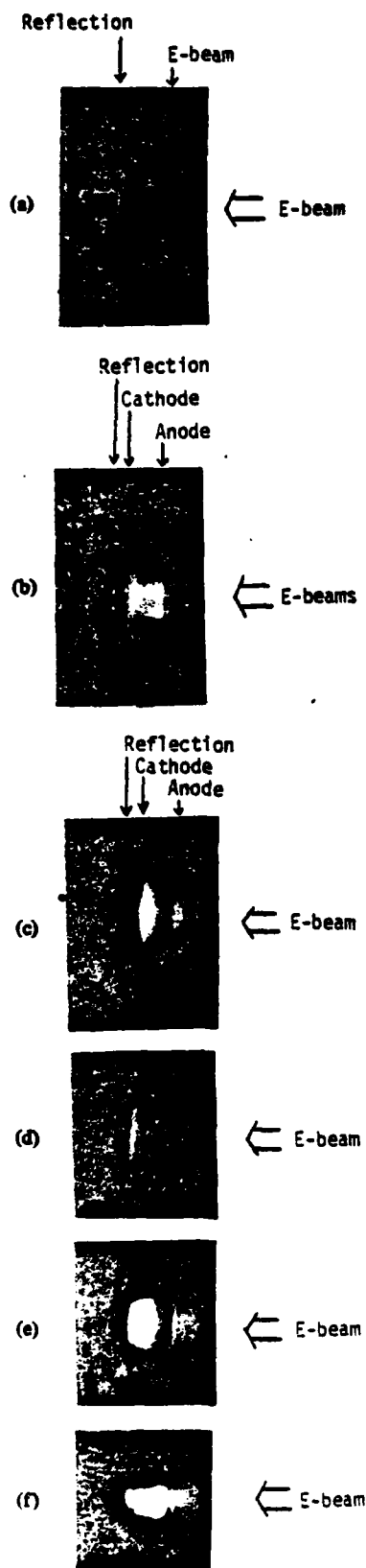


Fig. 8. Discharge channels when *e*-beam was injected from the anode. (a) *e*-beam only (gap voltage is zero). (b) Discharge channels initiated by 2 *e*-beams. (c) Discharge channel initiated by a 500-A, 10-ns, 35-keV *e*-beam. (d) Discharge channel initiated by a 440 A 60 keV 3-ns *e*-beam. ( $V_g = 72$  kV,  $V_{sb} = 160$  kV, 3 atm  $N_2$ ). (e) Discharge channel initiated by a 440 A, 60 keV, 3-ns *e*-beam. ( $V_g = 126$  kV,  $V_{sb} = 160$  kV, 3 atm  $N_2$ ). (f) Discharge channel initiated by a 192-A 35-keV 3-ns *e*-beam. ( $V_g = 156$  kV,  $V_{sb} = 160$  kV).

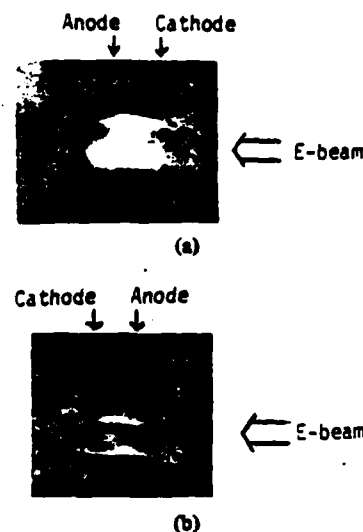


Fig. 9. Discharge channels initiated by a 4-A 150-keV 10-ns *e*-beam. (A 1-mm thick Al mask with 8 holes was put in front of the *e*-beam.) (a) Positive polarity. (b) Negative polarity.

in Fig. 8 for a negative target electrode. For the same polarity, the conducting channel luminosity varied as we changed the experimental conditions (e.g., *e*-beam current amplitude, *e*-beam pulse length, *e*-beam cross section, number of *e*-beams, gap voltage, etc.). The light distribution in the gap changes with polarity, indicating that there are different processes leading to the discharges. In general, the discharge channel is broad except when the amount of space charge induced by the beam is small. In this case, the discharge channels are filamentary (single or multiple), and large delays are observed (hundreds of nanoseconds). Fig. 9 is an illustration of this condition. In this case, a 4-A, 150-keV, and 10-ns *e*-beam has been used to trigger a spark gap pressurized to 3 atm of  $N_2$ . The gap voltage is close to self-breakdown voltage (i.e.,  $0.95 V_{sb}$ ). Multichannel discharges have also been achieved using multiple *e*-beams. Up to 8 channels have been simultaneously created (see Fig. 7(a)).

The various results discussed in the above paragraphs may be explained as follows. When the *e*-beam is injected into the gap towards a negatively charged electrode, it is retarded by both the gas and the electric field. The spatial distribution of the induced space charge is thus determined by the beam energy, the gas pressure, and the magnitude of the applied field. The distribution and amount of the induced space charge, together with the gap conditions, determine the properties of the discharge channels and current characteristics. Simple calculation shows that the current generated in the external circuit due to the motion of the space charge induced by a 1-ns, 500-A, 60-keV *e*-beam injected into a gap charged to 150 kV in 3 atm  $N_2$  is on the order of kiloampere. This explains the short delay times observed (nanosecond). Once the *e*-beam is injected into the gap, the ionized and excited gas molecules will emit photons in a short period of time. Those photons having low-absorption cross section may reach the cathode. If their energy is higher than the work function of the electrode material, they can release electrons via the photoelectric effect. This constitutes a supply of electrons distributed over a large area of the cathode. On their way to the anode, the photoelectrons form a number of avalanches. Since the avalanches are over-



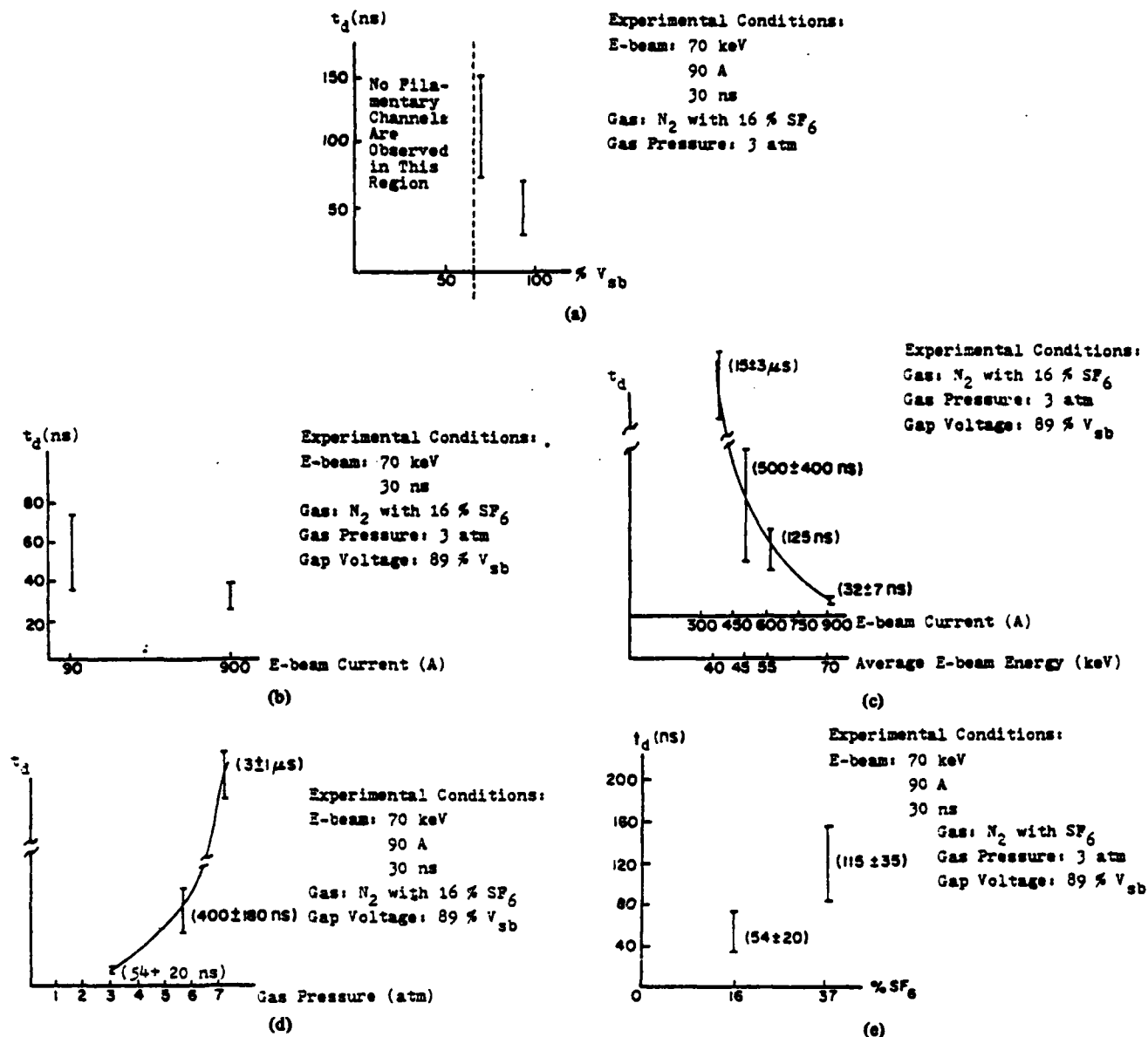


Fig. 10. Delay time versus e-beam and gap conditions with e-beam injected from anode. (a) Delay time versus percentage of  $V_{sb}$ . (b) Delay time versus e-beam current. (c) Delay time versus e-beam current and energy. (d) Delay time versus e-beam gas pressure. (e) Delay time versus percentage of  $SF_6$ .

lapping, the space charge enhanced field is uniform, and therefore, we see a broad discharge channel. This phenomenon is similar to that observed by Koppitz [8]. The avalanches evolve until the ion space charge resulting from the e-beam induced plasma is neutralized. This is seen in Fig. 8. If this space charge is small (for low e-beam current, for example) multiple avalanches will develop, resulting in a filamentary discharge, as shown in Fig. 9. When the target electrode is charged positive, the injected fast electrons can penetrate across the gap and create a conducting channel by ionizing the gas molecules. The conductivity of the channel depends on the amount of space charge introduced. The properties of this discharge are similar to the e-beam sustained discharge discussed in [3]. This experiment shows the fast turn-on of this mode of opera-

tion and its capability of delivering a  $0.5 \text{ kA/cm}^2$  discharge current density.

When mixtures of  $N_2$  and  $SF_6$  are used as the gas medium, the character of the discharge is different than when pure  $N_2$  is used. In general, when the gap voltage is higher than some threshold voltage  $V_t$  (Fig. 10(a)), the discharge channel is filamentary (single or multiple) with a discharge current pulse similar to the self-breakdown pulse. The threshold voltage  $V_t$  for the onset of this filamentary discharge depends on gas pressure, percentage of  $SF_6$ , e-beam conditions, etc. When the gap voltage is lower than this threshold, no filamentary arc channel is observed. The discharge current amplitude is then very small compared to that of self-breakdown. After the discharge stops, the voltage of the charged line drops to

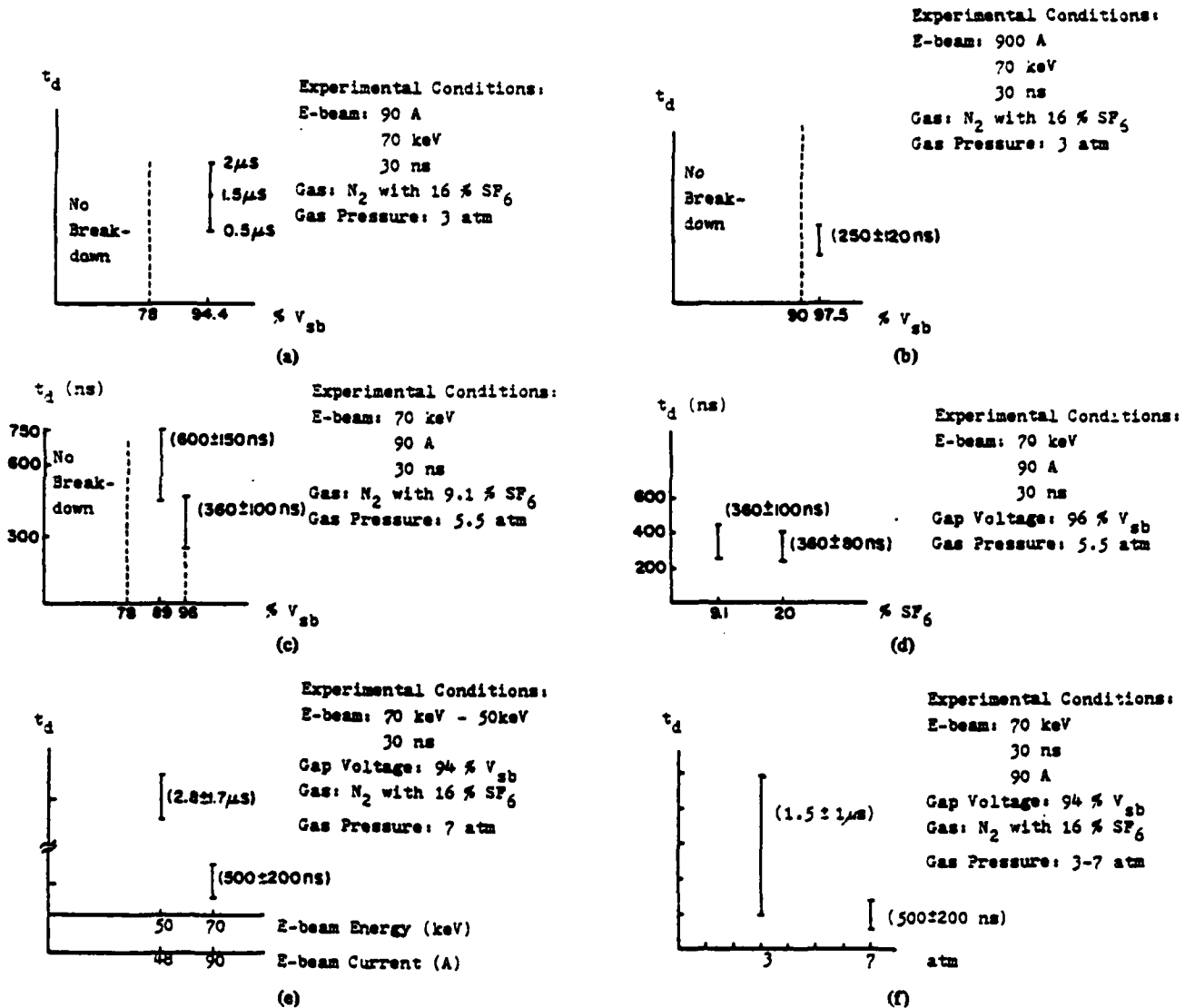


Fig. 11. Delay time versus *e*-beam and gap conditions with *e*-beam injected from cathode. (a) Delay time versus percentage of  $V_{sb}$ . (b) Delay time versus percentage of  $V_{sb}$ . (c) Delay time versus percentage of  $V_{sb}$ . (d) Delay time versus percentage of  $SF_6$ . (e) Delay time versus *e*-beam current and energy. (f) Delay time versus gas pressure.

only a fraction of its original voltage. These phenomena are observed for both gap voltage polarities.

The delay time, from the injection of *e*-beam to the detection of the discharge current pulse at the load, not including the delay time due to the transmission line for diagnostics, has been measured and is shown in Fig. 10 for a negative target electrode and in Fig. 11 for a positive target electrode. For the case of negative target electrode, the *e*-beam energy plays an important role in determining the delay time. From Fig. 10(b), we note that for a ten-fold increase in *e*-beam current, the delay time decreases by 70 percent. Moreover, from Fig. 10(c), we note that the delay time increases by 500 times when the average *e*-beam energy decreases to 60 percent and the *e*-beam current decreases to 33 percent. Therefore, we conclude that the delay time is a strong function of the average *e*-beam energy and a relatively weak function of the *e*-beam current. For

the case of a positive target electrode, both *e*-beam current and average energy show important effects on the delay time. This is shown in Fig. 11(a), 11(b), and 11(e). In Fig. 10(d) and 11(f), the dependence of the delay time on the gas pressure is displayed. The delay time increases with increasing gas pressure for the case of a negative target electrode, while it decreases with increasing gas pressure for the case of a positive target electrode. The dependence of the delay time on the ratio of mixture of N<sub>2</sub> and SF<sub>6</sub> is displayed in Figs. 10(e) and 11(d).

These observations can be explained as follows. The attachment coefficient of SF<sub>6</sub> is high for low-energy electrons and increases with decreasing ratio of electric field to gas pressure. Therefore, most of the low-energy electrons produced in the gap will attach to SF<sub>6</sub> to form negative ions. Since the drift velocity of these ions is low, the space charge current induced

in the external circuit right after the injection of the  $e$ -beam is small. When the target electrode is negative, the ionized gas close to the anode virtually extends the anode and enhances the electric field due to asymmetry and reduction of the cathode virtual anode distance. Since the net ionization coefficient, (the difference between ionization and attachment) is a strong function of the ratio of electric field to gas pressure, the electron number density close to the symmetrical axis of the electrodes grows faster than those at other places. When the injected  $e$ -beam has higher energy, it can penetrate farther. The electric field in the cathode virtual anode region determines the further development of the breakdown. Under some conditions, a filamentary arc channel may develop. Therefore, the delay time is strongly dependent on the  $e$ -beam penetration depth, which is a function of  $e$ -beam energy, gap voltage, and gas pressure. When the target electrode is positive, the inhomogeneous ionization of the gas by the non-monoenergetic  $e$ -beam and the resulting nonuniform distribution of space charge are thought to be the cause of the breakdown of the spark gap. When the gap voltage is lower than the threshold  $V_z$ , the space-charge enhanced electric field is not strong enough for the spark gap to break down. A diffuse discharge channel, which ceases before the charged line voltage drops to zero, is observed under this condition.

#### V. CONCLUSIONS

The fundamental processes leading to the collapse of the insulating property of the gas for the various experimental conditions studied have been elucidated. It has been shown that with  $e$ -beam triggering diffuse or multichannel discharges can be achieved. For high-power switching applications, the diffuse discharge channel obtained under certain conditions provides the beneficial characteristics of nonmeasurable delay and jitter, low electrode erosion, fast recovery (because it can be operated at a low percentage of  $V_{zb}$  and the gas is not fully

ionized), and low switch inductance. Moreover, multichannel discharge operation, shown possible with  $e$ -beam triggering, provides low gap resistance, low switch inductance, and low electrode erosion compared to that of a single discharge channel.

The ability to tailor the space charge induced by the  $e$ -beam to virtually create any type of discharge channel would make this scheme most desirable for spark gap operation. However, the requirements for the  $e$ -beam parameters, e.g., high  $e$ -beam current for diffused discharge, and high  $e$ -beam energy for fast breakdown of the spark gap when  $e$ -beam propagates against electric field, may limit the range of applicability. More detailed discussions about the parameters have been presented in Section IV.

#### REFERENCES

- [1] T. R. Burkes, M. O. Hagler, M. Kristiansen, J. P. Craig, W. M. Portnoy, and E. E. Kunhardt, "A critical analysis and assessment of high power switches," Report NP30, submitted to Naval Surface Weapons Center, Dahlgren, VA, 1978.
- [2] A. S. El'chaninov, V. G. Emel'yanov, B. M. Koval'chuk, G. A. Mesyats, and Yu F. Potalitsyn, "Nanosecond-range triggering of megavolt switches," *Sov. Phys. Tech. Phys.*, vol. 20, no. 1, p. 51, July, 1975.
- [3] R. O. Hunter, "Electron beam controlled switching," in *Proc. 1st IEEE Int. Pulsed Power Conf.*, paper IC8-1, Lubbock, TX, Nov., 1976.
- [4] K. McDonald, M. Newton, E. E. Kunhardt, M. Kristiansen, and A. H. Guenther, "An electron-beam triggered spark gap," *IEEE Trans. Plasma Sci.*, vol. PS-8, no. 3, p. 181, 1980.
- [5] Y. Tzeng, "The effect of space charge induced by an electron beam on spark gap operation," Master thesis, Texas Technical University, August, 1981.
- [6] R. M. Sternheimer, "The density effect for the ionization loss in various materials," *Phys. Rev.*, vol. 88, p. 851, 1982.
- [7] W. Heitler, *The Quantum Theory of Radiation*. Oxford: England: Oxford University Press, 1963.
- [8] J. Koppitz, "Nitrogen discharges of large cross section at high over-voltage in a homogeneous field," *J. Phys. D.: Appl. Phys.*, vol. 6, p. 1494, 1973.

## Project 2

Transient Processes in Laser-Triggered Breakdown

(R. Dougal, R. Bieseke, D. Pease, and P.F. Williams)

and

## Project 5

Excited State Spectroscopy of Electrically Excited Gases

(S.K. Dhali and P.F. Williams)

The primary goal of the research carried out under Projects No. 2 and 5 was to understand at a basic, physical level the processes active in the laser-triggered breakdown of spark gap switches. From the start, emphasis was placed on a combined experimental/theoretical attack on the problem. This strategy has proved very successful, and, although considerable fill-in work remains to be done, it is clear that we have accomplished our goal. The first major successes were in the experimental arena, where we obtained for the first time direct experimental evidence for the importance of streamers in the laser-triggered breakdown process, and for the interaction of the laser with the propagating streamer. More recently, important advances have been made in the numerical modelling of the propagation of these streamers. These theoretical studies are providing new information about charging polarity and voltage effects, as well as laser power and focusing effects on the crucial first stages of laser-triggered breakdown. The results of the overall program have clear importance to the understanding and design of laser-

triggered switches, but they also have an impact on more general fundamental questions relating to fast electrical breakdown of gases in general.

There have been several secondary research goals which have been set along the way. One such general goal was the development of optical diagnostic techniques to aid in the experimental studies of laser-triggered breakdown. Some of our ideas have proved successful, and others have not. Successful efforts in this area include the following:

1. The development and use of fast, time-resolved, optical emission spectroscopic techniques for studying laser-triggered breakdown [1].
2. The development and use of spectrally-resolved streak photographic techniques for studying laser-triggered breakdown [1].
3. The development and use of Stark broadening spectroscopic techniques for measuring electron densities and temperatures in a spark channel [2].
4. The development and use of laser-induced fluorescence imaging techniques for monitoring the migration of electrode vapor in a spark gap [3].
5. The development, characterization, and use of multiphoton ionization techniques as an experimental probe of space-charge dominated transport [4].
6. The development and use of a novel, numerical algorithm for calculating the electric field in cylindrically-symmetric geometry [5].

7. The development and use of modern, flux-corrected-transport numerical techniques to study problems in space-charge-dominated transport, such as streamer propagation [6].

The primary goal of the research carried out under these two projects has been achieved. In order to fill in some of the important details, work still remains to be done in several areas.

1. Further numerical studies of streamer propagation, especially under conditions directly relevant to laser-triggered switches, need to be done. This work is currently underway.
2. The computer program we have developed for studying streamer propagation simulates the first stages of a laser-triggered breakdown event. Standard techniques based on a rate equation approach should be able to describe the second, heating, stage of breakdown, and such a program should be written and coupled with the first. The overall program would then be a major step in developing a computer-aided design capability for spark gap switches.
3. The techniques and expertise we have developed in studying laser-triggered breakdown should be applied to the study of other types of triggered breakdown important to pulsed power switching technology. Efforts in this direction are underway.
4. Optical diagnostics, such as the laser-induced fluorescence imaging techniques we have developed, and either spontaneous or stimulated Raman scattering should be applied to the study

of recovery phenomena in higher power spark gap switches. The experimental work carried out in these two projects pertained to relatively high impedance, well controlled, systems which allowed easier comparison with the theoretical calculations.

5. There is a need for more experimental data about laser-triggered and other types of triggered breakdown. One effort in this direction, already underway, involves the acquisition and development of a high speed framing camera facility based on a state-of-the-art microchannel plate intensifier tube technique.

#### References

1. R.A. Dougal and P.F. Williams, "Fundamental Processes in Laser-Triggered Electrical Breakdown of Gases," submitted to J. Phys. D: Appl. Phys., and included as an Appendix to the report on Project No. 2.
2. S.K. Dhali, P.F. Williams, R.J. Crumley, and M.A. Gundersen, IEEE Trans. Plasma Sci., PS-8, 164 (1980).
3. R.A. Dougal, P.F. Williams, and D.C. Pease, Rev. Sci. Inst., 54, 572, (1983).
4. S.K. Dhali and P.F. Williams, "Multiphoton Ionization - A Potential Trigger and/or Control for Electrical Breakdown," Proc. 3rd IEEE International Pulsed Power Conf., Albuquerque, NM, 1981, p 151.
5. E.E. Kunhardt and P.F. Williams, "A Fast Algorithm for Numerically Integrating Poisson's Equation in Cylindrically-Symmetric Geometries", submitted to J. Comp. Phys.
6. S.K. Dhali and P.F. Williams, "Numerical Simulation of Space-Charge-Controlled Transport", to appear in Proc. 4th IEEE Pulsed Power Conf., Albuquerque, NM, 1983, p. 227.

## Project No. 3

Spark Gap Discharge and Erosion Phenomena

(A. Donaldson, C. Yeh, B. Maas, R. Ness

H. Krompholz, M. Hagler, M. Kristiansen, and L. Hatfield)

The work performed during the contract has been directed toward the understanding of the basic physical processes which affect the performance (voltage stability, lifetime, repetition rate, and hold-off voltage) of high energy spark gaps. The principal objective was to develop new and check currently existing physical models which describe the mechanisms of spark initiation, electrode erosion, gas recovery, and insulator flashover. The objective required:

1. Documentation of existing models and results,
2. Design of key experiments (in order to test the assumptions of each model) which:
  - a) generate the appropriate data base,
  - b) allow for isolation of fundamental model parameters,
  - c) provide for simulation outside the previously existing parameter regime.

The different experimental facilities required to achieve these objectives were constructed and are described in Table I. In addition, plans have been made to use a high repetition rate pulser (1 kpps) at Sandia National Laboratories for further studies. A summary of the accomplishments made at Texas Tech and the topics which remain to be studied are given for each of the spark gap performance areas in Tables II-V.



Table I  
High Energy Spark Gap Facilities

<u>Pulser</u>	<u>Characteristics</u>	<u>Use</u>
Mark I	3 kJ, 60 kV, 60 kA, 2 $\mu$ s (critically damped), two pulses, variable separation	Material Synergism [1,2] Recovery [3]
Mark II	8 kJ, 30 kV, 25 kA 25 $\mu$ s (rectangular), 5 pps	Erosion [4-7] Breakdown Initiation [8,9]
Mark III	18 kJ, 60 kV, 90 kA 12 $\mu$ s (rectangular)	Erosion (Single Shot)
Mark IV	3 kJ, 60 kV, 60 kA 2 $\mu$ s (critically damped)	Arc Voltage (for erosion and recovery models)
Mark V	18 kJ, 50 kV, 100 kA (oscillatory 200 kHz)	Erosion (Oscillatory) Energy Deposited vs Pulse Shape

#### Diagnostics

Electrical: Voltage, Current,  $dI/dt$

Optical: Mach Zehnder Interferometry, Schlieren Interferometry

Misc: Streak Camera, Rotating Drum Camera, Video Camera,  
Mass Spectrometer, Thermocouples, Optical  
Microscopes, Scanning Electron Microscope

#### Additional Facilities:

Electrode Cross Sectioning Equipment

Computer Controlled Data Acquisition System

Table II

Breakdown Initiation Accomplishments [1-4,8,9]

- Determined the importance of material synergism (insulator, gas and electrode) on the self-breakdown voltage distributions (SBVD)
- Measured the SBVD for a large number of experimental conditions (varying charging rate, insulator, gas, electrode, gas pressure, amount of irradiation, energy per shot, and pulse characteristics)
- Developed theoretically and verified experimentally a breakdown initiation model which incorporates all the relevant physical parameters (charging rate, surface structure, gas type and pressure, electrode geometry, and electron generation rate).

Implications of this model include:

The greater the spread in field enhancements, the greater the possible range in breakdown voltages.

The higher the pressure, the higher the required threshold field enhancement for a fixed voltage.

For a fixed distribution of field enhancements; the higher the pressure, the greater the possible spread in breakdown voltages.

The larger the gap spacing, the smaller the effect of surface microstructure.

The larger the microstructure, the greater the spread in breakdown voltage for a fixed distribution of field enhancements.

Table III

Erosion Accomplishments [1, 2, 4-7]

- Determined the role of many of the chemical processes occurring at the electrode surface for the following electrode-gas combinations: Graphite-N<sub>2</sub>, Graphite-SF<sub>6</sub>, Copper Tungsten-N<sub>2</sub>, and Copper Tungsten-SF<sub>6</sub> [1,2].
- Measured the electrode erosion for nine different electrode materials and three types of gases as a function of current, resulting in the following conclusions:
  1. The electrode erosion rates and mechanisms are highly polarity dependent and, thus, results for oscillatory and unipolar discharges can be considerably different.
  2. A large amount of the erosion is in the form of solid and molten material removed parallel to the electrode surface and, apparently, from the edge of the macroscopic craters found on the cathode.
  3. Cathode erosion rates are proportional to the total amount of charge transferred for a fixed repetition rate and pulse width.
  4. Stainless steel (304) may be an economical replacement for copper-tungsten composites as a cathode material for the conditions studied.
  5. Anode erosion rates were quite scattered, but, in general, were considerably less than the cathode erosion rates for all materials tested except stainless steel.
  6. No distinct correlation was found between the thermo-physical properties of the electrode materials and the amount of erosion.
- A physical understanding of the erosion process has been developed which explains the previously unresolved discrepancy between the theoretical erosion spot models based on Joule heating (erosion a function of  $\int i^2 dt$ ) and experimental results which show erosion to be a function of  $\int i dt$ , as well as several other current dependencies.
- The basic erosion mechanisms in stainless steel, e.g. crack formation due to material inhomogeneities, has been clarified.

Table IV

Recovery Accomplishments [3]

- Measured the recovery rate of high energy spark gaps for several electrode material and gas combinations as a function of gas pressure, gap spacing, and rate of applied voltage (in a sealed gap, i.e. no gas flow)
- Measured the self-breakdown voltage statistics for the 1st and 2nd pulses in a two-pulse recovery test
- Recorded on film the motion of hot gas and/or electrode debris from 1st pulse traveling at  $2 - 10 \times 10^2$  cm/sec.
- Observed restrike phenomena through the debris as a function of time between pulses
- Initiated a comparison of experimental results with recovery models.

Table V

Work Remaining to Be Done During Contract Period

## Breakdown Initiation

- Final Documentation of Results
- Development of E-Field Solver for Simple Geometries (as Time Allows)
- Pre-Fire Experiments

## Electrode Erosion

- Measurement of Energy Delivered to Electrode vs Pulse Shape
- Measurement of Erosion as a Function of Pulse Shape (Unipolar vs Oscillatory Discharges)
- Measurement of Erosion as a Function of Pressure
- Measurement of Erosion as a Function of Rep-Rate and Gas Flow
- Study of Damage to Electrode Surface for the Above Cases for both Multiple Shot and for a Single Shot

## Recovery

- Verification of Recovery Models
- Use of Model to Make Trend Predictions for Design of Sealed Spark Gaps

## References

1. Lloyd Gordon, "Material Studies in a High Energy Spark Gap," Ph.D. Dissertation, Texas Tech University, May 1983.
2. L.B. Gordon, et.al., "Material Studies in a High Energy Spark Gap," IEEE Trans. Plasma Sci. PS-10, 286 (1982).
3. C.H. Yeh, et.al., "Voltage Recovery Measurements in a High Energy Spark Gap", 4th IEEE Pulsed Power Conference, Albuquerque, NM, June 1983.
4. A.L. Donaldson, et.al., "Electrode Erosion in High Power Spark Gaps", IEEE Conference Record of 1982, 15th Power Modulator Symposium, June 14-16, 1982, Baltimore, MD, pp 84-88.
5. Donaldson, A.L., et.al., "Electrode Erosion in a High Energy Spark Gap", 4th IEEE Pulsed Power Conference, Albuquerque, NM, June 1983
6. Donaldson, A.L., et.al., "Electrode Erosion Phenomena in a High Energy Pulsed Discharge", Accepted for publication in IEEE Trans. Plasma Science, March 1984.
7. Jackson, G., et.al., "Surface Studies of Electrodes Used in Spark Gaps", 4th IEEE Pulsed Power Conference, Albuquerque, NM, June 1983.
8. Donaldson, A.L., et. al., "Modeling of Spark Gap Performance", 4th IEEE Pulsed Power Conference, Albuquerque, NM, June 1983 (Invited Paper).
9. Donaldson, A.L., et.al., "Modeling of the Breakdown Voltage Stability in a High Energy Spark Gap", submitted to Journal Appl. Phys.

## Project No. 4

Pulsed Power Surface Physics and Applications

(G.L. Jackson, L.L.Hatfield,  
M. Kristiansen, and G.R. Leiker)

The project "Pulsed Power Surface Physics and Applications" was started to complement the studies of spark gaps. The initial idea was to examine the surfaces of insulators used in spark gaps and to determine the physical processes responsible for insulator failure through flashover and bombardment by microparticles. At the time, most studies of insulators were incidental to other work on spark gaps, and systematic follow-ups on observed surface phenomena were rare. The exception is studies of insulator surface flashover, on which a great deal of work had been done.

We found that the published work on surface flashover was consistent for study of one material at a time, but that comparison of different materials gave large variances from one investigator to another. This is due to the diversity of methods employed by the various investigators. The flashover potential for Lucite, for example, has been reported to be from 30 kV/cm to 90 kV/cm depending on the author. This was the motivation for the measurements of the flashover potential of four polymer insulators in vacuum and in gases. These measurements were taken under well documented, closely controlled conditions, so that the comparisons between materials are meaningful.

The results of our work on surface flashover can be summarized as follows: [1,2]

1. We have made meaningful comparisons of the flashover potentials of four commonly used polymer insulators. This has been done in vacuum and in two different gases at one atmosphere.
2. A durable, high resistivity coating, which dramatically raises the vacuum flashover potential of three of the four polymers, has been discovered.
3. Our study of the effects of this coating has verified some aspects of the current theoretical models of flashover.
4. We have advanced an experimentally testable hypothesis concerning the role of surface charge and surface damage in flashover tests.
5. We have offered a hypothesis which explains the failure of some previous attempts at coating polymers to raise the flashover potential.

Problems which we have not solved include:

1. Exactly what is the structure of the coating we observe on our polymer test samples?
2. Can this coating be applied by some other method more suited to coating large insulators?
3. Does this coating actually have the secondary electron emission coefficient implied by our indirect evidence?



The results of our work on electrodes and insulators used in spark gaps may be summarized as follows: [3,4,5]

1. We have demonstrated beyond any doubt the importance of the synergism between the materials used in spark gaps. (Electrode, insulator, and gas.)
2. We have obtained experimental verification of the predicted effects of the electrode surface topography and composition on the self breakdown voltage statistics of a spark gap.
3. The basic processes responsible for erosion of the electrodes, have been identified for certain combinations of electrode and gas.

Questions which remain include:

1. Can the surface of an electrode be tailored to have and maintain characteristics which decrease the erosion rate and/or improve the self-breakdown voltage statistics?
2. Can the synergistic materials effects in spark gaps be employed to improve spark gap lifetime or performance?
3. In the graphite electrode-air combination, is the production of CO and CO<sub>2</sub> really responsible for the lack of carbon coating on the insulator surface?

## References

1. "Pulse Flashover of Solid Dielectrics in Vacuum", G.L. Jackson, L.L. Hatfield, M. Kristiansen, J. Marx, and A. Bowling, IEEE Transactions on Electrical Insulation, EI-18, 310 (1983).
2. "Pulsed Flashover of Solid Dielectrics in Gases", G. Jackson, L. Hatfield, G. Leiker, M. Kristiansen, and J. Marx, Proc. 4th IEEE Pulsed Power Conf., Albuquerque, NM, June 1983.
3. "Surface Studies of Dielectric Materials Used in Spark Gaps", G. Jackson, L. Hatfield, M. Kristiansen, M. Hagler, J. Marx. A.L. Donaldson, G. Leiker, R. Curry, and R. Ness, Journal of Applied Physics, 55, 262 (1984).
4. "Surface Studies of Electrodes Used in Spark Gaps", G. Jackson, L. Hatfield, M. Kristiansen, M. Hagler, A.L. Donaldson, R. Ness, and J. Marx, Proc. of the 4th IEEE Pulsed Power Conf., Albuquerque, NM, June 1983.
5. "Multichannel Surface Discharge Switch," D. Johnson, M. Kristiansen, and L. Hatfield, Annual Report of the Conf. on Electrical Insulation and Dielectric Phenomena, Amherst, MA, Oct. 1982.

## Project No. 6

Exploratory Concepts

(R. Curry, B. Maas, D. Johnson, L. Hatfield,  
K. Schoenbach, G. Schaefer, F. Williams, and M. Kristiansen)

The main objective of this project is to support a variety of smaller investigations in order to determine if they warrant further, more extensive investigations and support. This is essentially the "venture capital" part of the overall program. Many of these "mini-investigations" have, as expected, not proved successful but a significant part have also been found promising enough to warrant increased support. The main, successful, accomplishments are:

1. Feasibility studies of optically controlled switches were carried out to the level where they warranted separate funding (AFOSR-Project No. 8).
2. Feasibility studies of various opening switch concepts, especially the e-beam controlled opening switch, were carried out to the level where they warranted separate funding (ARO-Project No. 9).
3. Investigations of restrike phenomena in gas blown spark gaps were carried out to the level where they warranted separate funding (AFOSR Grant No. AFOSR-82-0327 to our ME Dept.).

4. Several novel opening switch ideas have been evaluated in cooperation with Project No. 9. Two of the more interesting ideas are being pursued in cooperation with research groups at the University of Illinois and at GTE Research Laboratory. Several other ideas have been judged either promising or impractical and documented in Annual Reports on this Program.
5. A system has been designed and constructed for measuring the time-dependent resistance of a spark gap arc during a discharge. This is a measurement of both considerable complexity and importance. The results will form an important input to our erosion modelling efforts (Project No. 3).
6. A surface discharge switch has been designed and constructed. The investigations have led to improved understanding of the optimum triggering conditions for these extremely low inductance switches [1,2]. These investigations will probably form the basis for a separate proposal for continued investigations of the limits to the maximum current per channel and the associated dielectric substrate erosion.
7. Current investigations of novel field distortion trigger concepts have shown promising, preliminary results.

## References

1. "Triggering of Surface Discharge Switches, R. Curry, D. Johnson, M. Kristiansen, L. Hatfield, A. H. Guenther, Proc. 4th IEEE Pulsed Power Conf., p. 174, Albuquerque, NM, 1983.
2. "Multichannel Surface Discharge Switch", Proc. Conf. on Electrical Insulation and Dielectric Phenomena, Amherst, MA, Oct., 1982 (with D. Johnson and L. Hatfield).

## Project No. 7

Electromechanical Pulse Device

(R.H. Dunlap and J.P. Craig)

This project element was finished in the previous contract period and a final report was included in the last Annual Report on this contract. The basic goal was to determine the feasibility of designing and constructing a repetitive ( $> 1000$  pps) Electromechanical Pulse Amplifier with very short pulse rise times ( $\sim 10$   $\mu$ s) and pulse widths ( $\sim 100$   $\mu$ s) compared to other electromechanical devices. The theory of the device was developed and a small scale model was constructed. Successful pulse compression and voltage gain were demonstrated but there was no net power gain due to the losses inherent in small scale models. The basic concept was verified, however, and further development awaits identification of applications which fits the optimum performance regimes of the Electromechanical Pulse Amplifier.

Projects 8 and 9  
"Optically Controlled Discharges  
and  
Opening Switches

(C. Harjes, G. Hutchinson, L. Thurmond, R. Cooper, K. Schoenbach  
G. Schaefer, H. Krompholz, L. Hatfield, and M. Kristiansen)

1. Introduction

The use of diffuse discharges as externally controlled switches was proposed and discussed independently by R. Hunter [1] from the USA and B. M. Kovalchuk and G. A. Mesyats, [2] from the USSR at the First Pulsed Power Conference in Lubbock, TX in 1976. In the following years extensive work on e-beam controlled diffuse discharges was performed in the USSR [3], whereas in the USA only relatively small efforts were made to advance the field of diffuse discharges as controllable pulsed power switches. One of the reasons for this lack of interest was the low efficiency of diffuse discharges, when used as fast opening switches with opening times of microseconds and less.

2. Gases for Diffuse Discharge Switches

The problem of switch efficiency is mainly caused by electron loss processes in the diffuse plasma. Loss processes, such as attachment, should be strong in order to reduce the plasma conductivity of the switch rapidly after turn off of the sustaining source, for instance an e-beam. On the other hand, lossy gases require a high-power e-beam source to sustain the discharge during the conductive phase of the switch.

At Texas Tech University efforts were made in 1980 [4] and 1981 [5,6] to explore various possibilities to "tailor" gas mixtures with respect to their optimum efficiency in diffuse discharge opening switches as part of inductive storage circuits. These efforts led to a set of criteria for optimum gas properties [6,7,8,9]:

- a) The drift velocity of electrons should be high at low electron energies and decrease at higher electron energies.
- b) For fast opening the diffuse discharge should be attachment dominated. The attachment rate coefficient should be small at low electron energies and increase with increasing electron energy in the range of opening switch operation.

To find gases and gas mixtures which show the desired behavior a literature search was performed. Additionally, SRI, Inc. was requested, through a subcontract, to investigate  $N_2O$ , one of the candidate gases [10]. Cooperation with JPL (S. Srivastava) was initiated, with the goal to examine other, similar gases, like  $SO_2$  for diffuse discharge switches. Informal contacts with the molecular physics group at Oak Ridge National Laboratory (L. Christophorou) led to the initiation of research efforts on opening switch gases there. The interaction was beneficial for both the group at Oak Ridge as well as at Texas Tech University. A formal joint research program is planned (a joint proposal to NSF is pending).



### 3. Control Mechanisms

Externally controlled diffuse discharges seem to offer the opportunity for fast as well as for repetitive opening switching. Diffuse discharges are advantageous mainly because of their moderate energy density. Also the discharge is not in local thermodynamic equilibrium (LTE), which offers the possibility of external control of opening and closing processes. Externally sustained discharges have widely been used for TEA laser discharges. Here the external control mechanisms provides the required ionization and the discharge can be operated at low values of  $E/N$  since Townsend ionization is not required. The most important processes that have been used are:

- 1) High energy electron beams
- 2) Broadband VUV sources.

Narrow bandwidth light sources (lasers) offer the advantage that the density of particles in individual states can be influenced and subsequently also the generating and depletion mechanisms of electrons in the gas discharges. Some of the processes considered for switching applications have been known as optogalvanic effects. They were used to indicate a wavelength specific response of a discharge such as in spectroscopy, impurity sensing, and laser frequency stabilization. For switching applications, however, the magnitude and the fast response are the important parameters. As part of this research project, optogalvanic processes with lasers have been screened for their possible use as control mechanisms for switches and the results were presented in two papers [9,11]. A shortened review is given in the following section.

The interaction of light with specific energy states of atoms and molecules can be used to increase or to decrease the conductivity by controlling either the electron generation or depletion. Optically increased conductivity can be accomplished by photoionization or excitation, with collisional assistance, or by photodetachment, which may be considered as an electron generation process if negative ions are present or as a process which eliminates electron losses via attachment. Optically decreased conductivity can be accomplished by optical quenching of excited states or by optically enhanced attachment.

The following processes can be used to increase the conductivity:

- (1) Single photon ionization: This is not a resonant process and the advantage of the laser as a narrow bandwidth source is not utilized.
- (2) Resonant two-step photoionization: This appears to be a more efficient way to generate electron-ion pairs. Consider that UV excimer lasers have produced significant electron densities in several organic molecules.
- (3) Multiphoton ionization: This will in general involve one or more nonresonant steps and the subsequent ionization rate will depend strongly on the intensity of the laser beam. Thus, it is not an efficient mechanism for producing large volume ionization. However, it may be a suitable mechanism for laser triggering, acting either on the electrode or in the gas.

- (4) Photoexcitation and subsequent collisional ionization: This has already been used in laser enhanced, ionization spectroscopy. An interesting mechanism is laser resonance pumping, which has been demonstrated in several alkali vapors. In this case, if the absorption of a resonant transition is saturated, then the density of the resonance state is nearly the same as that of the ground state. Here the probability for an electron to collide with an excited atom is very high; and, through super elastic collisions, the electrons can gain enough energy to ionize the gas.
- (5) Photoionization from collisionally excited states: This can result in a large effect in systems with high densities of excited species or in systems where the transition rate into such an intermediate state is large.
- (6) Photodetachment: This is one way to overcome attachment in a well defined switch period. In diffuse discharge opening switches attachers must be used to achieve fast opening, however, during the conduction phase, photodetachment may be used to eliminate electron losses via attachment [12].

Processes which can be used to decrease the conductivity are quenching of metastables and optically enhanced attachment:

- (1) Quenching of metastable: Atoms or molecules may also be suitable mechanisms to control the conductance of a discharge, particularly if the electron generation, dominated by two-step ionization via metastables, can be controlled. Quenching, as used here, describes the dissipation of energy

deposited in metastables in the discharge by exciting a higher lying level which is optically connected to the ground state. If this resonance radiation can escape the discharge vessel, the energy will not even contribute to heating of the ambient gas.

- (2) Optically enhanced attachment: This makes use of the fact that certain attachers have an increased attachment cross section in their rotationally and/or vibrationally excited states. As in gas discharges, there is always a certain rate of vibrational excitation by electron collisions. Only those systems are considered where an increase of the attachment rate becomes dominant if molecules in highly excited vibrational states are present. The considered generation mechanisms for molecules in these states are:
- a) (E V,R) transitions (transitions from electronically excited states to vibrationally and rotationally excited states), radiative or collisional.
  - b) photo dissociation.

Considering the, in general, low efficiency in producing laser photons, it does not seem efficient to use photons for the production of electrons starting from the ground state of a particle. For these purposes electron beams and broad band UV sources are cheaper and operate with high efficiency. An important exception may be to use photodetachment to overcome attachment in a short switch period. The main advantage of laser induced processes seems to be related to optically controlled attachment where the laser is used only in a short switch period.

These considerations have led to the concept of an electron beam sustained, optically assisted diffuse discharge switch which is now being investigated in further detail.

#### 4. Calculations

Models and computer codes for diffuse discharges have been developed for a long time. Important applications were gas discharge lamps and gas discharge laser. The TEA lasers show especially close similarities to discharges suitable for switching. However, the operating conditions, which the discharges must fulfill, are different for switching applications. Other discharge properties and mechanisms of importance in the discharge have to be considered and their collective influence on the coupling between the discharge and circuit must be optimized in a different way.

There are three different groups of parameters of diffuse discharges that have to be optimized simultaneously for switching applications: (1) the gas parameters, specially the attachment properties, as discussed in Section 2, (2) the external control mechanisms (which may mean several control mechanisms at the same time), as discussed in Section 3, and (3) the circuit properties for circuits appropriate to inductive energy storage systems. No calculations were published that incorporate all these parameters and allowed calculations of the transient behavior of such a discharge. We, therefore, developed a computer code and applied it to electron beam and optically controlled diffuse discharges.

This code was specially designed to allow fast calculations for different discharge and circuit parameters. The code use two independent steps. In a first step, all rate constants necessary for the calculation of all rates of the significant processes are calculated, depending on  $E/N$ , for a representative gas mixture. These calculations require knowledge of the  $E/N$  dependent electron energy distribution function or the calculation of this distribution function. In a second step a system of time dependent rate equations is solved, using the  $E/N$  dependent rate constants and the circuit equation to incorporate the feedback of the circuit. It is assumed in this code that the electron energy distribution function and subsequently the  $E/N$  dependent rate constants do not change significantly if the gas mixture is changed in a certain range around the value for which the rate constants have been determined in step one.

For the first calculations on an optically controlled discharge containing  $N_2$ ,  $NO$ , and an attacher, the rate constants were calculated using experimental data for the mean electron energy dependence on  $E/N$  and a Maxwellian energy distribution function. In the meantime, Monte Carlo calculations have been performed for a gas mixture containing  $N_2$  as a buffer gas and  $N_2O$  as an attacher, based on a set of experimentally evaluated cross sections [13]. The rate constants based on these calculations have then been used for calculations of an e-beam sustained discharge, assisted by photodetachment of  $O^-$  in the turn-on phase [14].

These calculations demonstrate the advantage of using electron beam controlled discharge switches with gas mixtures containing a buffer gas and admixtures of attachers with an attachment rate having a threshold at some  $E/N$  and then increasing with  $E/N$ . In the switch closing process, starting with a high value of  $E/N$ , photodetachment allows one to overcome the high losses during the closing phase [14].

## 5. Experimental Arrangements

### A. Electron-Beam Controlled Diffuse Discharge System [15]

An electron-beam controlled diffuse discharge system has been constructed to study the behavior of an e-beam sustained, attachment dominated diffuse discharge at

- a) high discharge current densities
- b) fast opening and closing times
- c) burst-mode operation.

The e-beam gun is constructed as a triode with a thermionic cathode. The e-beam can be operated at plate voltages up to 250 kV and current densities of up to  $4 \text{ A/cm}^2$  at total currents of 400 A. The voltage and current can be varied independently. The e-beam control system allows operation in a burst-mode with variable pulse durations and pulse separations in the 100 ns range. Turn-on and turn-off times of the e-beam are 10 ns. The switch system, which can be pressurized up to 10 atm, is part of a circuit with a PFN with variable impedance as the power source.

The e-beam switch apparatus allows independent variation of e-beam current and voltage at high current densities. Addi-

tionally, it offers the opportunity to investigate rep-rated switch operation in the 100 ns range.

#### B. Laser Controlled Diffuse Discharge System

Several laser controlled discharge systems have been constructed and operated to investigate the feasibility of optical control mechanisms in diffuse discharge switches.

In small scale dc discharge experiments optogalvanic effects were investigated in the discharge itself as well as in the flowing afterglow. The flowing afterglow allows investigations of the basic processes used in different optogalvanic effects since the feedback with the discharge can be eliminated. Experiments in the discharge itself allow the use of the feedback of the discharge to enhance the effect, especially if experiments are performed in a discharge operating regime close to instabilities. Experiments on photodetachment have been performed in gas mixtures containing attachers producing  $O^-$  [12].

High power discharge system experiments must be carried out to check the scaling laws for optogalvanic processes. A self sustained, high pressure, diffuse discharge system has been constructed and tested. The system consists of an oil filled, 50  $\Omega$  line, a laser triggered closing switch, and the discharge chamber. Integrated into the discharge chamber is a UV preionization system which is switched by a laser triggered gap, using the same laser to allow precise timing. A flashlamp pumped dye laser produces a rectangular pulse with a pulse length up to 500 ns and rise and fall times of 10 ns. This system fulfills the



following requirements for the production of diffuse discharges at high pressures, containing attachers:

1. voltage across the discharge gap large compared to the breakdown voltage,
2. fast voltage risetime,
3. uniform preionization,
4. uniform initial electric field.

It also satisfies the following requirement for optical control of the diffuse discharge:

1. optical access of the diffuse discharge
2. tunability of the laser
3. possibility to shape the laser pulse with rise and fall times in the order of the desired switching times.

## 6. Workshops

Solving the problem of developing a practical switch requires an extremely wide range of expertise. Researchers with backgrounds in circuit analysis, material properties, discharge physics, basic gas data determination, plasma chemistry, etc., are needed. The group at Texas Tech University tried from the beginning to obtain information on these fields through cooperation with various research groups in the United States. Besides personal contact it was tried to promote exchange of information through discussions at several workshops, organized by Texas Tech University. These workshops were:

- a) ARO Workshop on "Opening Switches," at Tamarron, Colorado in January, 1981.

- b) Meeting on "Diffuse Discharge Switches," in Lubbock, in September 1981.
- c) ARO Workshop on "Diffuse Discharge Opening Switches," at Tamarron, Colorado in January 1982
- d) NSF Supported, Joint US-FRG Seminar on "Externally Controlled Diffuse Discharges," at Bad Honnef, Germany, in August 1983.

These meetings were very successful, in that they helped to set the direction of research on diffuse discharge switches, not only at Texas Tech University, but in the USA in general. The group at Texas Tech University served as an organization center for several joint activities, especially in the field of the optical switch research.

## 7. References

1. R.O. Hunter, "Electron Beam Controlled Switching", Proc. 1st International Pulsed Power Conference, Lubbock, TX, 1976, Paper IC-8.
2. B.M. Kovalchuk, G.A. Mesyats, "Current Breaker with Space Discharge Controlled by Electron Beam", Proc. 1st IEEE International Pulsed Power Conference, Lubbock, TX, 1976, Paper IC-7.
3. S. Kassel, "Soviet Pulsed-Power Technology", Air Force Pulsed Power Lecture Series, Lecture #38, (1983), Coord: M. Kristiansen and A. Guenther.
4. K. Schoenbach, L. Hatfield, E. Kunhardt, "An Opening Switch Using a Divertor", First Annual Report on Coord. Research Program in Pulsed Power Physics, Dept. of Electrical Engineering, TTU, Lubbock, Tx, 1980, p. 158.
5. K.H. Schoenbach, M. Kristiansen, E.E. Kunhardt, L.L. Hatfield, and A.H. Guenther, "Exploratory Concepts of Opening Switches", Proc. ARO Workshop on Repetitive Opening Switches, Tamarron, CO, 1981, p. 65.

6. K.H. Schoenbach, G. Schaefer, E.E. Kunhardt, M. Kristiansen, L.L. Hatfield, and A.H. Guenther, "An Optically Controlled Diffuse Discharge Switch", Proc. 3rd IEEE Intern. Pulsed Power Conf., Albuquerque, NM, 1981, p. 142.
7. K.H. Schoenbach, G. Schaefer, M. Kristiansen, L.L. Hatfield, and A.H. Guenther, "Diffuse Discharge Opening Switches", Plenum Press, Series B, Physics, Vol. 89b, p. 415. (E. Kunhardt and L. Luessen, Editors).
8. K.H. Schoenbach, G. Schaefer, M. Kristiansen, L.L. Hatfield, and A.H. Guenther, "Optical Control of Diffuse Discharge Opening Switches", Proc. ARO Workshop on Diffuse Discharge Opening Switches, Tamarron, Co. 1982, p. 134.
9. K.H. Schoenbach, G. Schaefer, M. Kristiansen, L.L. Hatfield, and A.H. Guenther, "Concepts for Optical Control of Diffuse Discharge Opening Switches", IEEE Trans. Plasma Science, PS-10, 246 (1982).
10. L.C. Lee, C.C. Chiang, K.Y. Tanq, D.L. Huestis and D.C. Lorents, "Gaseous Electronics Kinetics for E-Beam Excitation of Cl, NO and N<sub>2</sub>O in N<sub>2</sub>", Molecular Physics Lab., SRI International, in Second Annual Report on Coord. Research Program in Pulsed Power Physics, Dept. of Electrical Engineering, TTU, Lubbock, Tx., 1982, p. 189.
11. G. Schaefer, K.H. Schoenbach, A.H. Guenther, and W.K. Pendleton, "Recent Advances in Optically Controlled Discharges", Proc. 4th IEEE Pulsed Power Conf., Albuquerque, NM, June 1983.
12. G. Schaefer, P.F. Williams, K.H. Schoenbach and J. Moseley, "Photodetachment as a Control Mechanism for Diffuse Discharge Switches," IEEE Trans. on Plasma Science, PS-11, 263, 1983.
13. G. Schaefer, K.H. Schoenbach, P. Tran, J.-S. Wang, and A.H. Guenther, "Computer Calculations of the Time Dependent Behavior of Diffuse Discharge Switches", Proc. 4th IEEE Pulsed Power Conf., Albuquerque, NM, June 1983.
14. G. Schaefer, K.H. Schoenbach, H. Krompholz, M. Kristiansen, and A.H. Guenther, "The Use of Attachers in Electron Beam Sustained Discharge Switches - Theoretical Consideration", submitted to Lasers and Particle Beams.
15. H. Haries, K.H. Schoenbach, G. Schaefer, H. Krompholz, and M. Kristiansen, "E-Beam Triode for Multiple Submicrosecond Pulse Operation", Proc. 4th IEEE Pulsed Power Conf., 1983, Albuquerque, NM.

SUMMARY OF WORK DURING THE LAST CONTRACT PERIOD  
(1982-83)

The program, during the last contract period had four projects devoted to closing switches, two to opening switches, and one to various exploratory concepts. Two additional projects, one on electron beam initiated triggering and one on electromechanical pulse generation (Projects No. 1 and 7) were completed earlier in the program and will not be discussed here.

Projects No. 3 and 4 were closely coordinated and primarily concerned with materials interactions in high power spark gaps. Substantial advances were made in understanding the material synergisms, the electrode erosion process, and the factors affecting the statistical distribution of self breakdown of the gaps. Various dielectric surface phenomena were also investigated in detail and a possible method for enhancing the voltage flashover strength for insulators in vacuum was discovered.

Projects No. 2 and 5 were likewise closely coordinated and primarily concerned with laser triggering phenomena in spark gaps and the development of new, optical diagnostic techniques. Substantial advances were made in understanding the important, initial, laser induced, breakdown processes and a rather detailed theoretical model was developed. This model is also important to the understanding of breakdown processes in general. The use of laser induced fluorescence diagnostic techniques also answered several questions related to metal vapor migration into the inter-electrode space.

In Project No. 6, we investigated several ideas. The main projects were surface discharge switching where the optimum conditions for switch triggering were determined and a system was developed for determining the time dependent arc resistance in a high power spark gap. Efforts were also initiated to improve field distortion triggering of spark gaps. Some initial investigations of solid state opening switches were also carried out in cooperation with Project No. 9.

Close cooperation was also maintained between Projects No. 8 and 9. Some of the main achievements include the development of a two-step computer simulation code which describes the important opening and closing phases of externally controlled switches. Several mechanisms for externally controlled discharges have been considered and two primary experimental facilities have been constructed along with several smaller ones. Cooperation has been established with other laboratories on other opening switch concepts.

## Project No. 2

Transient Processes in Laser-Triggered Breakdown

(R.A. Dougal, R. A Bieseke, D. Pease, and P.F. Williams)

## A. SUMMARY

The principal accomplishment during the contract period was the acquisition of a sizable body of experimental information concerning laser-triggering of breakdown in gas-filled gaps, and the development of a rather detailed model of laser-triggered breakdown based on this information. This model has important consequences for the design of laser-triggered spark gaps in that it suggests that the heating phase of the breakdown process plays an important role in determining the delay and jitter characteristics of the laser-triggered switch. This aspect of the breakdown cycle is not usually considered in previous treatments of the subject. The results of the experimental work also provides clear answers to several long-standing questions about the laser-triggering process in the fast triggering regime.

## B. ACCOMPLISHMENTS

The results of work carried out during the 1980-82 contract periods left us with a good, solidly-based qualitative understanding of laser-triggered breakdown in the fast, low-jitter

triggering regime [1]. Work carried out during the most recent contract period under this project has centered on improving this understanding both through obtaining more quantitative information and through carrying out corroborative experiments to verify or expand on certain key points. These efforts have been generally successful, and on this basis we have developed a rather detailed, experimentally-based model of laser-triggered breakdown.

Our work provides a solid, experimental basis for the streamer breakdown mechanism first suggested by Pendleton and Guenther [2]. We also find clear, unambiguous evidence for the interaction between the laser and the propagating streamer. Our model, along with the results of the numerical work discussed under Project No. 5, provides an answer for the long-standing question of why better triggering is observed with a positive struck electrode than with a negative none. We have also found evidence for the importance of the heating phase of breakdown in determining the delay and jitter in laser-triggered switching. Thus the switch closure characteristics depend not only on the propagation speed of the streamer, but also on the ionization left in its trail since this ionization provides an initial condition for the final heating phase. Finally, our model suggests that an additional, unexpected benefit of laser-triggering in the longitudinal geometry is the initial limitation of the incipient breakdown channel to a diameter determined by the dimensions of the focused laser beam. This limitation reduces the heating requirements for forming the initial spark

channel, and probably contributes to the very sharp turn-on characteristic of laser-triggered switches.

The results of our work, including a detailed description of our model and the experimental basis for it are described in a paper which has been submitted for publication to the Journal of Physics D: Applied Physics, and is attached as an appendix. Since this paper is intended to be a complete description of our work, there will be no further discussion here of these subjects.

#### C. REFERENCES

- [1] P. F. Williams, et. al., "Transient Processes in Laser-Triggered Breakdown," pp. 7-19, Third Annual Report on Coordinated Research Program in Pulsed Power Physics, AFOSR Contract No. F49620-79-C-0191 (1982).
- [2] W. K. Pendleton and A. H. Guenther, "Investigation of a Laser-Triggered Spark Gap," Rev. Sci. Instr. 36, 1546 (1965).



APPENDIX I

FUNDAMENTAL PROCESSES IN LASER-TRIGGERED  
ELECTRICAL BREAKDOWN OF GASES\*

R.A. Dougal<sup>†</sup>  
Department of Electrical Engineering  
Texas Tech University  
Lubbock, Texas 79409, U.S.A.

and

P.F. Williams  
Departments of Electrical Engineering and Physics  
Texas Tech University  
Lubbock, Texas 79409, U.S.A.

## ABSTRACT

We describe the results of an experimental study of the physical mechanisms important for laser triggering of spark gaps in the longitudinal, striking-electrode geometry. We present clear, new evidence for the propagation of a streamer in undervolted gaps, and for the interaction of the triggering laser with the streamer head. We find that the propagation conditions of the initial streamer markedly affect the subsequent heating of the incipient channel to form the spark. A model of the laser-triggered breakdown process based on these results is presented and discussed.

\*Preprint of article submitted to J. Phys. D: Appl. Phys.

\*Work sponsored by AFOSR.

<sup>†</sup>Present Address: Department of Electrical and Computer Engineering, University of South Carolina, Columbia, S.C. 29208, U.S.A.

## FUNDAMENTAL PROCESSES IN LASER TRIGGERED ELECTRICAL BREAKDOWN OF GASES

R.A. Dougal and P.F. Williams

### A. Introduction

Since Pendleton and Guenther (1965) first reported laser triggering of spark gap switches considerable work has been carried out to delineate the capabilities and limits of the triggering method (Guenther and Bettis 1978). From this work it has become apparent that several different techniques can be used to laser-trigger spark gaps, and that for each technique there are, depending on operating parameters, several modes of operation in which different physical mechanisms are important. In the work described here, we were primarily interested in studying the fundamental, physical mechanisms important for laser-triggering of spark gaps in the geometry of Fig. 1 for which the laser beam is parallel to the gap axis, and strikes an electrode. As a result of this work we now have a good, physically-based understanding of laser-triggered breakdown in this mode. The work also impacts understanding of conventional, over-volted breakdown in that it allows study of the basic processes under an unconventional set of experimental constraints.

In this geometry it is found experimentally that several modes of operation exist, depending on gap voltage and spacing, fill gas

composition and pressure, and laser power and focussing. The experiments we report here were conducted in  $N_2$  at 800 Torr with the laser focussed on or near one electrode, and with the minimum laser energy ( $\sim 10$  mJ.) necessary for low delay ( $< 10$  ns.), low jitter triggering. Several workers have presented theories for the laser triggering of breakdown in this mode. Guenther and Bettis (1967), largely on the basis of triggering delay studies, have suggested that the triggering laser pulse initiates an electron avalanche which grows until it reaches a critical size and becomes a streamer which rapidly bridges the gap, causing closure. From their results, they further suggested that in a range of conditions, the laser interacted with the streamer, preparing a path for it to follow and speeding its propagation. Deutsch (1968); Horii et. al. (1970); and Dewhurst, Pert, and Ramsden (1972); have suggested similar models. Lindner, et. al. (1975) have proposed an alternative mechanism for breakdown in which closure is due to the expansion of a conducting metal vapor plasma from the struck electrode into the gap.

We have obtained for the first time, clear experimental evidence for the streamer mechanism of Guenther and Bettis (1967), although we find that the laser produces sufficient free charge in the fireball that the avalanche growth stage is bypassed, and a streamer is initiated immediately. We also find very clear evidence for the interaction, first suggested by these authors, of the laser with the propagating streamer head. Besides speeding the streamer propagation, this interaction probably limits the diameter

of the incipient spark channel, reducing the heating requirements for ionization and gap closure, and thereby improving switch rise time.

Based on our experiments, we propose the following model of laser-triggered breakdown in the longitudinal, striking electrode geometry and in the fast triggering mode. The focussed incident laser rapidly heats the surface of the struck electrode, explosively evaporating electrode material which is then further heated and serves as a seed for heating of the fill gas, probably through an inverse bremsstrahlung, cascade ionization process (Zel'Dovitch and Raizer 1964, DeMichelis 1969, Ostrovskaya and Zaidel 1973, Morgan 1975, Raizer 1979). The result is a small protrusion of relatively dense plasma on the electrode surface which then shields itself from the applied field, thereby setting up a region of enhanced field at the tip. Electrons in this enhanced field region experience very high ionization rates and rapidly extend the protrusion into the gap as a streamer. In regions of high laser intensity, the velocity of the streamer is enhanced by interaction with the laser. This interaction may take the form of a direct ionization rate enhancement due to inverse bremsstrahlung heating near the streamer head, or an indirect rate enhancement due to vibrational or electronic excitation of the gas in front of the streamer. Of particular importance for cathode-directed streamers, the laser may also provide seed electrons in front of the streamer head.

At some point the laser-streamer interaction will cease, ei-

ther because the laser pulse ended or because the streamer reached the vicinity of the opposite electrode and was forced to branch away from the laser path in order to strike the electrode. We present evidence that the residual ionization left in the wake of the streamer is markedly different in the two (laser-assisted and non-assisted) regions. After the streamer has crossed, the gap is bridged by a thin, weakly conducting filament which is rapidly heated through ohmic heating. Due to this heating the gap current rises rapidly until a spark forms, closing the switch. Since the laser interaction limits the diameter of the streamer, the energy required to accomplish this heating can be considerably smaller than with conventionally triggered breakdown. Thus an additional effect of the laser-streamer interaction may be an improved switch rise time. Our model is supported by the results of several experiments we have conducted, and we will discuss the several aspects of the model separately.

#### B. Experimental Apparatus

A schematic diagram of the experimental setup for streak photography experiments is shown in Fig. 2. All laser-triggered breakdown experiments were conducted with the high vacuum cell shown in Fig. 3. The cell was designed to provide a clean, reproducible environment, and was constructed from a specially modified Varian cross with Conflat flanges. The electrodes are insulated

electrically from the cell with Corning Macor ceramic insulators, and o-rings are used for the ceramic-metal vacuum seal. The upper electrode is hollow and has an o-ring sealed quartz window at the bottom to allow longitudinal access for the triggering laser beam. The electrodes were machined to an approximately constant field profile, and the gap separation was 5 mm. The cell may be pumped out to a vacuum of  $< 1 \times 10^{-5}$  Torr with a cryogenic sorption pump and an ion pump, and then back filled. In all experiments reported here the cell was operated with 800 Torr of purified nitrogen. Pressure was measured with a digital guage.

The cell was designed to appear as a section of  $50\Omega$  transmission line to minimize reflections and provide a clean electrical diagnostic signal. The load resistor was composed of a number of 2 watt carbon composition resistors, chosen according to the specifications given by Martin, connected in series-parallel, and arranged in a radially symmetric manner. Gap current was measured by using a resistive voltage divider and a Tektronix Model 7834 storage oscilloscope with a specified rise time of 1.9 ns to monitor the load voltage. Voltage was applied to the cell through a length of RG-8/U coaxial cable charged by a regulated power supply in series with a large charging resistor. With properly matched load resistor the system produced a clean, rectangular current pulse when laser triggered. Fig. 4 shows a typical current oscillogram obtained with this apparatus.

The principal optical diagnostics used include time-resolved

spectroscopy and streak photography. The spectroscopy studies were carried out with the aid of a computer-controlled, reticon-based, optical multichannel analyzer system. Time resolution to 5 ns was possible with the system. The multichannel analyzer detector head was used in conjunction with a 0.5 m spectrograph to provide spectral dispersion.

Streak photography was accomplished with the use of a Hamamatsu Model C979 Temporal Dispenser, a microchannel plate intensified unit with intensifier gain of up to 3000. For all streak photographs shown here the input slit width was 100  $\mu$ . Images were either recorded directly onto 35 mm film, or recorded with a SIT vidicon and displayed on a video monitor with the aid of the Hamamatsu Model C1330 Temporal Analyzer. The Temporal Analyzer provided a real-time video readout and could digitize and store the image, although with decreased spatial resolution. With the weakest images there was insufficient light to expose the film, and it was necessary to digitize and store the image and then photograph the video monitor to obtain a hard copy.

At the highest gain settings the sensitivity of the system was sufficient that single electron emission from the streak tube photocathode was easily detectable. Although the gain of the system was quite high, it had limited rejection capability for intense, but out-of-time-frame emission, due probably to scattering in the electron optics of the streak tube. To improve this rejection capability a specially modified camera was used which allowed the

tube to be electronically gated off at the end of the sweep. This gating improved the rejection capability by several orders of magnitude in favorable cases, but it resulted in considerable image distortion just before the gating occurred. To further enhance the rejection of the system, and to provide information about the processes being observed, a spectral bandpass filter was in many cases used before the streak camera. Both narrow band interference filters and a monochromator were used for this purpose. Further discrimination against the intense emission from the spark was obtained on some occasions by using a short charging cable in order to limit the length of the current pulse.

The laser system used for triggering was a Quanta-Ray Model DCR-1A Nd:YAG laser which produced up to 800 mJ of 1.06 $\mu$  energy in an approximately 15 ns pulse. The temporal waveform of the pulse showed considerable mode beating with structure on the 1 ns time scale. When focussed with a simple spherical lens, there were also several hot spots in the focal region of the beam. Since only 10-20 mJ was typically needed, experiments were often run using a beam splitter to pick off about 10% of the output from the laser oscillator stage only.

### C. Results

The model of laser-triggered breakdown described in Section A



is supported by the results of a large number of experiments we have conducted. All experiments we discuss here were carried out with a fill gas of purified nitrogen at a pressure of 800 Torr and in the longitudinal, striking-electrode geometry. The results of experiments carried out in other geometries will be described in a forthcoming paper. In this section we discuss the results pertinent to the several aspects of the triggering model separately.

### 1. Initial Fireball Formation

A streak photograph showing the formation of the plasma fireball is shown in Fig. 5a. The luminous fireball expands initially at a speed of  $\sim 2 \times 10^7$  cm/sec. Since a metal atom with this speed would have kinetic energy of about  $10^4$  eV, the plasma likely is composed of excited fill gas atoms or molecules, and not metal vapor. Spectroscopy of the fireball showed there was a strong continuum component to the fireball emission during the rapid expansion phase, indicating a high degree of ionization in the fireball. During this time there was no indication of metal vapor line emission from the fireball away from the electrode surface, although the strong continuum emission could easily mask weaker line emission.

Further evidence that the fireball expansion results from laser heating of the fill gas at a moving interface rather than physical motion of an excited species is seen in Fig 5b. In this photograph, as discussed in the next section, the laser interacted

with the incipient spark channel, forming a hot spot about 1.7 mm above the struck electrode. This hot spot is not transparent to the laser, and the expansion of the primary plasma fireball is halted upon the appearance of the hot spot. The streak photo in Fig. 5c shows the formation of two secondary hot spot plasmas due to the laser interaction. These phenomena were quite repeatable.

## 2. Streamer Propagation

In conventional over-volted breakdown, the process is initiated by one or a few electrons (Llewellyn-Jones 1983). In order for a streamer to form, this initial charge density must be amplified through avalanching to some "critical" density, at which point the space charge resulting from shielding effects becomes large enough to modify the electric field locally. With laser-triggered breakdown, however, the focussed laser creates a plasma fireball on the surface of the struck electrode sufficiently dense to support streamer propagation. These streamers propagate rapidly across the gap and are responsible for the very fast breakdown of under-volted, laser-triggered gaps.

The results of several experiments provide evidence for the existence of these streamers. Of these, the most direct evidence is from high sensitivity streak photographs such as shown in Fig. 6 of the early stages of the breakdown event. Here the emission from most of the plasma fireball was blocked by a mask at the streak camera entrance slit to avoid swamping the electron optics. In

these photographs a weak luminous front is clearly seen propagating outwards from the struck electrode with an initial velocity of  $1-2 \times 10^8$  cm/sec, slowing to  $1-2 \times 10^7$  cm/sec. The front was consistently present in all streak photos taken under similar conditions, although there was considerable shot-to-shot variation in the front shape, probably reflecting variations in laser pulse intensity. We associate this front with the propagation of a streamer across the gap. In many shots the speed of the front decreased as it traversed the gap. This behavior is contrary to that of streamers observed in conventional over-volted breakdown (Timm 1973, Bayle et. al. 1975) and to expectations based on considerations of the increased field resulting from dropping the gap voltage across a decreasing distance. We believe these speed variations to result from laser enhancement of the streamer propagation. Enhancement is greatest near the struck electrode where the intensity of the focussed laser is largest, and decreases away from the focus. Depending on the streamer resistivity and other factors, this decreased enhancement may be partially offset by the increased field due to the "shorting out" effect discussed above.

Evidence linking these luminescence fronts with space-charge effects comes from the results of experiments we carried out using an electrode with a small well machined in the center as shown in Fig. 7. If the triggering laser is focussed on the bottom of the well, the plasma fireball thus formed will not initially feel the applied electric field and a streamer will not form, but in other respects the situation is very similar to that without the well.

Only after the expanding fireball has reached the top of the well where it experiences the applied field does a streamer form and breakdown occur.

These effects are seen clearly in the streak photographs and current traces we obtained for this case. Fig. 8 shows a typical current trace obtained under these conditions, and Figs. 9 and 10 show streak photographs. To illustrate the timing, the oscillogram in Fig. 8 was obtained by displaying the sum of signals proportional to the gap current and to the laser intensity as measured with a fast photodiode. On this scale there is no measurable gap current during the laser pulse. About 40 ns after the laser pulse significant gap current begins to flow and breakdown occurs in two steps similarly to overvolted breakdown.

In the streak photograph shown in Fig. 9, a weak luminous front is observed starting from the struck electrode about 25 ns after the laser trigger pulse. This time corresponds to the time required for the luminous fireball to expand a distance equal to the well depth. We believe that the luminous front results from a streamer traversing the gap. Due to the 25 ns delay, the laser is no longer on during the traversal time, and the streamer propagates without laser assistance. The streak photo in Fig. 9 was obtained using very high sensitivity, and a short charging cable to minimize the time-integrated light intensity. The photo shown in Fig. 10 was obtained with lower sensitivity, but with a 1  $\mu$ sec cable, in order to investigate the later stages of breakdown. After the

luminous front has crossed the gap, breakdown occurs in a manner very similar to that observed with weakly over-volted gaps.

### 3. Laser-Plasma Interaction

Our streak photographs provide very clear, unambiguous evidence for the strong interaction between the laser radiation and the incipient spark channel. In the streak photographs of Fig. 5 the laser was focussed slightly above the struck electrode. In Fig. 5a the applied voltage was below the threshold for laser triggering, in Fig. 5b a higher voltage, above triggering threshold, was applied, and a still higher voltage, near self breakdown, was applied in Fig. 5c. With voltage below threshold the primary plasma fireball expands smoothly under the intense laser radiation. Above threshold, the laser interacts with the propagating streamer, forming a secondary plasma hot spot at the focus of the lens. Farther above threshold, this hot spot forms sooner, and shortly thereafter a second hot spot forms farther up-beam. The laser intensity in the focal region of the lens is known to be highly inhomogeneous due to lens aberrations (Evans and Morgan 1969) and to the poor mode quality of the laser beam. Presumably this second hot spot forms at such a local maximum.

As discussed above, the cessation of growth of the primary plasma fireball upon the appearance of a secondary hot spot plasma clearly demonstrates that the hot spot plasmas are effectively opaque to the laser radiation and that the growth of the primary

plasma is the result of laser heating of the fill gas, and not of motion of excited species outwards from the struck electrode. Further, the appearance of the hot spot plasmas only when a voltage above threshold for triggering is applied unambiguously demonstrates that the laser interacts with some product of the initial breakdown process. Most likely, the interaction is with the electrons, and occurs as a result of an inverse bremsstrahlung, cascade ionization process.

#### 4. Channel Heating

After the streamer has traversed the gap there is a thin bridge of weakly conducting ionization left in its path. At this point the gap voltage has not yet collapsed, and energy is deposited into the incipient channel due to the resulting current flow. Because of this energy deposition the ionization of the channel increases, allowing more current to flow and increasing the rate of energy deposition. This recursive process continues until sufficient conductivity has been attained in the gap that the voltage collapses. We refer to this phase of breakdown as the heating phase, even though the existence of any type of thermodynamic equilibrium in the early stages of the phase is debatable.

Effects of this heating phase are clearly seen in streak photographs such as shown in Fig. 11. After the streamer has traversed the gap a diffuse glow appears in front of the electrode opposite the struck electrode. A few nanoseconds later, coincident

with the abrupt current increase, intense emission appears nearly simultaneously everywhere along the incipient channel except for this region of the diffuse glow. Finally this last dark region is breached by two luminous fronts advancing from each end. Spatially and temporally resolved spectroscopy shows, consistent with the findings of others (Stritzke et. al. 1977), that the emission from the streamer and the diffuse glow is molecular in origin, whereas the final, intense emission signalling spark channel formation is atomic or ionic in origin with a strong continuum component.

We may make use of these results to obtain information about the dynamics of the heating process. From the predominance of molecular emission during both the streamer and the diffuse glow phase, we conclude that there is not strong transfer of energy to the molecules during these periods. Further, the rotational bands of the C $\rightarrow$ B emission can be clearly distinguished in spectra of the diffuse glow, and a simple analysis of these bands shows that the rotational temperature is of the order of 300 K. Additionally, the vibrational lines observed in these spectra are predominantly from transitions with upper vibrational levels with low quantum number (mostly  $v'=0$  and  $v'=1$ ), implying only minimal vibrational heating of the gas as well. In contrast, if the electron density is  $10^{13}$  cm $^{-3}$ , equilibrium thermodynamics would predict a temperature of 8400 K. It is clear, therefore, that during the diffuse glow stage the free electrons are essentially decoupled from the rotational and vibrational modes of the molecules for the time scale of interest.

As the atomic, ionic, and continuum emission intensity in the incipient channel begins to appear the intensity of the molecular emission decreases, probably reflecting the rapid dissociation of the  $N_2$  molecules. The sudden appearance of the continuum emission implies a rapid thermalization of the electronic system in the incipient channel. Aside from the apparent substantial dissociation of the  $N_2$  molecules, spectroscopy provides little information concerning the degree of thermalization of the translational motions during the final stages of spark channel formation. In laser shadowgraphy experiments we see a very sharp and well defined shock wave formed coincident with the spark channel formation, but this shock could be the result of the molecular dissociation, rather than a true kinetic temperature increase.

Of specific interest is the reason for the appearance of the diffuse glow in front of the entrance electrode and for the subsequent anomalous behavior of the region. We believe these effects to be the result of differing residual ionization left in the path of the streamer, depending on whether or not the streamer was laser-assisted when it traversed the region. As the streamer propagates toward the entrance electrode, it must, because of the laser entrance hole, at some point depart from the gap axis in order to strike the electrode. At this time the laser interaction with the propagating head will cease, and the streamer propagation will be modified. Of course, if the streamer is delayed or propagates slowly, the laser pulse will turn off before the streamer reaches this point, and the anomalous region will extend farther



away from the entrance electrode. In either case, the residual ionization left in the path of the streamer will be different in the two regions (laser-assisted and non-assisted).

Figs. 12 and 13 show experimental evidence for this model. The figures show streak photographs of the breakdown for positive and negative struck electrode respectively, and for several different gap charging voltages, but otherwise identical conditions. It is evident that the length of the anomalous region increases with decreasing charging voltage. This effect is documented in Fig. 14 where the length of the luminous region displaying abrupt, uniform turn-on is plotted as a function of voltage. Also plotted in these figures is the corresponding delay to breakdown. It is clear that the length of the luminous region remains roughly constant over a range of voltages, but starts to decrease below about 80% of self breakdown. This behavior is qualitatively predicted by our model. For positive struck electrode and voltages above ~80% of self breakdown the laser-assisted streamer propagates rapidly enough to reach the vicinity of the entrance electrode while the laser is still on. Thus the length of the anomalous region is determined by the requirement that the streamer deviate from the gap axis in order to strike the electrode, and is therefore independent of charging voltage. For voltages below this value, the streamer has not traversed the gap when the laser pulse shuts off, and the length of the anomalous region is determined by how far the streamer had gotten before laser shut-off.

Deutsch reported similar behavior in experiments in which the variation in the laser-triggered spark was studied as a function of charging voltage and laser power. He found that there was a clear break in the spark channel, which he interpreted as implying a difference in initiating conditions for the channel on either side of the break. Further, he found that the position of the break moved away from the struck electrode as the gap charging voltage was increased, or the laser power increased.

Our delay data are also consistent with our model. In these experiments the laser pulse duration was  $\sim 15$  ns, and we see that the delay increases sharply at the point where the knee occurs in the length data. At this point the delay has increased to 20 ns. Bettis and Guenther (1970) report similar findings in that they observe that the delay as a function of charging voltage rises steeply for voltages below that which causes a delay roughly equal to the laser pulse width. This behavior is expected in a case where the propagation of laser-assisted streamers is substantially different than that of non-assisted streamers.

Additional support is provided by the results obtained with a recessed struck electrode as discussed in section C.2. A very similar structure consisting of a diffuse glow bridging the entire gap, followed by a V-shaped, brightly luminous region is observed in the streak photographs obtained with recessed electrode triggering, and from the timing it is known that in this case the streamer traverses the gap without laser assistance. Furthermore, similar

structures are observed in streak photographs of conventional over-volted breakdown in  $N_2$  (Doran 1968). The similarity of observed structures in the three cases is strongly suggestive of similar initiating processes, and supports the contention that the two distinct regions seen in the streak photos of Fig. 11 are the result of differences in the degree of laser interaction with the propagating streamer.

#### D. Conclusion

Through the use of sensitive, high speed streak photography and other optical diagnostics we have obtained for the first time direct evidence for the importance of a streamer mechanism in the initiation of breakdown in laser-triggered,  $N_2$ -filled spark gaps, and for the interaction of the laser with these propagating streamers. All work reported here was obtained in the longitudinal, striking-electrode triggering geometry, and in the fast triggering mode. Similiar, although less complete, studies have been carried out in other triggering geometries, and the results of these studies will be described in a forthcoming paper. Our work is aimed at understanding the laser-triggering of electrical breakdown in gases, but it additionally impacts understanding of conventional over-volted breakdown in that we are able to investigate the same physical phenomena under a different set of experimental constraints.

In order to understand quantitatively the breakdown process under these conditions, more theoretical work is needed. Of particular importance, and difficulty, is the quantitative understanding of the space-charge-controlled transport occurring in the streamer head. Analytic calculations describing these phenomena have proven quite difficult due to the non-linearity and the two-dimensional (at least) nature of the governing equations (Turcotte and Ong 1968, Albright and Tidman 1972, Klingbeil, et. al. 1972). The results of numerical solutions of these equations have been reported (Yoshida and Tagashira 1976, Davies et. al. 1977), but the algorithms used generally had difficulty dealing with the extremely sharp density gradients which develop in streamer heads. We are currently using a different algorithm, based on flux-corrected-transport (Boris and Book 1973, Zalesak 1979), which is specifically designed to deal with these steep gradients, to carry out numerical simulation of space-charge-controlled transport.

We thank A.H. Guenther, M.A. Gundersen, R.L. Redington, and K. Schoenbach for helpful discussions. The support of the Air Force Office of Scientific Research, and, in the early stages of the work, of the Research Corporation is gratefully acknowledged.

## REFERENCES

- Albright N W and Tidman D A 1972 Phys. of Fluids 15 86-90
- Bayle M, Bayle P, and Crokaert M 1975 J. Phys. D: Appl. Phys. 8 2181-2189
- Boris J P and Book D L 1979 J. Comput. Phys. 11 38-69
- DeMichelis C 1969 IEEE J. Quant. Elect. QE-5 188-202
- Deutsch F 1968 J. Phys. D: Appl. Phys. 1 1711-1719
- Dewhurst R J, Pert G J, and Ramsden S A 1972 J. Phys. D: Appl. Phys. 5 97-103
- Davies A J, Evans C J, Townsend P, and Woodison P M 1977 Proc. IEE 124 179-182
- Doran A A 1968 Z. Physik 208 427-440
- Evans L R and Morgan C G. 1969 Phys. Rev. Lett. 22 1099-1102
- Guenther A H and Bettis J R 1967 IEEE J. Quant. Elect. QE-3 581-588
- Guenther A H and Bettis J R 1978 J. Phys. D: Appl. Phys. 11 1577-1613
- Horii K, Noguchi T, and Yano M 1970 IEE Int. Conf. on Gas Discharges: IEE Conf. Publ. No. 90 pp 6-10
- Klingbeil R, Tidman D A, and Fernsler R F 1972 Phys. of Fluids 15 1969-1973
- Lindner F W, Rudolph W, Brumme G, and Fischer G 1975 Appl. Optics 14 2225-2228
- Llewellyn-Jones F 1983 "The Development of Theories of the Electrical Breakdown of Gases," in Electrical Breakdown and Discharges in Gases, Part A, ed. by E E Kunhardt and L H Leussen (Plenum, New York) pp 1-72
- Martin T H, "Effects of High Voltage Pulses on Various Resistors," Private Communication
- Morgan C G 1975 Rep. Prog. Phys. 38 621-665
- Ostrovskaya G V and Zaidel A N 1973 Usp. Fiz. Nauk 111 579-615 [Sov. Phys. Usp. 16 834-855]
- Pendleton W K and Guenther A H 1965 Rev. Sci. Inst. 36 1546-1550

Raizer Y P 1979 Journal de Physique 40 C7 141-147

Stritzke P, Sander I, and Raether H 1977 J. Phys. D: Appl. Phys. 10 2285-2300

Timm U 1973 J. Phys D: Appl. Phys. 6 1891-1898

Turcotte D L and Ong R S B 1968 J. Plasma Phys. 2 145-155

Yoshida K and Tagashira H 1976 J. Phys. D: Appl. Phys. 9 485-490

Zalesak S T 1979 J. Comput. Phys. 31 335-362

Zel'Dovitch Y B and Raizer Y P 1964 J. Exptl Theoret. Phys. (USSR) 47 1150-1161 [Sov. Phys. JETP 20 772-780]

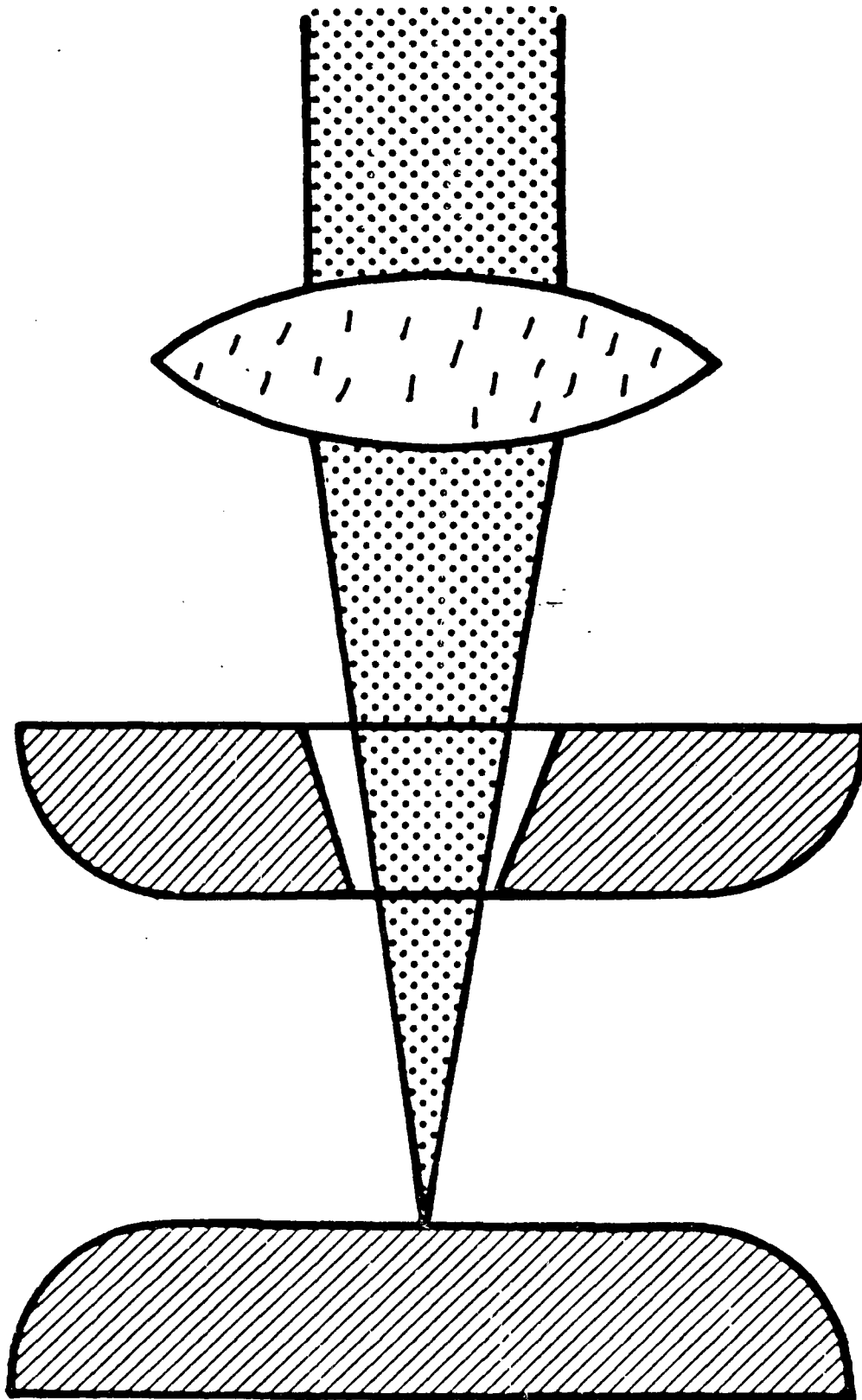
## FIGURE CAPTIONS

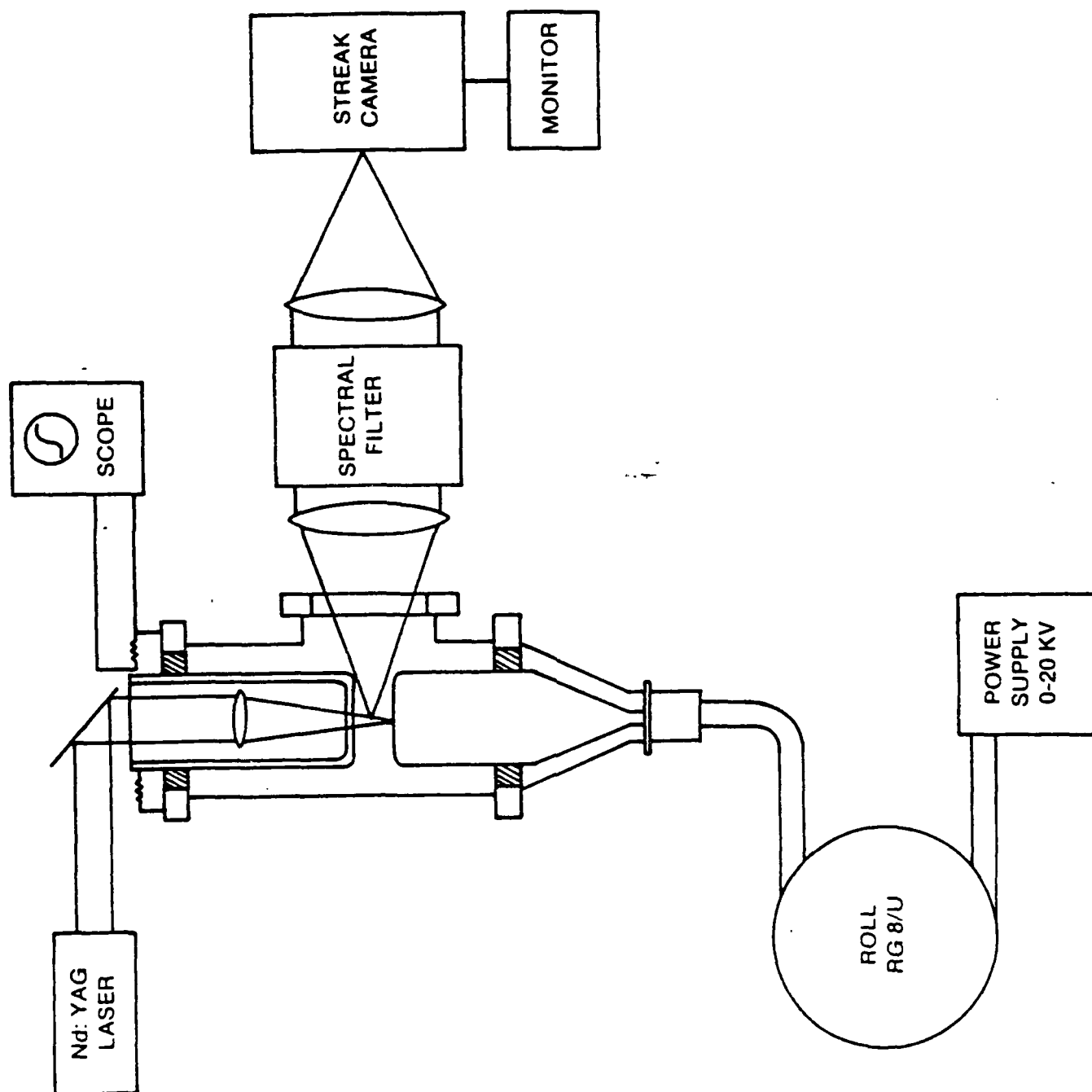
1. Schematic diagram of the longitudinal, striking-electrode triggering configuration used in most experiments reported in this paper.
2. Schematic diagram of the apparatus used for obtaining streak photographs of laser-triggered breakdown.
3. Schematic diagram of the cell used to contain the spark gap for laser-triggered breakdown experiments.
4. Oscillogram showing the gap current observed in experiments with laser-triggered breakdown in the longitudinal, striking-electrode geometry of Fig. 1. The horizontal scale is 10 ns/div and the vertical is 30 amps/div. Experimental conditions were: 800 Torr  $N_2$ ; 98% SBV; 10 mJ, 1.06  $\mu$ , 15 ns laser; 100 m, 1  $\mu$ s discharge cable; brass electrodes, 5 mm gap spacing.
5. Digitized streak photographs showing the formation of the plasma fireball produced by the triggering laser as it impinges on the struck electrode. The black islands centered in regions of high intensity are artifacts resulting from overloading the digitizer. Experimental conditions were: 800 Torr  $N_2$ ; 100 mJ, 1.06  $\mu$ , 15 ns laser; brass electrodes, 5 mm gap spacing. Charging voltages were: a) 54%; b) 81%; c) 98% of static breakdown voltage (SBV). The charging voltage in a) was below the triggering threshold.
6. Very high sensitivity, digitized streak photograph showing the early stages of the laser-triggered breakdown process. We identify the weak luminous front as being due to the passage of a streamer. Experimental conditions were: 800 Torr  $N_2$ ; 97% SBV; 10 mJ, 1.06  $\mu$ , 15 ns laser; stainless steel electrodes, 5 mm gap spacing; 30 cm discharge cable.
7. Schematic diagram showing the recessed electrode configuration used in the experiments discussed in the text.
8. Oscillogram showing the gap current observed in the recessed-electrode triggering geometry. For timing purposes, the trace shows the sum of the current from a high-speed photodiode monitoring the laser intensity, and the gap current. The first feature is due to the photodiode signal, and the plateau-like feature occurring later is due to the gap current. A second current rise starting about 90 ns after the peak of the laser intensity is visible, but somewhat attenuated due to non-linear behavior of the load resistor in this shot. The horizontal scale is 20 ns/div, and for the gap current the vertical is 50 amp/div. Experimental conditions were: 800 Torr  $N_2$ ;

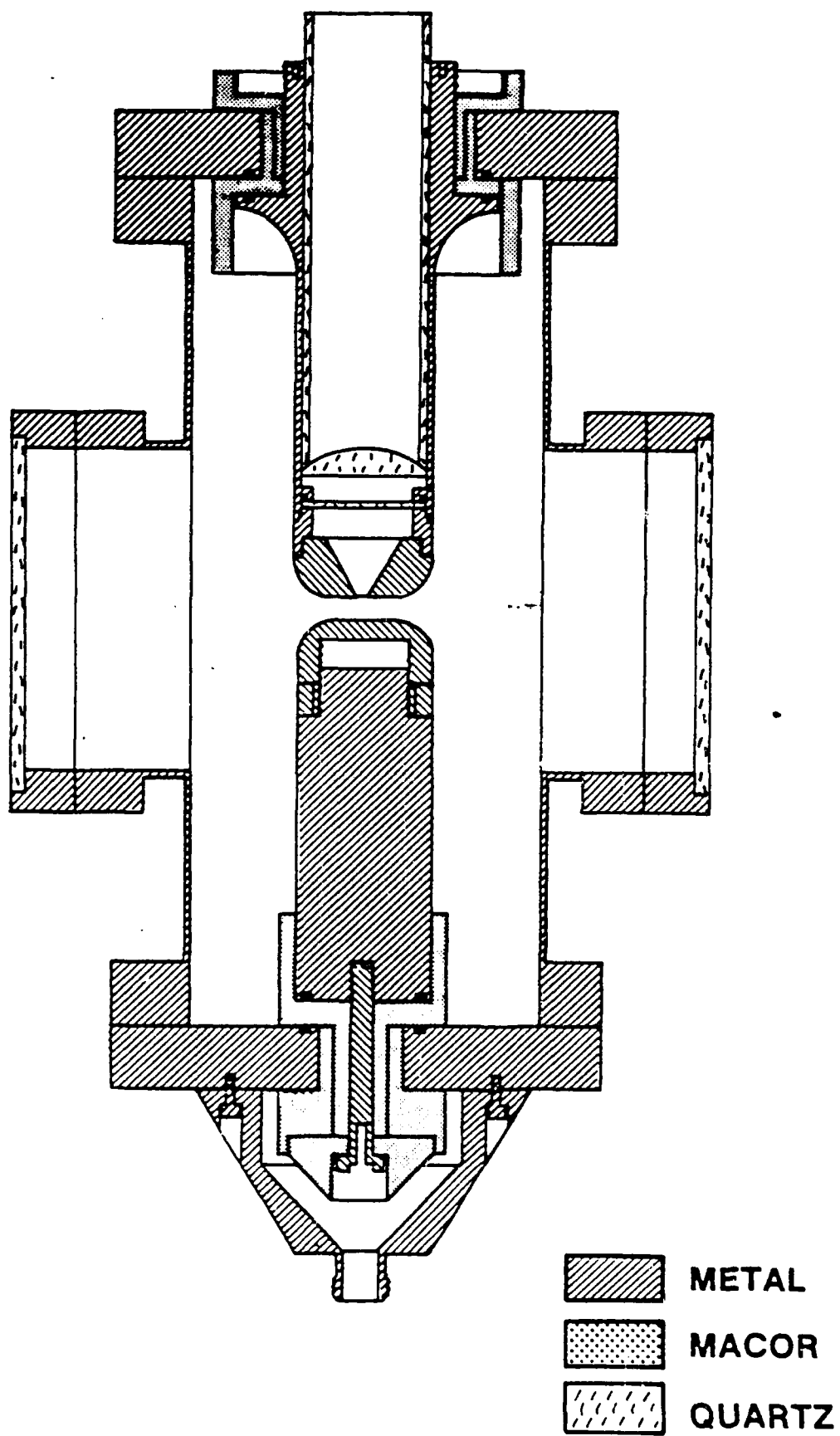
97% SBV; 10 mJ, 1.06  $\mu$ , 15 ns laser; stainless steel electrodes, 5 mm gap spacing.

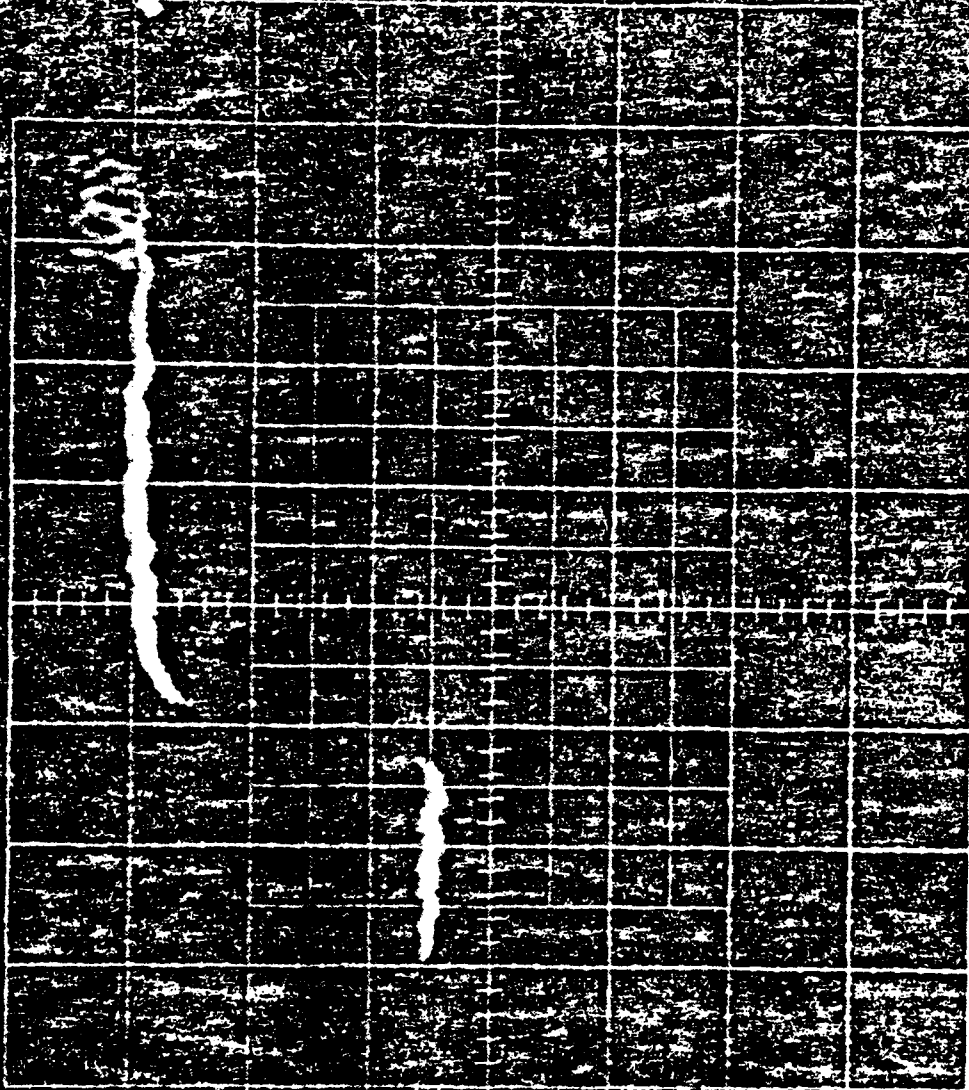
9. Very high sensitivity, digitized streak photograph showing the propagation of a streamer front for the recessed-electrode triggering geometry. The nearly-vertical white streak in the lower left corner of the photo is an artifact due to a reflection from the face of the video monitor. Experimental conditions were: 800 Torr  $N_2$ ; 95% SBV; 15 mJ, 1.06  $\mu$ , 15 ns laser; 30 cm charging cable; stainless steel electrodes, 5 mm gap spacing.
10. Streak photograph showing the longer term development of the breakdown with the recessed electrode geometry. The streak camera sensitivity was less than that used in Fig. 9 by a factor of approximately 1000. Experimental conditions were: 800 Torr  $N_2$ ; 95% SBV; 15 mJ, 1.06  $\mu$ , 15 ns laser; 100 m, 1  $\mu$ s discharge cable; stainless steel electrodes, 5 mm gap spacing.
11. Streak photograph showing the later stages of laser-triggered breakdown. The camera sensitivity is less than that used for Fig. 6 by a factor of approximately 1000. Experimental conditions were: 800 Torr  $N_2$ ; 20 mJ, 1.06  $\mu$ , 15 ns laser; 100m, 1  $\mu$ s discharge cable; stainless steel electrodes, 5 mm gap spacing.
12. Streak photographs of the later stages of laser-triggered breakdown for a positively charged struck electrode and several applied voltages. A wide (2 mm) entrance slit was used on the streak camera to reduce interpretational problems introduced by a non-vertical or crooked discharge channel. The constriction seen in the last 10 ns is an artifact produced by the application of a gating pulse to the streak tube in order to discriminate against the intense spark channel emission. Experimental conditions were: 800 Torr  $N_2$ ; 9 mJ, 1.06  $\mu$ , 15 ns laser; 100 m, 1  $\mu$ s charging cable; stainless steel electrodes, 5 mm gap spacing. Charging voltages were: a) 99%; b) 92%; c) 86%; d) 79%; e) 72%; f) 66% of static breakdown voltage.
13. Streak photographs of the later stages of laser-triggered breakdown for a negatively charged struck electrode and several applied voltages. Experimental conditions and charging voltage sequence were the same as used in Fig. 11.
14. Plots of the length of the luminous region displaying abrupt turn-on, and the delay to closure, as obtained from Figs. 12 and 13, as a function of applied voltage for: a) positive struck electrode; b) negative struck electrode.









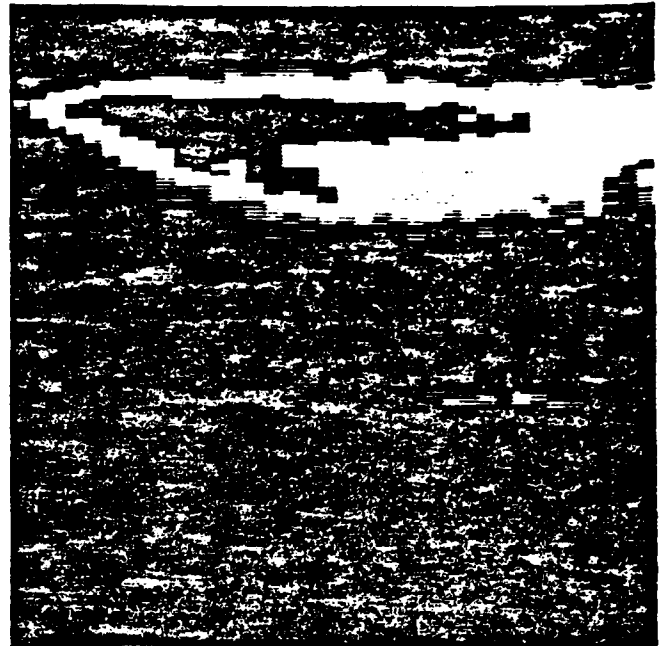


a)



5ns

b)

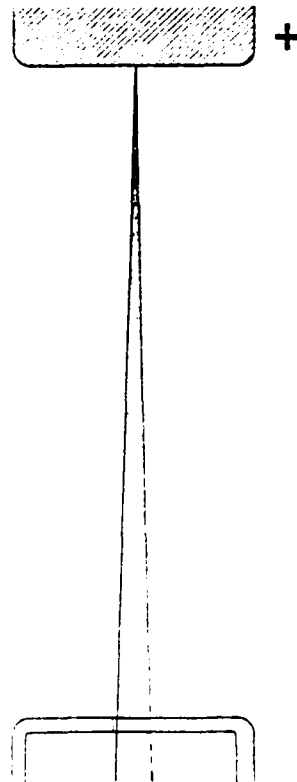


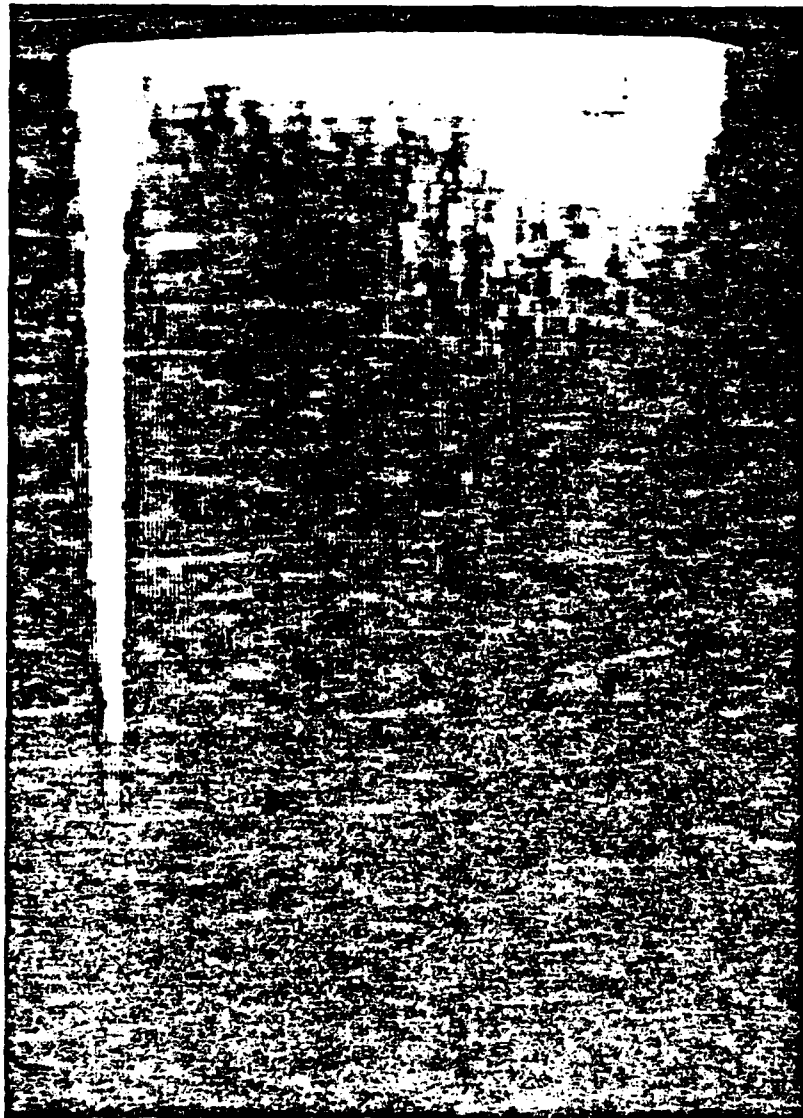
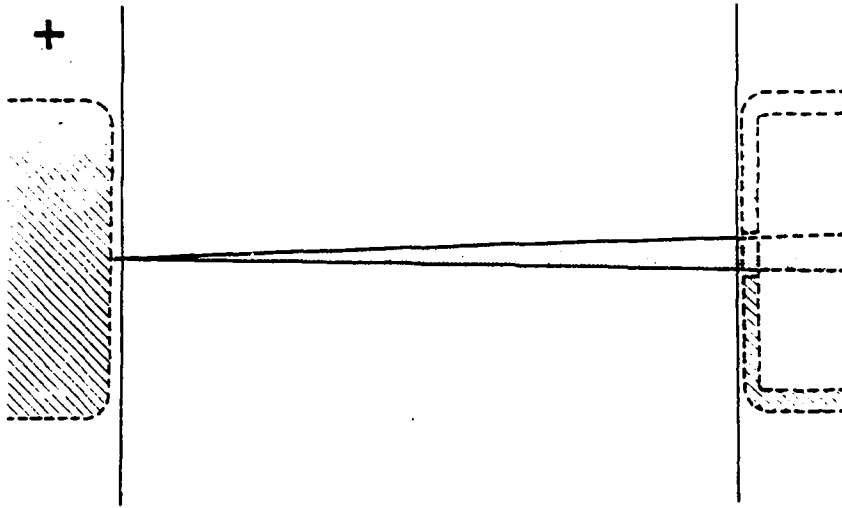
5ns

c)

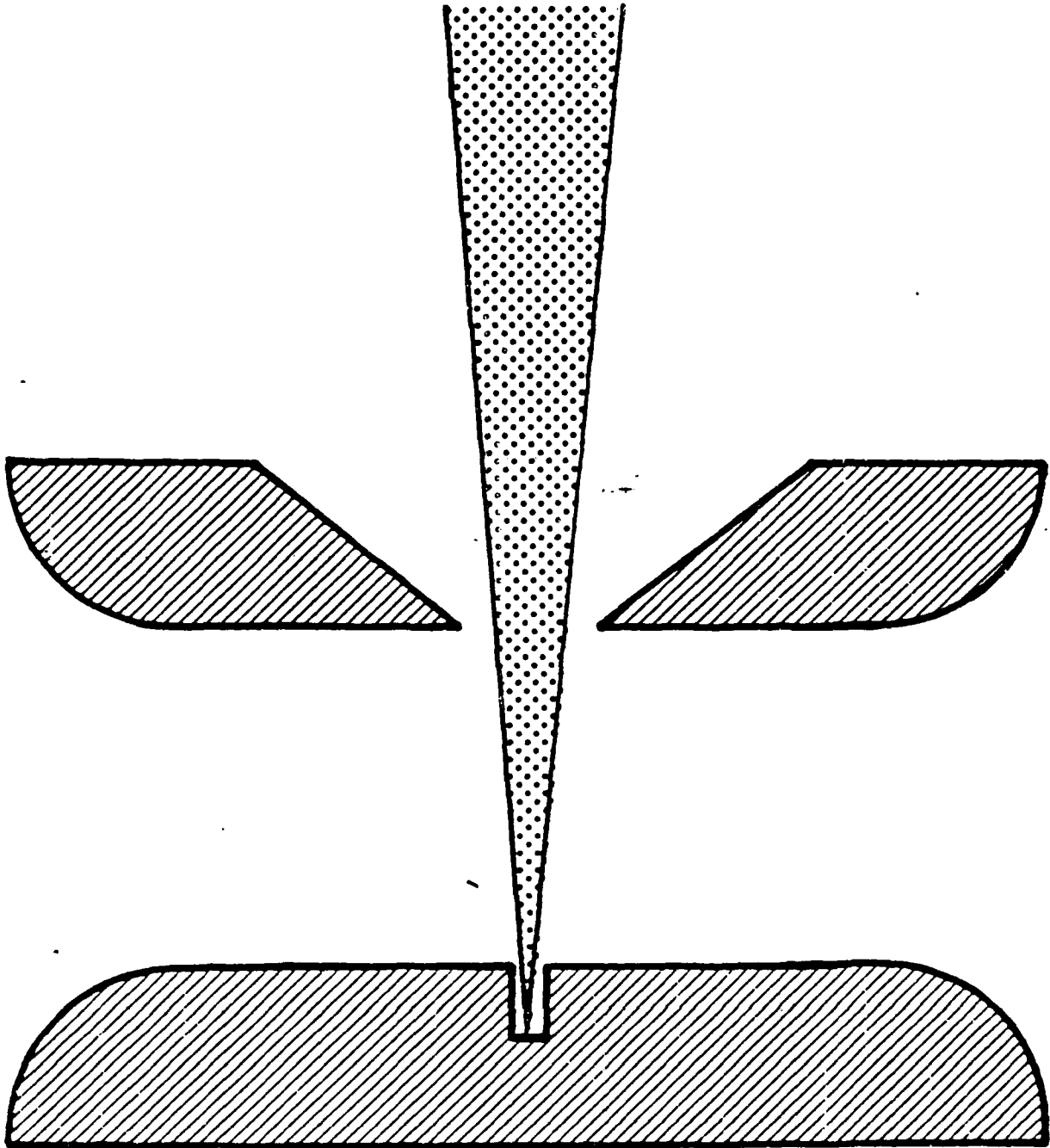


5ns





1ns



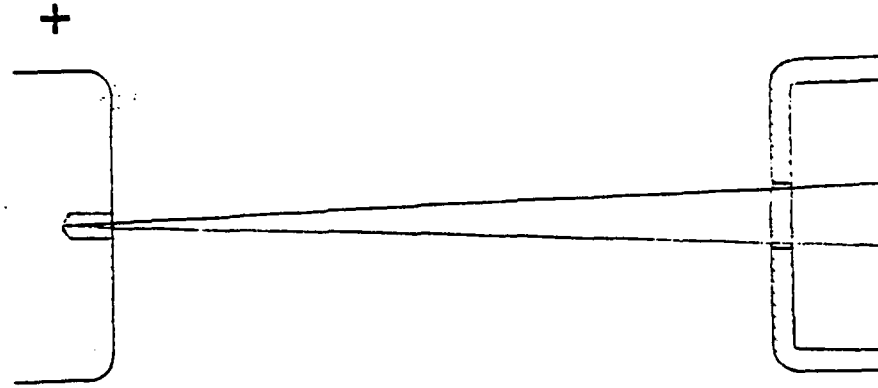


SW2

APR 2

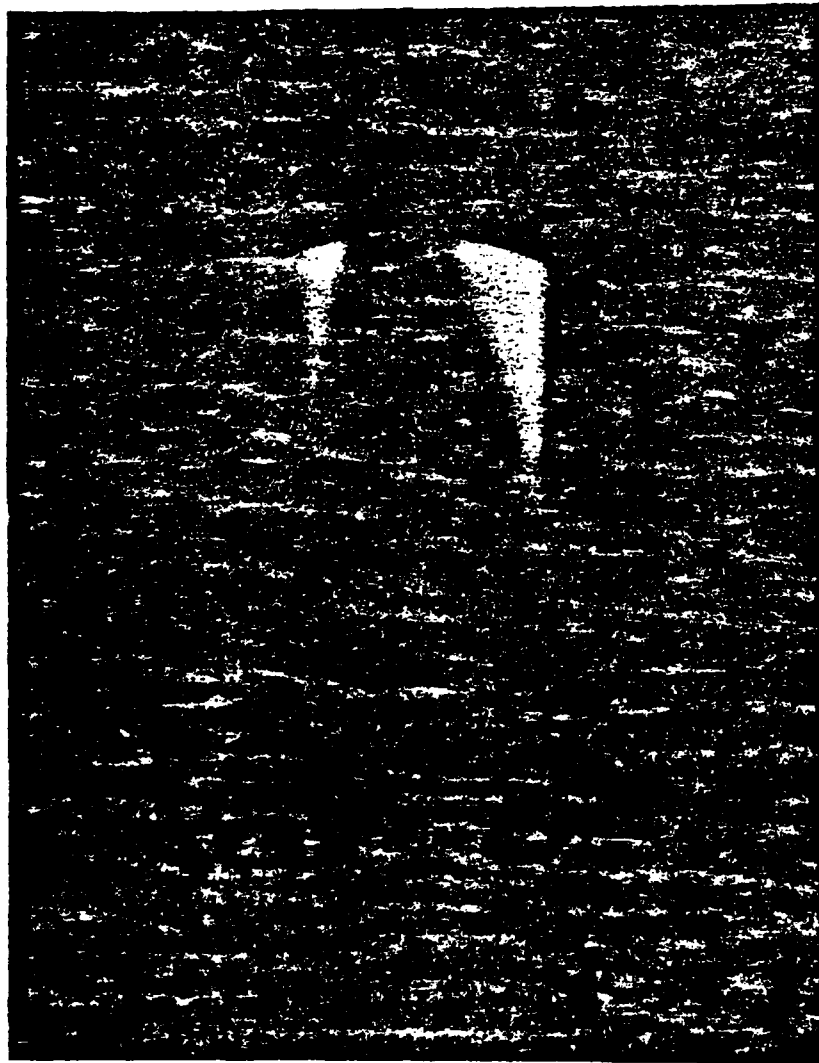
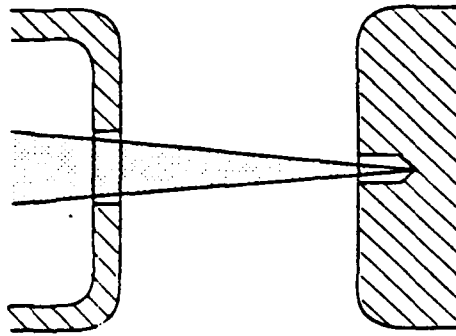
2/1





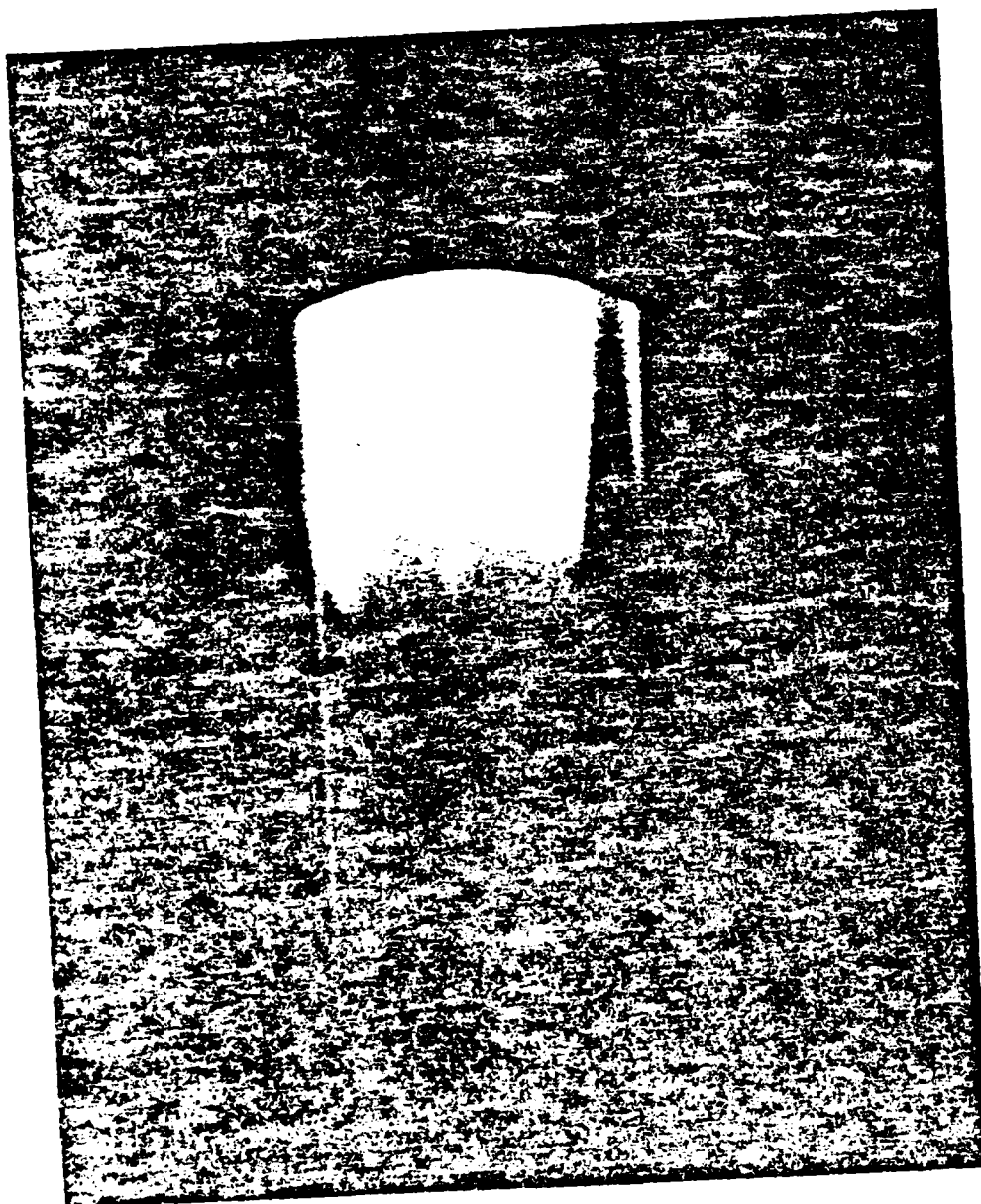
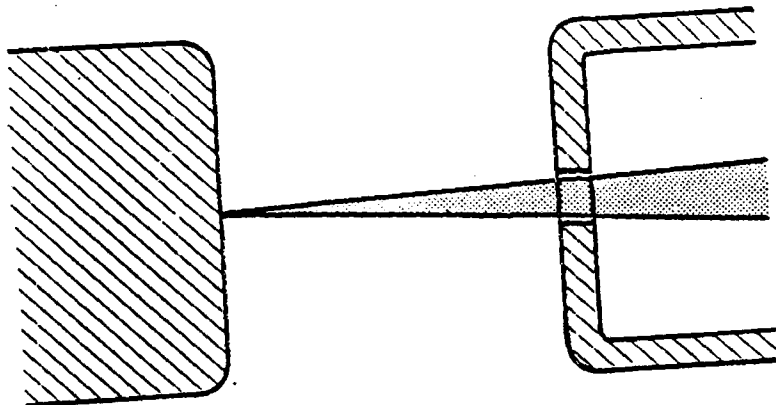
5ns

+



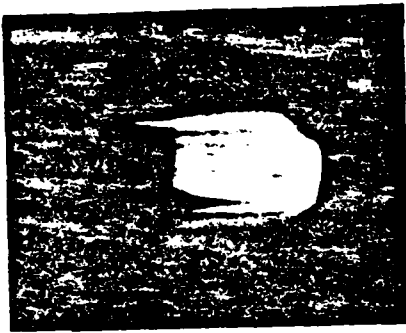
↑  
10ns

+



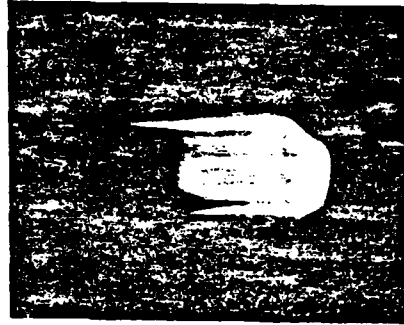
5ns

a)

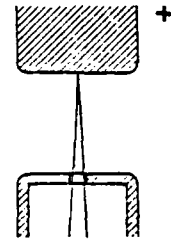


10ns

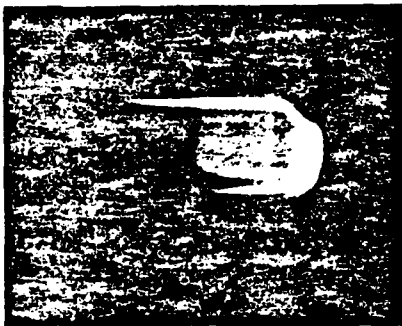
b)



10ns

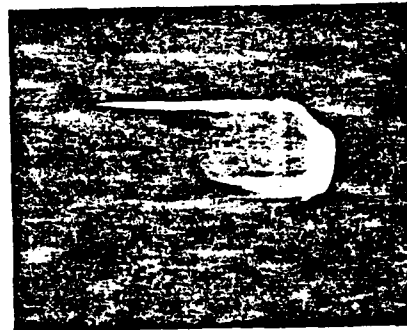


c)

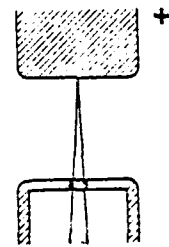


10ns

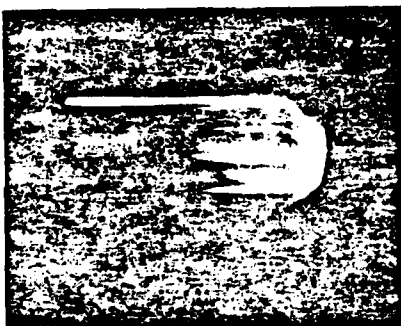
d)



10ns

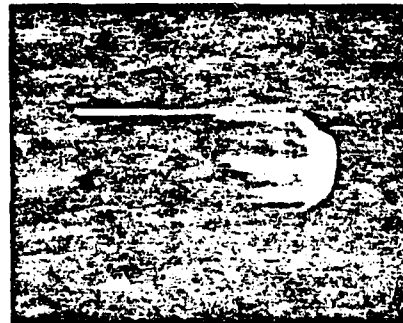


e)

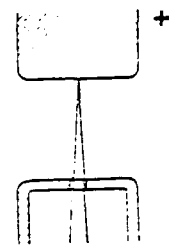


10ns

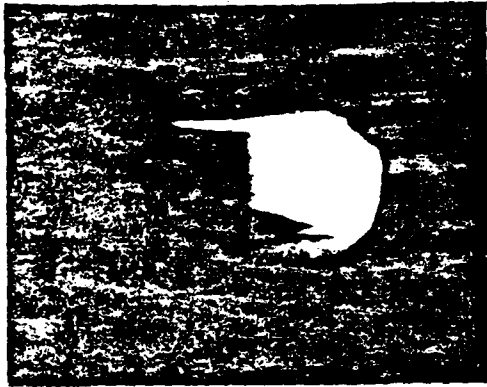
f)



10ns

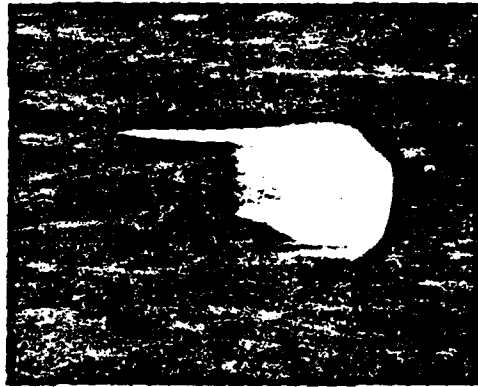


a)



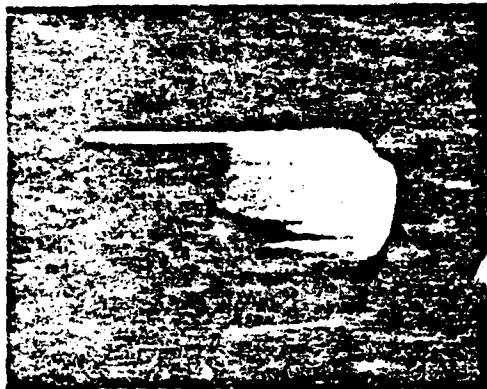
10ns

b)



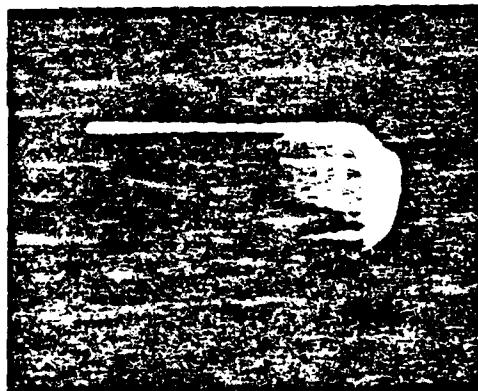
10ns

c)



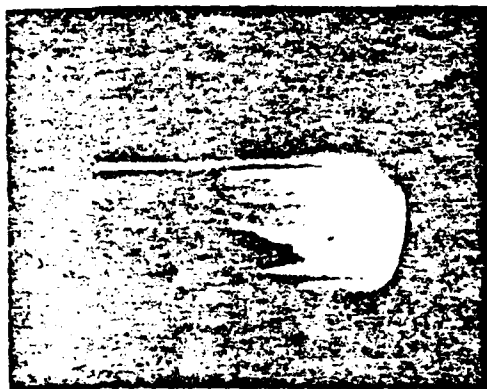
10ns

d)

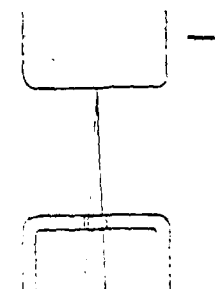
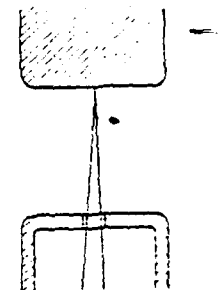
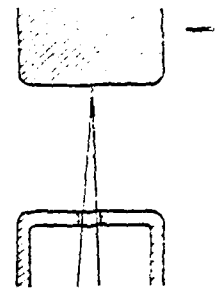
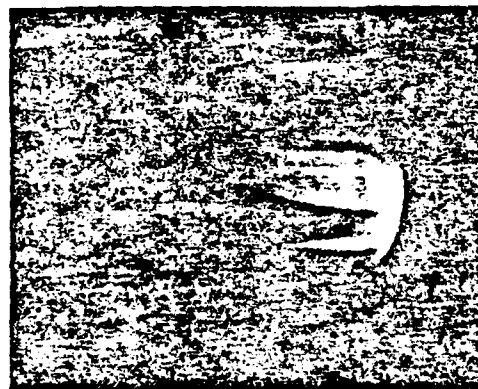


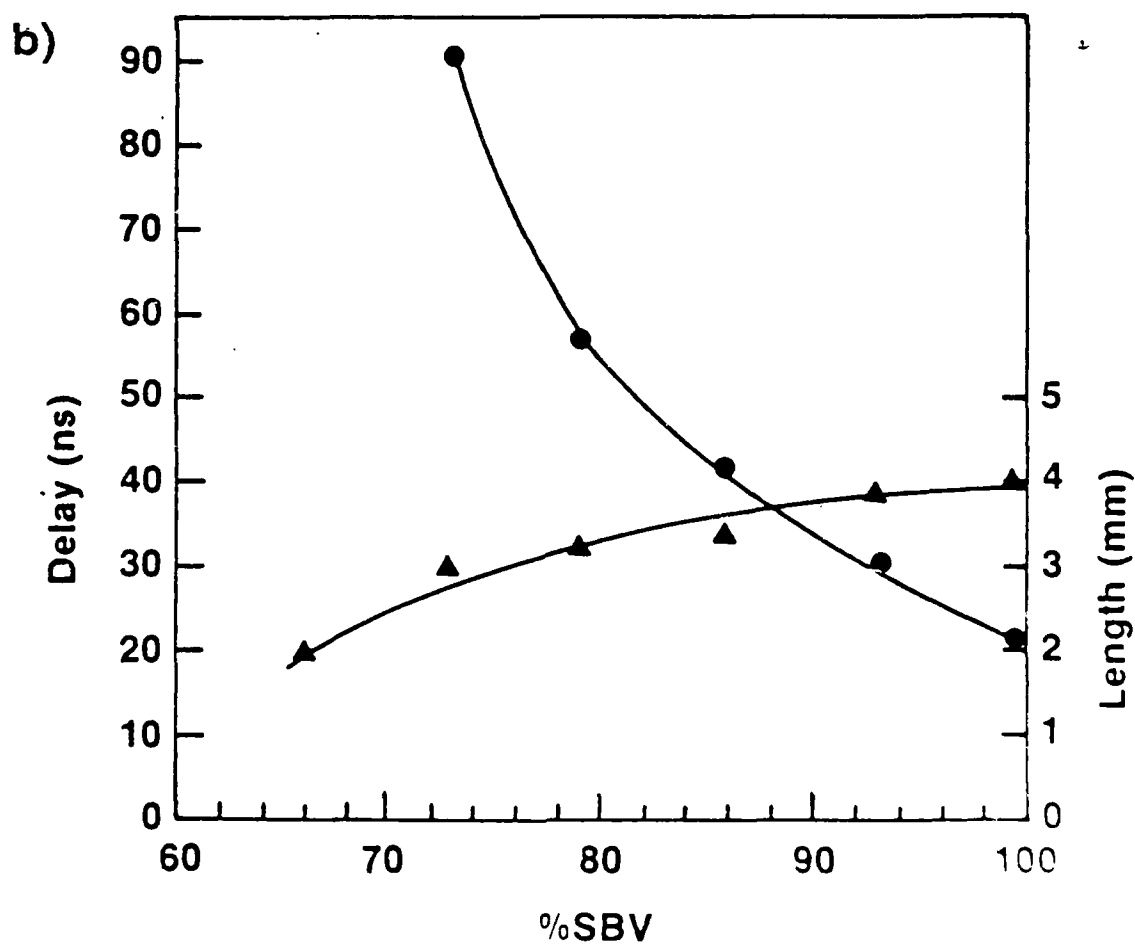
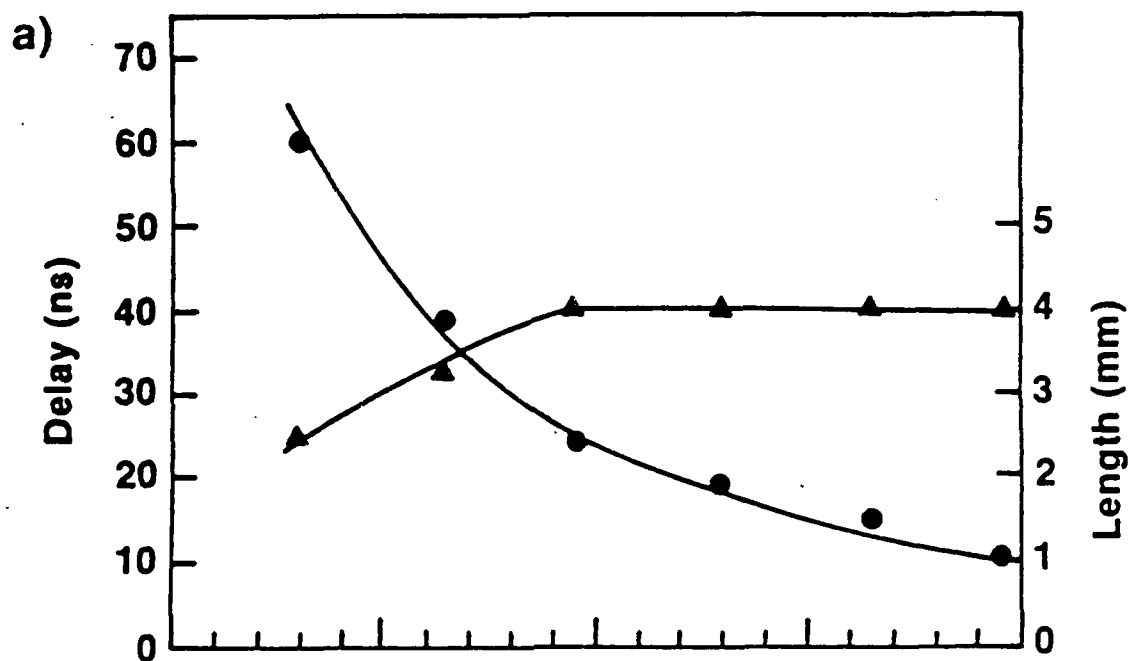
10ns

e)



f)





AD-A139 321

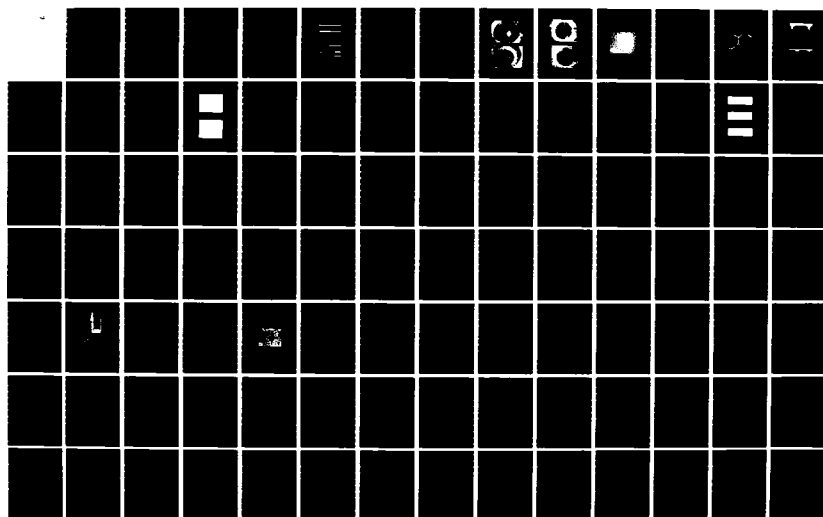
COORDINATED RESEARCH PROGRAM IN PULSED POWER PHYSICS  
(U) TEXAS TECH UNIV LUBBOCK DEPT OF ELECTRICAL  
ENGINEERING M KRISTIANSEN ET AL. 27 FEB 84  
AFOSR-TR-84-0174 F49620-79-C-0191

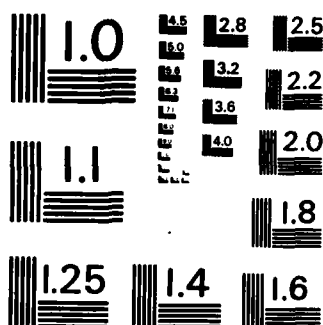
2/8

UNCLASSIFIED

F/G 10/2

NL





MICROCOPY RESOLUTION TEST CHART  
NATIONAL BUREAU OF STANDARDS-1963-A



## Project No. 3

Spark Gap Discharge and Erosion Phenomena

(A. Donaldson, C. Yeh, B. Maas, R. Ness,  
H. Krompholz, M. Hagler, M. Kristiansen and, L. Hatfield)

## A. SUMMARY

The work performed during the past year involves the main aspects limiting the performance of high energy, rep-rated spark gaps, namely, voltage breakdown stability, electrode erosion, and voltage recovery. The accomplishments during the contract period include:

1. A theoretical model which describes the selfbreakdown voltage distribution of a spark gap as a function of the relevant parameters, e.g. electrode surface conditions, gas type, gas pressure, and voltage ramp rate has been developed and experimentally verified. This model can be extended to the description of pulse charged and triggered spark gaps. For experimental verification of the model the necessary computer software has been developed and applied to calculations of the effects of surface microstructures on the static breakdown voltage distribution in  $N_2$  and  $SF_6$ .
2. A physical understanding of the erosion process has been developed which explains the previously unresolved discrepancy between the theoretical erosion spot models [1] based on joule heating (erosion a function of

$\int i^2 dt$ ) and experimental results [2-10] which show erosion a function of  $\int i dt$  and several other current dependencies.

3. The erosion rates as a function of current for a variety of parameters (electrode materials, gas type, pressure etc.) with unipolar discharges (Mark II) have been measured. A ringing discharge facility (Mark V) has been constructed which provide a high charge transfer per unit of stored energy.
4. The basic erosion mechanisms in stainless steel, e.g. crack formation due to material inhomogeneities, has been clarified.
5. Different diagnostic methods have been set up, including:
  - cross sectioning facility for first hand examination of electrode surfaces,
  - interfacing of a microprocessor controlled temperature aquisition system for measurement of electrode and gas temperature in order to get additional information with regard to energy balance,
  - optical diagnostics: a Schlieren technique for measuring the arc expansion vs. time and a Mach-Zehnder interferometer for observation and measurement of the motion of hot gas and/or electrode debris during spark recovery.
6. Measurement of the recovery rate statistics using a double pulse arrangement has been made for several electrode and gas combinations.

## B. MODELING OF SELF-BREAKDOWN VOLTAGE STATISTICS

A model has been developed which relates the electrode surface structure produced by a high energy discharge to the self-breakdown voltage statistics. This model, previously described in the Third Annual Report [11], includes all the parameters relevant for spark gap operation (electrode surface structure, gas type, gas pressure, and voltage ramp rate) and allows for the scaling, parameter optimization, and predictions needed to improve spark gap performance. Recently the model has been found to have a direct application for the design and improvement of pulse charged and triggered spark gaps [12]. Details of this model are given in the preprint of "Modeling of Self-Breakdown Voltage Statistics in High Energy Spark Gaps" in Appendix I and has been submitted to the Journal of Applied Physics.

## C. ELECTRODE EROSION

### 1. Material dependence as a function of current

Electrode erosion measurements as a function of current have continued on the Mark II generator. A large portion of this work is described in the paper "Electrode Erosion Phenomena in a High Energy Spark Gap" which has been accepted for publication in IEEE Trans. on Plasma Science and is attached as Appendix II. To date, nine different electrode materials have been tested in air and nitrogen. The erosion rates for these materials are shown in Figs. 1 and 2. Figure 1 indicates that stainless steel (304) has

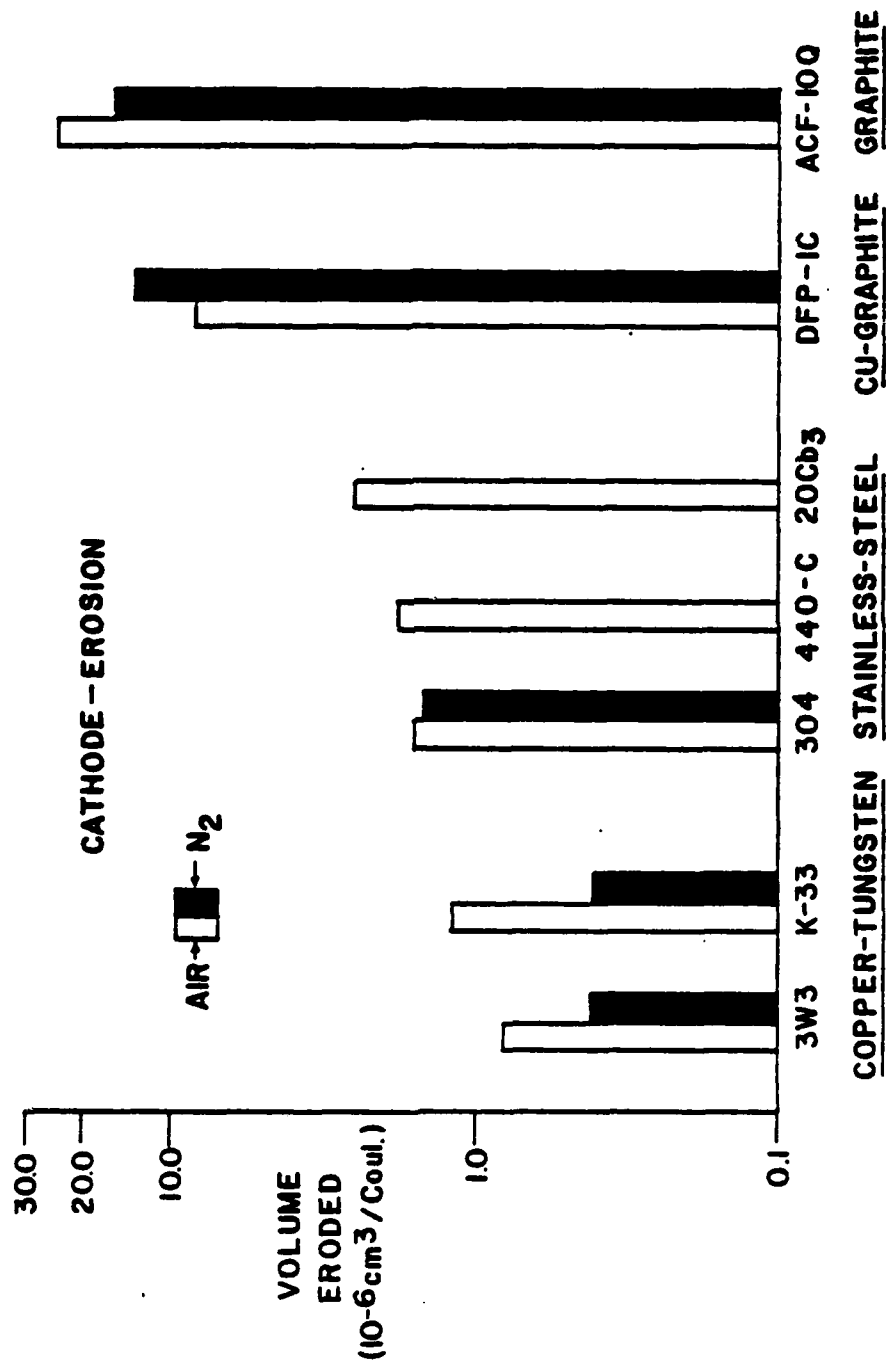


Fig. 1. Cathode Erosion Rates for Different Gases and Electrode Materials

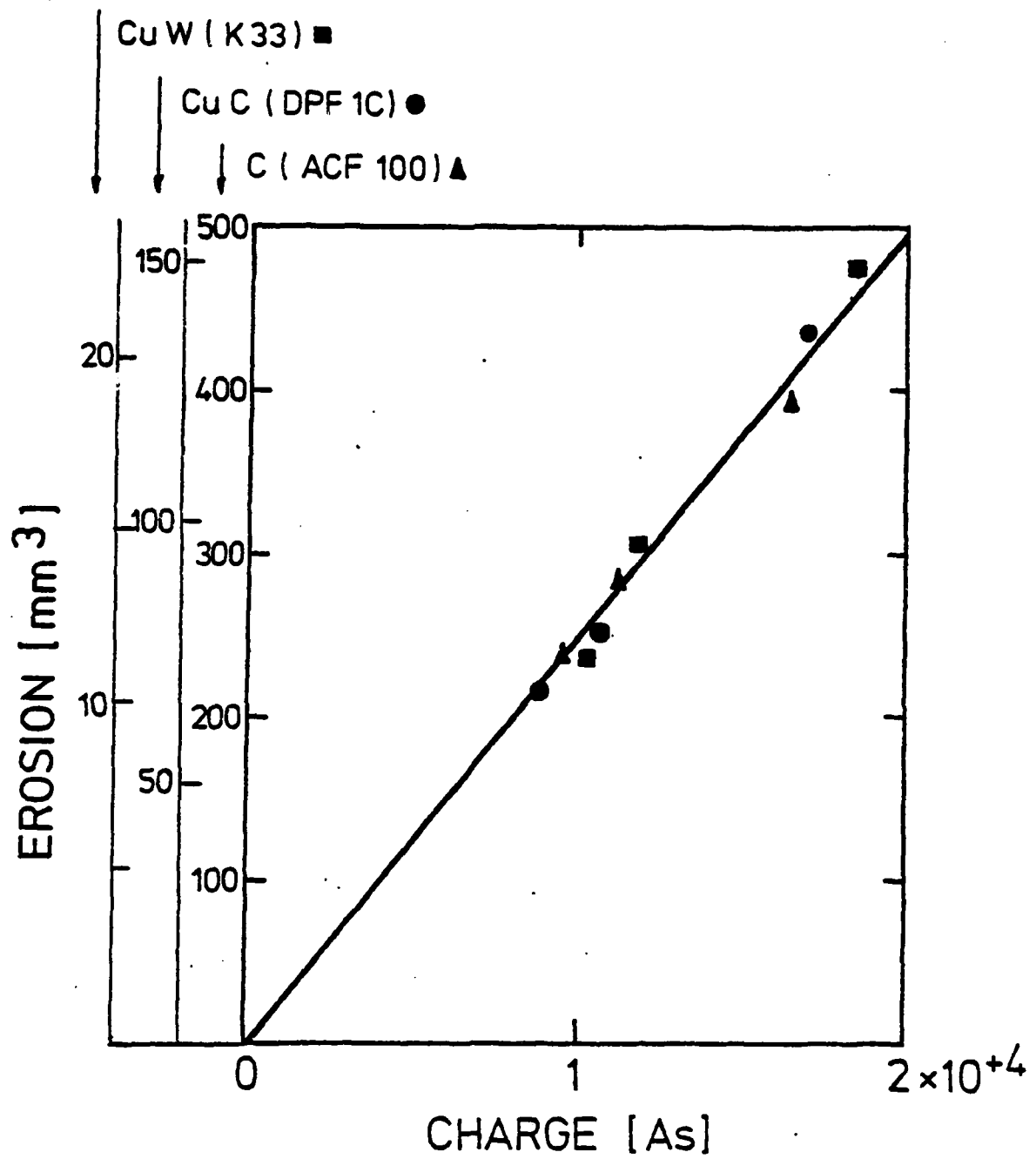
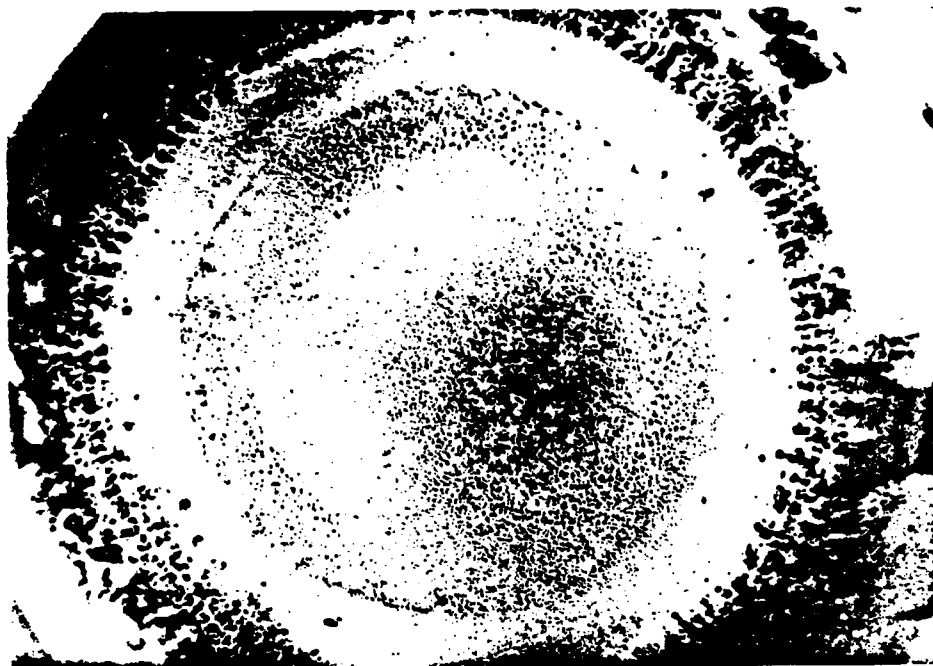


Fig. 2. Cathode Erosion Rates vs. Total Charge Transferred

a cathode erosion rate comparable to the more expensive copper-tungsten. As a result, several stainless steels (20Cb-3 and 440-C) which were known to have low erosion rates in MHD generators were tested as well. The surfaces of these electrodes are shown in Figs. 3 and 4. Neither of these steels were as good as 304 and the 20Cb-3 showed signs of gross material extraction.

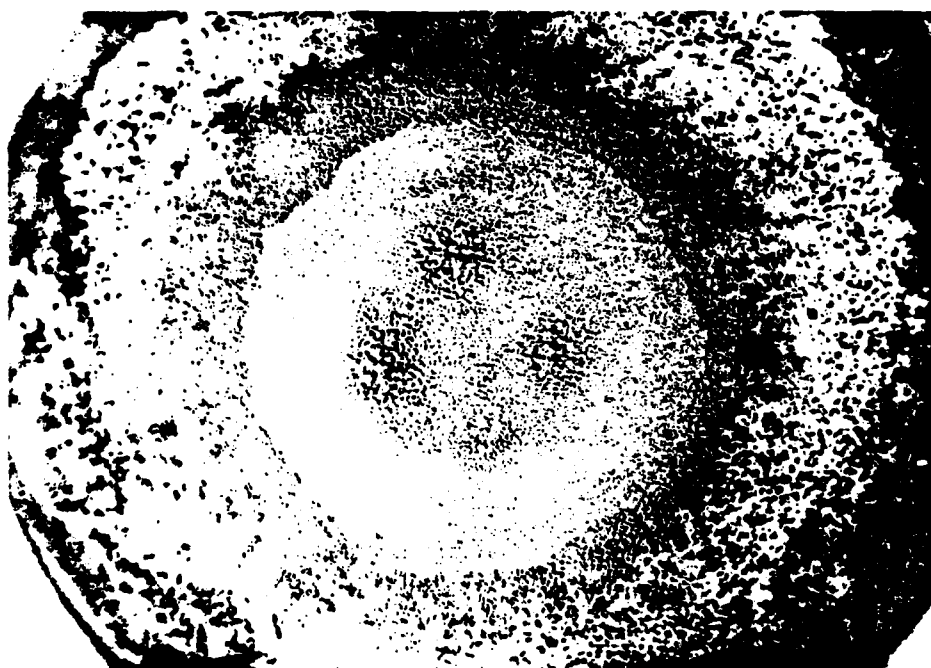
Figure 2 indicates that for air the cathode erosion rate is material dependent and varies linearly with  $\int i dt$ , or  $Q$ , for unipolar pulses. Although consistent with other experimental results this dependency of erosion on  $\int i dt$  is in apparent conflict with much theoretical work which assumes resistive heating at the arc attachment site to be responsible for the melting of electrode material and thus have a dependence upon  $\int i^2 dt$ . In contrast, an  $\int i dt$  dependence would seem to indicate that the source of energy for the erosion would come from the energy dissipated in the cathode fall, namely,  $\int V_{arc} i dt$ . However, as it will be shown, this is not necessarily the case. (The erosion mechanism was an issue of considerable debate in Russian literature and was never adequately resolved [13-14].)

Using the essential results of vacuum spark investigations [15], which can be applied to high pressure discharge experiments as far as electrode processes are considered, the basic erosion processes can be described as follows: The arc consists of filaments with individual points of attachment at the electrodes (cf. Fig. 5). At low pressures the current in each filament has been found to be constant [16] and, is in general, a function of electrode material, gas type, and pressure. Thus, the number of attachment sites  $N$  is a function of the total current  $I$  at any



a) Cathode

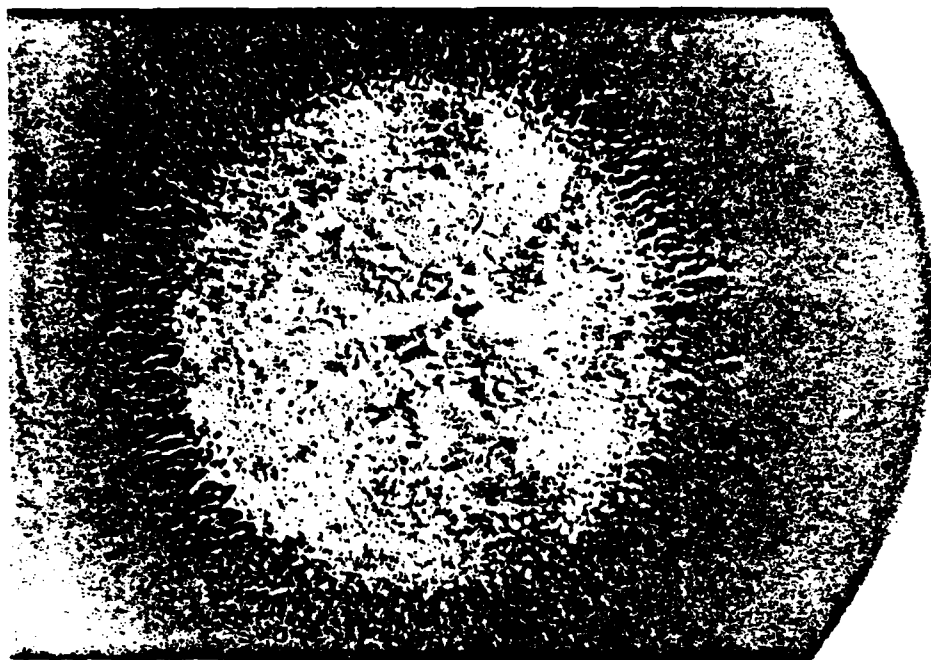
1 cm



b) Anode

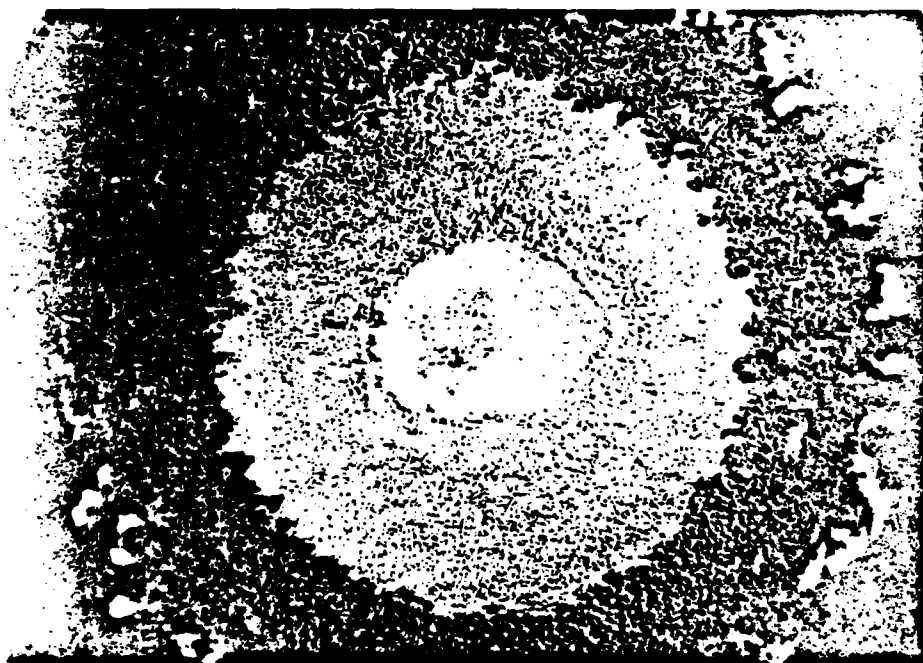
1 cm

Fig. 3. Electrode Surfaces for Stainless Steel (440-C)  
Run in Nitrogen



a) Cathode

1 cm

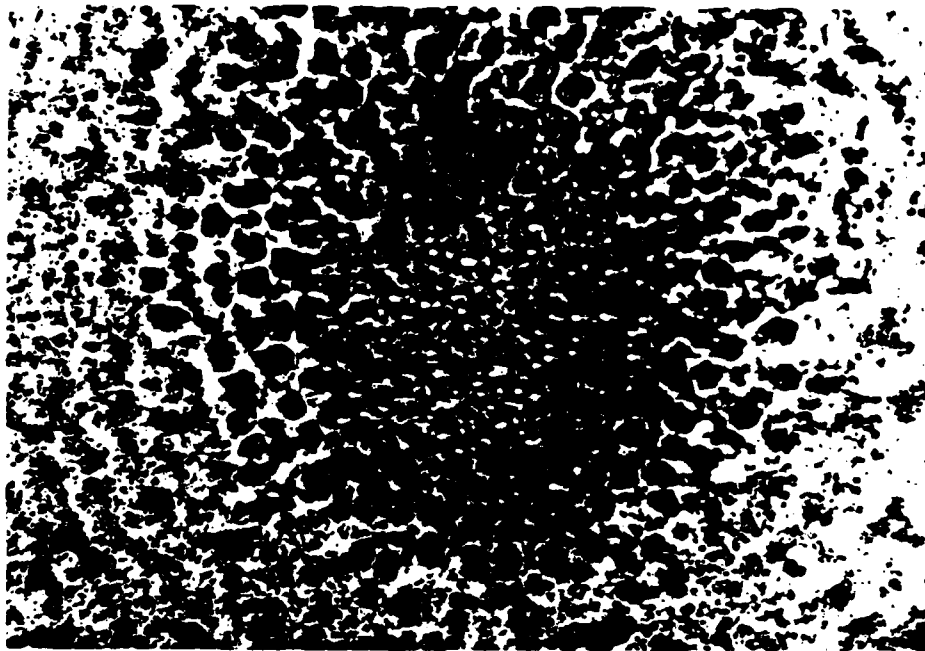


b) Anode

1 cm

Fig. 4. Electrode Surfaces for Stainless Steel (20 Cb-3)  
Run in Air





1 mm

Fig. 5. Surface of a Stainless Steel Cathode (304) Run in Air After a Single Discharge (20 kA, 25  $\mu$ s)

given time. Regardless of the erosion dependence on current for each filament, the total erosion will then be proportional to the number of sites and thus proportional to the total current, if one assumes that the lifetime for each filament is the same. If the attachment lifetime, which is known to be a function of electrode material, gas type, and pressure and is generally ~ 100 ns, is allowed to change during the current pulse itself, then virtually any functional dependence on current could result.

## 2. Surface analysis

Surface analysis work continued on the spark gap electrodes [17]. Cross sections were made of several electrodes in order to study the depth of the erosion damage. For the case of stainless steel electrodes in air and nitrogen the results proved to be quite interesting and gave considerable insight into the physics of the erosion process. Figure 6 shows a top view of the central region of a stainless steel (304) cathode run in air. The hexagonally shaped regions, 100-200  $\mu\text{m}$  wide, are of considerable importance since the boundaries or cracks show evidence of enhanced erosion. Cross sections of this electrode are shown in Fig. 7 and were analyzed by Paul Predecki at Denver Research Institute. His analysis showed that:

- 1) the cracks oriented themselves along magnesium sulfide "stringers" which were present in the stainless steel,
- 2) the density of the stringers is quite high and the hexagonal regions were a result of a combination of biaxial tensile forces produced during the temperate cycling created by the arc and the enhanced chemical attack which resulted at the stringer locations,

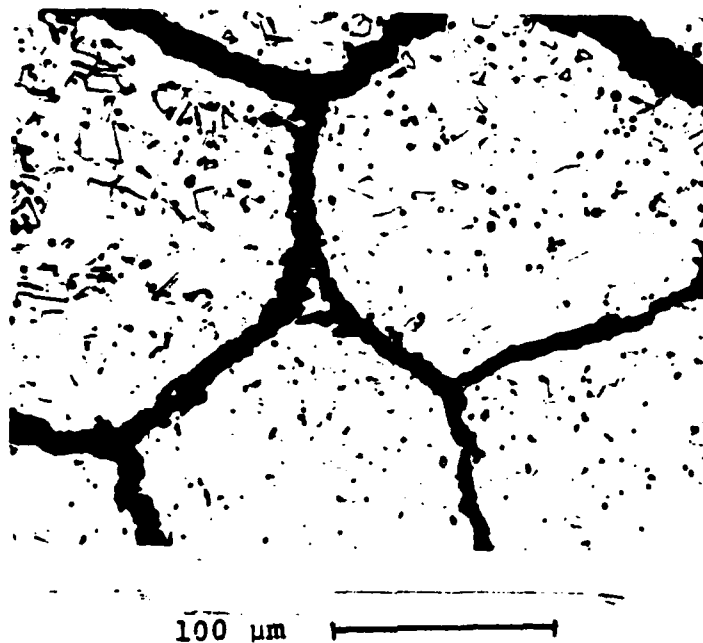


Fig. 6. Surface of the Central Region of a Stainless Steel (304)  
Cathode Run in Air



a) Cathode in Air

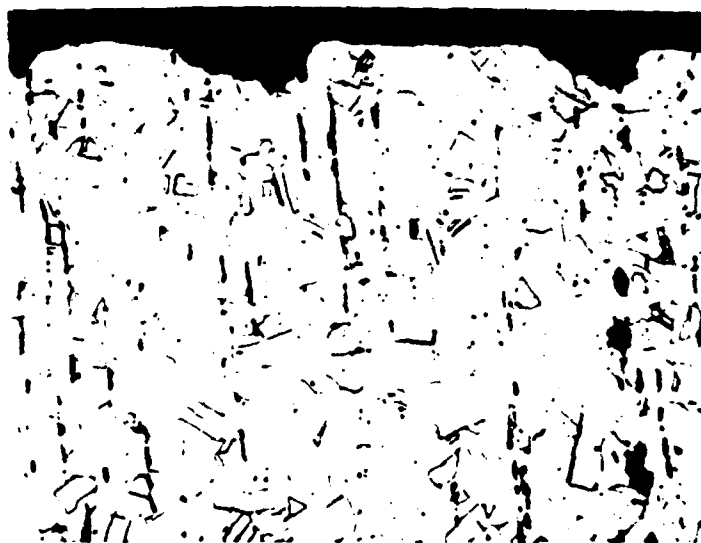
100  $\mu\text{m}$ b) Cathode in  $\text{N}_2$ 100  $\mu\text{m}$ 

Fig. 7. Cross Sections of the Central Region of a Stainless Steel (304) Cathode Run in Air and  $\text{N}_2$

- 3) the depth of the cracks was considerably less in nitrogen (20  $\mu\text{m}$ ) than in air (80  $\mu\text{m}$ ), presumably due to less chemical attack or by a reduction in the temperature cycling in nitrogen, and
- 4) except at the cracks, the depth of damage, as evidenced by melting or chemical composition changes, was generally less than 10  $\mu\text{m}$ .

As a result of this work, efforts are being made to obtain stainless steels with fewer stringers and a cross-sectioning facility has been assembled in our laboratory to allow in-house electrode inspection.

### 3. Energy Deposition

The study of the energy deposition in a spark gap is important for modeling electrode erosion and voltage recovery. The experimental work is divided into two parts: the measurement of the arc resistance and the measurement of the energy deposited in the electrode. The arc resistance is ideally calculated from the following equation in which all the terms are functions of time.

$$V_1 - V_2 = i \left( R_{\text{arc}} + R_{\text{shaft}} + dL_{\text{arc}}/dt + dL_{\text{shaft}}/dt \right) \\ \left( + \frac{di}{dt} L_{\text{arc}} + L_{\text{shaft}} \right), \quad (1)$$

where  $V_1$  and  $V_2$ , the anode and cathode voltages, and  $i$  and  $\frac{di}{dt}$  are all measured directly from probes. The shaft resistance,  $R_{\text{shaft}}$ , has been determined using skin depth calculations [18] and  $L_{\text{arc}}$  has been calculated from Braginskii's equation [19]. The arc inductance will be verified experimentally using the Schlieren

diagnostic system shown in Fig. 8 to measure the radial expansion rate of the arc. The shaft resistance will also be verified experimentally by differential voltage measurement along the shaft. A computer program is currently being developed to solve Equation 1 for  $R_{arc}$  with the use of this information and the digitized probe data.

To calculate the energy deposited in the electrode an experiment is being planned which is similar to the one described in detail by Carder [6]. Basically the experiment consists of measuring the temperature of a thermally isolated electrode after a fixed number of pulses have occurred. A microprocessor controlled temperature acquisition device has been interfaced to our laboratory computer and the required thermocouples will be assembled shortly. It is anticipated that the energy deposition to the electrodes will be calculated for a wide variety of pulse conditions and thus aid in the development of an erosion model.

#### 4. Ringling Discharge Experiment (Mark V)

In order to study electrode erosion as a function of pulse shape, and for higher levels of Coulomb transfer, a ringling discharge facility (Mark V) has been constructed. The design is essentially the same as that for Mark IV except that the load is shorted to produce an oscillatory current, and the electrodes are water cooled. A typical pulse with approximately 90% reversal is shown in Fig. 9. Typical operating parameters are currently:

Ringling frequency	50-200 kHz
Peak current	100 kA
Total charge stored	0.5 Coulombs/shot
Total charges transferred	10 Coulombs/shot
Discharge voltage	50 kV

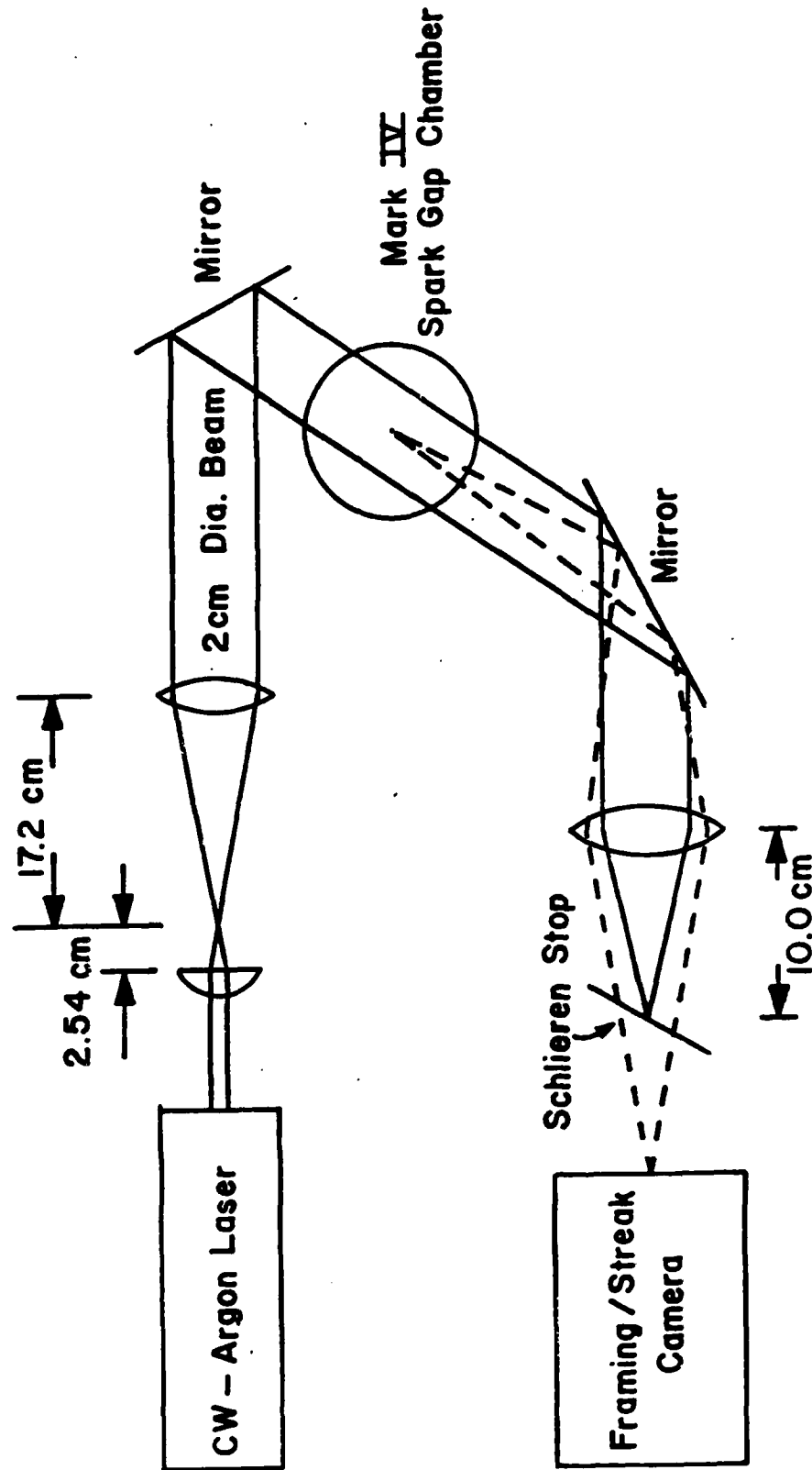
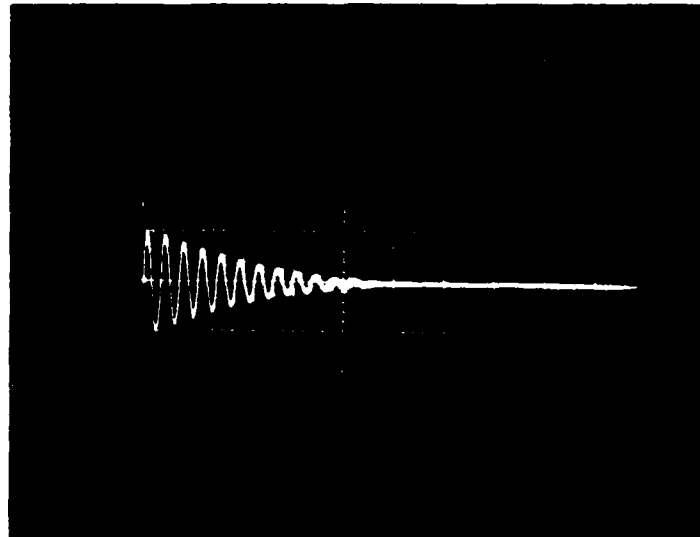
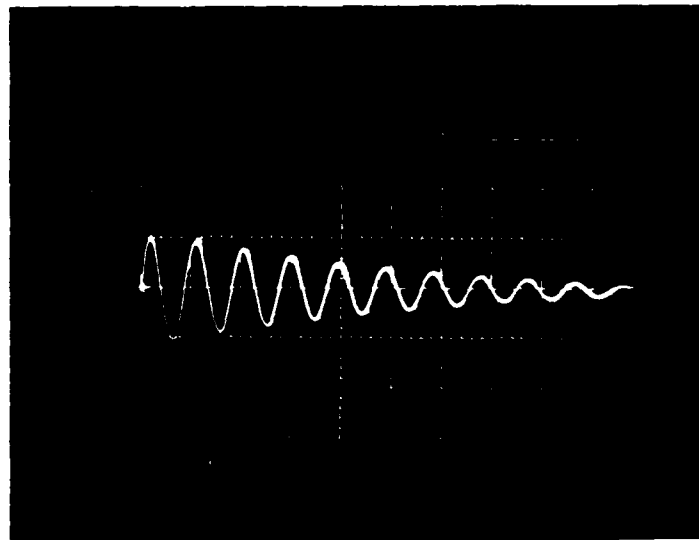


Fig. 8. Mark IV Schlieren Set-up



a) Vertical: 10 kA/div, Horizontal 50  $\mu$ s/div



b) Vertical: 10 kA/div, Horizontal 20  $\mu$ s/div

Fig. 9. Mark V Ringing Discharge Waveforms in Air



Initial experiments will include measuring the electrode erosion rates as a function of the charge transferred in order to compare them with the unipolar results.

#### D. VOLTAGE RECOVERY

Voltage recovery measurements have been performed on the Mark I generator for graphite, stainless steel and copper-tungsten electrodes in air or nitrogen at pressures up to 2 atmospheres. The results of this work are discussed in Appendix III "Voltage Recovery Measurements in a High Energy Spark Gap". In addition to the data presented there, Figs. 10 through 15 show the statistics of the recovery breakdown voltages for both the first and second pulses. These statistics are important for at least two reasons:

- 1) it shows that a considerable spread exists for the second pulse data which suggests that recovery will have to be defined in terms of the lower edge of the voltage distribution instead of the mean voltage, and
- 2) it provides a large data base to check the range of applicability of the statistical model discussed earlier for significantly higher charging rates (270 kV/ms).

A Mach Zehnder interferometer system (Fig. 16), complete with a He-Ne laser and a high speed camera, has been used to record density fluctuations on the Mark I system. First results (Fig. 17) show density variations  $\Delta n/n \leq 0.5$  propagating with extremely slow velocities (250-750 cm/sec.) in the radial

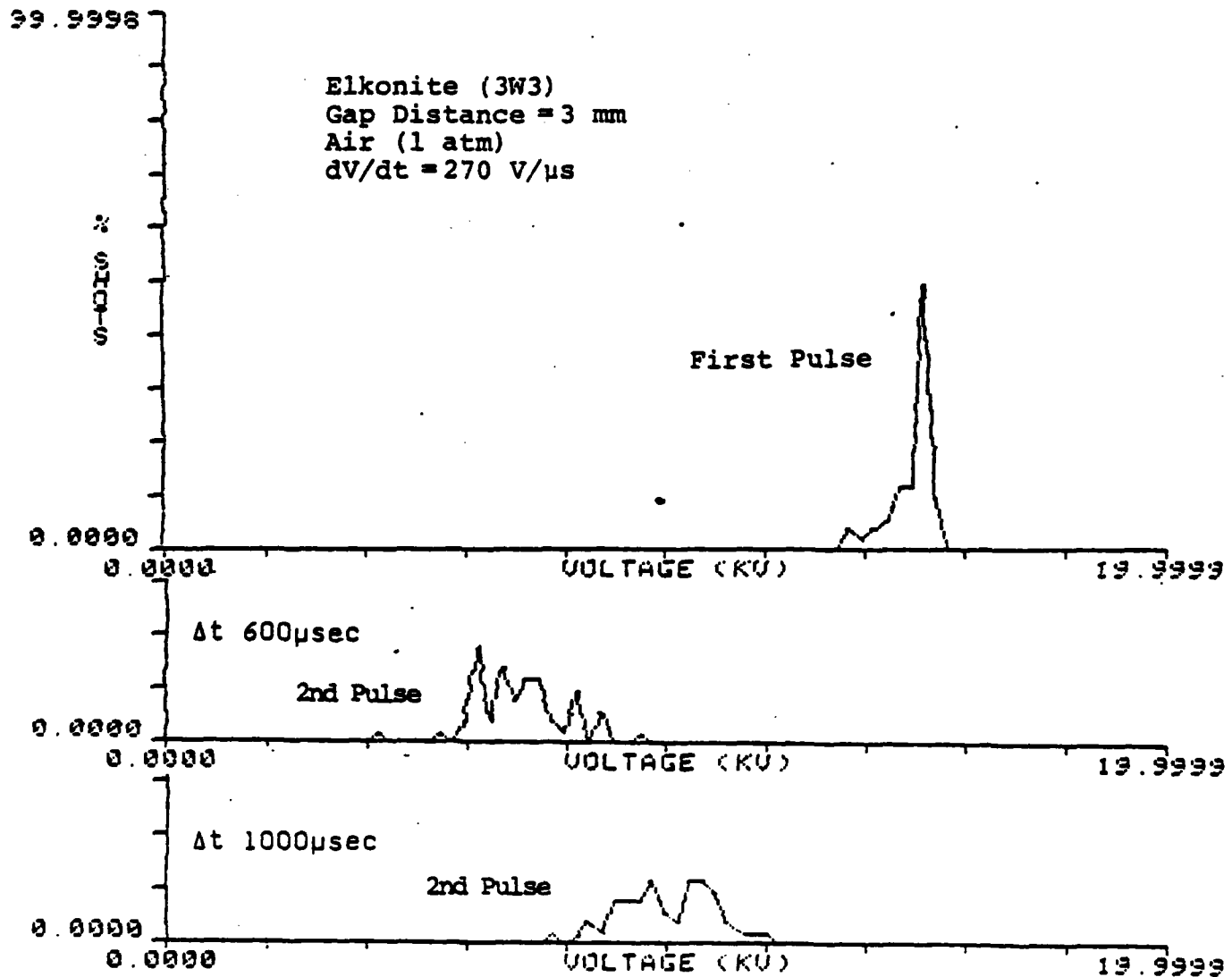


Fig. 10. Voltage Statistics of Pulse Pair for Different Delay Times

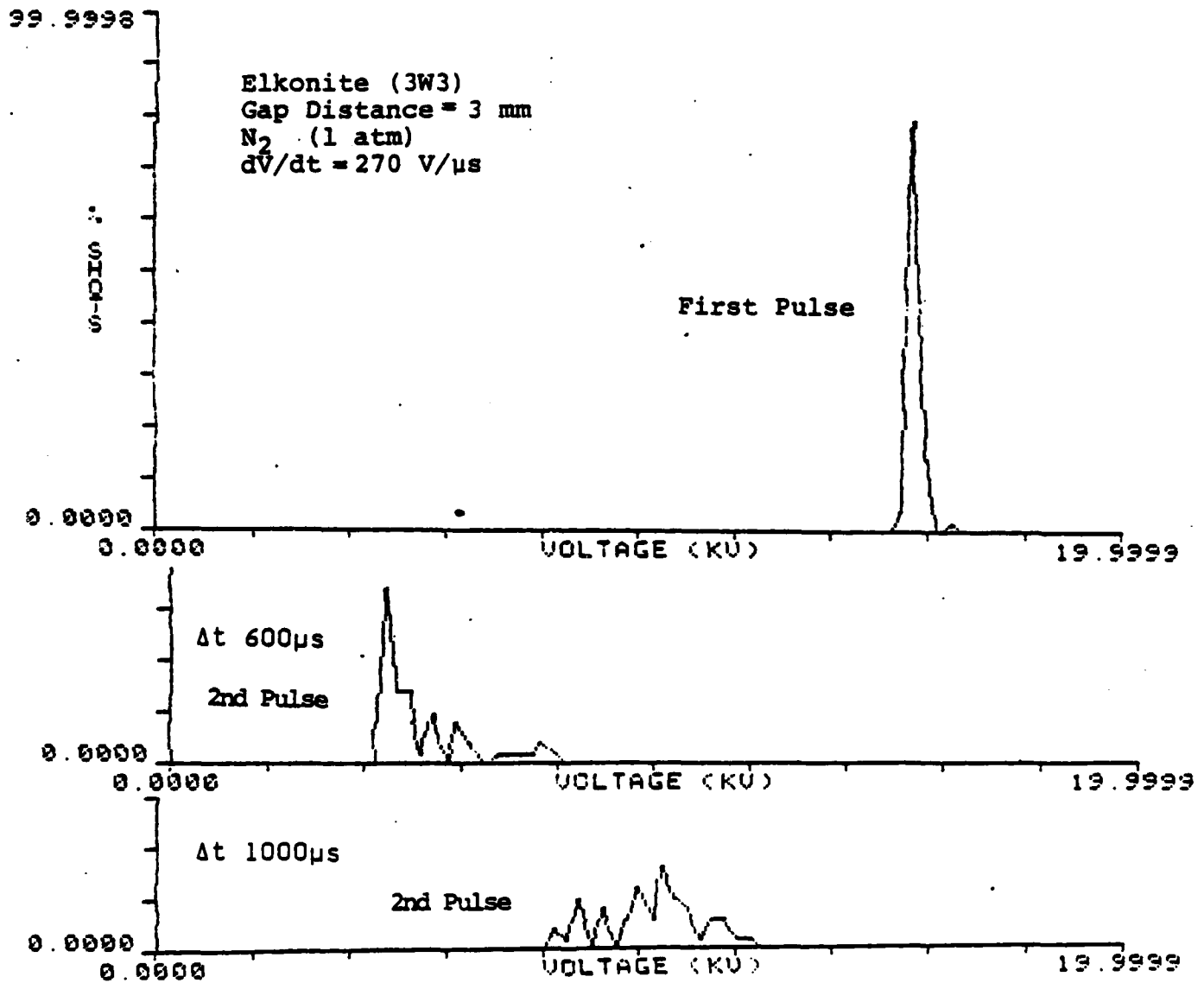


Fig. 11. Voltage Statistics of Pulse Pair for Different Delay Times

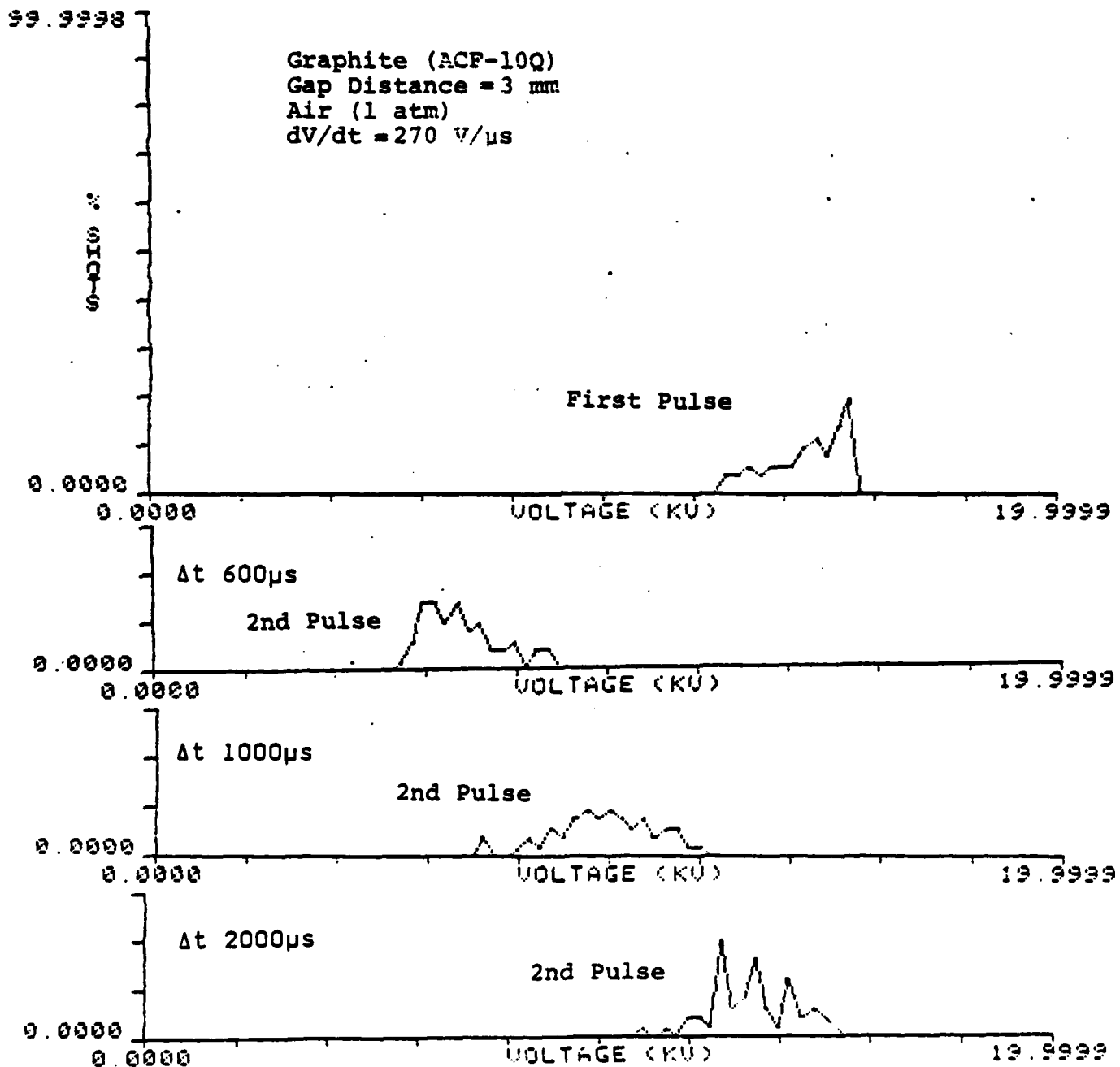


Fig. 12. Voltage Statistics of Pulse Pair for Different Delay Times

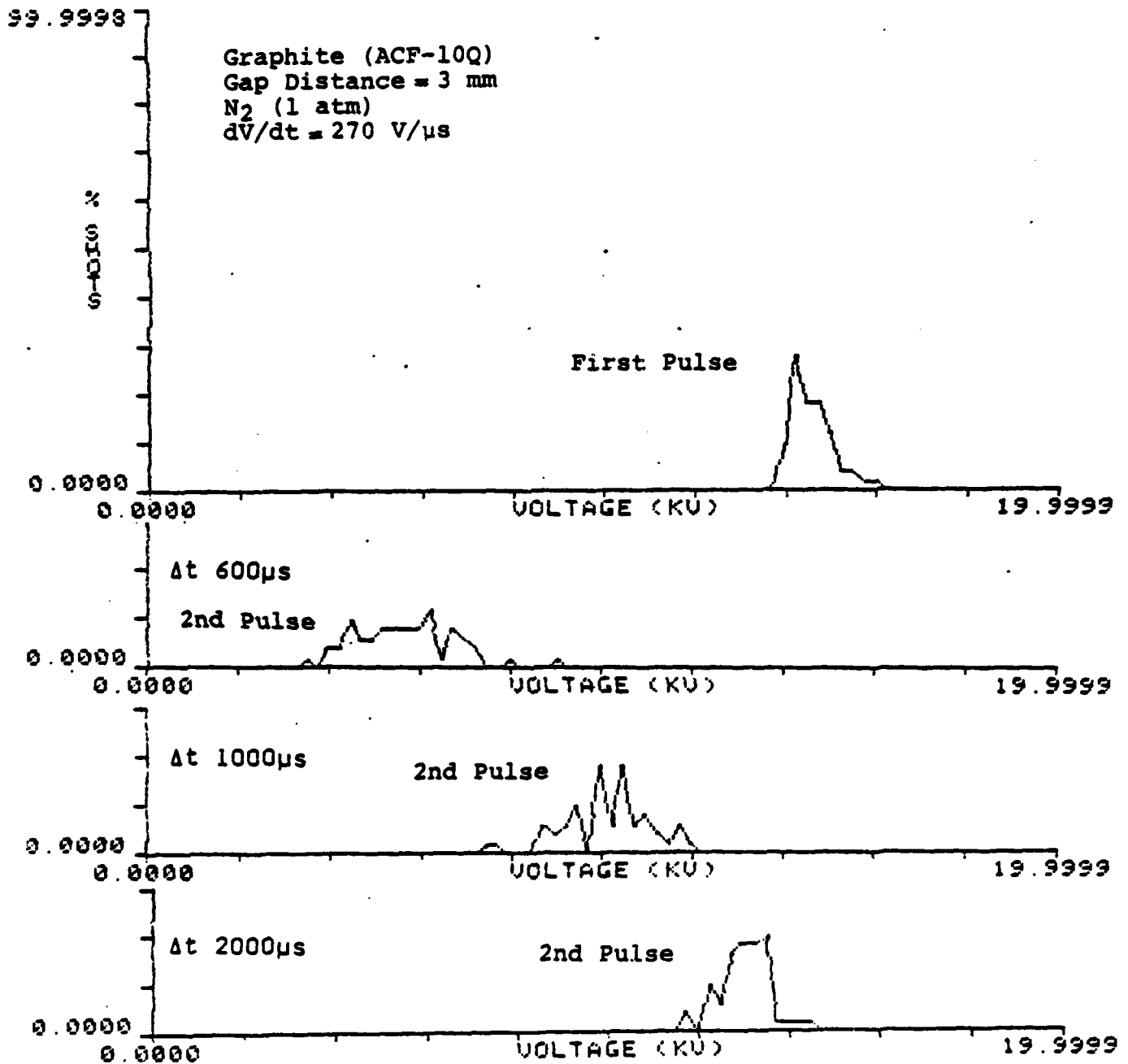


Fig. 13. Voltage Statistics of Pulse Pair for Different Delay Times

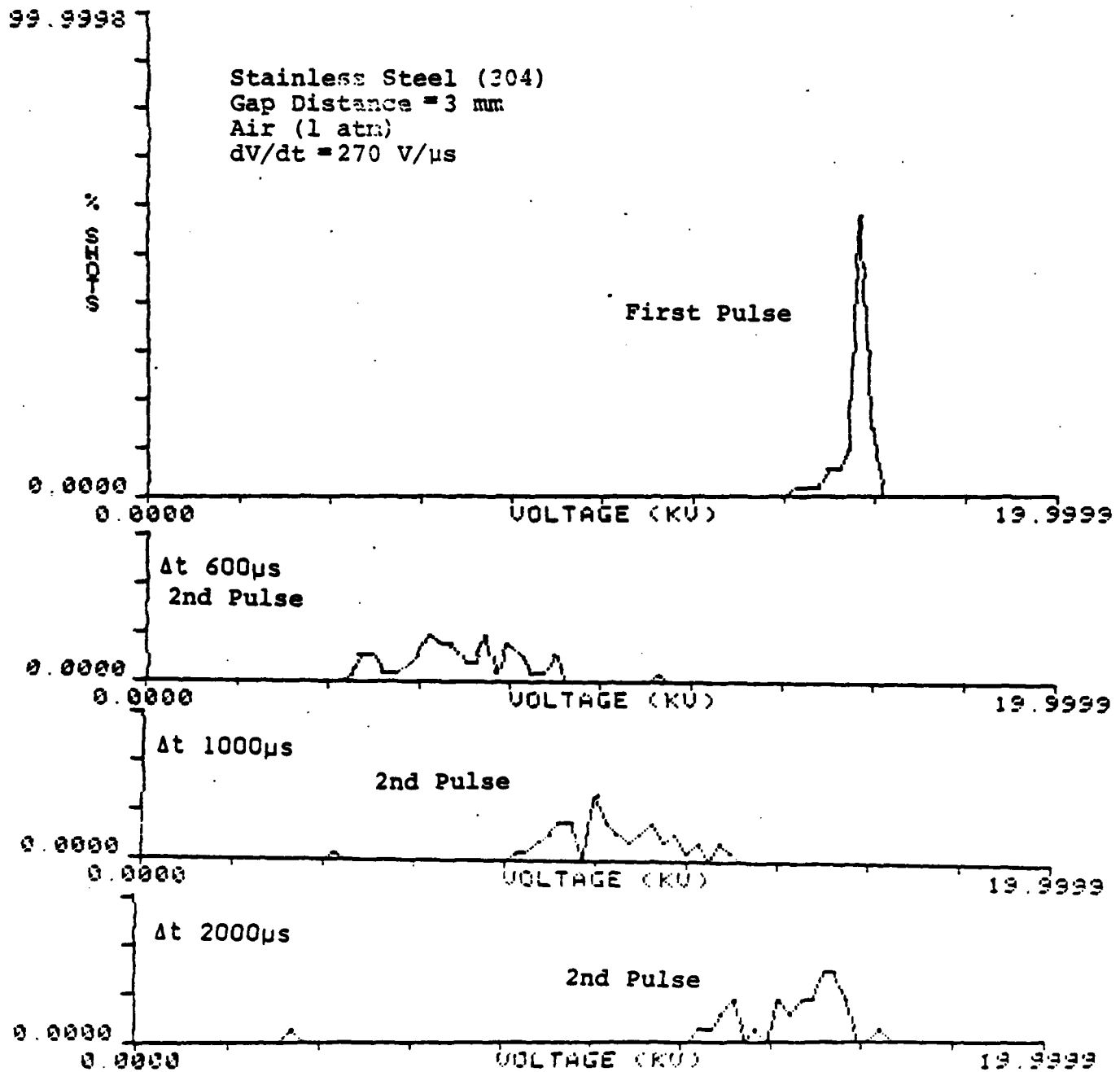


Fig. 14. Voltage Statistics of Pulse Pair for Different Delay Times

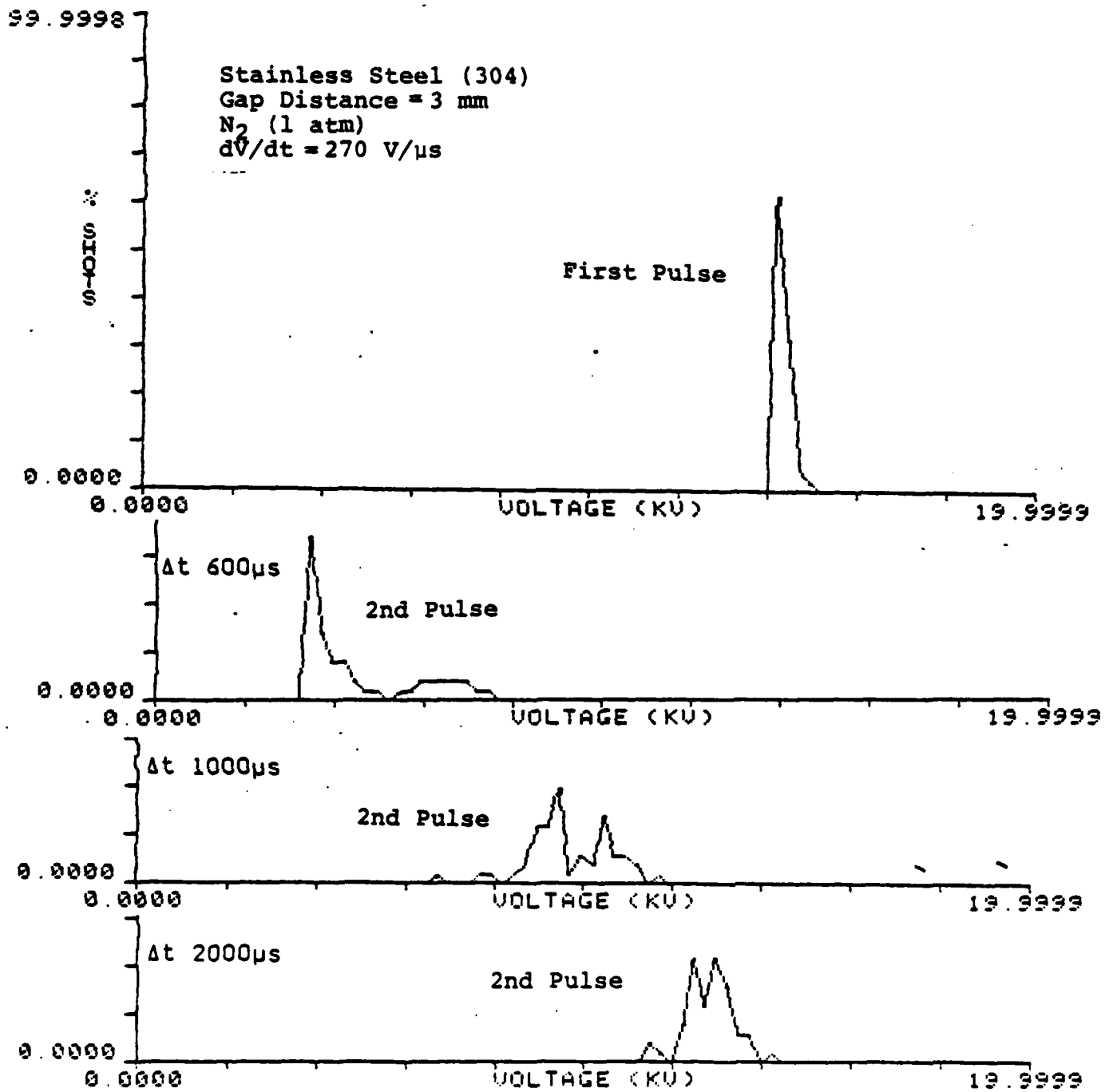


Fig. 15. Voltage Statistics of Pulse Pair for Different Delay Times

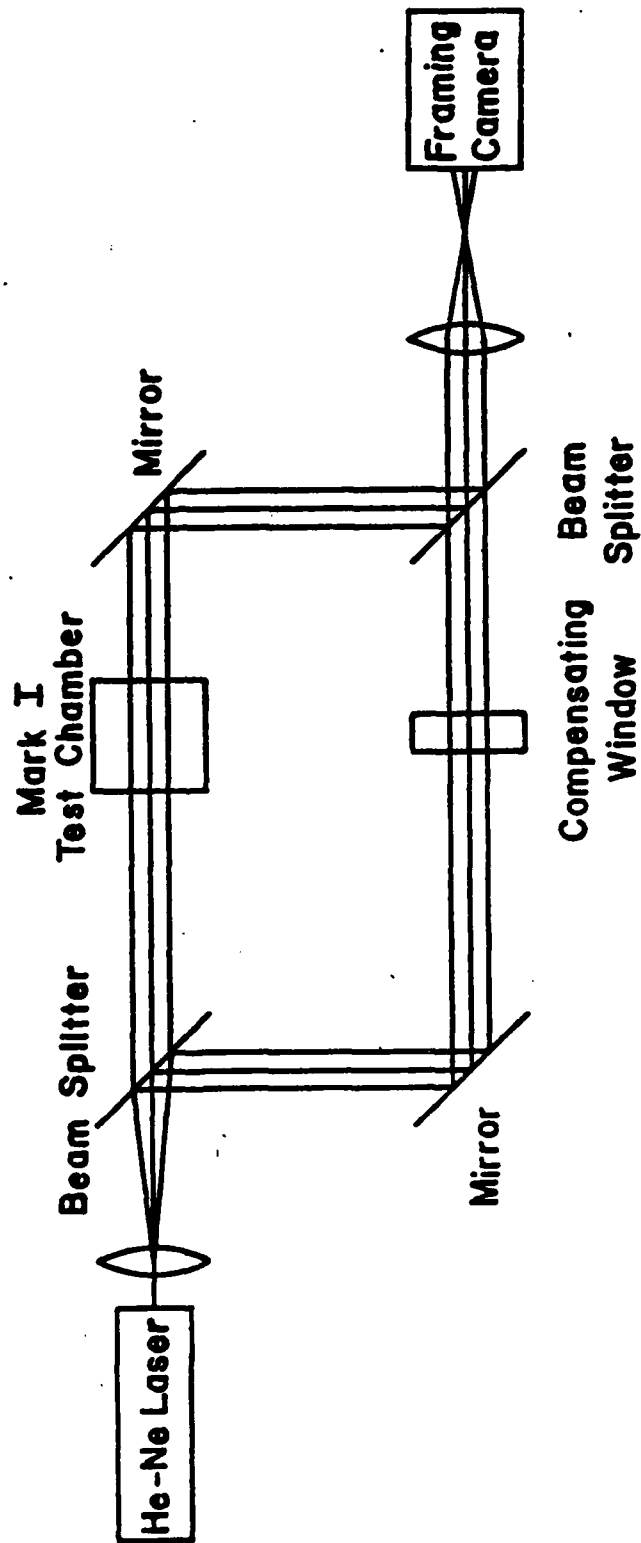


Fig. 16. Mach Zehnder Interferometry Set-up for Mark I Recovery Studies



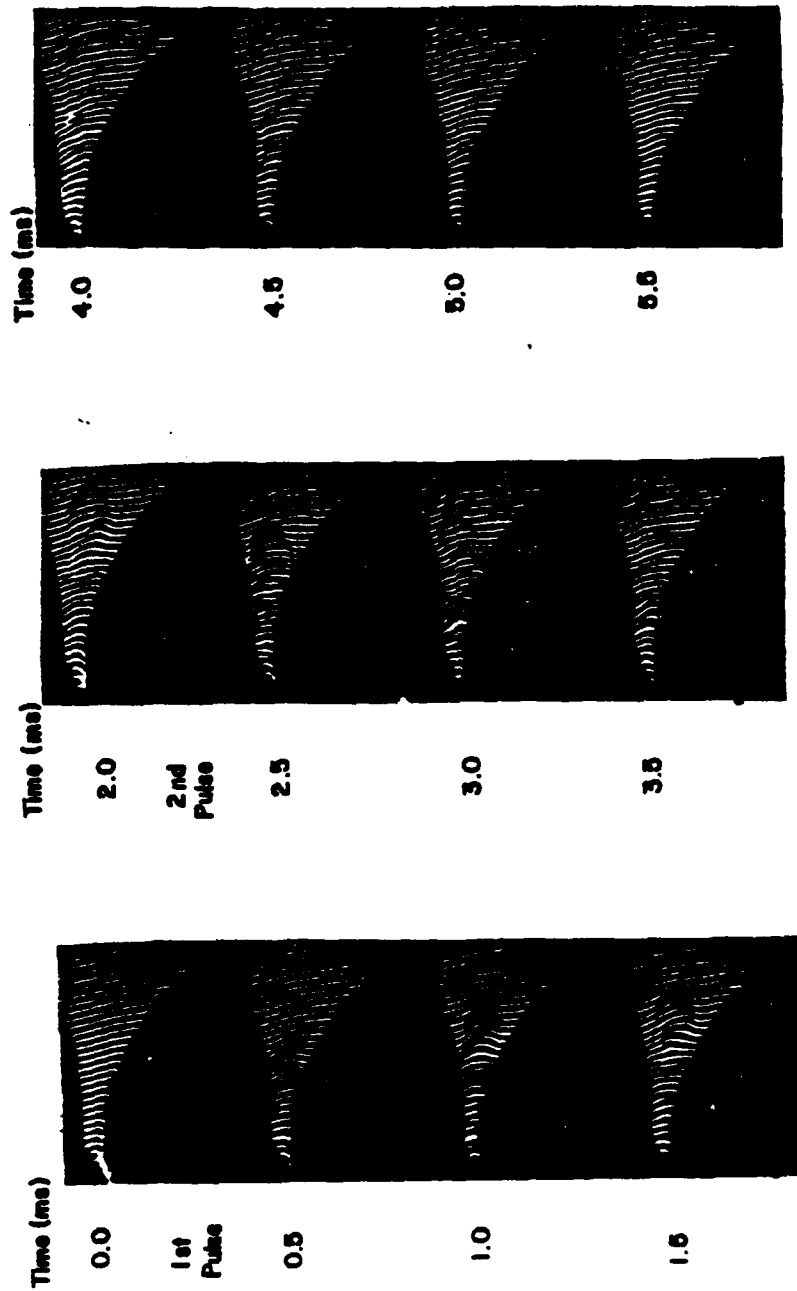


Fig. 17. Interferograms of Mark I First and Second Pulse Recovery  
Framing Interval: 0.5 ms, Exposure Time: 6  $\mu$ s

direction for times up to several milliseconds after the current pulse.

The time scale for these processes appears related to the measured recovery times, but a final explanation of these density variations requires additional experiments (for instance, extension to faster time scales to measure also the well known arc expansion/shock wave propagation and the use of material sensitive diagnostics, e.g. laser induced fluorescence (LIF)).

#### E. REFERENCES

1. V.E. Il'in and S.V. Lebedev, Sov. Phys. Tech. Phys., 7, 717 (1963).
2. S. Levy, U.S. Army Research and Development Lab., TR-2454, (April 1964).
3. G.S. Belkin and V.Ya Kiselev, Sov. Phys. Tech. Phys., 11, 280 (1966).
4. G.S. Belkin, Sov. Phys. Tech. Phys., 13, 1256 (1969).
5. J.E. Gruber and R. Suess, Max Planck Inst. fur Plasmaphysik, Garching bei Munchen, IPP 4/72, (Dec. 1969).
6. B. Carder, Physics International Report, PIIR 12-74, (Dec. 1974).
7. G.S. Belkin and V.Ya. Kiselev, Sov. Phys. Tech. Phys., 23, 24 (1978).
8. Y. Kawakita, et. al., 3rd IEEE Int. Pulsed Power Conf., Albuquerque, NM, 444, (June 1981).
9. K.J. Bickford, et. al., 15th Power Modulator Symposium, Baltimore, MD, (June 1982).
10. A.L. Donaldson, et. al., to appear in IEEE Trans. on Plasma Science.
11. Third Annual Report on Coordinated Research Program in Pulsed Power Physics, December 1, 1982, AFOSR Contract # F 49620-79-C-0191.

12. T. Martin, Sandia National Laboratory, private communication.
13. K.K. Namitotkov, Sov. Phys. Tech. Phys., 12, 714, (1967).
14. G.S. Belkin and V.Ya Kiselev, Sov. Phys. Tech. Phys., 12, 719 (1967).
15. J.C. Sherman, et.al., 4th IEE Int. Gas Discharge Conference, IEE Publ. # 143., 94 (1976).
16. R. Basharov, et.al., Sov. Phys Tech. Phys., 12, 1383 (1968).
17. G. Jackson, et. al, 4th IEEE Int. Pulsed Power Conf. Albuquerque, NM, (June 1983).
18. H. Knoepfel, Pulsed High Magnetic Fields, North Holland Publishing Company, Amsterdam-London, (1970).
19. S.I. Braginskii, Sov. Phys. JETP 34, 1068 (1958).

## APPENDIX I

MODELING OF SELF-BREAKDOWN VOLTAGE STATISTICS  
IN HIGH ENERGY SPARK GAPS\*

A. L. Donaldson, R. Ness, M. Hagler, M. Kristiansen  
Department of Electrical Engineering/Computer Science  
and

L. L. Hatfield  
Department of Physics  
Texas Tech University, Lubbock, Texas 79409

Abstract

A model which incorporates the influence of electrode surface conditions, gas pressure, and charging rate on the voltage stability of high energy spark gaps is discussed. Experimental results support several predictions of the model; namely, that increasing pressure and the rate of voltage charging both produce a broadening of the self-breakdown voltage distribution, whereas a narrow voltage distribution can be produced by supplying a copious source of electrons at the cathode surface. Experimental results also indicate that two different mechanisms can produce this broadening, both of which can be taken into account with the use of the model presented. Further implications of the model include changes in the width of the self-breakdown voltage probability density function as the primary emission characteristics of the cathode are modified by, for example, oxide or nitride coatings and/or deposits from the insulator. Overall, the model provides a useful and physically sound framework from which the properties of spark gaps under a wide variety of experimental conditions may be evaluated.

---

\* Submitted to Journal of Applied Physics

### Introduction

Low-jitter, triggered spark gaps are needed for a wide variety of switching applications, including fusion machines<sup>1</sup>, weapons systems, and high energy physics experiments. To achieve low jitter, the switch should be triggered as close to the self-breakdown voltage as possible. Thus, an ideal switch should have a delta function for the self-breakdown voltage probability density function. In actual operation the self-breakdown voltage will be somewhat erratic, and in most cases "prefires", or breakdown voltages which are significantly less than the mean, will occur. The self-breakdown voltage density functions and the respective distributions for these cases are shown in Fig. 1. This paper presents a model which incorporates the processes which can produce the voltage distribution shown in Fig. 1b. The problem of prefires is not addressed here but is being considered for future work.

Numerous studies<sup>2-6</sup> have shown that the choice of gas, electrode, and insulator material can significantly influence the width and shape of the actual voltage density function. More specifically, several studies<sup>7-9</sup> have suggested a correlation of the statistical distribution in the self-breakdown voltage of a spark gap and the properties of the cathode surface, including its microstructure. The data have been interpreted in terms of models that consider:

- 1) the effect of the field enhancement, due to cathode microstructure, and the effect of lower surface work functions, resulting from surface coatings, on the generation rate of electrons at the cathode<sup>7,10,11</sup>,

- 2) the effect of the field enhancement on Townsend's first ionization coefficient,  $\alpha$ ,<sup>7,12,13</sup>, and
- 3) the effect of the surface coatings and the applied field on the secondary emission coefficient,  $\gamma$ , at the cathode<sup>14</sup>.

These models usually include the concept of waiting-for-an-electron, in that breakdown is assumed to occur when the first electron appears at the cathode after a breakdown condition (usually the Townsend condition) has been satisfied<sup>a</sup>. The theoretical model presented here includes all of these mechanisms by which the cathode surface can affect the statistical distribution in the breakdown voltage, and includes the field enhancement effects on the cathode surface in a new way.

### Theoretical Model

#### General Case

Consider a spark gap subjected to a monotonically increasing applied voltage,  $v(t)$ . Denote the breakdown voltage, a

---

<sup>a</sup> It should be noted that Hodges<sup>10</sup> took into account the Wijsman probability<sup>15</sup> which allows for no breakdown to occur even if the above criteria are satisfied. However, this effect was ignored in the present analysis since the Wijsman probability goes from 0 to 1 quite rapidly near self-breakdown and the modeling of this effect is quite uncertain for electronegative gases at higher pressures<sup>11</sup>.

random variable, as  $V$ . The field enhancement factor,  $M$ , defined as the ratio of the enhanced electric field at the cathode with microstructure to the electric field without microstructure, is also considered to be a random variable (the underlying sample space is the geometrical surface of the cathode). The random variable  $M$  is characterized by a probability density function,  $p_M(m)$ . A basic assumption of the model is that the gap breaks down when an electron is born at a site on the cathode surface where  $M$  is as large as or larger than the value that satisfies the breakdown condition (perhaps Townsend or streamer) at the particular voltage applied. We denote this threshold value of the field enhancement as  $m_t(v)$ . Physically we expect that  $m_t(v)$  is a monotonically decreasing function of  $v$  ( $\partial m_t(v)/\partial v < 0$ ), an increasing function of pressure ( $\partial m_t(v)/\partial p > 0$ ), and that  $m_t(0) = \infty$  and  $m_t(v_{\max}) = 1$ . Figure 2 shows an actual calculation of  $m_t(v)$  using a model microstructure described in Appendix A. The trends for this model are listed in Table I.

We now calculate the probability,  $p_t$ , that the gap breaks down during the time between  $t$  and  $t + \Delta t$  and hence at a voltage between  $v$  and  $v + \Delta v$ . For  $\Delta t$  small, the probability ( $\Delta p_t$ ) that an electron is born between  $t$  and  $t + \Delta t$  at a site where  $M$  takes a value between  $m$  and  $m + \Delta m$  is

$$\Delta p_t = \frac{i_e(m, v(t))}{e} \Delta t p_M(m) \Delta m \quad (1)$$

The quantity  $e$  is the charge on an electron and  $i_e$  is the primary electron current generated at the cathode. In general,  $i_e$  could be generated by:

- a) cosmic rays ionizing the gas in front of the cathode surface<sup>16</sup>,
- b) Fowler-Nordheim field emission<sup>17</sup>, and/or
- c) Schottky field assisted thermal emission<sup>10</sup>.

These emission processes could occur directly from the cathode material or from compounds existing on the cathode surface whose work function is usually lower than that of the metal and which can be effectively lowered even further by surface charging. Thus, in general,  $i_e$  could be a function of total cathode surface area, voltage, field enhancement, temperature, and work function. The last three are also functions of the position on the surface. For the following formulation, however, we will represent  $i_e$  as an explicit function of field enhancement and voltage only.

If  $\Delta t$  is large compared with the time of avalanche formation (see Appendix B), then the probability that the gap breaks down between  $t$  and  $t + \Delta t$  is

$$p_t(\Delta t) = \frac{\Delta t}{e} \int_{m_t(v)}^{\infty} i_e(m, v(t)) p_M(m) dm \quad (2)$$

Let the random variable  $T$  represent the time elapsed before breakdown of the gap. Then, from Eq. (2), the probability density function for  $T$  is readily seen to be<sup>18</sup>



$$p_T(t) = f(t) \exp \left[ - \int_0^t f(\tau) d\tau \right] \quad (3)$$

where

$$f(t) = \frac{1}{e} \int_{m_t(v(t))}^{\infty} i_e(m, v(t)) p_M(m) dm. \quad (4)$$

Since, by assumption,  $v(t)$  is a monotonic function of  $t$ , then the probability density function for the breakdown voltage,  $v$ , is<sup>19</sup>

$$p_V(v) = p_T(t(v)) \left/ \left| \frac{dv}{dt} \right| \right. \quad (5)$$

or<sup>20</sup>

$$p_V(v) = \frac{\lambda(v)}{v'} \exp \left[ - \int_0^v \frac{\lambda(\eta) d\eta}{v'} \right], \quad (6)$$

where  $v'$  is the derivative of the charging voltage with respect to time  $(dv(t)/dt)$  and

$$\lambda(v) = \frac{1}{e} \int_{m_t(v)}^{\infty} i_e(m, v) p_M(m) dm. \quad (7)$$

It is easy to see that

$$F_V(v) = \int_0^v p_V(\xi) d\xi = 1 - \exp \left[ - \int_0^v \frac{\lambda(\eta) d\eta}{v'(\eta)} \right], \quad (8)$$

where  $F_V(v)$  is the cumulative probability distribution for the random variable,  $v$ . Equation (8) shows that the width of the self-breakdown voltage distribution: 1) decreases with increasing  $i_e$ , 2) increases with increasing  $m_t$  caused by, for example, an increase in operating pressure, and 3) increases with increasing  $v'$ , the charging rate. Note that  $v'$  is to be evaluated at  $v$ , and hence can be considered as a function of  $v$ , namely,  $v' = v'(v)$ .

If  $v(t)$  is a ramp, then  $v' = v_0'$ , a constant. If  $v(t)$  is an RC charging waveform, then  $v' = (v_0 - v)/RC$  where  $v_0$  is the charging voltage. If  $v(t) = A(1 - \cos \omega t)$  for  $0 \leq \omega t \leq \pi$ , then  $v' = \omega \sqrt{v(2A - v)}$ .

From Equations (7) and (8), it is easy to show<sup>20</sup> that

$$\frac{1}{e} \int_{m_t(v)}^{\infty} i_e(m, v) p_M(m) dm = \frac{v' p_V(v)}{1 - F_V(v)} \quad (9)$$

Notice that all the terms on the right hand side of Eq. (9) can be measured experimentally. This will hold true for the special cases discussed below as well. This is an important result, for even when  $i_e$  depends on (implicit) variables other than  $m$  and  $v$ , the function  $v' p_V(v)/(1 - F_V(v))$  should still describe the results.

### Special Cases

To proceed further, consider two special cases of the model. First, suppose that  $i_e(m, v)$  is constant so that field enhancement distribution effects from the cathode surface microstructure and waiting-for-an-electron effects are the primary physical mechanisms included in the model. This circumstance is likely to hold, for example, when the cathode is illuminated with sufficiently intense ultraviolet radiation so that any field emission current is dwarfed by photoelectric current, which should be independent of  $M$  and  $V$ . If  $i_e = i_{eo}$ , a constant, then Eq. (9) gives

$$\frac{i_{eo}}{e} [1 - F_M(m_t(v))] = \frac{v' p_V(v)}{1 - F_V(v)} \quad (10)$$

where  $F_M(m)$  is the cumulative probability distribution for the random variable,  $M$ . If we know  $m_t(v)$ , we can determine  $F_M(m)$  by plotting  $F_M(m_t(v))$  versus  $m_t(v)$ . Therefore, for this special case it is possible, in principle, to deduce  $F_M(m)$  from  $p_V(v)$  (self-breakdown voltage histogram) under a given set of conditions and thus predict  $p_V(v)$  (or  $F_V(v)$ ) for a different  $v'$  or gas pressure (which affects  $m_t(v)$ ), for example. For this special case, Eq. (8) becomes

$$F_V(v) = 1 - \exp \left[ - \frac{i_{e0}}{e} \int_0^v \frac{[1 - F_M(m_t(\eta))]}{v'} d\eta \right] \quad (11)$$

Consider now a second special case in which  $p_M(m) = \delta(m - m_0)$ , where  $\delta(\cdot)$  is the Dirac delta function and  $m_0$  is a constant. In this case the field enhancement is assumed to be uniform (that is, sufficiently characterized by its mean value rather than its distribution) so that the primary effects included are the voltage dependence of the primary electron current,  $i_e$ , and waiting-for-an-electron. In this case Eq. (8) becomes

$$F_V(v) = 1 - \exp \left[ - \frac{1}{e} \int_{v_t}^v \frac{i_e(m_0, \eta) d\eta}{v'} \right], \quad (12)$$

where  $v_t$  is the threshold voltage, and  $m_t(v_t) = m_0$ , while Eq. (9) becomes

$$i_e(m_0, v) = \frac{v' p_V(v)}{1 - F_V(v)}. \quad (13)$$

### Experimental Arrangement

The experimental arrangement and the system diagnostics used to test the theoretical results are shown in Fig's. 3 and 4. The construction of this facility and the development of the modeling software is described elsewhere<sup>9,21</sup>. The test circuit shown in Fig. 4 consists of a high energy (2 kJ) pulse forming network (PFN) and a low energy (<1 mJ) RC probing circuit. The PFN is used to generate an electrode surface which is characteristic of a high energy switch. The RC probing circuit is used to generate the voltage distributions with a low energy, low current pulse so that the equilibrium temperature is reached prior to each shot. This low energy circuit is also used so that the surface microstructure will not be altered significantly from shot to shot. The pressure in the spark gap could be raised to 3.5 atmospheres and the voltage ramp rate could be varied from 3 to 60 kV/s by changing  $R_C$ . A 5 Watt UV lamp was used to generate additional electrons at the cathode surface when needed.

A testing sequence consisted of firing 2000 - 7000 shots at high energy, waiting approximately one hour for the electrode to cool, and proceeding with several series of 500 low energy shots with different  $i_e$ ,  $v'$ , and pressure.<sup>b</sup> Figure 5 shows a typical electrode surface generated by the high energy pulses for the case of 304 stainless steel run in one atmosphere of nitrogen gas

---

<sup>b</sup> The Kolmogorov - Smirnoff<sup>22</sup> test indicates that this number of shots should determine  $F_V(v)$ , within a confidence level of 99%, to an accuracy of 7%.

at a gap separation of 5 mm. Examination of the electrode surface after application of the low energy pulses indicates that no significant changes had occurred which might alter the breakdown statistics.

### Experimental Results

Several experiments were performed to verify the model's predictions for the effect of  $i_e$ ,  $v'$ , and pressure on the probability density function  $p_v(v)$ . In the first experiment, an UV source was used to generate a continuous supply of photoelectrons at the surface of a stainless steel electrode in air. Figure 6 shows that, without UV, the density function is very broad; indicating that the cathode surface is a very poor emitter of electrons. However, with the UV source on, the density function collapsed to the lowest value of breakdown voltage. Nitta, et al.<sup>23</sup>, observed the same effect in  $\text{SF}_6$  at pressures up to 2 atm. This result is significant for at least two reasons. First, it supports the waiting-for-an-electron concept as one mechanism responsible for statistical variation in the self-breakdown voltage; and second, it provides an externally controllable experimental "switch" where the effect of waiting-for-an-electron can be turned on or off. The behavior observed is consistent with Eq. (8).

A second experiment consisted of varying the voltage ramp rate  $v'$  from 3 kV/s ("slow" ramp) to 30 kV/s ("fast" ramp). According to the model (Eq. (8)), if you are waiting for an electron to appear, then the faster the ramp rate, the higher the breakdown voltage will be when the electron appears and thus the

greater the scatter in the density function,  $p_V(V)$ . Figure 7 shows that this effect was indeed observed. Also, from Eq. (8), the density function for the slower ramp rate could be theoretically calculated from the data for the fast ramp rate. Figure 7 shows this result for the assumption  $i_e = i_{e0}$ , a constant. The result is fair, indicating that for better agreement a more realistic expression for  $i_e$ , perhaps  $i_e(m, V)$ , would have to be used.

Previous work<sup>13,24-26</sup> has shown that with the presence of cathode microstructure, an increase in pressure can lead to significant deviations from the Paschen curve breakdown voltage if the product of the protrusion height and the pressure is greater than a gas dependent threshold. For example, Berger<sup>13</sup> calculated that pressure-height products of  $30 \mu\text{m}\cdot\text{atm}$  for  $\text{SF}_6$  and  $200 \mu\text{m}\cdot\text{atm}$  for air would be required for the onset of breakdown voltage modifications due to enhanced ionization occurring near the microstructure. Avrutskii<sup>8</sup> stated that an increase in pressure should lead to an increase in scatter in the breakdown voltage, but no data were given. Thus, in order to understand the effect of pressure on the breakdown voltage statistics for a surface with large protrusions, the brass sample shown in Fig. 8 was generated and the breakdown voltages were recorded for pressures up to 3.5 atmospheres. (Earlier work in electrode erosion showed that brass electrodes in high energy operation can form protrusions up to  $500 \mu\text{m}$ <sup>21</sup>.) Figure 9 clearly shows an increase in scatter, especially at the low end, in the density function  $p_V(V)$  for higher pressures. If the effect is due to field enhancements, then the calculated range of  $m$ 's at any pressure should be

the same since the distribution of surface field enhancements is not changing from shot to shot. For  $p = 1.7$  atm, the range of  $m$ 's, calculated using the model in Appendix A, was 1 - 2.93; for  $p = 2.5$  atm, the range was 1 - 3.63.

Increased scatter has also been observed for electrode surfaces with microstructures much smaller than the amount required to affect the breakdown voltage. Figure 10 shows the breakdown voltage distribution as a function of pressure for graphite electrodes in air. The electrode surface had no protrusions greater than  $10\text{ }\mu\text{m}$ . Although the pressure-height product is an order of magnitude less than the amount required to affect the breakdown voltage by enhanced ionization<sup>13</sup>, there is still a significant spreading of the distribution at higher pressures. Unlike the results for the brass electrodes, the spreading occurs at the high end of the distributions, i.e., for voltages larger than those calculated from the Townsend breakdown criteria for a gap without protrusions, and  $M = 1$ . Whereas the results for brass indicated a lowering of the Townsend breakdown criteria due to enhanced ionization, the results for graphite indicate that a different mechanism is producing the scatter at high pressures; seemingly, by altering the effective generation rate of electrons.

The pressure data were also found to be of importance for analyzing the different  $i_e$  cases which were studied theoretically. Figure 11 shows theoretical plots of the quantity

$v'p_V(v)/(1-F_V(v))$  for the three physical cases discussed earlier: a)  $i_e = i_e(m_0, v)$ ,  $m_0$  is a constant over the entire surface (Eq. (13)); b)  $i_e = i_{e0}$  is a constant (Eq. (10)); and c) the most general case,  $i_e = i_e(m, v)$  which assumes a distribution of surface field enhancements (Eq. (9)). A Gaussian distribution in field enhancements was used for cases b) and c). The function  $m_t(v)$  was calculated using the model described in Appendix A and a Schottky emission current was used for  $i_e(m, v)$ . Case a) illustrates that if there is no spread in the distribution for  $M$  (Eq. (13)), then an increase in pressure will correspond simply to a higher emission current because of the higher breakdown voltage, which is typical for a field dependent Schottky or Fowler-Nordheim emission mechanism<sup>10</sup>. A higher emission current at higher pressure would imply narrower statistics, but experimental results indicate just the opposite; namely, broader statistics at higher pressures. However, in case b) for a fixed voltage, the increase in pressure has the effect of raising the threshold,  $m_t$ , required for breakdown, which raises  $F_M(m_t(v))$ , and thus the function  $v'p_V(v)/(1-F_V(v))$  is multivalued and decreases with increasing pressure (Eq. (10)). For case c)  $v'p_V(v)/(1-F_V(v))$  is also multivalued and decreases with increasing pressure, but in a different way (Eq. (9)). For a fixed voltage, and assuming that the surface features do not change with pressure, the integrand is constant with increasing pressure. However, the lower limit on the integral, namely  $m_t(v)$ , increases with increasing pressure which has the effect of reducing the value of the function.



Figure 12 is a plot of the function  $v'p_V(v)/(1-F_V(v))$  from experimental data for the pressure data of Figure 9. From this plot it is clearly seen that the experimental data are inconsistent with the theoretical results for case a) (a constant M surface). Thus, the effect of a distribution in field enhancements should be considered in the analysis of the breakdown statistics. In addition, the function  $v'p_V(v)/((1-F_V(v)))$  increases very rapidly with voltage and only very extreme values for the work function,  $\phi < 0.5$  eV, and field enhancement,  $M > 50$ , could give reasonable agreement between the experimental data and the Fowler-Nordheim or Schottky field emission mechanisms.

### Conclusion

A model has been described which correctly accounts for the influence of pressure,  $v'$ ,  $i_e$ , and surface microstructure on the self-breakdown voltage statistics. The model's importance in the area of pulse-charged and triggered switches stems from the fact that the statistics for these systems have been recently shown<sup>27</sup> to be heavily dependent on the self-breakdown statistics discussed in this paper.

Using this model, theoretical and experimental results show:

- 1) The spread in self-breakdown voltages in a spark gap is a function of the charging rate ( $v'$ ) and the cathode surface properties which determine the electron emission current  $i_e$  and the distribution of field enhancement sites  $F_M(m)$ .

2) Increasing  $i_e$  provides a practical method for reducing the width of the self-breakdown voltage density function. This can be accomplished with an external UV source, by sandblasting the electrodes to supply a large number of low work function emitting sites<sup>27</sup>, or perhaps with an electron emission agent introduced into the cathode material<sup>28</sup>.

3) The spread in self-breakdown voltages increases with increasing pressure, and/or increasing charging rate.

4) Increasing pressure had two distinctive effects on the breakdown voltage distributions. For large microstructures ( $>200 \mu\text{m}$ ) on brass electrodes, increasing pressure led to increased scatter at the lower end of the distributions as a result of enhanced ionization near the microstructure. For small microstructures ( $<10 \mu\text{m}$ ) on graphite electrodes, an increase in pressure led to increased scatter at the high end of the distributions which presumably was due to a lowering of the effective electron emission current,  $i_e$ .

5) The function  $v'p_V(v)/(1-F_V(v))$ , which can be computed directly from self-breakdown voltage data, is useful for determining the nature of  $i_e$  for a given set of conditions.

### Acknowledgments

The authors are indebted to B. Conover, P. Krothapalli, K. Rathbun and A. Shaukat for their work on the construction of the experiment and the implementation of the data acquisition system. In addition, a special thanks goes to M. Byrd, J. Clare, R. Davis, L. Heck, R. Higgenbotham, M. Katsaras, and M. C. McNeil for their work on the manuscript.

This work was supported by the Air Force Office of Scientific Research.

### Appendix A

The Townsend breakdown criterion for a spark gap with microstructure is given by

$$\int_h^d \bar{\alpha} dz = K \quad (A-1)$$

where  $\bar{\alpha}$  is the effective ionization coefficient of the gas which is equal to  $\alpha - \eta$ ; and where  $\alpha$  is the Townsend first ionization coefficient,  $\eta$  is the attachment coefficient,  $h$  is the protrusion height,  $d$  is the gap spacing, and  $K$  is a function of  $E/p$  and is obtained from empirical data. The microstructure modifies the voltage which satisfies Eq. (A-1) by altering the electric field and thus  $\alpha$  in the region near the protrusion. One can model the protrusion several ways<sup>12,29</sup>, but the semi-ellipsoidal model shown in Fig. A1 was chosen because the electric field along the  $z$  axis was known analytically and could be expressed in terms of the field enhancement  $M$ . The field for this configuration is given by

$$E(z) = E_0 \left( 1 + (M-1) \frac{h^3}{z^3} \right) \quad (A-2)$$

where

$$E_0 = \frac{d}{\int_h^d E(z) dz / (d-h)}. \quad (A-3)$$

The field enhancement factor  $M$  is related to  $b$ , the radius of the base of the protrusion, and  $h$ , the protrusion height, by the equation

$$M = \frac{c^2}{1-c^2} \left( \frac{1}{2c} \ln \frac{1+c}{1-c} - 1 \right)^{-1}, \quad (\text{A-4})$$

where

$$c = 1 - b^2/h^2.$$

The coefficients  $\bar{\alpha}$  and  $K$  were obtained from the literature<sup>13,30</sup>. Thus, Eq. (A-1) was solved for a variety of conditions and plotted in Fig's. A2-A4. It should be remembered that these graphs are useful only for showing trends since actual surface structure effects are not as simple as a single ellipsoid. Also, it was assumed that  $\alpha$  takes on its equilibrium value instantly, when in reality it would gradually approach its equilibrium value within a few collision paths. This effect was modeled in Fig. A5 and the calculated results in Fig. A6 show that if one takes this into account the effect would be to smooth the surface out or to reduce protrusion effects.

Thus, the values obtained for the breakdown voltage using equilibrium values of  $\alpha$  are lower limits for a given set of conditions.

### Appendix B

In the main body of the paper, it was assumed that the time for avalanche formation (formative time) is sufficiently short so that the applied voltage changes only negligibly ( $<100$  V) during this time. For  $\text{SF}_6$  and air at 1 atm, the maximum formative times are approximately  $100 \mu\text{s}$ <sup>31,32</sup> and thus, for charging rates less than  $1000 \text{ kV/s}$ , this assumption was valid.

If the formative time is not negligible, then it is considered to be a random variable,  $T_f$ , with a probability density  $p_{T_f}(t)$ . The increase in applied voltage during  $T_f$  is a random variable,  $V_f$ . Because the voltage and time are monotonically related<sup>18</sup>

$$p_{V_f}(v) = p_{T_f}(t) \left| \frac{dv}{dt} \right| \quad (\text{B-1})$$

Under these circumstances, the gap breakdown voltage is not simply  $V$ , the applied voltage when the first electron is born at a site at the cathode surface where  $M > m_t$ , but rather the sum of  $V$  and  $V_f$ , which will be called  $U$ .

$$U = V + V_f \quad (\text{B-2})$$

Thus,  $U$  is the sum of two random variables. Its probability density is therefore given by<sup>33</sup>

$$p_U(v) = \int_{-\infty}^{\infty} p_{V,V_f}(v-u,u) du \quad (\text{B-3})$$

where  $p_{V,V^\dagger}(\cdot,\cdot)$  is the joint probability density for  $V$  and  $V^\dagger$ . If  $V$  and  $V^\dagger$  are statistically independent, then this result simplifies to<sup>34</sup>

$$p_U(v) = p_V(v) * p_{V^\dagger}(v) \quad (B-4)$$

where the asterisk denotes convolution in  $v$ ,  $p_V(v)$  is given by Eq. (6) and  $p_{V^\dagger}(v)$  is found using Eq. (B-1). The random variables  $V$  and  $V^\dagger$  are simply transformations of  $T$  and  $T^\dagger$ . Therefore<sup>35</sup>,  $V$  and  $V^\dagger$  will be statistically independent if the formative time,  $T^\dagger$ , does not depend on the time,  $T$ , required for an electron to be born at a site on the cathode surface where  $M \gg m_t$ .

Notice that if the formative time is negligible, then  $p_{V^\dagger}(v)$  becomes  $\delta(v)$ , a Dirac delta function, so that

$$p_U(v) = p_V(v) * \delta(v) = p_V(v) \quad (B-5)$$

This case is the one assumed in the body of the paper.

### References

- 1) R. A. White, Proc. of 3rd IEEE International Pulsed Power Conf., Albuquerque, N.M., (June 1981).
- 2) L. B. Gordon, M. Kristiansen, M. O. Hagler, H. C. Kirbie, R. M. Ness, L. L. Hatfield, and J. N. Marx, IEEE Trans. on Plasma Science, PS-10, 286 (1982).
- 3) E. I. Zolotarev, V. Mukhin, L. E. Polyanskii, and V. N. Trapeznikov, Sov. Phys. Tech. Phys., 21, 340 (1978).
- 4) Physics International Report PISR-127-4, Physics International Co., 2700 Merced Street, Saneandro CA 94577 (July 1969).
- 5) M. T. Buttram, Sandia National Lab Report, Sand 81-1552 (1981).
- 6) T. H. Martin, Air Force Pulsed Power Lecture Note #11, Plasma and Switching Laboratory, Department of Elec. Eng. Texas Tech University (1983).
- 7) V. A. Avrutskii, Sov. Phys. Tech. Phys., 18, 389 (1973).
- 8) V. A. Avrutskii, G. M. Goncharenko, and E. N. Prokharov, Sov. Phys. Tech. Phys., 18, 386 (1973).
- 9) R. M. Ness, Masters Thesis, Texas Tech University, (August 1983).
- 10) R. V. Hodges, R. C. McCalley, and J. F. Riley, Lockheed Missiles and Space Company Report, LMSC-0811978 (1982).
- 11) R. V. Hodges and J. F. Riley, Lockheed Missiles and Space Company Report, LMSC-0877208 (1983).
- 12) A. Pedersen, IEEE Trans. on Power Apparatus and Systems, PAS-94, 1749 (1975).
- 13) S. Berger, IEEE Trans. on Power Apparatus and Systems, PAS-95, 1073 (1976).
- 14) W. S. Boyle and P. Kisliuk, Phys. Rev. 97, 255 (1955).
- 15) R. A. Wijsman, Phys. Rev. 75, 833 (1949).
- 16) M. W. Watts, 5th Int. Conf. on Gas Discharge, University of Liverpool, 11-14 Sept. 1978, 297, (IEE London 1978).
- 17) R. H. Fowler and L. Nordheim, Proc. Roy. Soc. 199, 173-181 (1928).
- 18) W. B. Davenport, Jr. and W. L. Root, An Introduction to the Theory of Random Signals and Noise (McGraw-Hill, New York, 1958) pp. 113-117.



- 19) Ref. 18, pp. 32-34.
- 20) M. O. Hagler, A. L. Donaldson, and R. M. Ness, Texas Tech University Pulsed Power Lab Notes, TTU-EEPP-83-1.
- 21) A. L. Donaldson, Masters Thesis, Texas Tech University, (August 1982).
- 22) R. C. Pfaffenberger and J. H. Patterson, Statistical Methods for Business and Economics, R. D. Irwin, Inc., Homewood, IL, (1977), p. 685.
- 23) T. Nitta, N. Yamada, and Y. Fujiwara, IEEE Trans. on Power Apparatus and Systems, PAS-93, 623 (1974).
- 24) S. Berger, IEEE Trans. on Power Apparatus and Systems, PAS-96, 1179 (1977).
- 25) C. M. Cooke, IEEE Trans. on Power Apparatus and Systems, PAS-94, 1518 (1975).
- 26) I. W. McAllister, Elektrotechnische Zeitschrift-A, 99, 283 (1978).
- 27) T. Martin, Sandia National Labs, private communication, October 1983.
- 28) V. I. Krizhanovskii, A. I. Kuz'michev, G. V. Levchenko, R. B. Luban, and A. I. Shendakov, Sov. Phys. Tech. Phys., 26, 1204 (1981).
- 29) T. J. Lewis, J. of Applied Phys., 26 1405 (1955).
- 30) J. Jones, J. Phys. D., 1, 769 (1968).
- 31) L. H. Fisher, Phys. Rev. 72, 423 (1947).
- 32) P. Narbut, E. Berg, C.N. Workes, and T. W. Dakin, AIEE Trans., 78, 545 (1959).
- 33) J. M. Wozencraft and I. M. Jacobs, Principles of Communication Engineering, Wiley, New York, (1965), pp. 68-69.
- 34) Ref. 32, p. 72.
- 35) Ref. 32, p. 77.

## List of Figures

- Fig. 1. The Self-Breakdown Voltage Probability Density Function,  $p_V(v)$ , and its Distribution Function,  $F_V(v)$  for:  
a) Ideal Spark Gap; b) Actual Spark Gap, c) Actual Spark Gap with Prefires.
- Fig. 2.  $m_t(v)$  vs.  $V$  for Two Different Pressures in Nitrogen.
- Fig. 3. Experimental Arrangement and System Diagnostics.
- Fig. 4. Test Circuits.
- Fig. 5. Stainless Steel Electrode After 2200 High Energy Discharges in Nitrogen: a) Cathode Surface-Top View (Marker is 4 mm); b) Cathode Surface-Side View (Marker is 1 mm).
- Fig. 6. Self-Breakdown Voltage Probability Density Function for Stainless Steel in Air, With and Without UV.
- Fig. 7. Self-Breakdown Voltage Probability Density Function for Different Charging Rates.
- Fig. 8. Surface of Brass Cathode used for Pressure Studies (Marker is 4 mm).
- Fig. 9. Self-Breakdown Voltage Probability Density Function for Brass Electrodes in Air at Different Pressures.
- Fig. 10. Self-Breakdown Voltage Probability Density Function for Graphite Electrodes in Air at Different Pressures.
- Fig. 11. Theoretical Plots of  $v'p_V(v)/(1-F_V(v))$  for: a)  $i_e = i_e(m_0, v)$ ; b)  $i_e = i_{e0}$ ; and c)  $i_e = i_e(m, v)$ .
- Fig. 12. Experimental Plots of  $v'p_V(v)/(1-F_V(v))$ .
- Fig. A1. Elipsoidal Surface Protrusion Model.
- Fig. A2.  $m_t(v)$  vs.  $V$  as a Function of Pressure in Nitrogen.
- Fig. A3.  $m_t(v)$  vs.  $V$  as a Function of Pressure in  $\text{SF}_6$ .
- Fig. A4.  $m_t(v)$  vs.  $V$  as a Function of Protrusion Height for two Different Pressures in Nitrogen.
- Fig. A5. a) Electric field across the gap; b)  $\alpha$  With and Without Correction Factor for Nonequilibrium Values Over a Distance  $S$ .
- Fig. A6.  $m_t(v)$  vs.  $V$  With and Without Equilibrium  $\alpha$  Correction in Nitrogen.

TABLE 1

General trends for the threshold field enhancement  $m_t(v)$  calculated for an ellipsoidal protrusion in a uniform field using the Townsend breakdown criteria in  $N_2$  and the streamer criteria in  $SF_6$ .

<u>TREND</u>	<u>IMPLICATION</u>
T-1: $\frac{\partial V}{\partial m_t} > 0$	The greater the spread in field enhancements, the greater the possible range in breakdown voltages.
T-2: $\frac{\partial m_t}{\partial p} > 0$	The higher the pressure, the higher the required threshold field enhancement for a fixed voltage.
T-3: $\frac{\partial}{\partial p} \left( \frac{\partial V}{\partial m_t} \right) > 0$	For a fixed distribution of field enhancements, the higher the pressure, the greater the possible spread in breakdown voltages.
T-4: $\frac{\partial}{\partial d} \left( \frac{\partial V}{\partial m_t} \right) < 0$	The larger the gap spacing, the smaller the effect of surface microstructure.
T-5: $\frac{\partial}{\partial h} \left( \frac{\partial V}{\partial m_t} \right) > 0$	The larger the microstructure, the greater the spread in breakdown voltage for a fixed distribution of field enhancements.

NOTE: All trends for  $SF_6$  are greater than the trends for nitrogen.

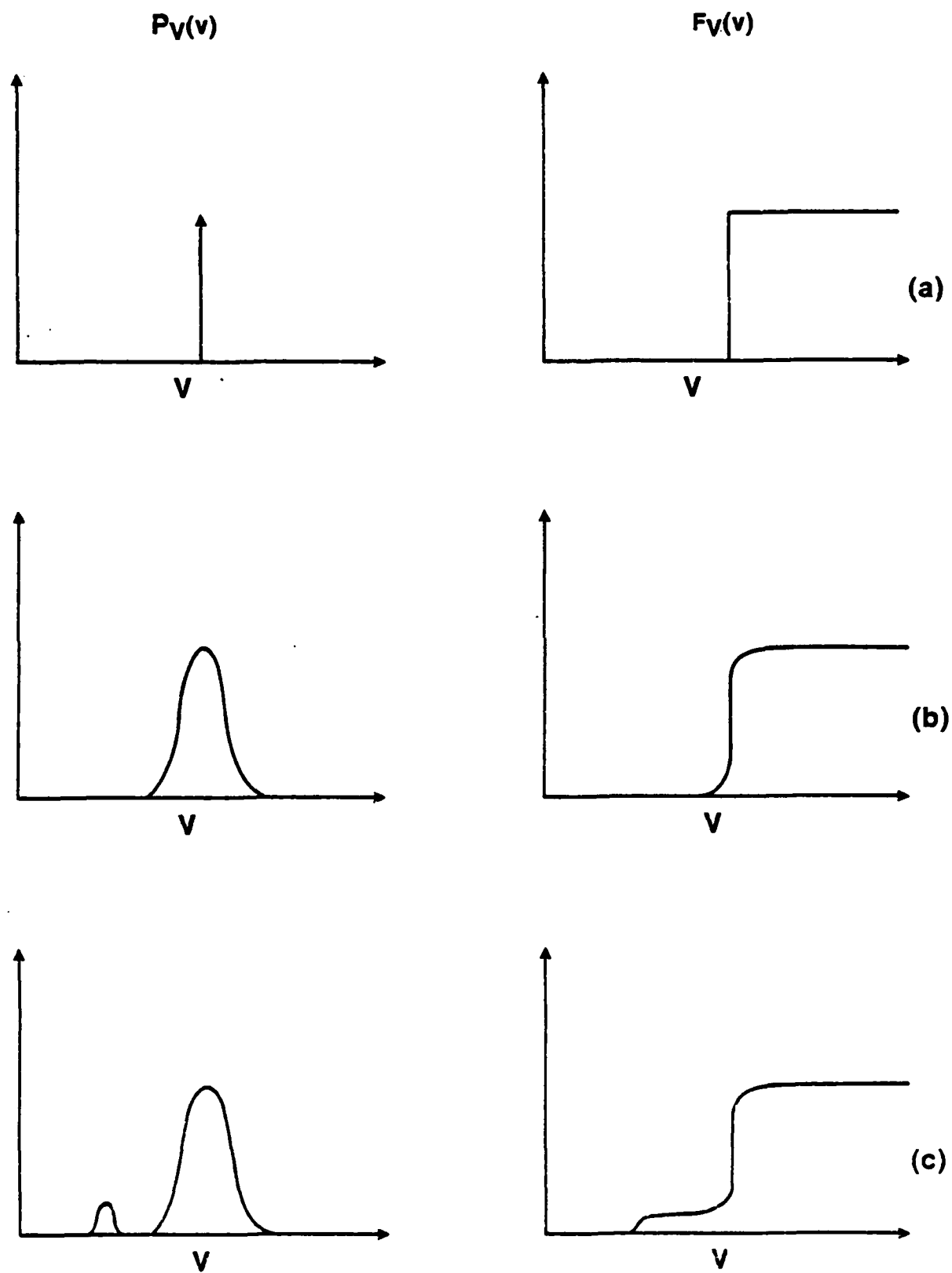


Fig. 1

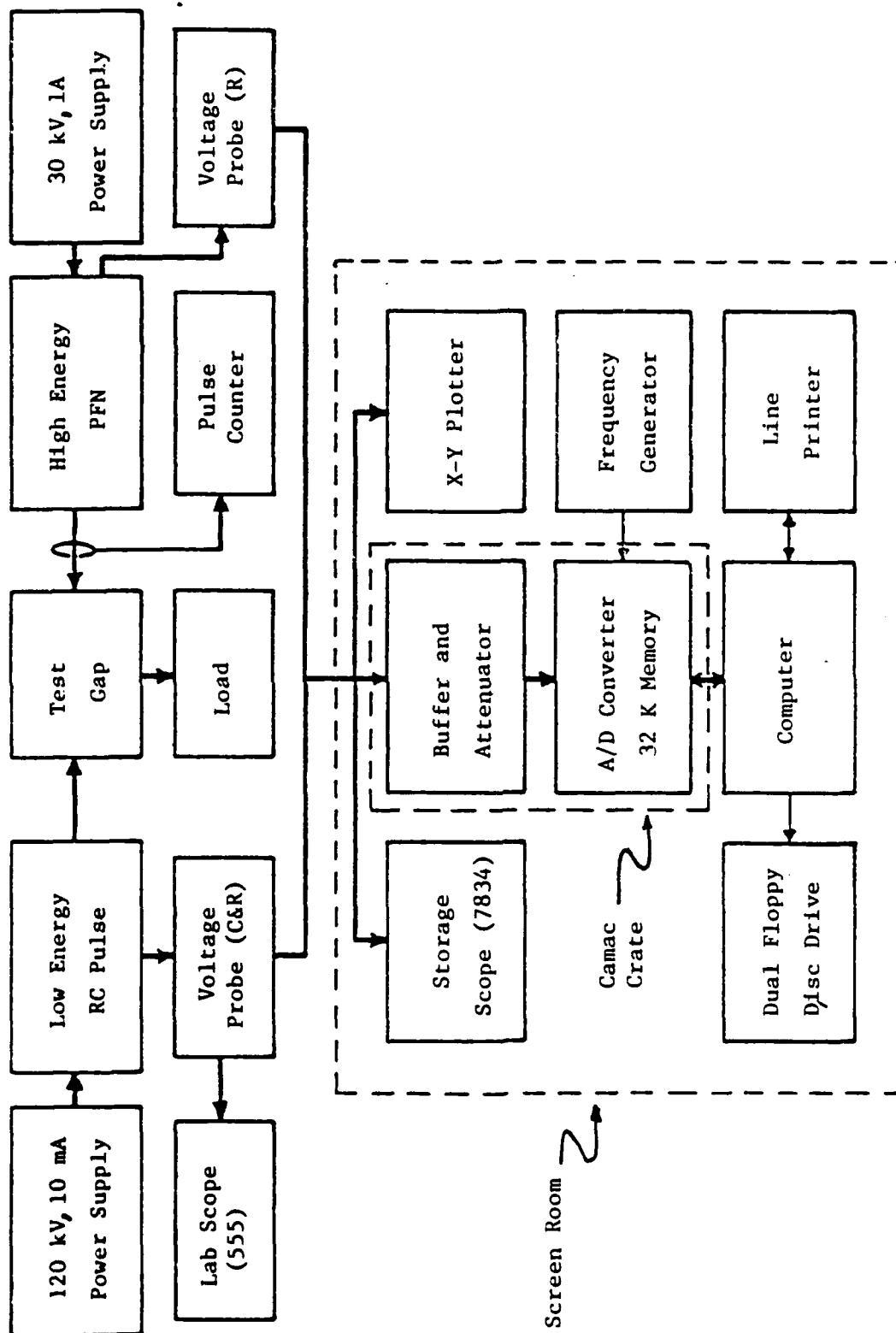


Fig. 2

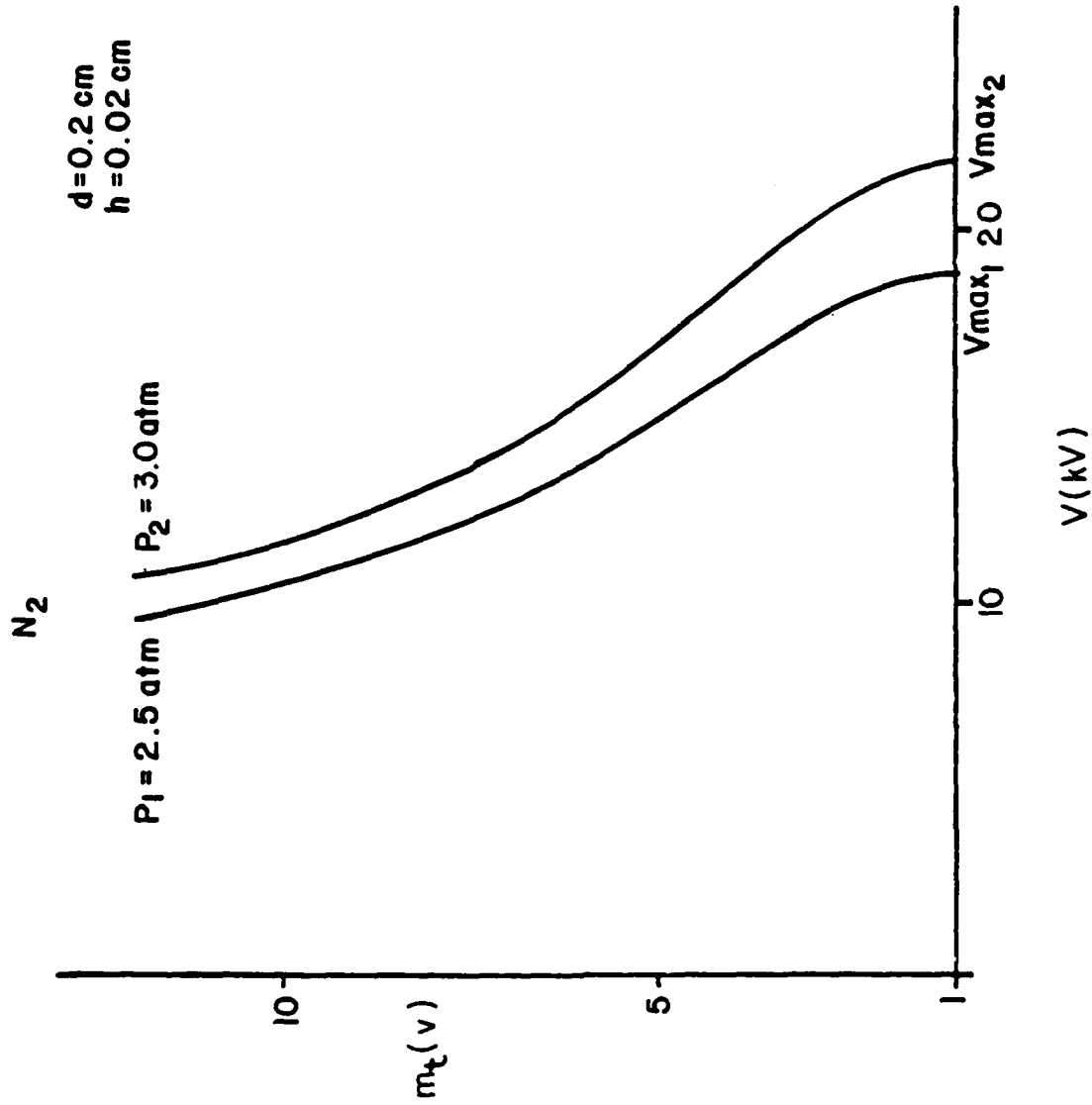
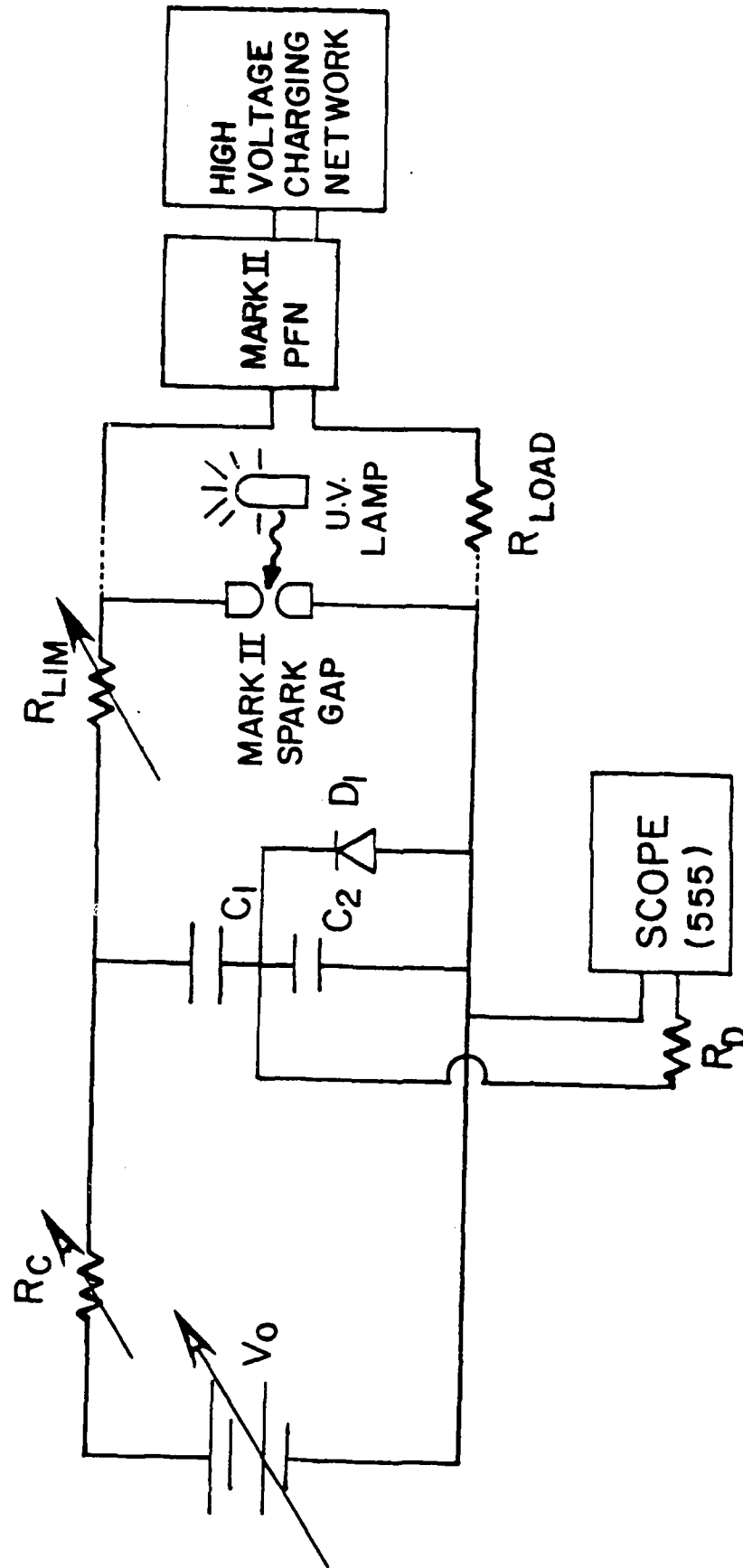


Fig. 3



LOW ENERGY PROBING CIRCUIT FOR  
TESTING BREAKDOWN INITIATION MODEL

Fig. 4

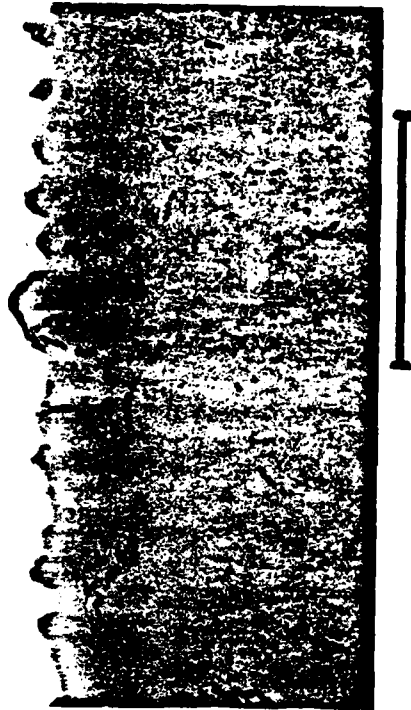


Fig. 5



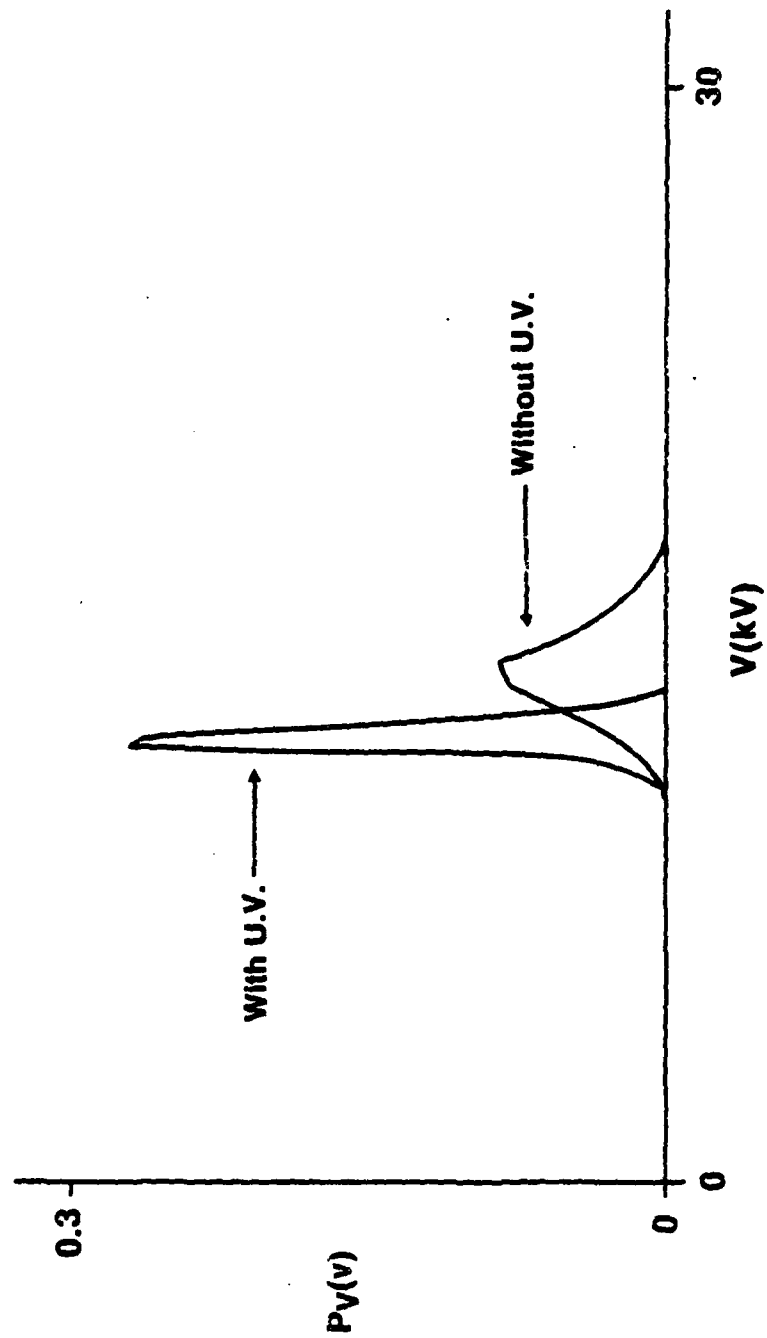


Fig. 6

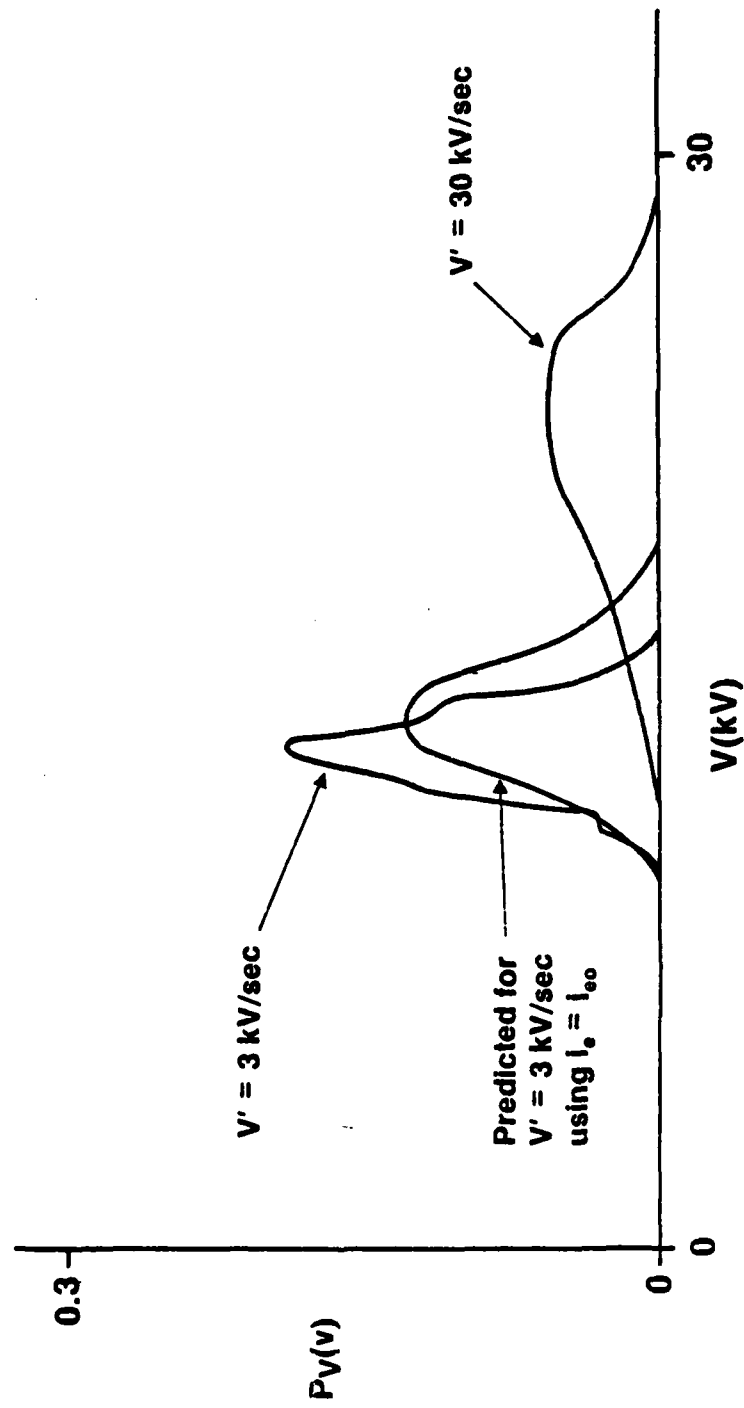


Fig. 7

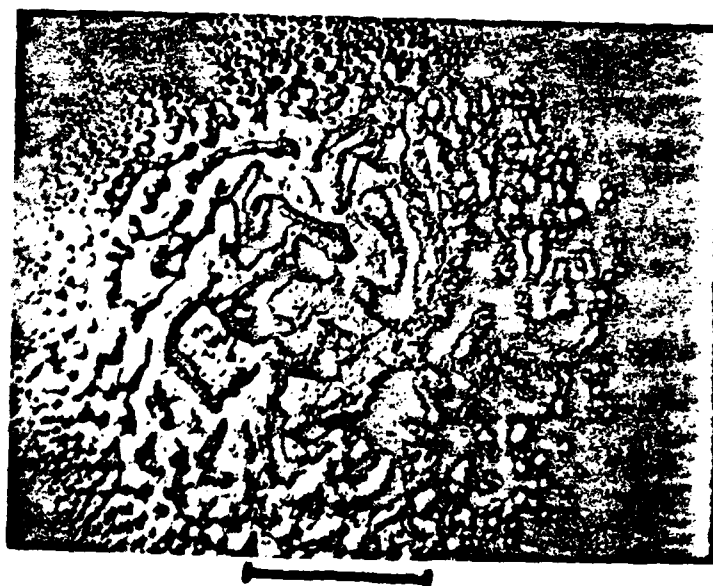


Fig. 8

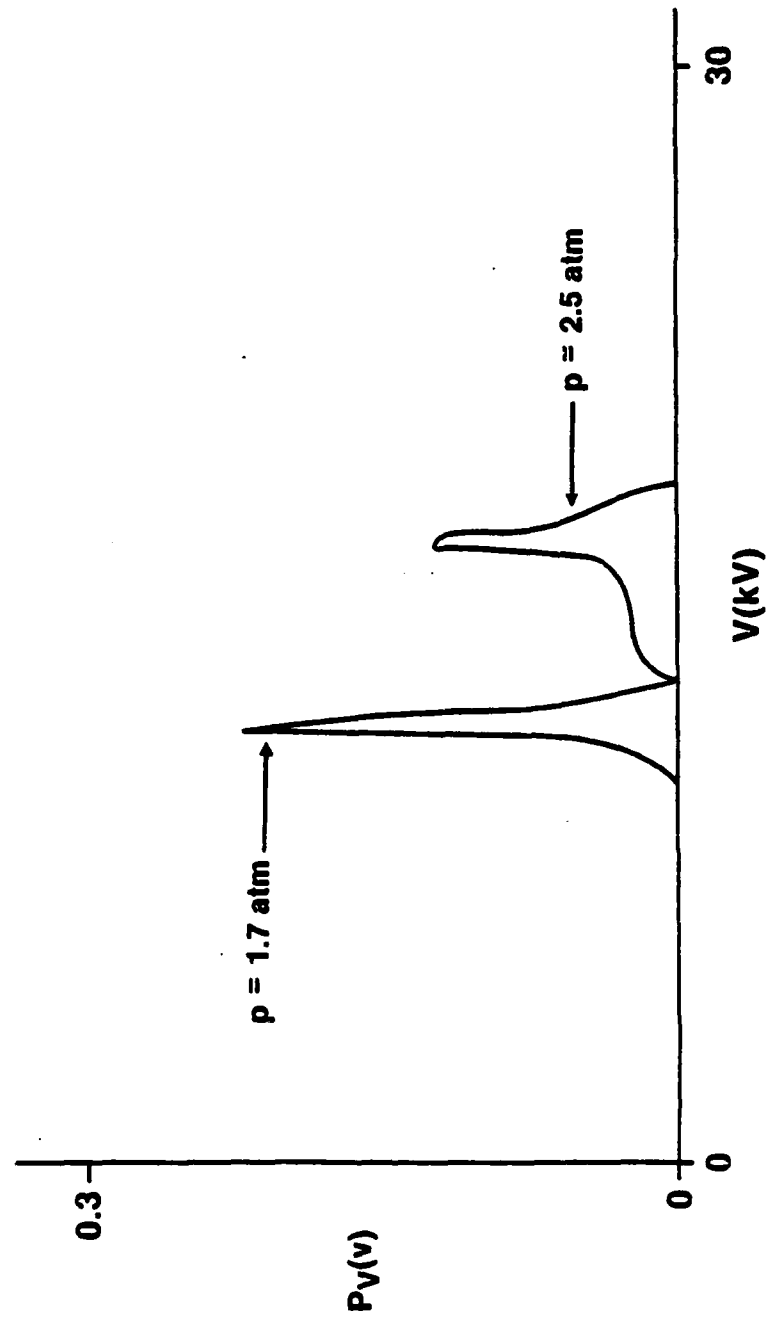


Fig. 9

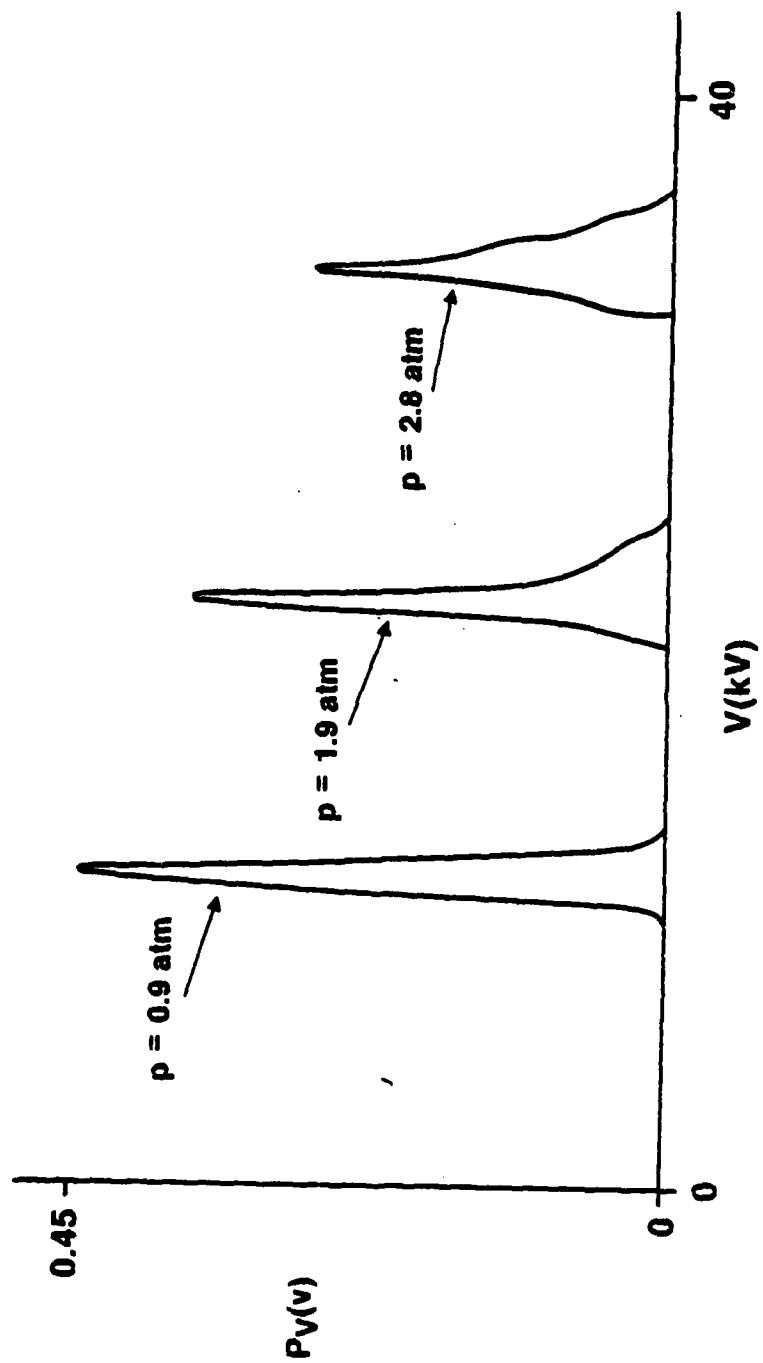


Fig. 10

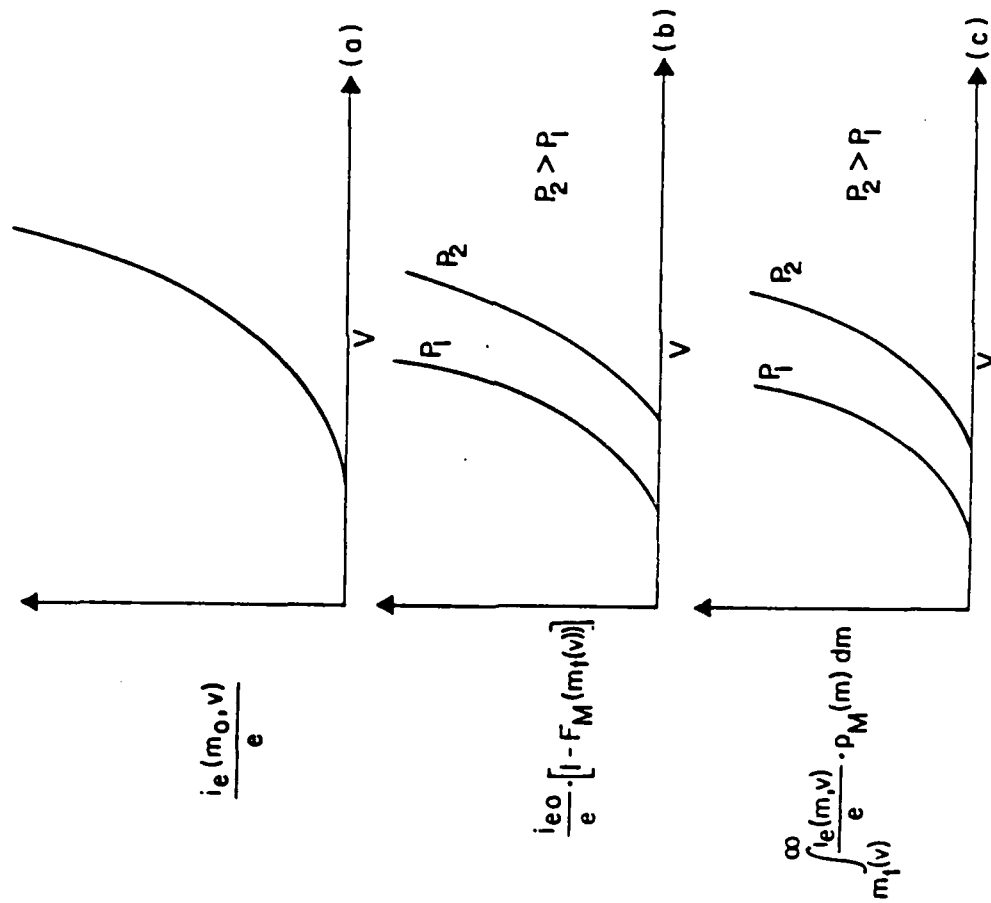


Fig. 11

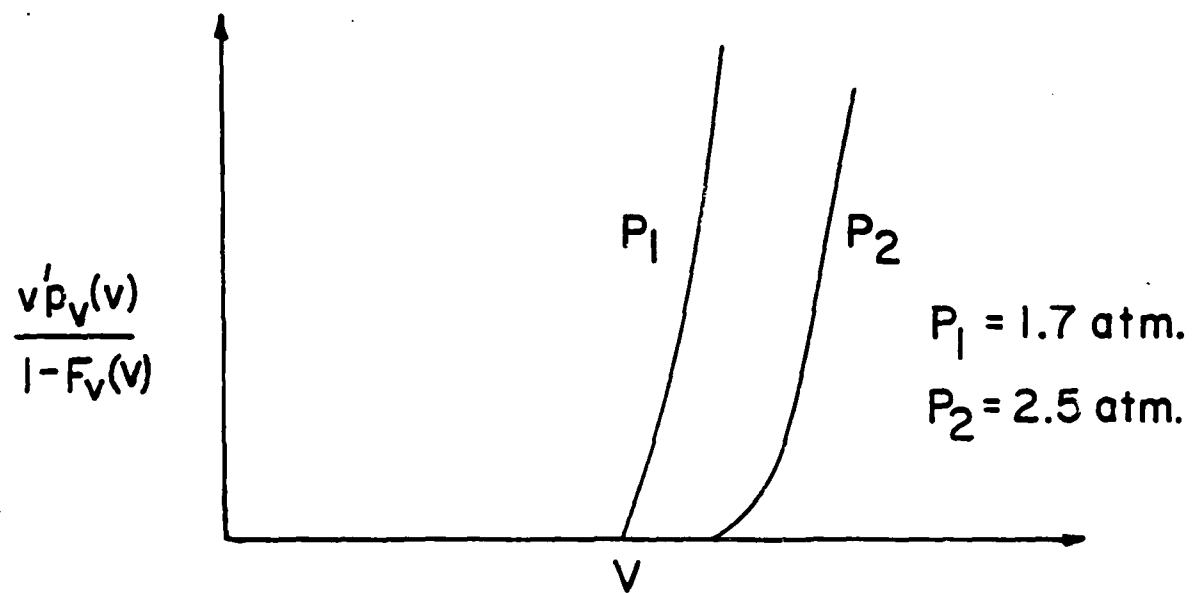


Fig. 12

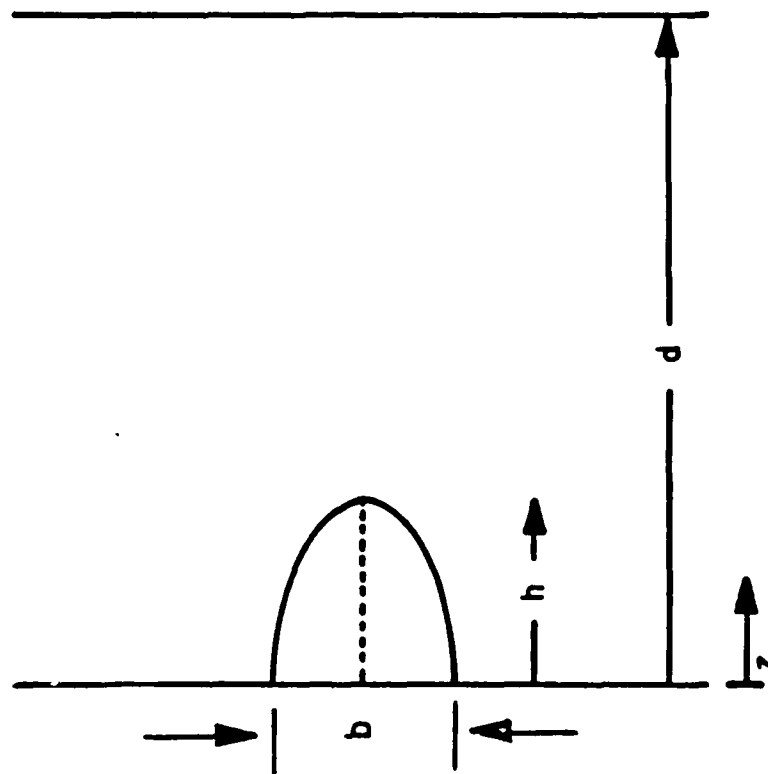


Fig. A1



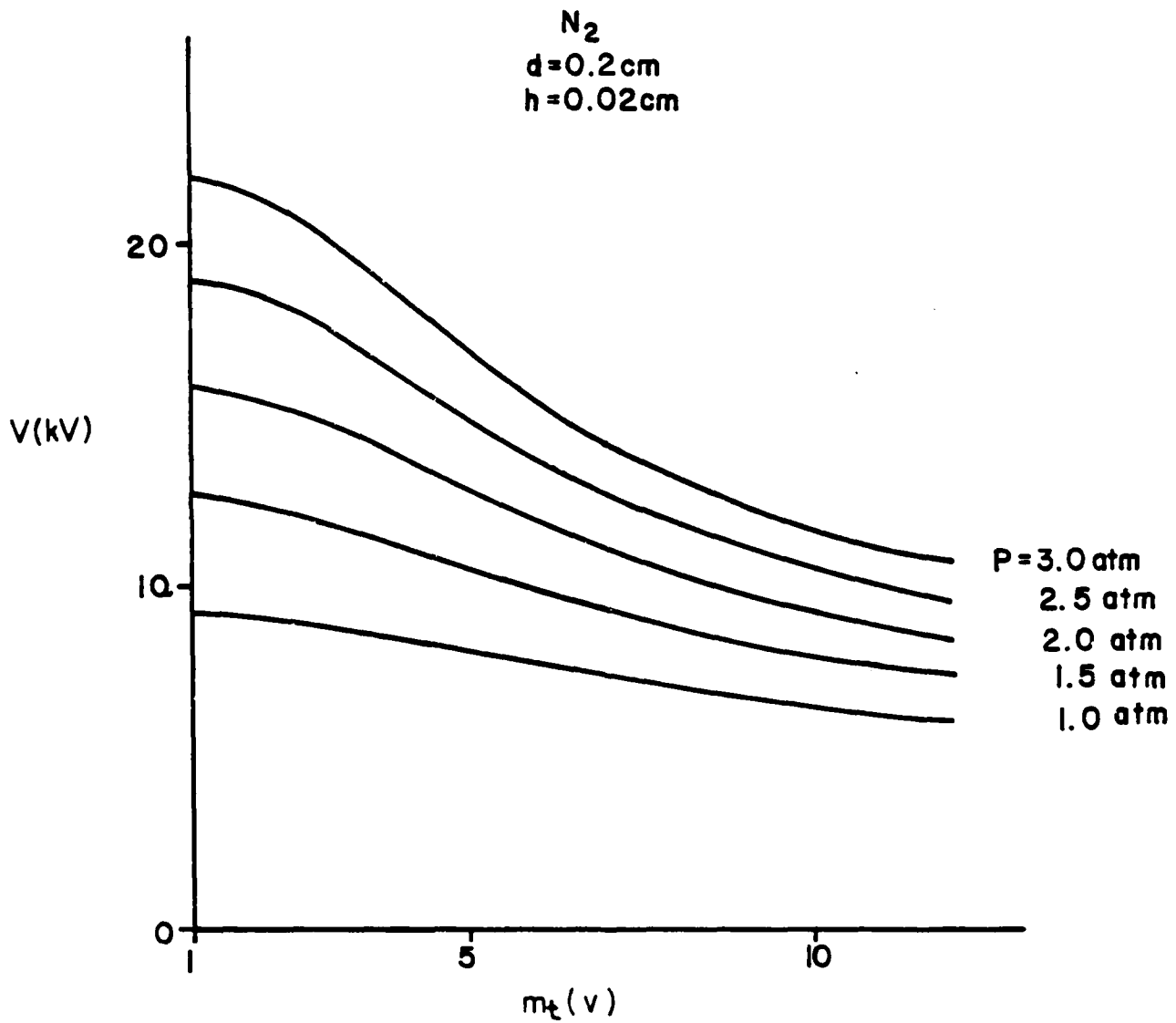


Fig. A2

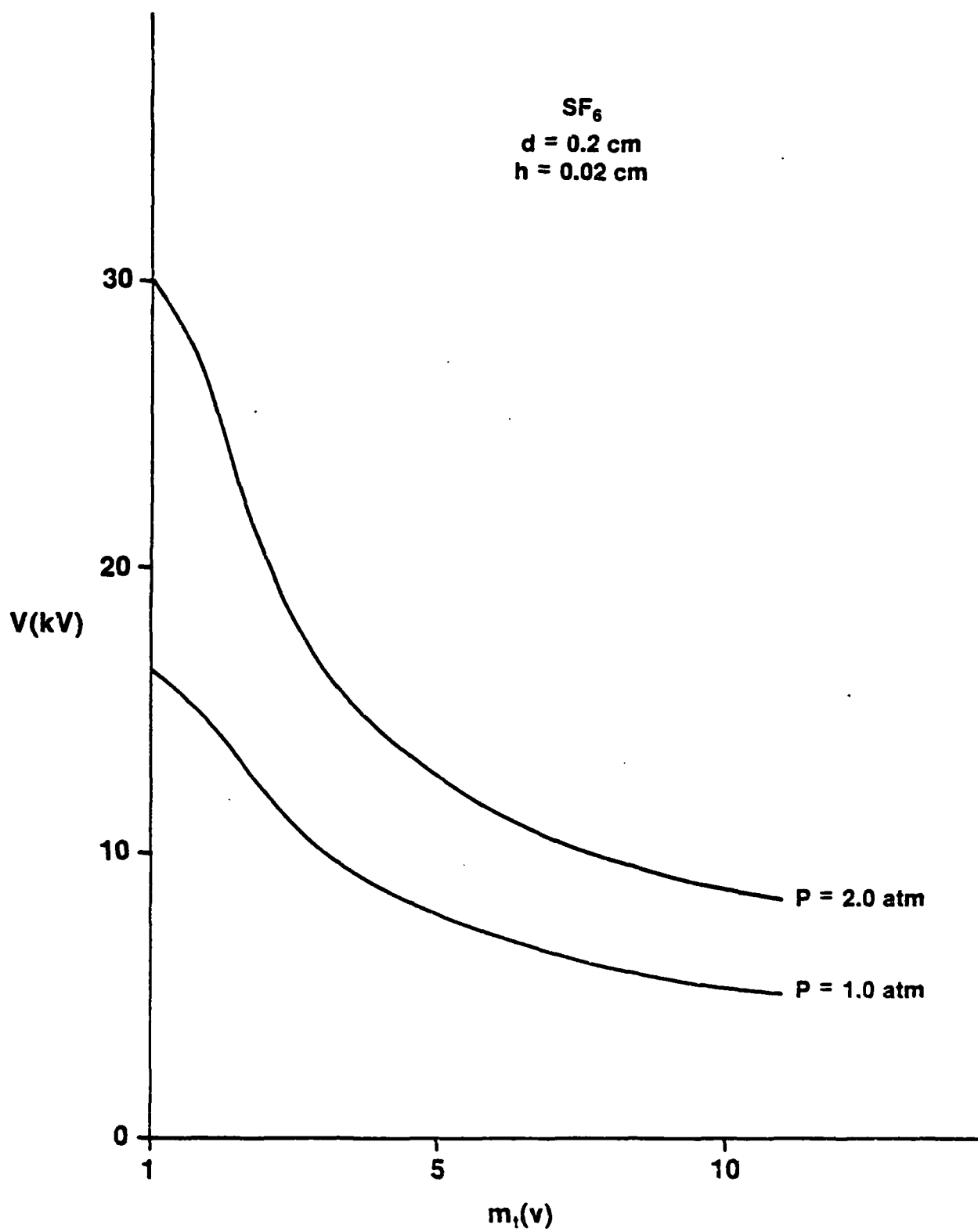


Fig. A3

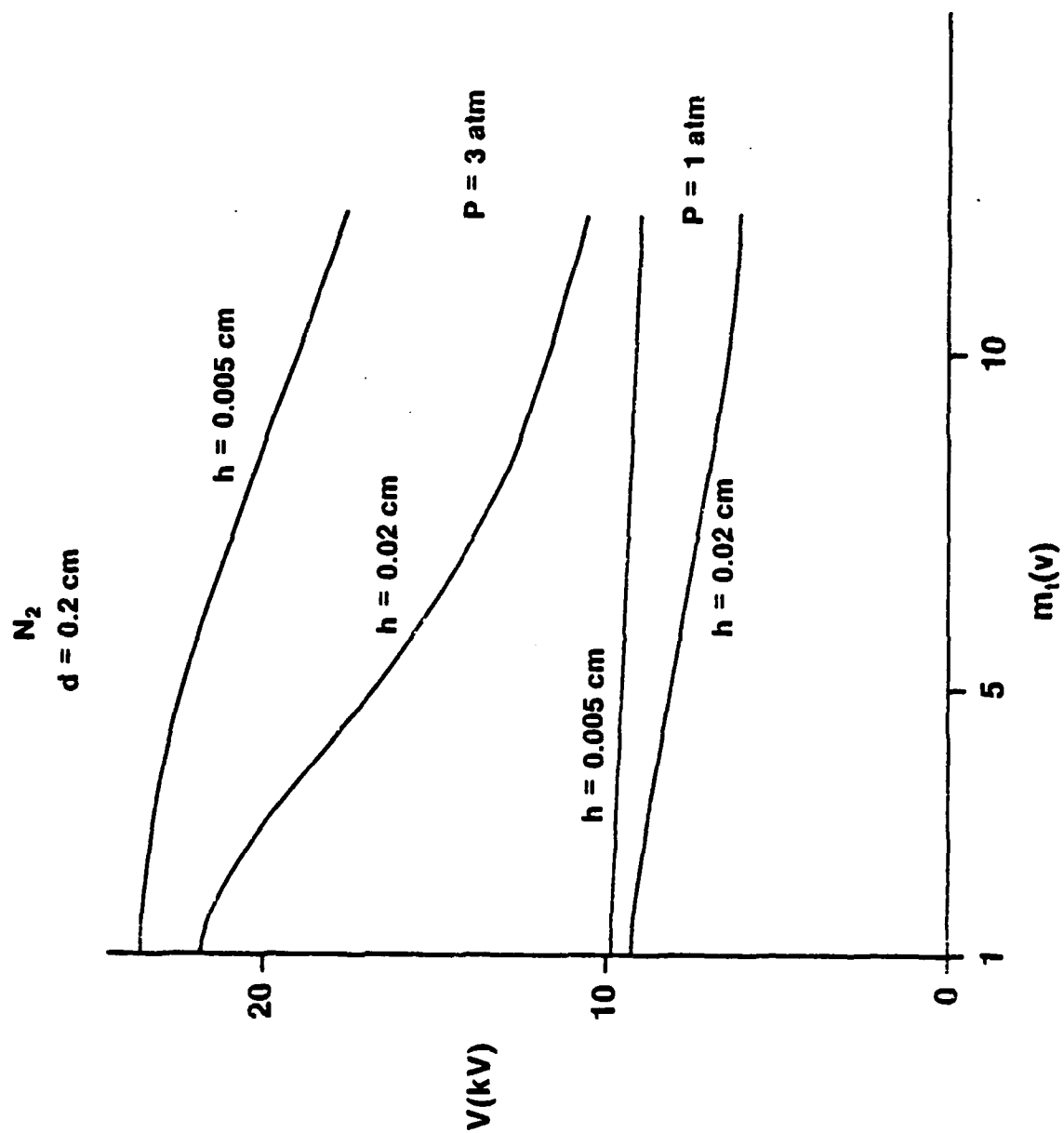


Fig. A4

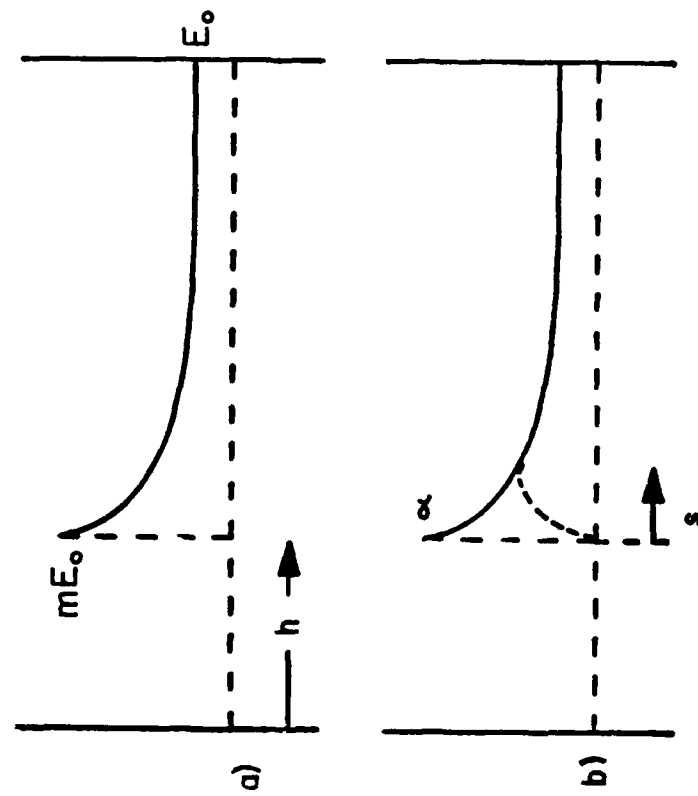


Fig. A5

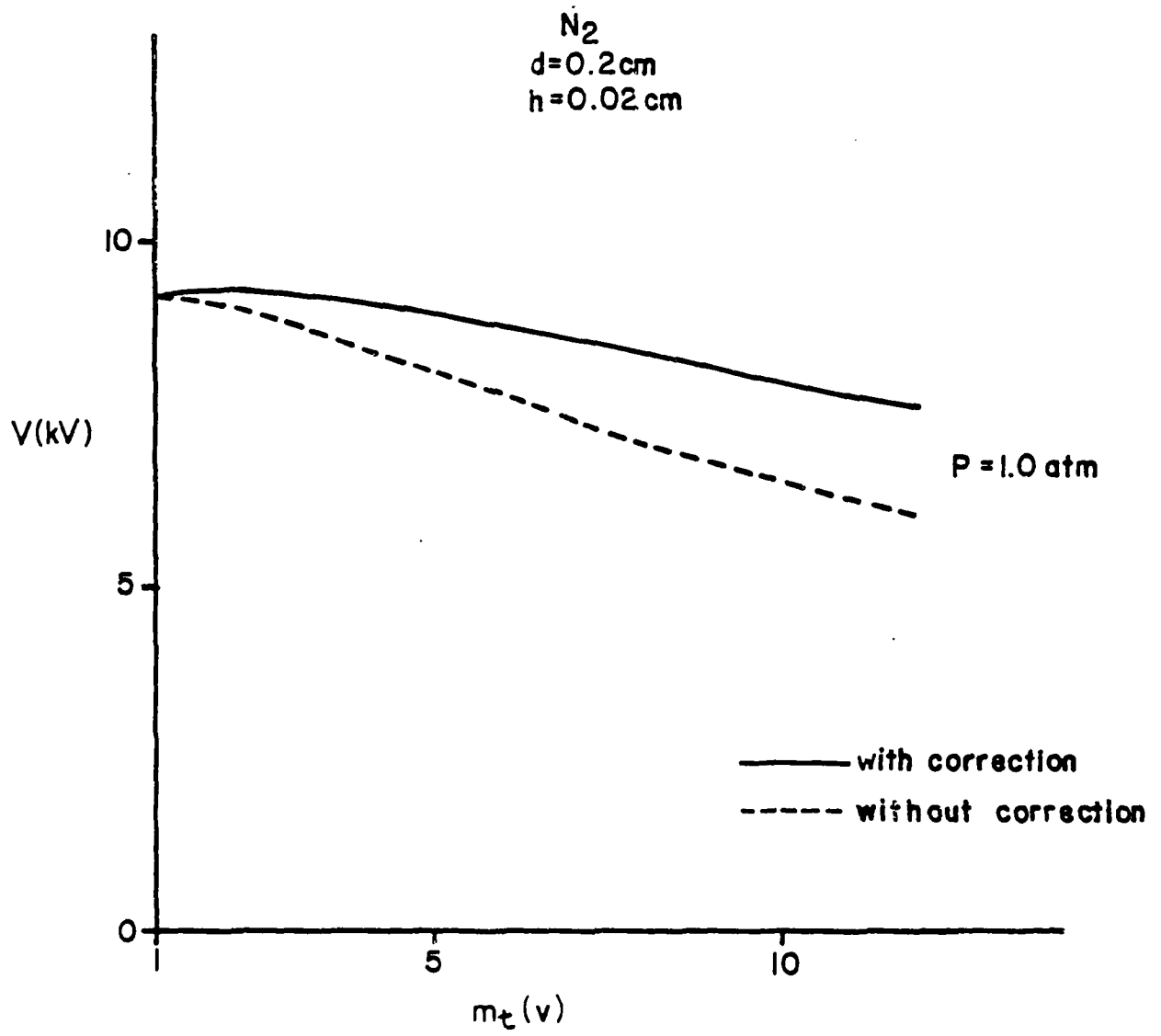


Fig. A6

## Appendix II

ELECTRODE EROSION PHENOMENA  
IN A HIGH ENERGY PULSED DISCHARGE

A.L. Donaldson, M.O. Hagler, and M. Kristiansen

Plasma and Switching Laboratory

Department of Electrical Engineering

G. Jackson\* and L. Hatfield

Department of Physics

Texas Tech University

Lubbock, Texas 79409

Abstract

The erosion rates for hemispherical electrodes, 2.5 cm in diameter, made of graphite, copper-graphite, brass, two types of copper-tungsten, and three types of stainless steel have been examined in a spark gap filled with air or nitrogen at one atmosphere. The electrodes were subjected to 50,000 unipolar pulses (25  $\mu$ s, 4-25 kA, 5-30 kV, 0.1-0.6 Coul/shot) at repetition rates ranging from 0.5 to 5 pulses per second (pps). Severe surface conditioning occurred, resulting in the formation of several spectacular surface patterns (craters up to 0.6 cm in diameter and nipples and dendrites up to 0.2 cm in height). Surface damage was limited to approximately 80  $\mu$ m in depth and

---

Accepted for publication - IEEE Trans. on Plasma Science, March, '84.

\* Present address: BDM Corp. Huntsville, Alabama 35803

was considerably less in nitrogen gas than in air. Anode erosion rates varied from a slight gain (a negative erosion rate), for several materials in nitrogen, to  $5 \mu\text{cm}^3/\text{Coul}$  for graphite in air. Cathode erosion rates of  $0.4 \mu\text{cm}^3/\text{Coul}$  for copper-tungsten in nitrogen to  $25 \mu\text{cm}^3/\text{Coul}$  for graphite in air were also measured.

### Introduction

High energy spark gaps with lifetimes of  $10^8$  shots are seen as one of the critical components in pulsed power systems used for particle beam systems, lasers, nuclear isotope separation, electromagnetic pulse simulation, and thermonuclear fusion reactors. The performance of a pressurized spark gap as a high energy, rep-rated switching device is typically characterized by its hold-off voltage, recovery time, delay time, and jitter, [1]. The switch lifetime is determined by the electrode erosion, gas decomposition and disassociation, and insulator damage that occur as energy is dissipated in the switch [2].

The purpose of this study was to measure the erosion rate of different electrode materials as a function of current in order to generate a data base from which theoretical models describing the complex erosion processes could be developed and verified. In addition, the electrode and insulator surfaces were examined in an effort to define the electrode erosion characteristics and to reduce the material parameter space used in further studies.

## Experimental Apparatus

### Spark Gap

The spark gap shown in Fig. 1 was designed to facilitate frequent electrode and insulator replacement and to allow for accurate control over electrode alignment and gap spacing. The electrodes are composed of three parts: the brass support (which also serves as a channel for gas flow), the brass adapter, and the electrode tip. The hemispherically shaped electrode tips are 2.5 cm in diameter and are made from the various materials studied. The Lucite inserts provide protection for the main gap housing and also provide a surface which gives a permanent history of the discharge debris which is deposited on the walls.

### Test Circuit and Conditions

Numerous experimentors have measured erosion rates for high current (10-800 kA), oscillatory discharges [3-7]. A few have studied erosion rates in high current ( $<10$  kA), unipolar discharges using brass and copper electrodes only [8,9]. A test circuit capable of delivering a unipolar pulse was chosen for this study, both to simplify separate investigations of the erosion processes at the anode and the cathode and to simulate more closely certain applications. The circuit, shown in Fig. 2, consists of a six-section Rayleigh pulse forming network (PFN) which is resistively charged to the self-breakdown voltage of the spark gap by a 30 kV, 1 A, constant voltage power supply. When the gap breaks down, the PFN is discharged into a matched,  $0.6\Omega$ , high power load. Further details of the test circuit and load



design are discussed elsewhere [10]. The waveform of the discharge current is shown in Fig. 3. The test conditions are summarized below:

Voltage	< 30 kV
Current	< 25 kA
Total Capacitance:	21 $\mu$ F
Charge/shot	< 0.6 Coul
Energy/shot	< 9 kJ
Pulse width:	25 $\mu$ s
Rep-rate:	0.5-5 pps
Gas:	Air or N <sub>2</sub>
Pressure:	1 Atm (absolute)
Flow rate:	1 Gap volume every 5 sec
Gap spacing:	< 0.8 cm

#### Materials Tested

The electrode materials tested were: brass (SAE 660), stainless steel (304, 20Cb-3, 440-C) [11], copper-tungsten (K-33 [12], 3W3 [13]), graphite (ACF-10Q), and copper-graphite (DFP-1C) [14]. This combination of materials allowed for:

- 1) a comparison with existing data for brass and stainless steel [3,4,8,15].
- 2) utilization of materials which experimentally have given good spark gap performance [3,6,16].
- 3) the testing of several new materials, namely copper-graphite, and the stainless steels 20Cb-3 (previously used in highly corrosive environments in MHD generators)

and 440-C (a high strength stainless steel).

The thermophysical properties of these materials are given in Table I.

### Experimental Results

#### Erosion Characteristics

The change in mass of the spark gap electrodes after 50,000 shots was measured with an analytical balance with a precision of  $\pm 5$  mg. The individual test conditions and resulting erosion rates are given in Table II. Although many authors report erosion rates in  $\mu\text{g}/\text{Coul}$ , the actual factor determining lifetime is the volume eroded, hence the units  $\mu\text{cm}^3/\text{Coul}$ . The results for brass are discussed later because of the failure of the electrodes due to gross material extraction.

Material: A ranking of the volume erosion rate for each material investigated, from smallest to largest, is:

Cathode: CT-3W3( $\text{N}_2$ ), CT-K-33( $\text{N}_2$ ), CT-3W3(Air), CT-K-33(Air),  
SS-304( $\text{N}_2$ ), SS-304(Air), SS-440-C(Air), SS-20Cb-3  
(Air), CG (Air), CG( $\text{N}_2$ ), G( $\text{N}_2$ ), G(Air)

Anode: CT-3W3(Air), CT-K-33(Air), SS-440-C(Air), CG( $\text{N}_2$ ),  
SS-304(Air), SS-20Cb-3(Air), G(Air) (The rest of  
the anodes showed no net erosion).

As expected, the copper-tungsten composites gave the lowest volume erosion rate. Somewhat surprising, however, was the excellent performance of the stainless steels (304 and 440-C) and the poor performances of the graphite materials as cathodes. From the results obtained for stainless steel in a pulsed discharge, it is seen that the high erosion rate reported by Gruber and Suess

[3], for an oscillatory discharge, was possibly a result of using a stainless steel which, according to the work reported here, is a poor anode material. Previous studies [6,15], which indicated that graphite was highly resistant to erosion were done at a much slower repetition rate (0.03 pps) and, therefore, gave a significantly lower erosion rate ( $<1\mu\text{cm}^3/\text{Coul}$ ). More recent results by Bickford [16] at 1000 pps gave an erosion rate of  $41\mu\text{cm}^3/\text{Coul}$  which is reasonably close to the value of  $25\mu\text{cm}^3/\text{Coul}$  measured in this experiment. A summary of the erosion rates found by other investigators is given in Table III. If one takes into account the lower values of current used in this study, then the results obtained in this experiment are in generally good agreement with the measurements of other investigators.

Polarity: Unlike previous experiments, where oscillatory current conditions masked any polarity effect, a distinct difference in the cathode and anode erosion rate and, most likely, the erosion mechanisms themselves were observed using a unipolar pulse. The ratio of cathode to anode erosion, for those materials which had significant anode erosion, varied from 1.5 in stainless steel (304) to 16 in copper-graphite. Carder [8] reported ratios of 2.5 to 5 for brass under similar conditions. Previous experiments, which gave cathode to anode erosion ratios less than one, were done at much higher pulse repetition rates (10-1000 pps) [15-18]. In addition, the results obtained by Petr [18] were done with smaller anode diameters and gap spacings (both  $<2.5\text{ mm}$ ).

In general, anode erosion rates were somewhat scattered, and thus, general trends were hard to obtain, given the limited data base. However, some agreement with an anode erosion rate proportional to  $Q^{1.5}$  was observed for graphite. A similar dependence has been found experimentally and derived theoretically by numerous other investigators [19-21].

Some anodes actually gained mass, which indicated that material was being transferred from the cathode to the anode and/or chemical reactions were forming compounds on the anode. The material transfer was demonstrated experimentally when a stainless steel cathode was found to deposit molten material on a graphite anode. Gray and Pharney [22] proposed a reasonable model for this effect at low currents, which is based upon the reduction of the ion bombardment force on the molten cathode material during the fall of the current pulse.

Cathode erosions in air are plotted in Fig. 4 as a function of the total charge transferred in 50,000 shots ( $\int i dt$ )\*. The actual experimental variable used to change the current was the gap spacing. Thus, from these data, there is no way to isolate the effect of increasing gap spacing and increasing current. For a given cathode material these results indicate a linear dependence of the erosion rate on the quantity  $Q = \int i dt$  over the entire range of currents. Since the energy in the arc is equal to  $\int V_{arc} i dt$ , this seemed to indicate that the main source of energy producing molten material and subsequent vaporization and droplet ejection is in the cathode fall region of the arc (ion impact heating) and not the localized  $i^2 R$  losses (Joule heating) in the

---

\* Note that the constant slope implies constant erosion rate per Coulomb.

material. (A similar statement by Belkin [5] touched off a heated debate in the literature [23], [24].) Although both experimental [25] and theoretical results [26] exist which support this result it will be shown that you can obtain erosion rates proportional to any reasonable function of current, even  $\int i dt$ , with Joule heating. Also, it should be mentioned that cathode and anode fall voltages are not known for short pulse, high current arcs which make it hard to check the erosion dependence on  $\int V_{arc} i dt$ .

Current: In order to understand the erosion dependence on current one should consider the following: the high current arc in both vacuum and pressurized gaps is known [9, 27] to consist of many individual filaments, each of which is attached to the electrode and forms a microscopic crater. Even if the erosion at each crater site is due to Joule heating [21, 28] the total erosion is a function of the filament current and the temporal history of each attachment site. For example, under certain circumstances it has been shown [9, 27] that the current per filament and the attachment lifetime are approximately constant. Thus, regardless of the erosion dependence on current at each individual attachment site, the total erosion would be a function of  $\int i dt$  since the total number of sites would be a linear function of current. This also explains why no clear dependence of erosion on the thermophysical properties  $[T_{mp}, d, k, c, \rho]$  has been consistently measured in experiments. Thus, to understand the erosion process correctly, one not only has to model the erosion mechanism occurring at each filament attachment site correctly, which will certainly depend on  $T_{mp}, d, k, c, \rho$  [21],

but also a model must exist which specifies the filament current and the temporal history of its attachment site. Excellent models exist for filament motion in low current, low pressure arcs [28], and high current arcs in vacuum [27], but it is not anticipated that any one model will suffice for the wide range of conditions encountered in high energy switches.

Gas: The erosion rate for copper-graphite, was slightly higher in nitrogen than in air whereas the rates for most of the other materials were smaller in nitrogen, by a factor of 2-3. In addition, the cross sections of the electrodes, shown in Figs. 5 and 6, show a significant reduction in the depth and amount of damage when the gas is nitrogen rather than air. The gas may affect the erosion in one or more of the following ways:

- 1) by forming chemical compounds on the electrode surface which alter:
  - a) the thermal stability [29],
  - b) the current density at individual attachment sites in the arc [30], and
  - c) the lifetime of each attachment [30],
- 2) by producing accelerated chemical reactions at the electrode surface [31], particularly at impurity sites or at the magnesium sulfide stringer locations in stainless steel [32],
- 3) by altering the cathode and anode fall voltages, particularly at higher pressures.

### Surface Conditions

The surface of the electrode tips and the insulator inserts were examined after 50,000 shots. The analysis techniques utilized were Auger electron spectroscopy (AES), scanning electron microscopy (SEM), and optical microscopy.

Brass: The surfaces of the brass electrodes are shown in Figs. 7 and 8. Large scale melting is evident, with dendrites or metallic protrusions up to 0.2 cm long existing on the surface. The self-breakdown voltage for these electrodes dropped from 20 kV to 3 kV in approximately 2000 shots as a result of macroscopic field enhancements. In addition, the voltage self breakdown distribution was characterized by a series of "jumps" thought to be due to large particles being "blown" off the ends of the protrusions. Originally it was thought that the material being "pulled out" of the bulk electrode was lead, but the results of the AES analysis shown in Fig. 9 indicate the surface consists primarily of carbon, copper, and oxygen, with a notable absence of zinc and lead. From these results and those found by Marchesi and Maschio [6], it is obvious that brass has only limited use in repetitive operation at higher levels of charge transfer.

Although the mechanism for the material extraction is not completely understood, Belkin [33] showed that the electromagnetic  $\vec{J} \times \vec{B}$  force resulting from the discharge can play an important role at large currents. In addition, Fitch and McCormick [34] observed gross material extraction from stainless steel electrodes as a result of asymmetrical current connections.

Cathode: The cathodes for most of the remaining materials are shown in Figs. 10-12. Considerable erosion has taken place, especially on the graphite materials. The stainless steel and copper-tungsten cathodes show evidence of severe melting. Although it is not easy to see in the photographs, all cathodes showed a distinct tendency to form a large scale crater whose diameter increases with increasing gap spacing and current. Similar macroscopic cratering was observed by Watson [35] who explained the results with the use of a hydromagnetic flow model. The idea of using a cathode cup in spark gaps is not new [36, 37], but it is interesting that the electrode erosion produces this shape. The location of the current attachment at the cathode should depend on the minimum electrical path length seen by the electron avalanche prior to breakdown. Thus, the erosion pattern and the corresponding erosion rate may be highly geometry dependent.

Anode: The anodes, corresponding to the cathodes shown in Figs. 10-12, are shown in Figs. 13-15. The graphite and copper-graphite anode erosion occurs primarily in a band, 0.8 cm wide, with the inner radius located 0.3 cm from the center of the electrode. This pattern is consistent with the results of Johnson and Pfender [38] which showed that an annular-shaped attachment region of high current density can exist at the anode. The copper-tungsten and stainless steel anodes indicate that melting and vaporization have taken place over the entire surface. Like the pattern at the cathode, the diameter of the anode erosion region increases with increasing current.



Insulator: A typical insulator insert, for eight of the possible combinations of electrode material and gas, is shown in Figs. 16 and 17. The insulator surfaces are covered by a coating of recondensed electrode material. The one notable exception was graphite electrodes in air, in which case no coating was found on the insulator surface. A dramatic difference is seen in Fig 16, in the case of a graphite electrode run in nitrogen. The entire insulator surface is covered with a thick coating of fluffy black material which is thought to consist of monoatomic layers of amorphous carbon [31].

All insulators were covered with solid particles, 10-100  $\mu\text{m}$  in size, distributed within a 5 cm band centered on a plane passing through the center of the gap and parallel to the electrode surfaces. This indicates that a considerable portion of the solid or molten material is ejected parallel to the electrode surfaces. Daalder [39] has reported similar results for vacuum arcs and McClure [40] has developed a model which shows that the ion recoil pressure of a vacuum arc plasma is sufficient to remove molten material from a cathode spot crater with velocities of  $2 \times 10^3 - 2 \times 10^4$  cm/sec parallel to the electrode surface. The values of velocity from McClure's model are in good agreement with the experimental findings of Udris [41].

Recent studies in vacuum arcs by Farrall [42] and Shalev [43], which have characterized the size and flux of the ejected particles as a function of current, indicate that the maximum number of particles are released at, or just following, the current maximum. Since the arc attachment region will reach its

maximum diameter at the current maximum then one would expect droplets of material to separate from the electrode at the crest or edge of the macroscopic crater. An SEM examination of the surface of the stainless steel (304) electrodes shows considerable agreement between the size and shape of the electrode surface features existing at the edge of the macroscopic crater, which is shown in Fig. 18, and a 50  $\mu\text{m}$  stainless steel (304) particle found on the insulator and shown in Fig. 19. A thorough characterization of the particles found on the insulators used in this experiment is given by Jackson, et.al. [44]. The presence of similar particles has been shown to have serious effects on the flashover potential of the insulator at high pressures for particle bigger than 35  $\mu\text{m}$  and densities of 20 particles/mm [45]. Thus, the electrode erosion mechanism affects the switch lifetime, not only as a result of the erosion itself, but also by coating the insulating materials with conductive particles.

### Conclusions

The erosion rate and surface damage of the electrodes was determined for several materials utilized in a high energy spark gap. The results from these preliminary studies have led to the following conclusions:

- 1) The electrode erosion rates and mechanisms are highly polarity dependent and thus, results for oscillatory and unipolar discharges can be considerably different.

- 2) A large amount of the erosion is in the form of solid and molten material removed parallel to the electrode surface and, apparently, from the edge of the macroscopic craters found on the cathode.
- 3) Cathode erosion rates are proportional to the total amount of charge transferred for a fixed repetition rate and pulse width.
- 4) Stainless steel (304) may be an economical replacement for copper-tungsten composites as a cathode material for the conditions studied.
- 5) Anode erosion rates were quite scattered, but, in general, were considerably less than the cathode erosion rates for all materials tested except stainless steel.
- 6) No distinct correlation was found between the thermophysical properties of the electrode materials and the amount of erosion.

In order to develop a more precise understanding of the effects of electrode erosion on switch performance, the following objectives are being considered for future work:

- 1) Measure the erosion rate as a function of pressure ( $10^{-2}$  to 4 atm) and rep-rate (1-1000 pps), and gas flow rate for a few of the more promising electrode-gas-insulator combinations.
- 2) Study the attachment of the arc to the electrode surface for a single shot as a function of pulse shape and peak current.

- 3) Compare the relative erosion rates for oscillatory and unipolar pulses which have different peak currents but transfer the same net charge.
- 4) Measure the voltage drop in the arc for pulsed currents in order to calculate the energy dissipated in the gap region.
- 5) Measure energy delivered to electrodes as a function of pulse shape, previously done by Carder [8], and compare these results with those computed from the arc voltage measurements in 4).

#### ACKNOWLEDGEMENTS

This work was supported by the Air Force Office of Scientific Research. The authors wish to express their sincere appreciation to the following people for their various contributions to this work and its preparation: A. Bowling, M. Byrd, J. Clare, B. Conover, J. Davis, B. Maas, C. Mueller, R. Ness, S. Prien, K. Rathbun, A. Shaukat, and A. Williams.

## LIST OF REFERENCES

- [1] T.R. Burkes, et. al., "A Critical Analysis and Assessement of High Power Switches," NSWC Dahlgren Lab. Report NP 30/78, 189-202, (1978).
- [2] L.B. Gordon, et. al., "Material Studies in a High Energy Spark Gap," IEEE Trans. on Plasma Science, PS-10, <sup>286</sup>A (1982).
- [3] J.E. Gruber and R. Suess, "Investigation of the Erosion Phenomenon in High Current, High Pressure Gas Discharges," Max Planck Inst. fur Plasmaphysik, Garching bei Munchen, IPP 4/72, (Dec. 1969).
- [4] R.A. Burden and T.E. James, "Statistical Performance Data for a High Current 60 kV Spark Gap Switch," Proc. 7th Symp. Fusion Technology, Grenoble, France, 24-27, (Oct. 1972).
- [5] G.S. Belkin, and V. Ya. Kiselev, "Electrode Erosion in Pulsed High-Current Discharges," Sov. Phys. Tech. Phys., 11, 280-283 (1966).
- [6] G. Marchesi and A. Maschio, "Influence of Electrode Materials on Arc Voltage Waveforms in Pressurized Field Distortion Spark Gaps," 5th Int. Conf. on Gas Discharges, 145-148 (Sept. 1978).
- [7] Y. Kawakita, et. al., "A 150-kV, 100-kA Spark Gap Switch for Marx Generators," 3rd IEEE Int. Pulsed Power Conf., Albuquerque, New Mexico, 444-447 (June 1981).

- [8] B. Carder, "Gas Spark Gap Electrode Heating and Erosion," Physics International Report, PIIR 12-74, (Dec. 1974).
- [9] R. Basharov, et. al., "Erosion of Cathode Material in a Pulsed Discharge Between Parallel Electrodes," Sov. Phys. Tech. Phys., 12, 1383-1390 (1966).
- [10] A.L. Donaldson, "Electrode Erosion Measurements in a High Energy Spark Gap," MS Thesis, Texas Tech University, (August 1982).
- [11] Carpenter Technology Corporation - Reading, Pennsylvania
- [12] Schwarzkopf Development Corporation - Holliston, Massachusetts.
- [13] Contacts Metals Welding - Indianapolis, Indiana
- [14] Poco Graphite - Decatur, Texas
- [15] D. Affinito, et. al., "Design and Structure of an Extended Life High Current Spark Gap," IEEE Trans. on Plasma Science, PS-7, 162-163 (1979).
- [16] K.J. Bickford, et. al., "Spark Erosion Characteristics of Graphite and CO Gas," IEEE Conference of 15th Power Modulator Symposium, Baltimore, Maryland 89-92 (June 1982).
- [17] G.S. Belkin, "Vaporization of Metal Electrodes by Pulsed Currents," Sov. Phys. Tech. Phys., 13, 1256-1260 (1969).
- [18] R.A. Petr, "Erosion Phenomena of Arcing Electrodes," MS Thesis, Texas Tech University, (May 1980).
- [19] H.W. Turner and C. Turner, "Choosing Contact Materials," Electronics and Power, 14, 437-439 (1968).

- [20] E.M. Williams and R.E. Smith, "Phenomena Accompanying Transient Low-Voltage Discharges in Liquid Dielectrics," IAE Trans. Part 1, 74, 164-169 (1955).
- [21] V.E. Il'in and S.V. Lebedev, "Destruction of Electrodes by Electric Discharges of High Current Density," Sov. Phys. Tech. Phys. 7, 717-721 (1963).
- [22] E.W. Gray and J.R. Pharney, "Electrode Erosion by Particle Ejection in Low-Current Arcs," J. of Appl. Phys., 45, 667-671 (1974).
- [23] K.K. Namitokov, "Electrode Erosion in High-Current Pulsed Discharges," Sov. Phys. Tech. Phys., 12, 714-716 (1967).
- [24] G.S. Belkin and V. Ya. Kiselev, "Features of Electrode Erosion Due to High Current Pulses," Sov. Phys. Tech. Phys. 12, 719-720 (1967).
- [25] S. Levy, "Spark-Gap Erosion Studies," USAELRDL Report No. 2454, U.S. Army Electronics Research and Development Labs, Fort Monmouth, New Jersey (April 1964).
- [26] B. Juttner. "Cathode Heating by Vacuum Arcs: A Survey," Beitrage aus der Plasma Physik, Band 22-Heft 5, 453-462 (1982).
- [27] J.C. Sherman, et.al., "The Spontaneous Formation of Cathode Spots in High-Current Triggered Vacuum Switches and an Estimate of the Cathode Spot Current Density on Copper," Proceedings of the 4th International Conference on Gas Discharges, Swansea, UK, 94-97 (1976).

- [28] A.E. Guile, "Joule Heating in Emitting Sites on Various Nonrefractory Arc Cathodes," *Proc. IEE*, 127, 452-457 (1980).
- [29] E.I. Zolotarev, et. al., "Breakdown-Voltage Stability of Gas-Filled Switches for Voltage Pulse Generator," *Sov. Phys. Tech. Phys.* 21, 340-344 (1976).
- [30] A.E. Guile and A.H. Hitchcock, "Arc-Cathode Craters on Copper at High Currents and With Reduced Gas Pressures," *Proc. IEE*, 125, 251-256 (1978)
- [31] L.B. Gordon, "Material Studies in a High Energy Spark Gap," Ph.D. Dissertation, Texas Tech University, (May 1983).
- [32] "Carpenter 20Cb-3 Stainless Steel," Carpenter Technology Corp., Reading, PA, p. 9 (1980).
- [33] G.S. Belkin and V. Ya. Kiselev, "Effect of the Medium on the Electrical Erosion Electrodes at High Current," *Sov. Phys. Tech. Phys.* 23, 24-27 (1978).
- [34] R.A. Fitch and N.R. McCormick, "Low-Inductance Switching Using Parallel Spark Gaps," *Proc. IEE (London)* 106A, 117-130 (1959).
- [35] A. Watson, "Fast Rising Heavy Current Spark Damage to Electrodes," 2nd IEEE International Pulsed<sup>Power</sup> Conference, Lubbock, TX, 471-474 (June 1979).
- [36] F.S. Goucher, et. al., "Spark Gap Switches for Radar," *Bell Sys. Tech. Journal*, 25, 563-602 (1946).
- [37] A.E. Bishop and G.D. Edwards, "Low-Inductance 100 kV Switch (Spark Gap) for Starting, Diverting, and Clamping Capacitor Discharges," *Proc. IEE*, 113, 1549-1556 (1966).



- [38] D. Johnson and E. Pfender, "Modeling and Measurement of the Initial Anode Heat Fluxes in Pulsed High-Current Arcs," *IEEE Trans. on Plasma Science*, PS-7, 44-48 (1979).
- [39] J.E. Daalder, "Cathode Spots and Vacuum Arcs," *Physica*, 104c, 91-106 (1981).
- [40] G.W. McClure, "Plasma Expansion as a Cause of Metal Displacement in Vacuum-Arc Cathode Spots," *J. of Appl. Phys.* 45, 2078-2084 (1974).
- [41] Y. Udriş, "On the Emission of Cathode Material Particles in Low Pressure Arc Discharges," *Proc. of the Int. Conf. on Gas Discharges*, IEE London, 108-112 (1970)
- [42] G.A. Farrall et.al., "The Time-Resolved Characterization of Erosion Products from High-Current, Copper Vacuum Arcs," *IEEE Trans. on Plasma Science*, PS-11, 132-138 (1983).
- [43] S. Shalev et.al., "In Situ Determination of Macroparticle Velocities in a Copper Vacuum Arc," *IEEE Trans. on Plasma Science*, PS-11, 146-151 (1983).
- [44] G. Jackson, et. al., "Surface Studies of Dielectric Materials Used in Spark Gaps," (Texas Tech University) to be published in *Journal of Applied Physics*. Dec, 1983.
- [45] B.F. Hampton and S.P. Fleming, "Impulse Flashover of Particle Contaminated Spacers in Compressed Sulfur Hexafluoride," *Proc. IEE.* 120, 514-522 (1973).

Table 1. Electrode Material Properties

Material	Composition	$T_{mp}$ (°C)	$d$ (kg/m <sup>3</sup> )	$k$ (W/m °K)	$c$ (kJ/kg °K)	$\rho$ (10 <sup>-6</sup> Ωcm)
Brass	Cu 83%, Pb 7% Sn 7%, Zn 3%	980	8700	120	0.36	6.7
Stainless steel (SS) (304)	Fe 69%, Cr 19% Ni 9%, Mn 2%	1430	8000	16	0.56	72
Stainless steel (SS) (20Cb-3)	Fe 41%, Ni 33% Cr 19%, Cu 3%	1370	8100	13	0.50	108
Stainless steel (SS) (440-C)	Fe 79%, Cr 17% C 1%, Mn 1%	1370	7600	24	0.44	60
Copper-tungsten (CT) (K-33)	W 67%, Cu 33%	Cu 1080 W 3400	14000	270	0.25	3.4
Copper-tungsten (CT) (3W3)	W 68%, Cu 32%	"	"	230	NA	3.4
Graphite (ACF-10Q) (G)	C 100%	4200*	1830	87	0.80	2700
Copper-graphite (CG) (DFP-1C)	C 84%, Cu 16%	Cu 1080	2970	175	0.84	178

$T_{mp}$ : Melting Temperature,  $d$ : Density,  $k$ : Thermal Conductivity,  $c$ : Specific Heat,  $\rho$ : Resistivity,

\*graphite sublimes

Table II. Electrode Erosion Rates

Electrode	Gas	V	Q	CE	AE
Stainless steel (304)	Air	10.3	0.21	1.8	1.2
Stainless steel "	Air	10.6	0.22	1.5	1.0
Stainless steel " [1]	Air	18.0	0.37	1.6	1.5
Stainless steel (440-C)	Air	12.4	0.26	1.8	0.5
Stainless steel (20Cb-3)	Air	10.0	0.21	2.5	0.9
Stainless steel (304) [2,3]	N <sub>2</sub>	7.8	0.16	0.7	+0.0
Copper-tungsten (K-33)	Air	9.5	0.20	1.2	0.4
Copper-tungsten "	Air	11.5	0.24	1.2	0.3
Copper-tungsten "	Air	18.0	0.37	1.2	0.5
Copper-tungsten (3W3)	Air	15.8	0.32	0.8	0.2
Copper-tungsten (K-33) [3]	N <sub>2</sub>	14.8	0.31	0.4	0.4
Copper-tungsten (3W3)	N <sub>2</sub>	16.4	0.34	0.4	+0.0
Copper-graphite (DFP-1C)	Air	8.3	0.17	8.5	0.4
Copper-graphite "	Air	16.2	0.34	8.6	+0.0
Copper-graphite " [3]	Air	11.4	0.24	7.2	0.0
Copper-graphite " [3]	N <sub>2</sub>	14.8	0.31	13.5	0.8
Graphite (ACF-10Q)	Air	9.2	0.19	24.1	3.5
Graphite "	Air	10.6	0.22	24.6	3.6
Graphite "	Air	16.0	0.33	23.5	5.0
Graphite " [3]	N <sub>2</sub>	12.9	0.27	15.7	0.0

V: Average Voltage, kV; Q: Charge/shot, Coulombs; CE: Cathode erosion,  $\mu\text{cm}^3/\text{Coul}$ ; AE: Anode erosion,  $\mu\text{cm}^3/\text{Coul}$ ; [1] - 32,000 shots, [2] - 22,000 shots, [3] - Experiment performed at approximately 85% of maximum power, + indicates that an increase in mass was measured.

Table III. Summary of Comparable Erosion Results

Investigator	Erosion Rate ( $\mu\text{m}^3/\text{coul}$ )	Material	Gas	Current (kA)	Waveform
Affinito [15]	1	Graphite	N <sub>2</sub> (2 atm)	100	Oscillatory (0.03 pps)
Belkin [17]	0.7-1.4	Brass	Helium (1 atm)	40	Oscillatory
Bickford [16]	5	Copper-tungsten	CO (1 atm)	1.5	Unipolar (1000 pps)
	6	Stainless-steel	"	"	"
	41	Graphite	"	"	"
Burden and James [4]	5	Brass	Air (1.25 atm)	400	Oscillatory
Carder [8]	3-5	Brass	N <sub>2</sub> (2 atm)	10-22	Unipolar (1 pps)
Gruker and Sues [3]	2-10	Copper-tungsten	Air (1 atm)	40-170	Oscillatory
	5-40	Brass	"	"	"
	20-40	Stainless-steel	"	"	"
Kawakita [7]	80	Copper-tungsten	SF <sub>6</sub> (4 atm)	100	"

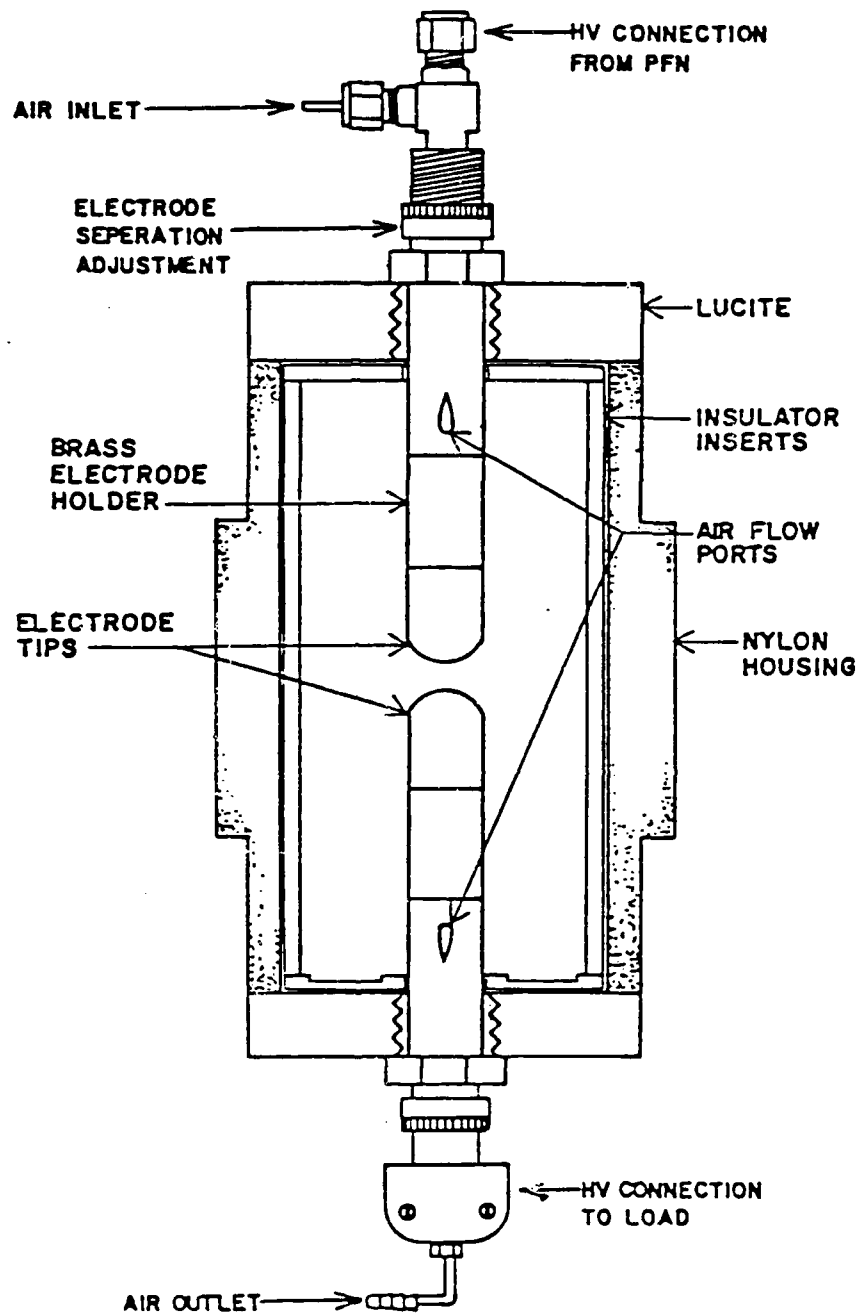
## List of Figures

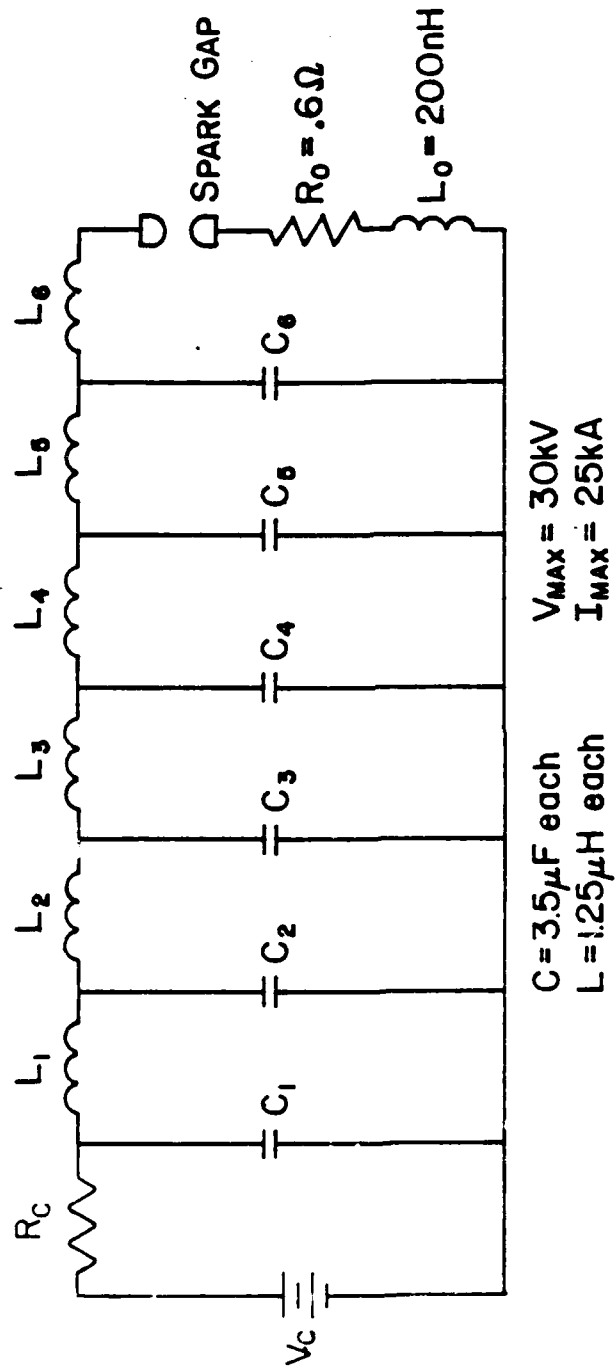
- Fig. 1 Spark Gap for Erosion Studies
- Fig. 2 Test Circuit for Erosion Studies
- Fig. 3 Current Pulse
- Fig. 4 Cathode Erosion Rates for Different Electrode Materials
- Fig. 5 Cross Section of Stainless Steel (304) Cathode in Air
- Fig. 6 Cross Section of Stainless Steel (304) Cathode in Nitrogen
- Fig. 7 Surface of Brass Electrodes in Air
- Fig. 8 Surface of Brass Electrodes in Nitrogen
- Fig. 9 Auger Electron Spectroscopy Surface Analysis of Brass Electrodes
- Fig. 10 Graphite and Copper-Graphite Cathode Surfaces in Air
- Fig. 11 Stainless Steel (304) and Copper-Tungsten (K-33) Cathode Surfaces in Air
- Fig. 12 Stainless Steel (304) and Copper-Tungsten (K-33) Cathode Surfaces in Nitrogen
- Fig. 13 Graphite and Copper-Graphite Anode Surfaces in Air
- Fig. 14 Stainless Steel (304) and Copper-Tungsten (K-33) Anode Surfaces in Air
- Fig. 15 Stainless Steel (304) and Copper-Tungsten (K-33) Anode Surfaces in Nitrogen
- Fig. 16 Insulator Inserts Exposed to Graphite and Copper-Graphite Electrodes in Air and Nitrogen

Fig. 17 Insulator Inserts Exposed to Stainless Steel (304) and  
Copper-Tungsten (K-33) Electrodes in Air and Nitrogen

Fig. 18 Scanning Electron Microscope Picture of Stainless Steel  
(304) Electrode Surface

Fig. 19 50  $\mu$ m Stainless Steel (304) Particle on Lucite Insulator







AD-A139 321

COORDINATED RESEARCH PROGRAM IN PULSED POWER PHYSICS  
(U) TEXAS TECH UNIV LUBBOCK DEPT OF ELECTRICAL  
ENGINEERING M KRISTIANSEN ET AL 27 FEB 84

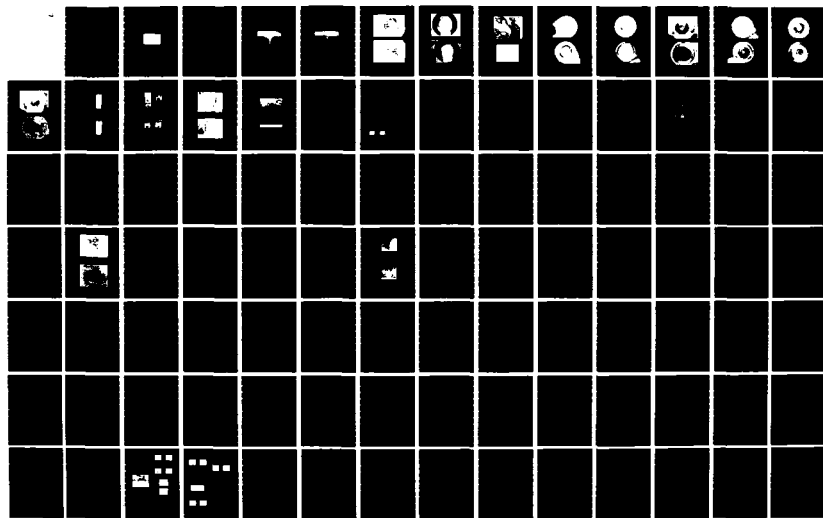
3/8

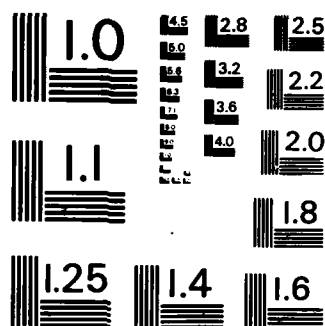
UNCLASSIFIED

AFOSR-TR-84-0174 F49620-79-C-0191

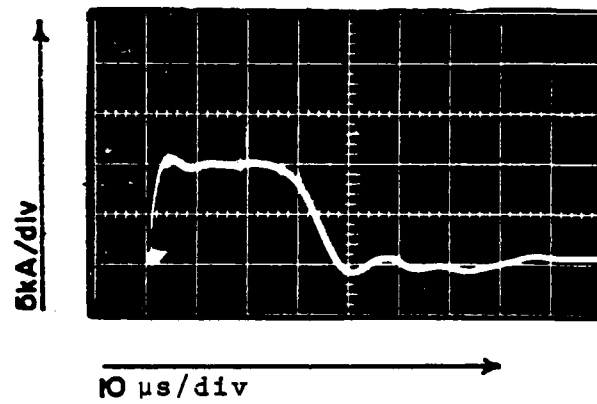
F/G 10/2

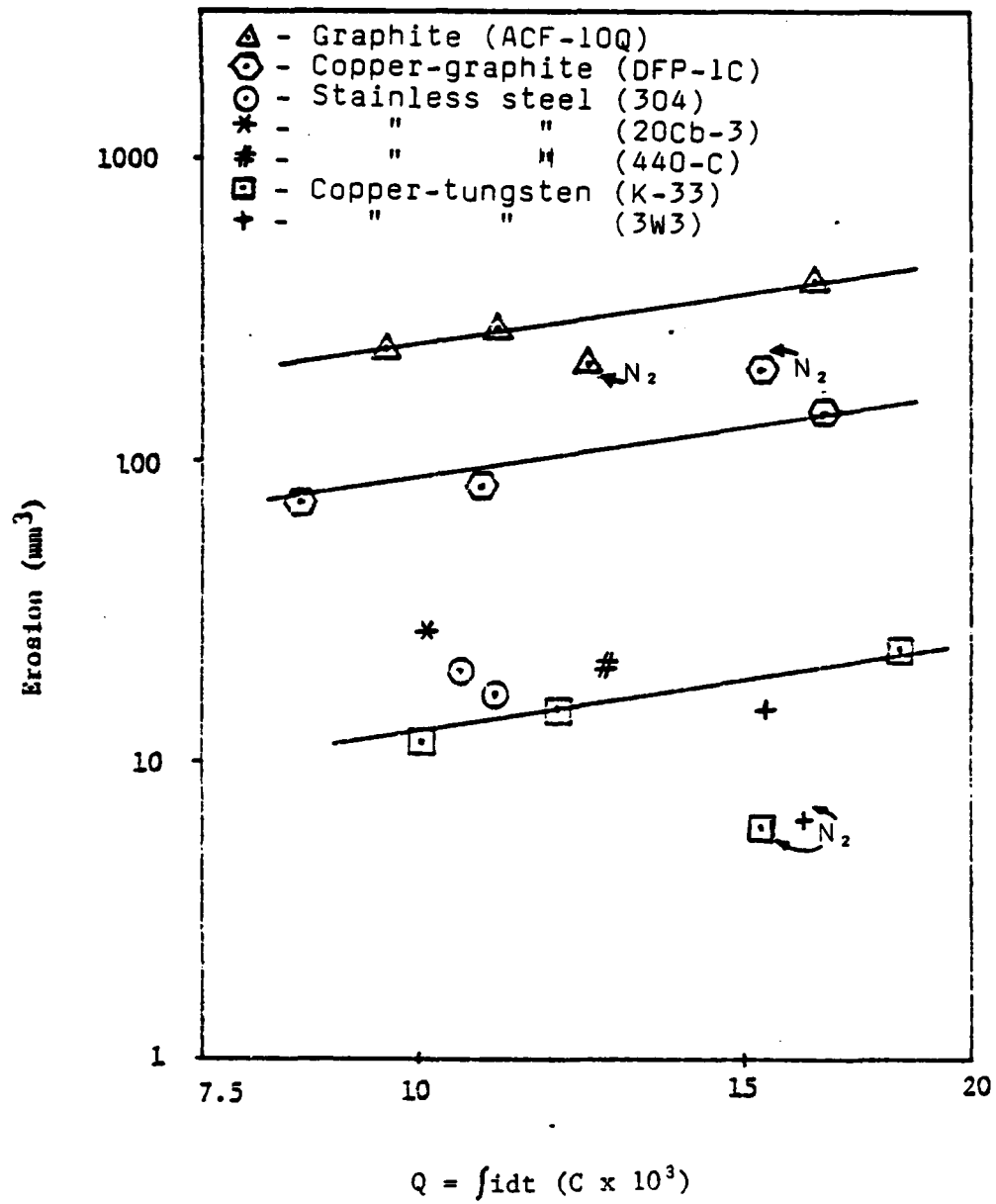
NL

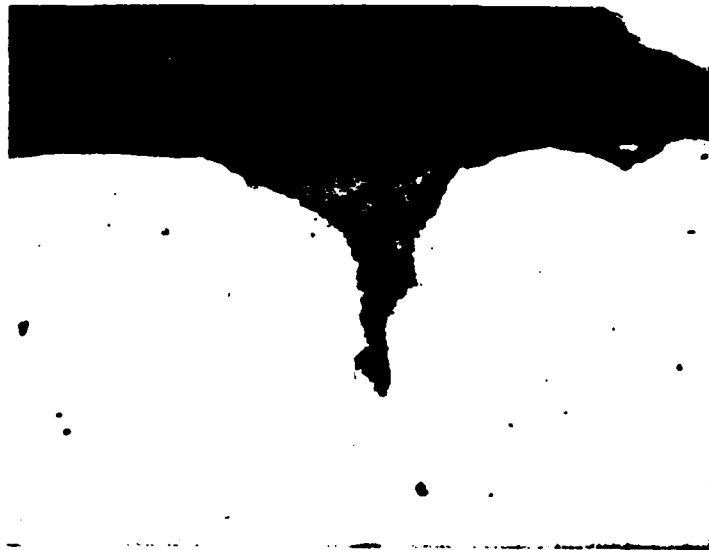




MICROCOPY RESOLUTION TEST CHART  
NATIONAL BUREAU OF STANDARDS - 1963 - A



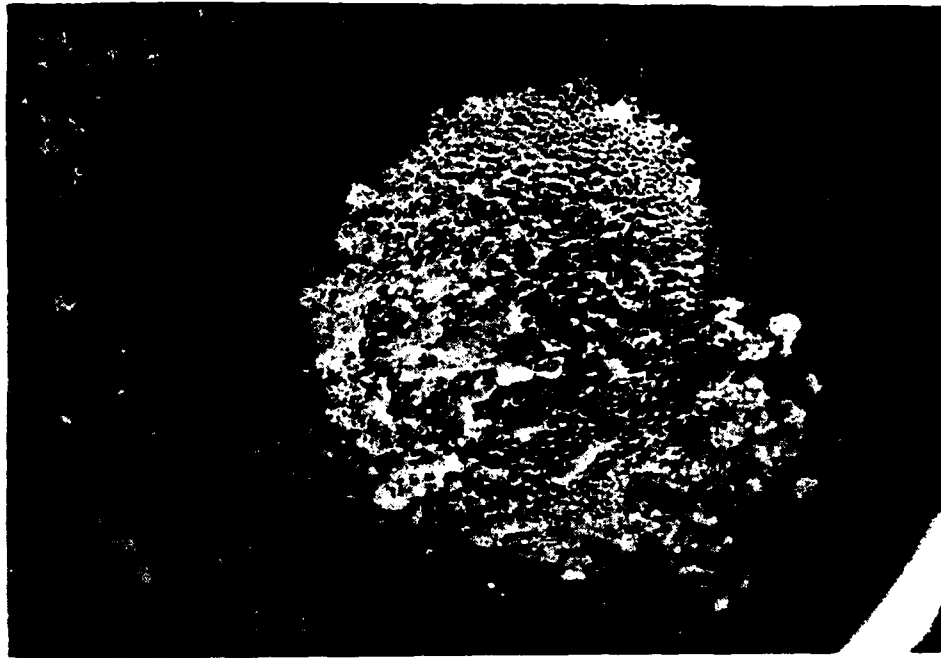




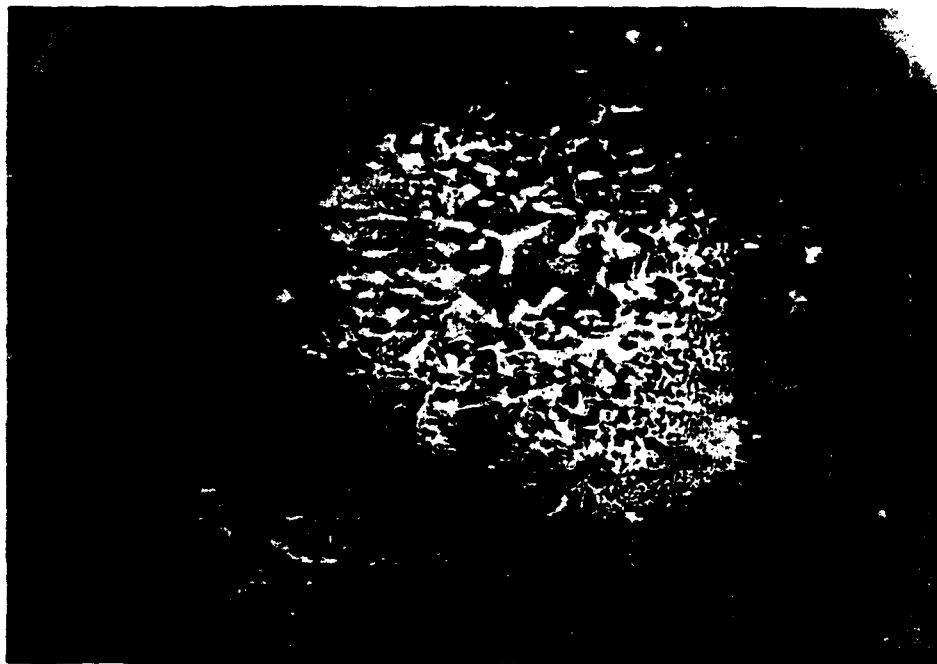
50  $\mu\text{m}$  |



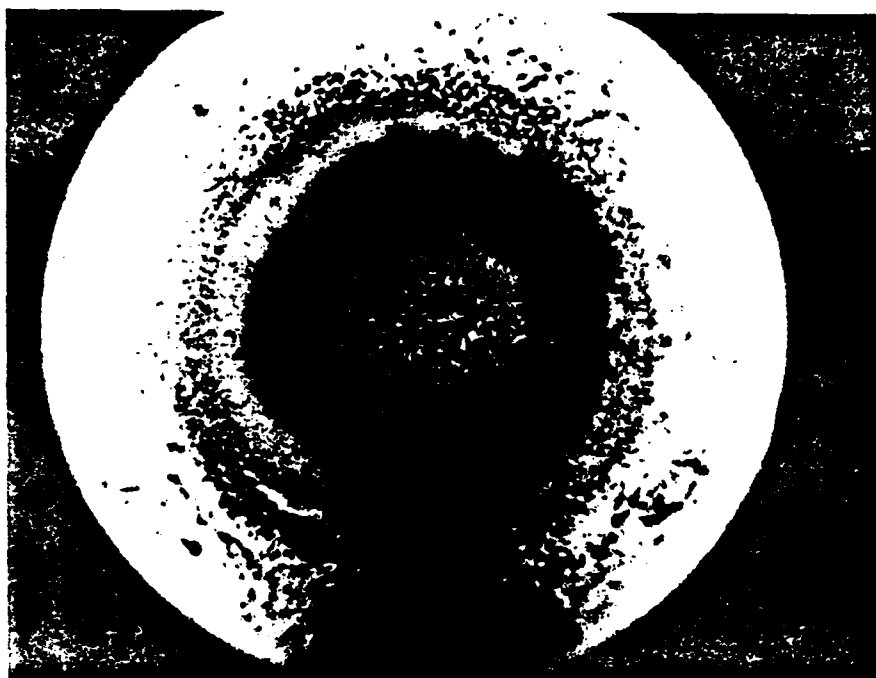
50  $\mu\text{m}$



a) Anode 1mm —



b) Cathode 1mm —




a) Anode

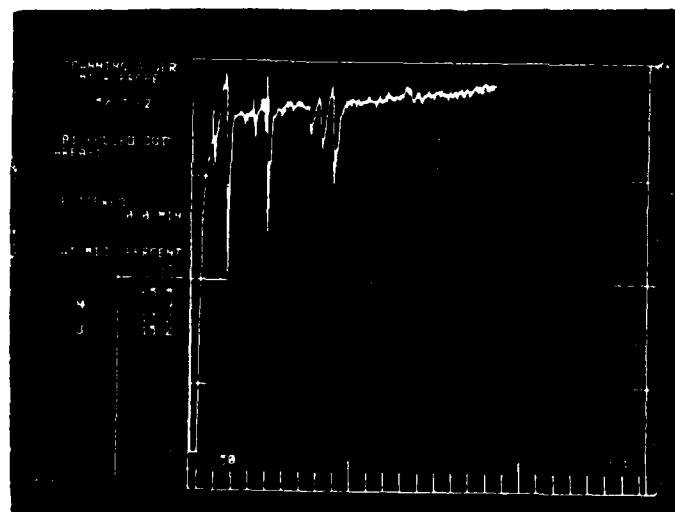


b) Cathode

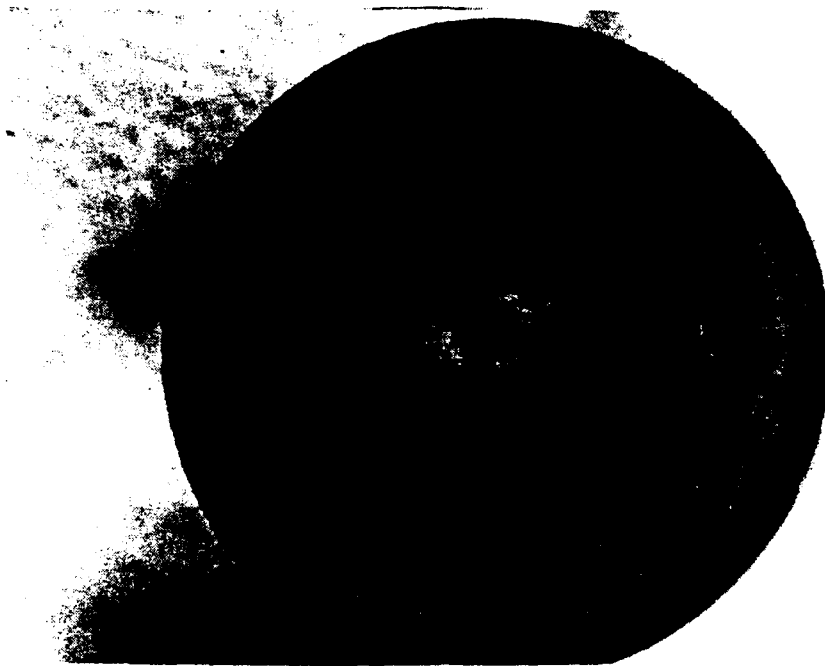




a) Cathode 250  $\mu\text{m}$  



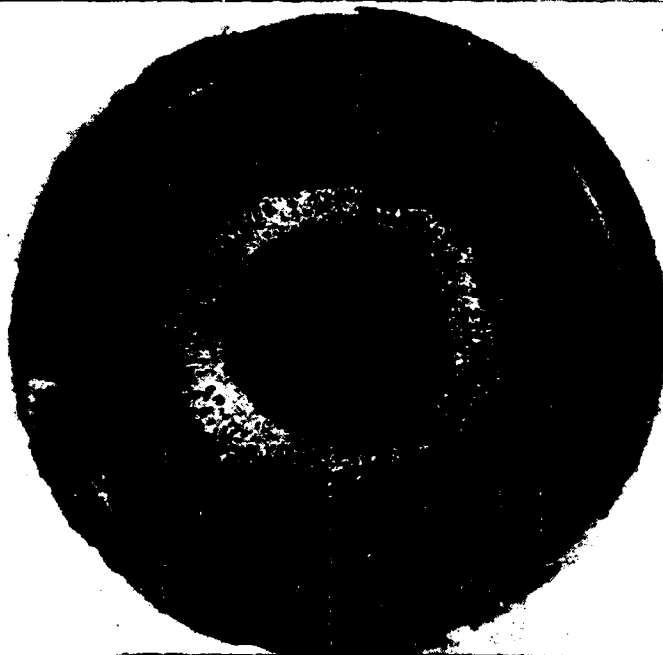
b) Auger Spectrum



a) Graphite



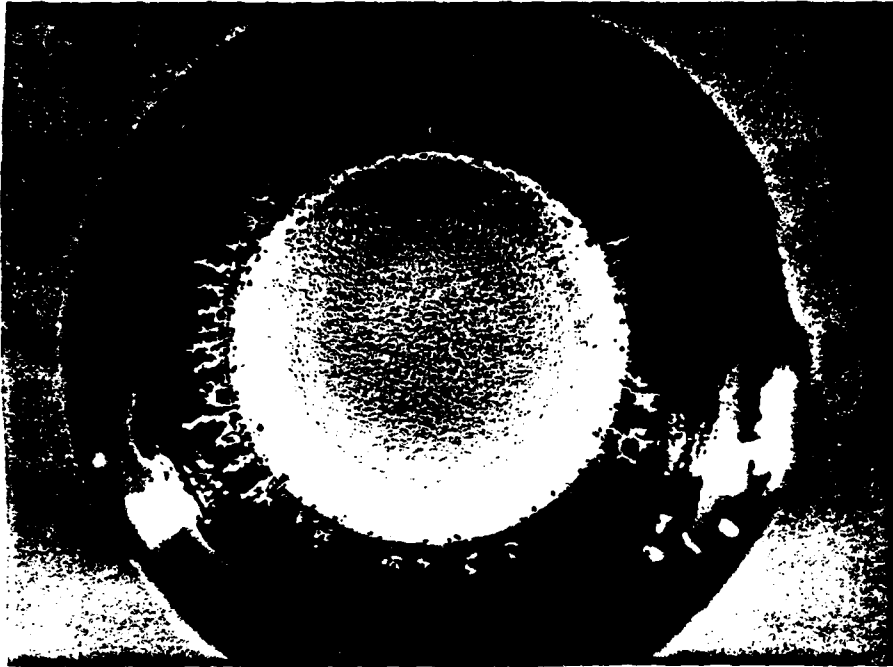
b) Copper-Graphite



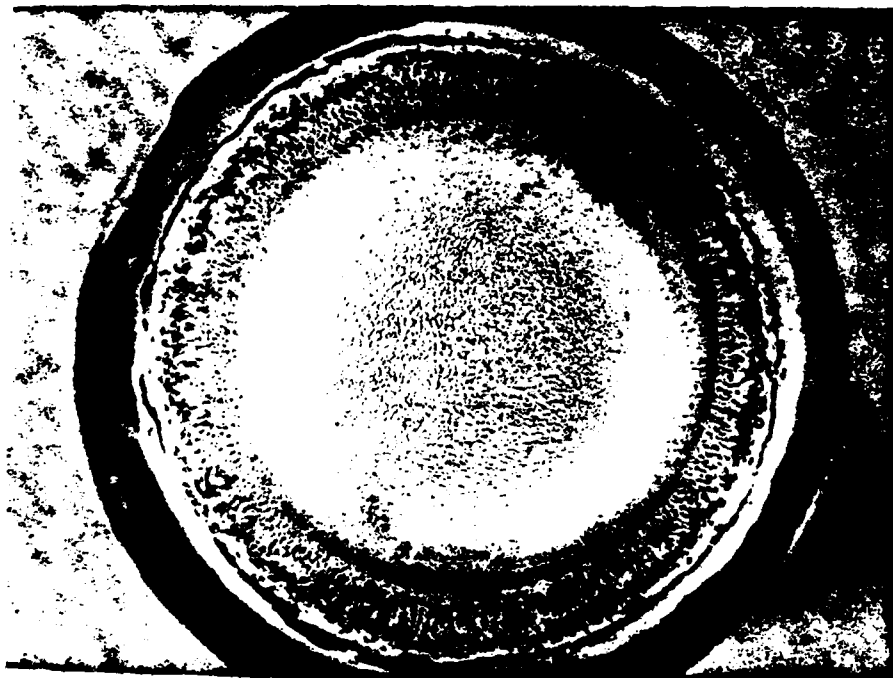
a) Stainless Steel



b) Copper-Tungsten



a) Stainless Steel



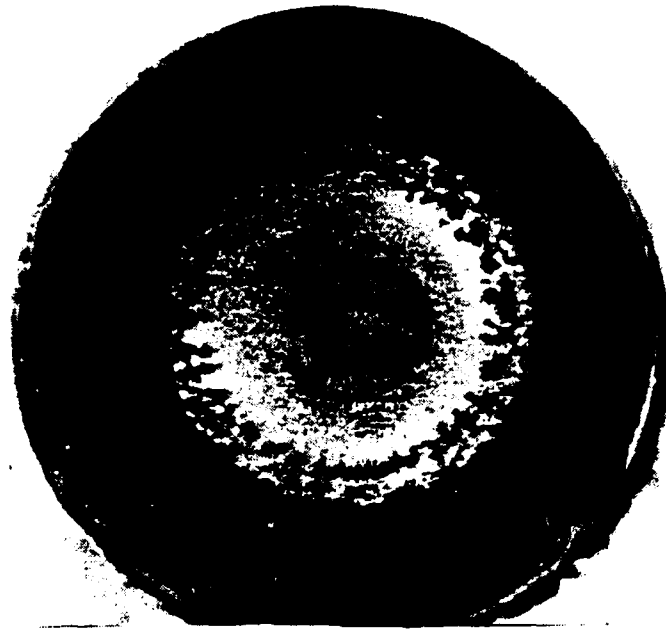
b) Copper-Tungsten



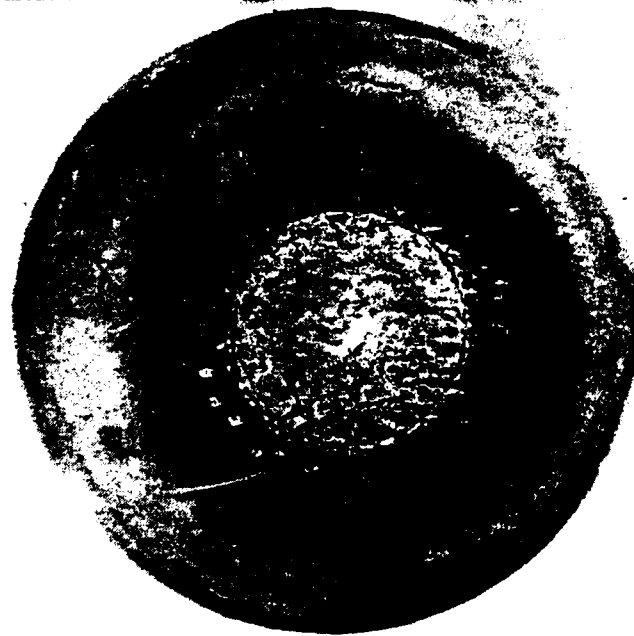
a) Graphite



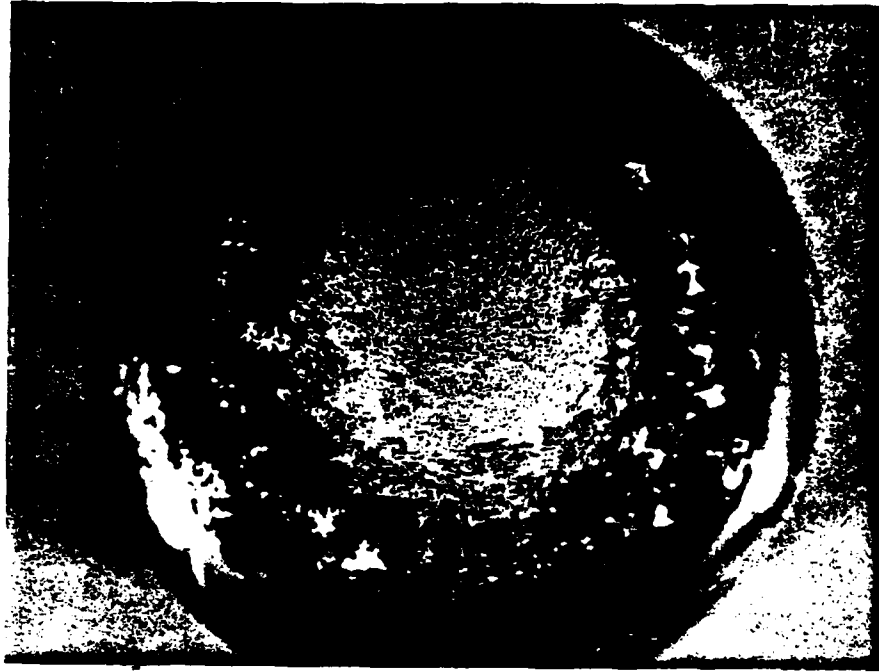
b) Copper-Graphite



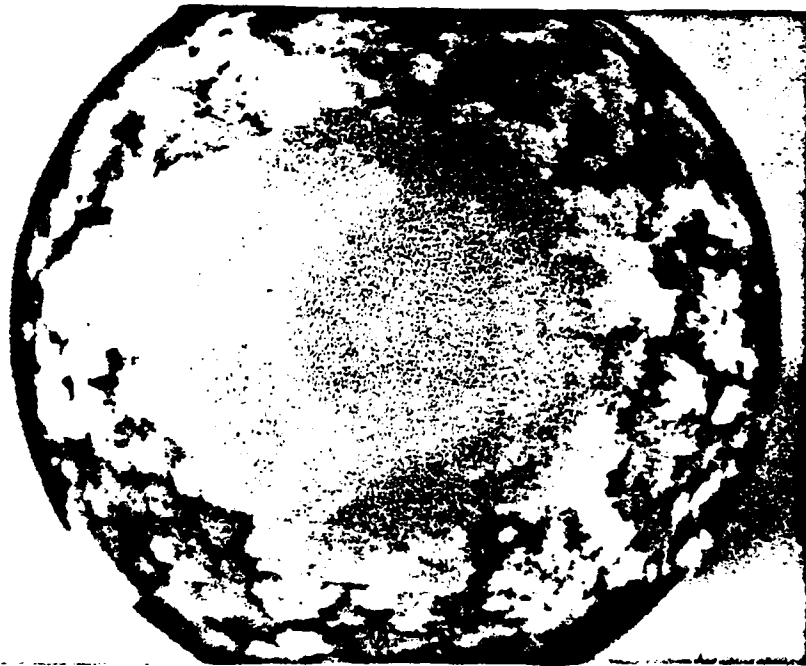
a) Stainless Steel



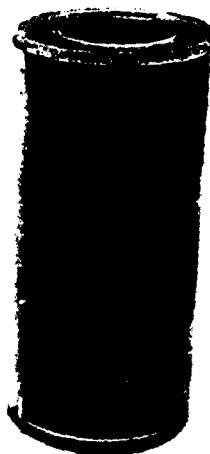
b) Copper-Tungsten



a) Stainless Steel



b) Copper-Tungsten



Nitrogen

Air

a) Graphite

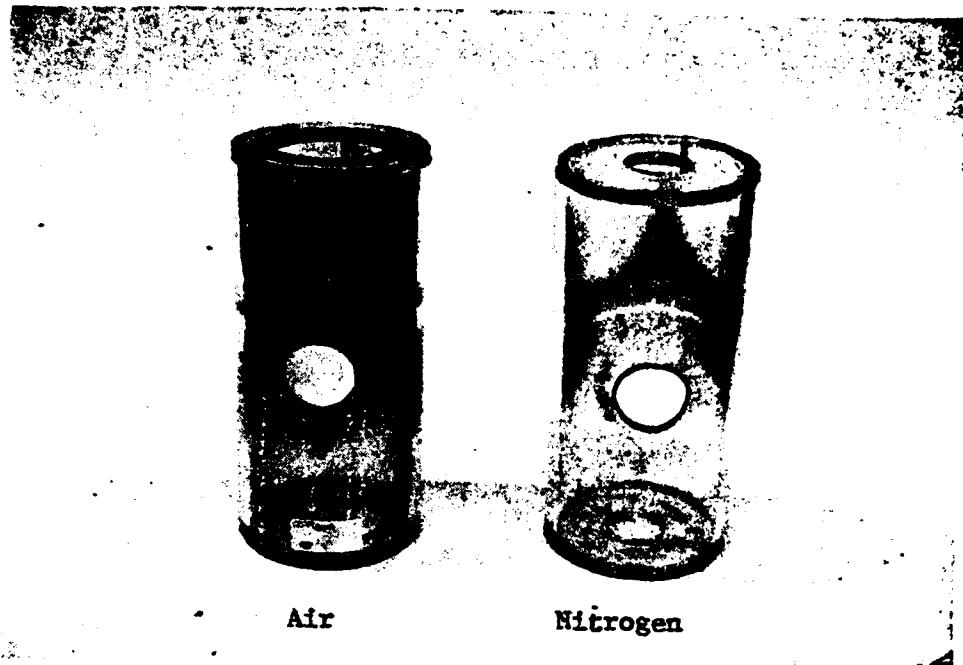


Nitrogen

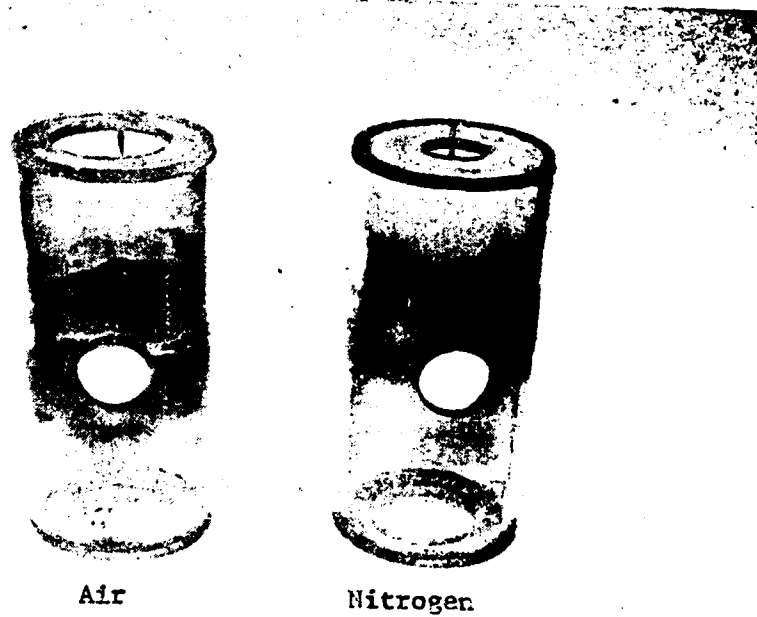
Air

b) Copper-Graphite





a) Stainless Steel



b) Copper-Tungsten



a) Outer Edge



b) Outer Edge Enlarged



00306 20KV 50U

VOLTAGE RECOVERY MEASUREMENTS IN A HIGH ENERGY SPARK GAP\*

C.H. Yeh, M. Hagler, and M. Kristiansen  
Plasma and Switching Laboratory  
Department of Electrical Engineering  
Texas Tech University  
Lubbock, Texas 79409

Abstract

Voltage recovery is discussed for a spark gap with 2.5 cm diameter, hemispherical electrodes made of graphite, stainless steel, or copper-tungsten and filled with air or nitrogen at one to two atmospheres pressure. The driving circuit delivers two, (1-cos $\omega t$ ), 200 Joule (max) pulses with a delay time variable from 10  $\mu$ s to more than 1 second. The rise time of the voltage pulse was varied from 25 kV/ms to 300kV/ms. Histograms of the self-breakdown and recovery voltages were recorded with an on-line data acquisition system. The results showed that the energy transfer and charging rate are the main factors in free (no gas flow) voltage recovery.

Introduction

Various pulsed power systems require high energy, rep-rated switching devices. Gas filled spark gaps are commonly used and offer the advantages of low losses and moderate shock problems in rep-rated operation.<sup>1</sup> In order to operate a spark gap in a rep-rated mode one must consider the electrode heating and erosion, the gas cooling rate, the deionization rate of the discharge plasma, and the de-excitation rate of the gas. To fully restore the dielectric strength of a gas-insulated spark gap after a discharge, it is essential to remove the charge carriers generated during the discharge and to recover the predischage temperature in the interelectrode gas.

Moran et. al. used a two-pulse method to measure the electric strength of various gases in a small pressurized spark gap.<sup>2</sup> Investigations were made to determine the electric strength of the gas as a function of time after breakdown with different pressures for a low energy (0.4 J), short gap spacing (0.127 mm), spark gap. They concluded that the recovery time decreases as the gas pressure increases.

The purpose of the study reported here was to measure the percentage voltage recovery of a spark gap with high energy discharges (up to 200 J) from two, (1-cos  $\omega t$ ), pulses. The voltage recovery for different electrode materials, gas types and pressures, and gap spacings were examined.

Experimental Apparatus

Spark Gap

The spark gap assembly shown in Figure 1 was designed to allow frequent and easy replacement of electrodes, adjustment of gap spacing, and operation with a variety of gas types and pressures. The

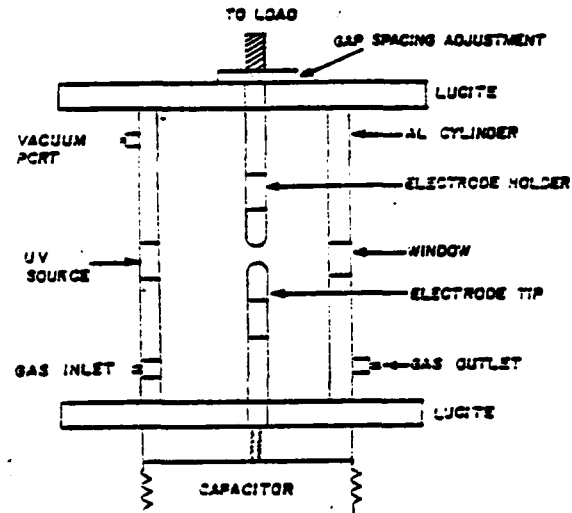


Fig. 1 Spark Gap for Recovery Studies

electrode assembly consists of stainless steel electrode holders and the electrode tips. The hemispherically shaped electrode tips are 2.5 cm in diameter and are made from the various materials studied. The upper electrode is adjustable and connects to a 1 ohm resistor. The electrode materials tested were stainless steel (304), graphite (ACF-10Q), and copper-tungsten (3W3). The gas types tested were air and nitrogen. Ultraviolet radiation from a low pressure mercury lamp was directed through a UV transmitting window onto the cathode in order to reduce statistical time lags.

Recovery Test Circuit

The recovery test circuit, shown in Figure 2, consists of two identical charging systems. When spark gap TSG1 is triggered,  $C_1$  discharges through  $R_1$ ,  $L_1$ , TSG1, and  $D_1$  into capacitor  $C_L$ . The voltage across  $C_L$  is

$$V_{CL} = V_0 \frac{C_1}{C_1 + C_L} (1 - \cos \omega t) \exp \left( -\frac{R_1}{2L_1} t \right),$$

where  $V_0$  is the initial voltage across  $C_1$ .

$$Q = C_1 C_L / (C_1 + C_L)$$

$$\frac{R_1}{2L_1} \ll \left( \frac{1}{L_1 C} \right)^{1/2}$$

$$\text{then } \omega \approx \left( \frac{1}{L_1 C} \right)^{1/2}$$

\*Supported by the Air Force Office of Scientific Research

If  $L_1 = 0$ , the voltage across  $C_L$  is

$$V_{CL} = V_0 \frac{C_1}{C_1 + C_L} (1 - \exp(-\frac{t}{R_1 C}))$$

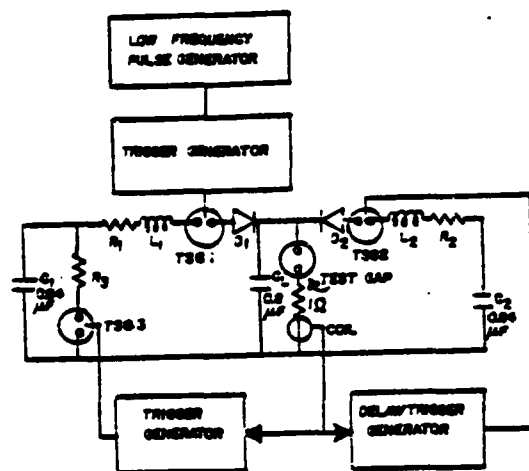


Fig. 2 Test Circuit for Recovery Studies

After the main spark gap self-breaks, capacitor  $C_L$  discharges through the main gap and the 1 ohm load to give a critically damped current pulse, as shown in Figure 3(a). The UV source insures that the main gap fires during the voltage rise. After the desired time delay, the second pulse is generated by triggering TSG2 which discharges  $C_2$  through  $R_2$ ,  $L_2$ , TSG2, and  $D_2$  into capacitor  $C_L$ . The capacitors  $C_1$  and  $C_2$  were charged through diodes and charging resistors (1 M $\Omega$ ) with one power supply (not shown in the diagram). The time between the pulse pairs is 7.5 sec which is set by a low frequency pulse generator to insure that the main gap has recovered fully. The output from the delay generator which controls the time delay (from 10  $\mu$ s to more than 1 s) between the two pulses is used to trigger TSG2. The delay generator is triggered by the current signal from the first breakdown pulse. The voltage pulse pair across  $C_L$  is shown in Figure 3(b).

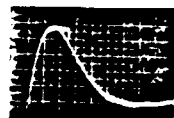


Fig. 3(a) Discharge Current



Fig. 3(b) Voltage Pulse Pair

The voltage is measured with a resistive voltage divider across the capacitor  $C_L$ . A Pearson coil measures the discharge current. The breakdown voltages of the pulse pairs are recorded by an on-line computer (Lecroy Model 2264 waveform digitizer and Model 3500 computer). The sampling rate is 1  $\mu$ s for the waveform digitizer. The data are stored on a floppy disc for further analysis of the recovery.

The diode stacks  $D_1$  and  $D_2$  consist of sixty 1N3766R diodes in series to obtain a PIV of 30 kV. The triggered spark gap, TSG3, discharges the residual voltage on  $C_1$  through  $R_3$  (2  $\Omega$ ) after the main spark gap breakdown. The charging rate of capacitor  $C_L$  is changed by choosing the values of  $L_1$ ,  $L_2$  and  $R_1$ , and  $R_2$ .

#### Experimental Results and Discussion

The percentage voltage recovery for different electrode materials in nitrogen at a gap spacing of 1.2 mm ( $L_1, L_2 = 1.1$  mH,  $R_1, R_2 = 37.5 \Omega$ ) is shown in Fig. 4. Each point (.5, 1.0, 2.0, 3.0 ms) represents the average value of 50 shots. The

#### % VOLTAGE RECOVERY

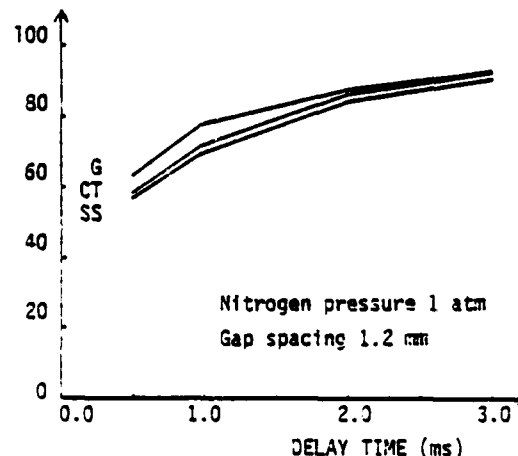


Fig. 4 Percentage Voltage Recovery with Different Electrodes (G: Graphite, CT: Copper-Tungsten, SS: Stainless Steel)

voltage across  $C_1$  and  $C_2$  is 15 kV. The average voltage and energy of the first pulse are 6.0 kV and 15.1 J, respectively. The thermal diffusivities of graphite<sup>3</sup> (0.594 cm<sup>2</sup>/sec), and copper-tungsten<sup>5</sup> (0.771 cm<sup>2</sup>/sec for K33, not available for 5X3) are larger than that of stainless steel (0.36 cm<sup>2</sup>/sec), and the percentage voltage recovery of graphite and copper-tungsten are slightly faster than that of stainless steel. These results indicate a weak dependence of voltage recovery on the electrode material. The thermal diffusivities of air and nitrogen are similar<sup>6</sup>. The percentage voltage recovery for the three electrode materials is slightly higher (5.0%) in air than in nitrogen. The statistical variation of the second breakdown voltage for copper-tungsten and stainless-steel in air is very large after a delay of 1 ns due to surface conditions which were changed by the first pulse (and the fact that the gap is not highly overvoltaged for  $t < 1$  ns). The surface is smoothed by the first pulse so that the required breakdown voltage is increased. The percentage voltage recovery is higher

than 90% after a 2 ms delay in air and a 3 ms delay in nitrogen for the three electrode materials.

The percentage voltage recovery decreases as the gap spacing increases from 1.2 mm to 3.1 mm at 1 atm, as shown in Fig. 5. The initial voltage across  $C_1$

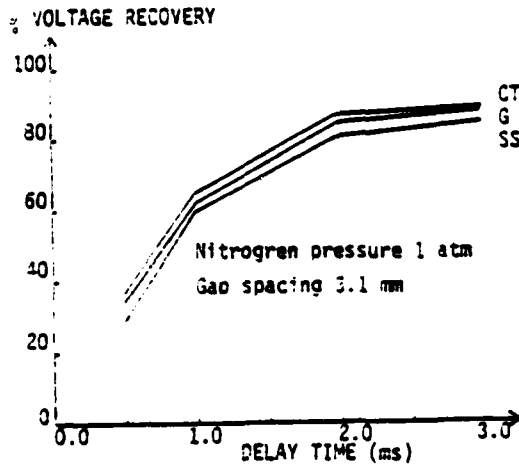


Fig. 5 Percentage Voltage Recovery with Different Electrodes (CT: Copper Tungsten, G: Graphite, SS: Stainless Steel)

and  $C_2$  is 25 kV at a gap spacing of 3.1 mm. The average voltage and energy of the first pulse are 10.8 kV and 49.0 J, respectively.

For a graphite electrode in nitrogen at a gap spacing of 1.2 mm ( $L_1, L_2 = 1.1$  mm,  $R_1, R_2 = 37.5 \Omega$ ), the percentage voltage recovery decreases as the pressure increases from 1 atm to 2 atm (abs), as shown in Fig. 6. The average voltage and energy of

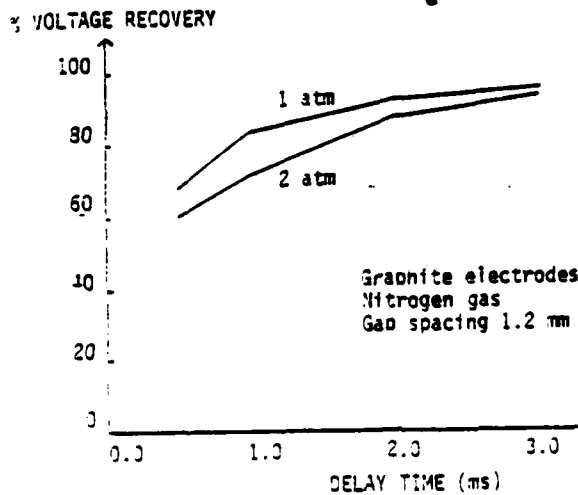


Fig. 6 Percentage Voltage Recovery at Different Gas Pressures

the first pulse are 3.4 kV and 29.6 J for 1 atm, and 16.3 kV and 105 J for 2 atm, respectively. The charging rates are 170 kV/ms and 300 kV/ms for 1 and 2 atmospheres respectively. There are three competing processes which determine the breakdown voltage recovery at higher pressures. One is the higher first pulse energy which causes higher ionization,

the second is higher gas density which causes higher charged particle recombination, and the third is the higher  $dV/dt$  caused by charging toward a higher breakdown voltage. The standard deviation of the first pulse data is 2% for 2 atm in nitrogen. The standard deviation of the second pulse data decreases from 10% at a delay time of 0.5 ms to 3% at 3 ms, as shown in Fig. 7.

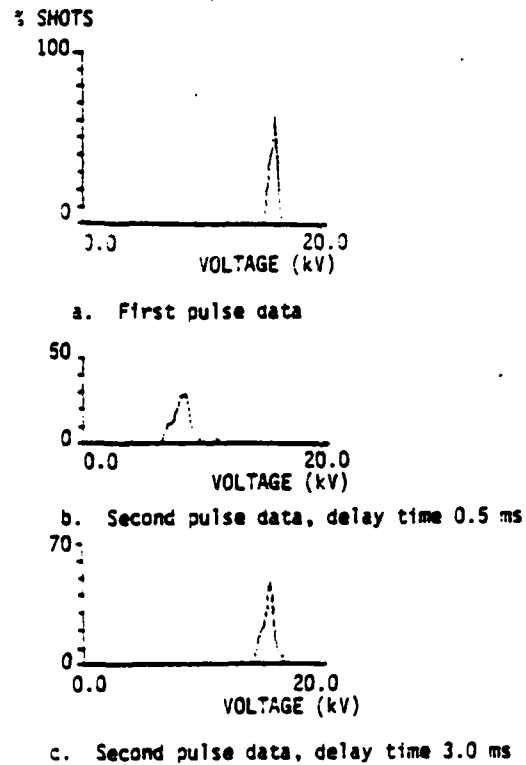


Fig. 7 Voltage Distribution for Different Delay Times

The percentage voltage recovery with different charging rates for graphite electrodes in nitrogen at a gap spacing of 1.2 mm is shown in Fig. 8. The

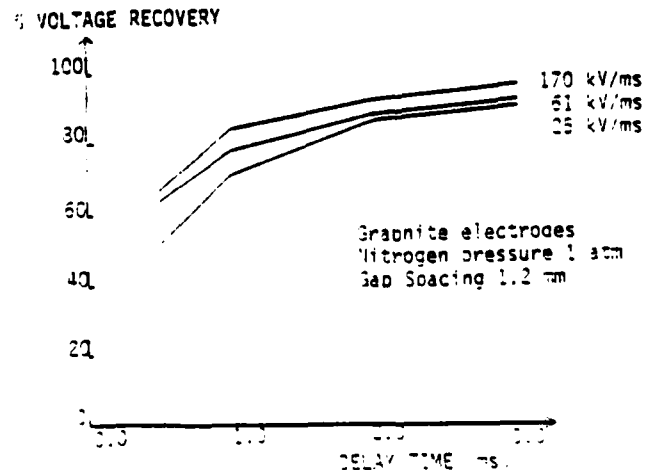


Fig. 8 Percentage Voltage Recovery for Different Charging Rates

charging rates are 170 kV/ms ( $L_1, L_2 = 1.1$  mH,  $R_1, R_2 = 37.5 \Omega$ ), 61 kV/ms ( $R_1, R_2 = 150 \Omega$ ), 25 kV/ms ( $R_1, R_2 = 450 \Omega$ ) for the three curves, respectively. Even though there is a UV-source, the spark gap is still waiting a short time for the initial electron to occur at the cathode surface to initiate the avalanche processes. The avalanche process also requires a certain time to reach the breakdown criterion. The faster rising pulses thus result in higher breakdown voltages than the slower rising ones.

### Conclusion

The standard deviation of first pulse data is larger in air than in  $N_2$ . The standard deviation of second voltage pulse data is larger than that of the first pulse data due to the statistical properties of the ionization processes and the initial temperature and charged particle conditions.

There is no significant difference in the percentage voltage recovery for graphite and copper-tungsten electrodes in air or nitrogen gases. The electrodes of higher thermal diffusivity have slightly higher percentage voltage recovery. The percentage voltage recovery in air is slightly faster than that in nitrogen.

The percentage voltage recovery depends on the initial temperature in the gas and electrodes, the charged particle recombination and the charging rate. The larger the gap spacing or the higher the pressure, the more energy is dissipated in the gap and the percentage voltage recovery will be lower if the pulse energy is the dominant factor.

### References

1. T.R. Burkes, et. al., "A Critical Analysis and Assessment of High Power Switches," NSWC Dahlgren Lab, Report NF 30/78, 177 (1978).
2. S.L. Moran, et. al., "Recovery of Electric Strength in Pressurized Spark Gaps," 15th Power Mod. Symposium, 99 (1982).
3. Poco Graphite, Decatur, Texas.
4. Schwarzkopf Development Corporation, Holliston, Massachusetts.
5. Contacts Metals Welding, Indianapolis, Indiana.
6. F. Kreith, Principles of Heat Transfer, New York : Intext Educational Publishers, 636 (1973).

## Project No. 4

Pulsed Power Surface Physics and Applications

(L.L. Hatfield, M. Kristiansen,  
G.L. Jackson, and G.R. Leiker)

## A. INTRODUCTION

The tasks performed during the course of this project naturally divide into two categories. The first is the measurement of the flashover potential of dielectrics before and after they have been exposed to the by-products of an arc in vacuum. This work is finished and is reported on in detail in a Ph.D. dissertation and several publications [1]. A brief report on the results is given below. The second category is the analysis of the surfaces of electrodes and dielectrics used in spark gaps and surface discharge switches. Projects 3 and 6 generated the samples for these studies which have produced a number of conclusions important to the understanding of erosion and breakdown statistics. Many of these conclusions have been presented in conference proceedings and journal articles [2].



## B. SURFACE FLASHOVER OF DIELECTRICS

### 1. Pulsed Flashover in Vacuum

#### a. Experimental Procedure

The four polymer dielectrics tested were Lexan, Lucite, Delrin, and Blue Nylon. Figure 1 shows the experimental setup. The samples were solid cylinders, one centimeter high and 6.35 cm in diameter. The samples tested for flashover (the upper sample in Figure 1) were placed between brass electrodes designed to give a uniform field. The lower samples were placed between brass electrodes designed to give a uniform field. The lower samples were never subjected to an electric field but were illuminated by the surface discharge ignitor plug and therefore, served as control samples. The spectroradiometer was used to measure the spectrum of the radiation from the ignitor plug in the region above 2000 Å. The photodiode and pulse counter were used to count the number of ignitor plug arcs during irradiation of a sample. The chamber containing the electrodes could be evacuated to  $1 \times 10^{-6}$  Torr and backfilled with dry gas. The pulse applied to the electrodes was a 5/135  $\mu$ s, double exponential, derived from a Marx bank erected into an RC load. The maximum voltage obtainable was 163 kV. A jet engine ignitor plug mounted on the wall of the chamber was used to expose the samples to the by-products of an arc in vacuum. The plug was pulsed at the rate of 5 pps with 2 joules of electrical energy per pulse. During exposure to this arc the electrodes and dielectric sample were rotated at 2.67 rpm to ensure uniform surface exposure of the dielectric cylinder [3].

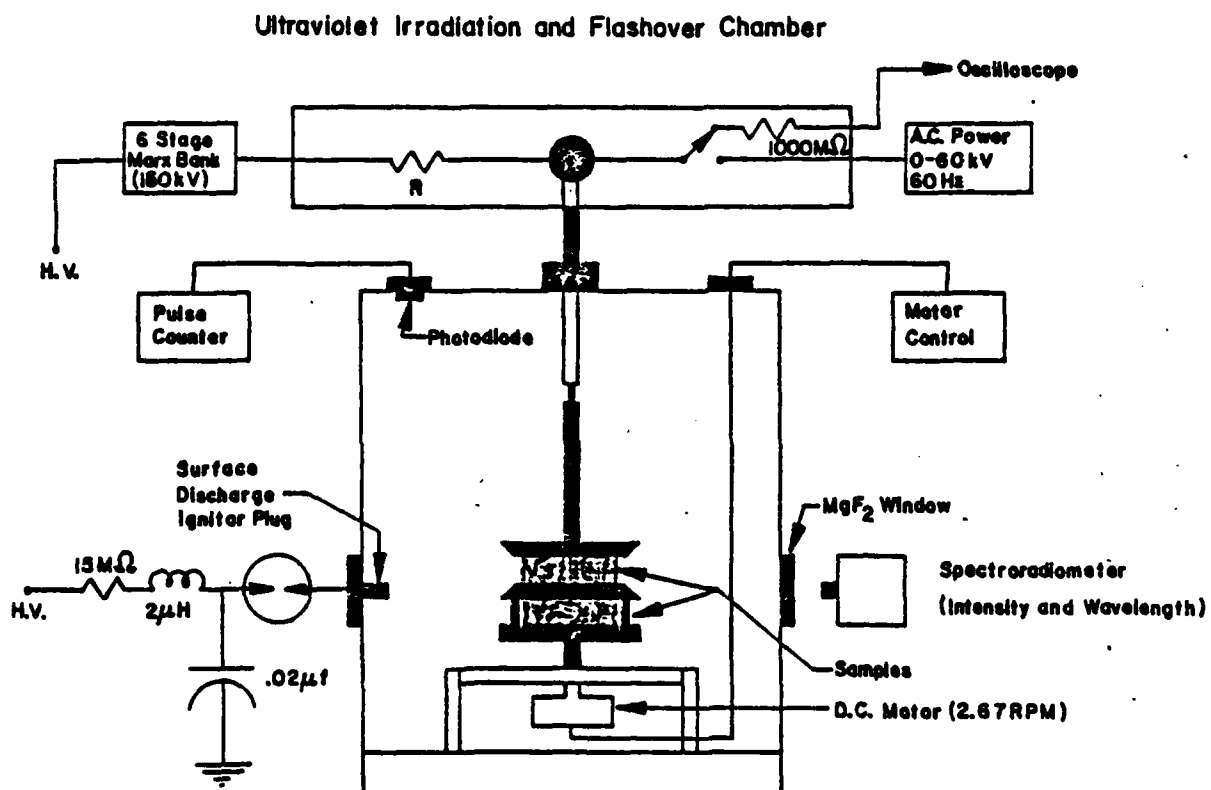


Fig. 1 Schematic representation of experimental setup.

Virgin and exposed dielectric samples were subjected to the same procedures throughout the flashover measurements. Also, all four materials were treated in the same way. For example, all samples were polished to a fine finish ending up with one micron alumina grit, and then cleaned with cyclohexane. A sample was then outgassed at  $1 \times 10^{-6}$  Torr for 24 hours to remove absorbed water. The sample was then conditioned with 60 Hz a.c. at up to 70% of the previously determined a.c. flashover voltage. The only difference in treatment between virgin and exposed samples was that exposed samples were subjected to 80,000 shots from the ignitor plug before undergoing the a.c. conditioning.

The flashover potential measurements were made immediately after the a.c. conditioning. Pulses were applied at 15 minute intervals until successive arcs occurred at the same location on the cylinder, indicating the formation of a track on the surface. Before formation of the track the arcs occur at random positions on the cylinder.

The voltage across the sample, derived from a resistive divider, was displayed on an oscilloscope and photographed for later analysis. The oscilloscope full scale sweep time was 10  $\mu$ s, so that if the flashover did not occur during the rising portion of the 5/135  $\mu$ s applied pulse, then the event was not recorded. However, the experimenter watching the sample through a window in the chamber could tell whether or not a flashover occurred at later times.

## b. Experimental Results

Table I lists the flashover potentials for the four polymer dielectrics with and without exposure to the vacuum arc. Lucite, Lexan, and Delrin samples which had been exposed to the arc in vacuum did not flash over during the rising portion of the applied pulse. This means that 163 kV/cm is a lower limit for the pulsed flashover field of those samples. The increases in flashover potential for these insulators, after exposure to the arc, were unexpectedly large (e.g. > 50% for Lexan).

Table I

### Insulator Flashover Electric Fields, in Vacuum

INSULATOR	FLASHOVER FIELD	FLASHOVER FIELD
	Virgin Samples	Exposed Samples
Lucite	$95 \pm 4$ (kV/cm)	$\geq 163$ (kV/cm)
Lexan	$104 \pm 3$ (kV/cm)	$\geq 163$ (kV/cm)
Delrin	$113 \pm 4$ (kV/cm)	$\geq 163$ (kV/cm)
Blue Nylon	$115 \pm 4$ (kV/cm)	$100 \pm 4$ (kV/cm)

The Blue Nylon samples exhibited a slightly lower flashover potential after exposure to the arc. The uncertainties attached to the values given in Table I are the standard deviations obtained using all measurements on all samples of that particular polymer (exceptions to this are discussed below). In most cases,

during the first two or so shots the sample apparently is being conditioned, while the last few shots are those which occur after a track has formed. Figure 2 shows the flashover voltage versus shot number for two virgin samples and one irradiated sample of Lexan. The first two shots and the last shot for each virgin sample were not used to determine the average value or the standard deviation. Four virgin and four exposed samples were measured for each polymer. Depending on the material, between three and twenty shots could be obtained on a sample before a track formed. Figure 3 shows the unusual behavior of Lucite samples. After two shots on virgin Lucite samples a track formed on the sample surface and a crater formed on the cathode at the location of the surface track. Exposed samples of Lucite never flashed over so those trials are plotted in Fig. 3 at 163 kV/cm as a lower limit. Exposed Lexan did flash over at 163 kV/cm but, on the first three shots the flashovers occurred after the oscilloscope trace was off scale. Therefore, in Fig. 2 these points are plotted at 163 kV/cm. Lucite was the only material for which craters were observed on the cathode after the flashover measurements.

SEM (Scanning Electron Microscopy), ESCA (Electron Spectroscopy for Chemical Analysis), and FTIR (Fourier Transform Infrared Spectroscopy) in the ATR (Attenuated Total Reflection) mode were used to study the surfaces of the samples after the flashover tests. SEM shows that exposed samples have a lower secondary electron emission (SEE) coefficient (at 5 keV incident electron energy) than the unexposed samples. But the track formed by a flashover on an exposed sample has a larger SEE than the adja-

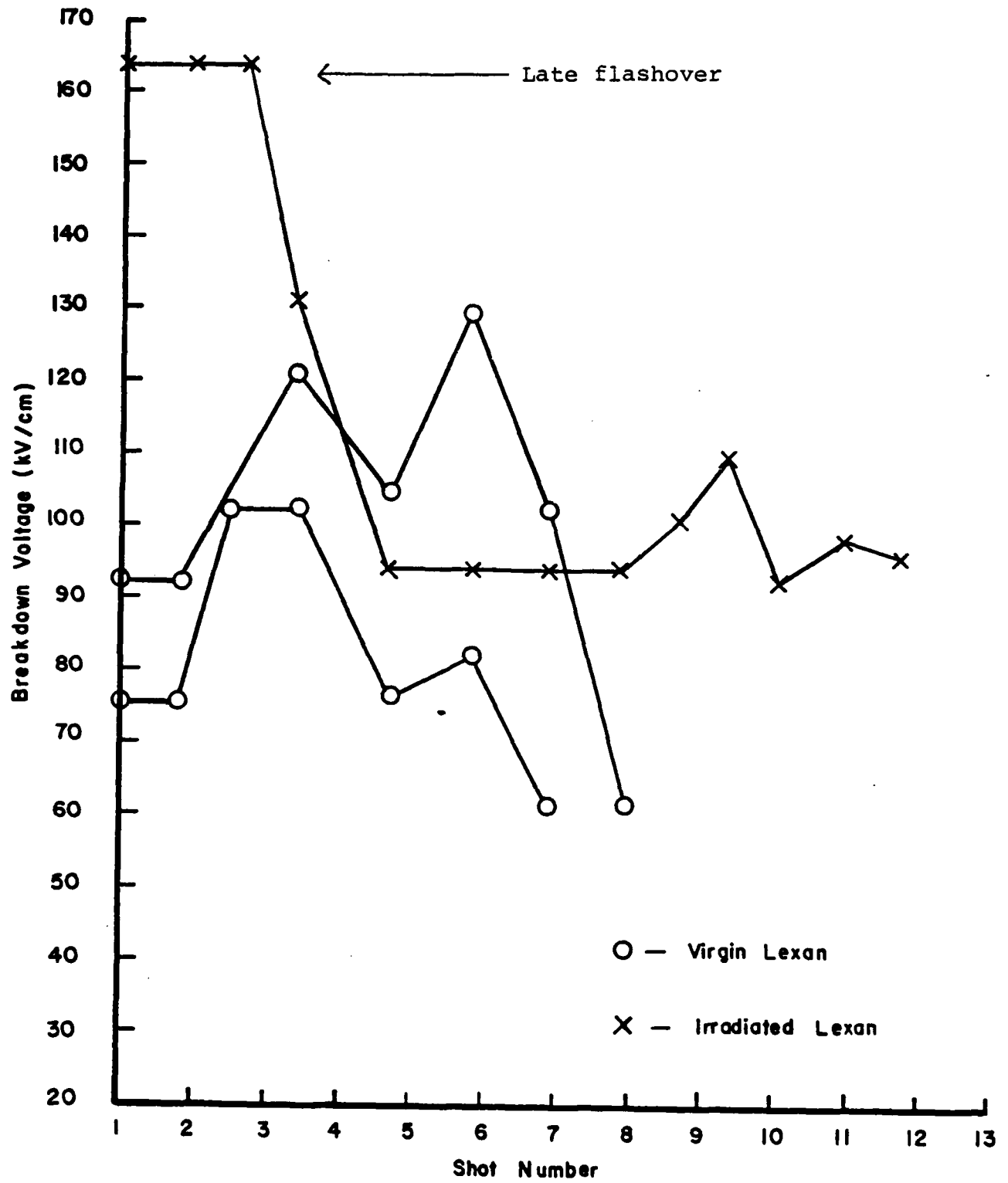


Fig. 2 Flashover potential of Lexan

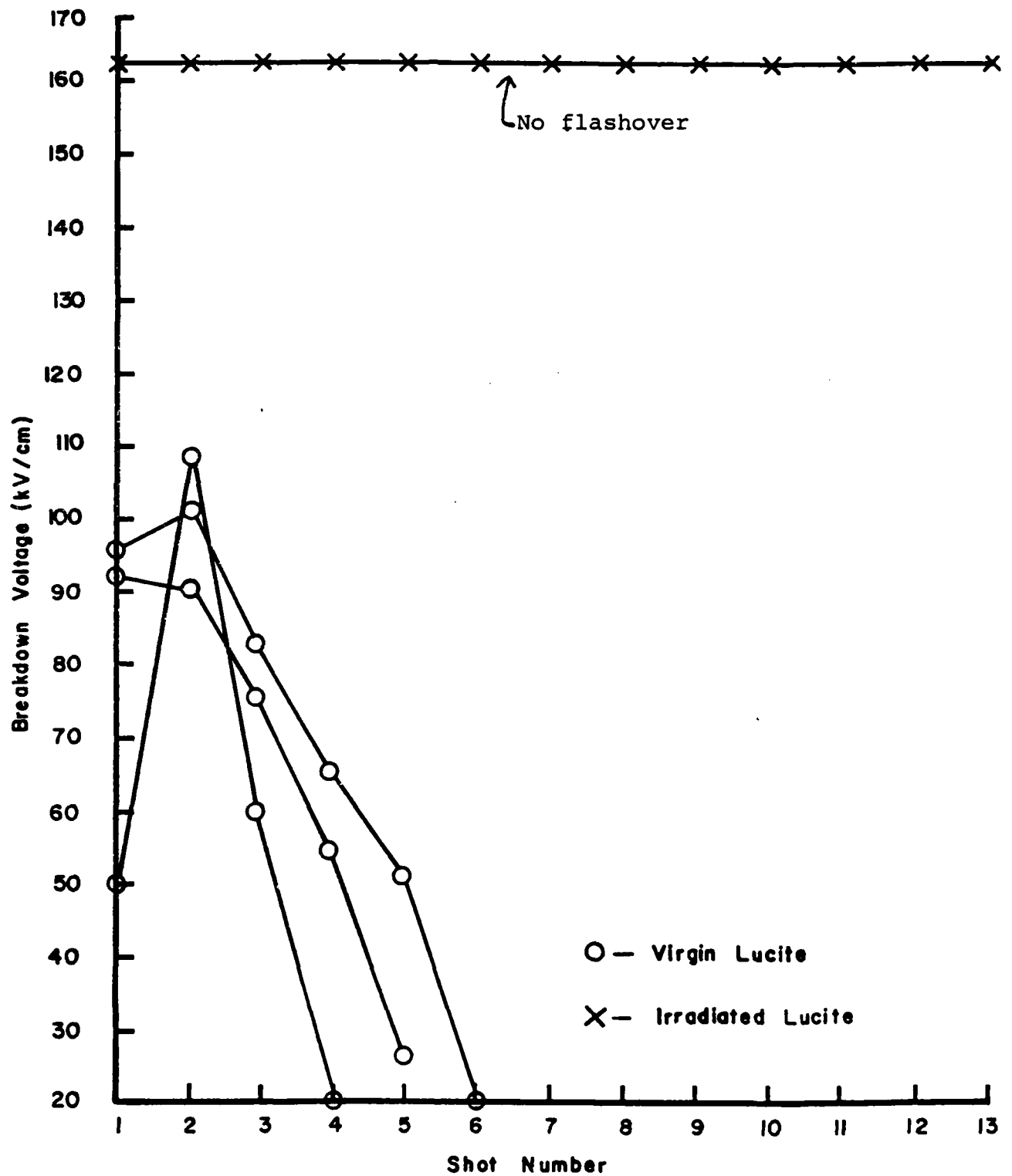


Fig. 3 Flashover potential of Lucite

cent undamaged surface. This suggests that exposure to the ignitor plug arc in vacuum produces a coating or damaged layer on the dielectric surface.

ESCA data from the surfaces of the exposed samples indicates that all the polymers are coated with a carbon-oxygen compound which exhibits both single and double C-O bonds and has the ESCA spectrum typical of a polymer. No sign of the underlying substrate (Lucite, Lexan, etc.) is seen. To substantiate this, a flat piece of boron nitride was exposed to the arc in vacuum for 80,000 shots and analyzed with ESCA. The results were identical to those using the polymers with no sign of the underlying substrate. The ESCA data do not have sufficient resolution to determine the exact structure, however. FTIR in the ATR mode on an exposed Lucite sample gives only the Lucite spectrum. From this and the ESCA spectrum we conclude that the coating is more than 50 to 100 Å thick and less than 200 to 500 Å thick.

Table II lists the results of surface resistivity measurements on virgin and exposed samples. Exposed samples have a surface resistivity two orders of magnitude less than virgin samples, but the resistivity is still  $10^{12}$  ohms or greater. This is too high to result in significant electric field grading by the coating during the applied flashover pulse. A simple calculation shows that the surface resistance ( $R_s \sim 6 \times 10^{13}$  ohms) for these samples combined with the capacity of the measuring system ( $C \sim 100$  pf) result in a  $1/e$  leakdown time of about 15 minutes for surface charge. We conclude that this explains the 15 minute wait between flashover measurements required to get consistent data. Measurements conducted with a five minute wait gave  $\pm 100\%$



scatter! This could be an important factor in high voltage systems with insulating surfaces that become charged during successive voltage pulses.

Table II

## Surface Resistivity of Virgin and Exposed Insulators

<u>Insulator</u>	<u>Surface Resistivity</u>
Lucite (virgin)	$4 \times 10^{16}$ ohms
Lucite (irradiated)	$3 \times 10^{12}$ ohms
Lexan (virgin)	$2 \times 10^{13}$ ohms
Lexan (irradiated)	$3 \times 10^{12}$ ohms
Delrin (virgin)	$5 \times 10^{14}$ ohms
Delrin (irradiated)	$2 \times 10^{12}$ ohms
Blue Nylon (virgin)	$7 \times 10^{12}$ ohms
Blue Nylon (irradiated)	$2 \times 10^{12}$ ohms

## c. Damage due to flashover

After the flashover measurements the samples were examined for tracks on the surface. All materials except Lucite exhibited visible tracks at the place where multiple flashovers occurred. Also, for all but Lucite, small particles of the polymer material were found firmly attached to the electrode surfaces around the perimeter of the sample. The behavior of Lucite was different in several aspects. As noted above, only one or two flashover pulses

could be applied to unexposed Lucite samples before the arcs began to occur at always the same location on the surface, indicating the formation of the track. The formation of a track was also indicated by successively lower flashover voltages after the first one or two shots. But, when the samples were removed and examined, no track could be found. Examination of the cathode always revealed a crater, about 10  $\mu\text{m}$  deep and 2  $\mu\text{m}$  in diameter, at the location of the repeated flashovers. We must conclude that the crater is the cause of the lowered flashover potential and the successive arcs at the same position. The effects of such imperfections on the electrode surfaces have been studied by others [4]. Since Lucite is the only material for which a crater appeared, some property peculiar to the Lucite must be responsible. Table I shows that the flashover potential is not higher for Lucite than for the other materials and therefore the total energy in the arc is not larger. The arc could have a larger current density which would promote the formation of craters. How the current density is related to the properties of the insulator material is not presently understood.

## 2. Pulsed Flashover in Gases

The flashover potentials of Lucite, Lexan, Delrin, and Blue Nylon were measured at three different pressures in nitrogen gas and in a mixture of 80%  $\text{N}_2$ , 20%  $\text{SF}_6$ . The procedure was the same as that used in vacuum, except the chamber was back filled with the gas to the desired pressure just before the measuring sequence began. Table III lists the results for the two gases and for exposed and unexposed samples. There are notable

Table III

Nitrogen Gas

<u>Insulator</u>	<u>635 Torr</u>	<u>317 Torr</u>	<u>12.7 Torr</u>
Lucite (virgin)	44 kV/cm	22 kV/cm	5 kV/cm
Lucite (irradiated)	48 kV/cm	18 kV/cm	14 kV/cm
Lexan (virgin)	57 kV/cm	35 kV/cm	9 kV/cm
Lexan (irradiated)	65 kV/cm	44 kV/cm	13 kV/cm
Delrin (virgin)	44 kV/cm	25 kV/cm	4 kV/cm
Delrin (irradiated)	44 kV/cm	28 kV/cm	13 kV/cm
Blue Nylon (virgin)	44 kV/cm	26 kV/cm	5 kV/cm
Blue Nylon (irradiated)	44 kV/cm	22 kV/cm	11 kV/cm

80% N<sub>2</sub> + 20% SF<sub>6</sub>

<u>Insulator</u>	<u>635 Torr</u>	<u>317 Torr</u>	<u>12.7 Torr</u>
Lucite (virgin)	80 kV/cm	34 kV/cm	11 kV/cm
Lucite (irradiated)	80 kV/cm	33 kV/cm	13 kV/cm
Lexan (virgin)	87.2 kV/cm	24 kV/cm	12 kV/cm
Lexan (irradiated)	67.6 kV/cm	25 kV/cm	12 kV/cm
Delrin (virgin)	79.3 kV/cm	28 kV/cm	3 kV/cm
Delrin (irradiated)	72.6 kV/cm	31 kV/cm	3 kV/cm
Blue Nylon (virgin)	80.2 kV/cm	26 kV/cm	3 kV/cm
Blue Nylon (irradiated)	77.4 kV/cm	31 kV/cm	3 kV/cm

differences between the results for the two gases. Unlike the vacuum case, there was no conditioning during the first few shots. In  $N_2$  gas the flashover potential remained constant for pulses applied at 15 minute intervals until a track developed after only 3 or 4 shots. In the 80%  $N_2$ , 20%  $SF_6$  mixture, 20 to 40 shots were taken without a decrease in the flashover potential, despite the fact that the energy in the arc was 4 times greater. (The flashover potential in the mixture was twice that in pure  $N_2$  and the energy dissipated in the arc is approximately the energy stored in the coaxial cable and parallel plate capacitor which holds the sample.)

The values listed in Table III show that at about 1 atmosphere (635 Torr) the surface modification of the dielectric sample by the vacuum arc has little effect on the flashover potential. At 317 Torr the trend is uncertain. At 12.7 Torr there is clearly a large increase in flashover potential for exposed samples tested in  $N_2$  but not for those tested in the gas mixture. It is apparent that  $SF_6$  either obviates the influence of the dielectric surface condition or changes the surface of the dielectric.

Surface analysis of the samples flashed over in  $N_2$  show chemical bonding of nitrogen on the surface where there was a flashover, although the ESCA resolution is not good enough to identify the bond uniquely. On the same samples, at positions where there was no flashover, only adsorbed nitrogen is observed. The same results were obtained for samples tested in the gas mixture except that, of course, chemically bonded fluorine is found on the surface where a flashover occurred.

differences between the results for the two gases. Unlike the vacuum case, there was no conditioning during the first few shots. In  $N_2$  gas the flashover potential remained constant for pulses applied at 15 minute intervals until a track developed after only 3 or 4 shots. In the 80%  $N_2$ , 20%  $SF_6$  mixture, 20 to 40 shots were taken without a decrease in the flashover potential, despite the fact that the energy in the arc was 4 times greater. (The flashover potential in the mixture was twice that in pure  $N_2$  and the energy dissipated in the arc is approximately the energy stored in the sample capacitor system.)

The values listed in Table III show that at about 1 atmosphere (635 Torr) the surface modification of the dielectric sample by the vacuum arc has little effect on the flashover potential. At 317 Torr the trend is uncertain. At 12.7 Torr there is clearly a large increase in flashover potential for exposed samples tested in  $N_2$  but not for those tested in the gas mixture. It is apparent that  $SF_6$  either obviates the influence of the dielectric surface condition or changes the surface of the dielectric.

Surface analysis of the samples flashed over in  $N_2$  show chemical bonding of nitrogen on the surface where there was a flashover, although the ESCA resolution is not good enough to identify the bond uniquely. On the same samples, at positions where there was no flashover, only adsorbed nitrogen is observed. The same results were obtained for samples tested in the gas mixture except that, of course, chemically bonded fluorine is found on the surface where a flashover occurred.

### 3. Surface Flashover Model

There is no generally applicable theoretical model of surface flashover. The model published by Hackam and Pillal [5], which is based on an earlier model proposed by Anderson and Brainard[6], treats d.c. charged systems in vacuum. In this model electrons are field emitted from the cathode at low applied fields due to field enhanced enhancement at the cathode-dielectric-vacuum (the so-called triple point) junction. These electrons are accelerated by the applied field and some strike the dielectric surface. This causes emission of secondary electrons and desorption of gas from the surface. The secondary emission plays two roles. It modifies the current on the dielectric surface and causes charging of the surface. If the secondary electron emission coefficient (SEE) is greater than one, the surface current will increase and the surface will accumulate a positive charge. Positive charge on the surface increases the fraction of available electrons which strike the surface, leading to a runaway electron current avalanche. The significance of the desorbed gas is that as the gas density near the surface increases and the current builds up, the system approaches the conditions necessary for a Townsend breakdown. All of this depends on the SEE and the SEE depends on the incident electron energy and the properties of the dielectric surface. The incident electron energy is determined by the applied field and the field due to the charged dielectric surface. Although a detailed analysis is not available, it appears that the system will come to equilibrium at an incident electron energy for which the SEE equals one.

This model is formulated for a d.c. applied field. However, if the equilibration time is very short compared with the time required for the applied field to increase significantly, then the d.c. condition applies to the pulsed case also. For our system the calculated equilibration time is a few ns, while the risetime of the applied voltage is 5  $\mu$ s. The d.c. assumption is, therefore, valid for our system.

Using this model, the coating which accumulates on our dielectric samples, due to exposure to the ignitor plug arc, can affect the flashover potential by changing either the SEE or the rate of desorption of adsorbed gas. We have made no measurements of the gas desorption rate, but the SEM data definitely show a lower SEE for coated samples at an incident electron energy of 5 keV. This result was obtained by viewing small pieces of coated and uncoated samples side-by-side in the SEM and also by viewing a tracked region on a coated sample. In both cases the coated surfaces appear darker, indicating a smaller SEE. Quantitative measurements of the SEE are beyond the scope of this work but could be done in our laboratories. Measurements of the gas desorption rate could also be done in our laboratories but would require resources not provided under this project.

The above model can also be applied to flashover in gases. At the two higher pressures used in our measurements the desorption of gas from the surface is unimportant because the gas density is already sufficient for a Townsend breakdown. Or, in other words, the electron mean free path between collisions with gas molecules is comparable to the mean path length between collisions with the dielectric surface. This implies that the

surface SEE does not play a role in the flashover at the two higher pressures and the data presented in Table III bear that out. Although virgin and exposed samples of the same material exhibit different flashover potentials in some cases, there is no consistency in going from one material to the other or from pure  $N_2$  to the mixture with  $SF_6$ .

Results from other investigators show that the dielectric surfaces in this experiment probably will be charged after application of a high voltage pulse whether or not a flashover actually occurs [7]. We have made no surface charge measurements on our samples and, therefore, are not prepared to comment on the differences between coated and uncoated samples.

At the lower pressure (12.7 Torr) shown in Table III the mean free path of the electrons in the gas is larger than the length of the trajectory followed by the electrons between collisions with the surface. This means that surface effects should be important, and indeed, the arguments using the lowered SEE for coated samples are consistent with the data for flashover in pure  $N_2$ . But the data from the mixture of 80%  $N_2$  - 20%  $SF_6$  imply that the  $SF_2$  greatly decreases the role of surface effects even at 12.7 Torr.

The  $SF_6$  has a large electron attachment coefficient for low energy electrons [8]. Low energy electrons field emitted from the triple point will be attached, as will low energy secondary electrons emitted from the dielectric surface. The first process will raise the flashover potential of any dielectric compared to that in pure  $N_2$ . The attachment of secondaries makes the SEE of the dielectric surface less important. Table III shows a very low



flashover potential for Delrin and Blue Nylon at 12.7 Torr in 80%  $N_2$  - 20%  $SF_6$ . Blue Nylon was also the only material that had a lower flashover potential in vacuum after exposure to the ignitor plug. Using the SEM we have discovered that the coating on the Blue Nylon is discontinuous, due to some peculiarity of the nylon surface. Delrin, on the other hand, gave results comparable to Lucite and Lexan when tested in vacuum and the coating on Delrin appears to be continuous. One possible explanation is that attachment of surface emitted secondaries by  $SF_6$  is not effective in the Delrin case. If the SEE of the Delrin surface (coated or uncoated) goes above 1 for incident electron energies that lie in the region for which the attachment coefficient of  $SF_6$  is small, then the  $SF_6$  would be ineffective in suppressing the buildup of surface current and surface charge. In fact, the data in Table III imply that the  $SF_6$  molecules are less effective than the  $N_2$  molecules at 12.7 Torr, i.e., the flashover potential for Delrin is larger in  $N_2$  gas than in the mixture.

As mentioned above, the number of flashover trials before formation of a track was much larger in the mixture than in pure  $N_2$ . To demonstrate that this much higher damage threshold was due to the  $SF_6$ , a Lucite sample was tested in a pure  $SF_6$  atmosphere at 127 Torr, the partial pressure of the  $SF_6$  in the mixture at 635 Torr. No track formed, even after 25 flashover arcs. Several possibilities are suggested. Since tracking depends on the current density in the arc, perhaps the current density is less when  $SF_6$  is present. Tracking also depends on the peak current in the arc, however, measurements with a B-dot probe showed the peak current in our apparatus to be independent of

the gas in the chamber. The most likely explanation is that SF<sub>6</sub> molecules, adsorbed on the dielectric surface, attach low energy electrons, producing a large negative surface charge which drives the arc away from the surface. This last suggestion could be tested using streak photography but that would require a geometry in which the location of the flashover is known in advance. In our apparatus, the flashovers occur at random locations on the surface of the cylinder (until a track forms).

Others have tried coating dielectrics with low SEE materials in order to raise the flashover voltage [9]. Because of some notable failures (Cu<sub>2</sub>O<sub>3</sub> coatings, for example) considerable skepticism about the utility of this approach exists. However, the coating on our samples does not exhibit the shortcomings of some of the ones tried previously. It adheres strongly to the surface and is removed only by mechanical abrasion or by a high peak current arc along the surface. It has a large surface resistivity so that joule heating during the applied voltage pulse is not a problem. In addition, we have demonstrated that the effect persists after exposure to ambient air and subsequent application in a vacuum system.

The practical questions which remain are, exactly what is the composition and structure of the coating, and could it be applied by some other method, suitable for large surface areas? This technique could then be extremely valuable to high voltage insulator designs and construction for vacuum and low pressure systems.

### C. SURFACE ANALYSIS OF ELECTRODES AND INSULATORS

Samples of electrodes and insulators used in the Mark I and II spark gaps and samples from insulators used in the surface discharge switch were analyzed to characterize the surfaces and surface changes. Those findings which relate directly to the operation of the switches are presented in the Project 3 and 6 reports. Many of the surface analysis results have already appeared in print [10]. A summary of the results is presented here.

#### 1. Electrodes

Three dimensional analysis using stereo SEM micrographs has been applied to electrode samples from the Mark II spark gap. This technique allows measurements of the heights and base diameters of protrusions on the electrode surface. The distribution of the sizes of such protrusions plays an important role in the modeling of the self-breakdown voltage statistics studied in Project 3. All results on the sizes of these protrusions (which appear as the result of operating the spark gap) fully support the model. In particular, the prediction by the model that protrusions with less than a certain height to base diameter ratio have no effect on the breakdown statistics below a certain gas pressure has been verified. This has been extremely important in understanding why the electrode surface structure dominates the breakdown statistics in some cases but not in others.

A second example of the necessity of surface studies of electrodes is shown in Fig. 4. The central regions of two stainless steel electrodes, one used in nitrogen gas (Fig. 4a), and

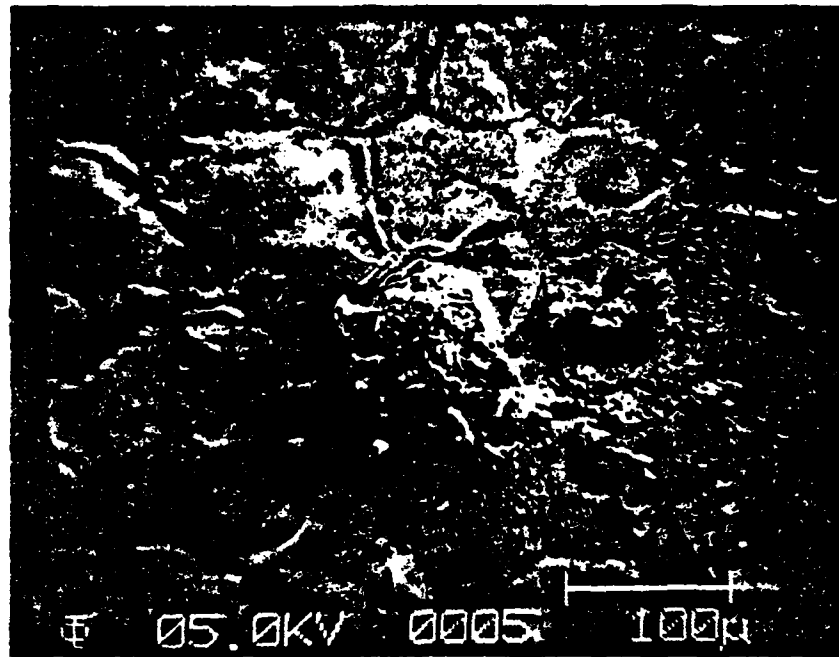


Fig. 4a Inner region of stainless steel electrode  
used in nitrogen gas

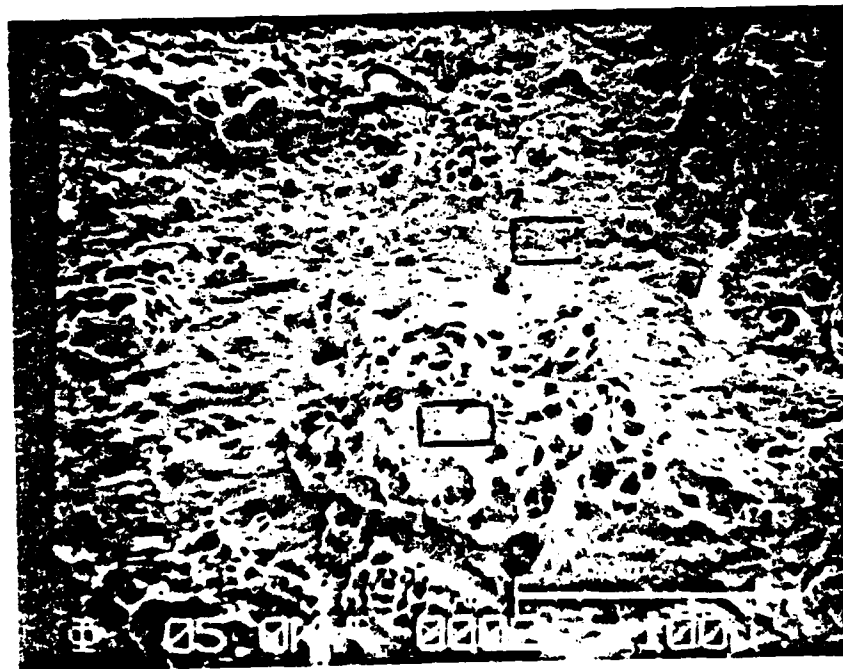


Fig. 4b Inner region of stainless steel electrode  
used in air

## D. SURFACE ANALYSIS OF ELECTRODES AND INSULATORS

Samples of electrodes and insulators used in the Mark I and II spark gaps and samples from insulators used in the surface discharge switch were analyzed to characterize the surfaces and surface changes. Those findings which relate directly to the operation of the switches are presented in the Project 3 and 6 reports. Many of the surface analysis results have already appeared in print [10]. A summary of the results is presented here.

### 1. Electrodes

Three dimensional analysis using stereo SEM micrographs has been applied to electrode samples from the Mark II spark gap. This technique allows measurements of the heights and base diameters of protrusions on the electrode surface. The distribution of the sizes of such protrusions plays an important role in the modeling of the self-breakdown voltage statistics studied in Project 3. All results on the sizes of these protrusions (which appear as the result of operating the spark gap) fully support the model. In particular, the prediction by the model that protrusions with less than a certain height to base diameter ratio have no effect on the breakdown statistics below a certain gas pressure has been verified. This has been extremely important in understanding why the electrode surface structure dominates the breakdown statistics in some cases but not in others.

A second example of the necessity of surface studies of electrodes is shown in Fig. 4. The central regions of two stainless steel electrodes, one used in nitrogen gas (Fig. 4a), and

one used in air (Fig. 4b) exhibit quite different topographies. This is due to the chemical reactions promoted by the arcs and the resulting high temperatures. The constituents of the stainless alloy readily form oxides but will also form nitrides. AES applied to both samples showed oxides and nitrides on the sample used in nitrogen but only oxides on the ones used in air. In addition, results from Project 3 show that a stainless steel electrode used in nitrogen exhibits a much narrower self-breakdown voltage distribution than stainless steel used in air. Also, the electrode used in air suffers a greater erosion rate. These dramatic differences prompted a more sophisticated study of the surface and bulk changes of these electrode samples [11]. Some of the results are already available and are incorporated into the Project 3 report.

One of the surface properties of electrodes, important in spark gap operation, is the electron emissivity of the surface. Oxides and nitrides are known to have higher emissivities than pure metal surfaces. The narrow distribution of self-breakdown voltages for stainless steel in nitrogen may be due to the nitrides on the surface. The emissivity enters the  $V_{SB}$  statistics through the initial electron current factor,  $i_e$ , as described in the Project 3 report. Quantitative results on this point would require in-situ measurements of the emissivity which are beyond the scope of the present project but which could be done in our laboratories.

Studies of the surfaces of K-33 and graphite electrodes also led to results which can be applied to the  $V_{SB}$  statistics and erosion models. K-33 samples, analyzed using AES, typically show

regions which are excellent insulators. The composition of these regions could not be determined using AES because of the extremely large accumulated surface charge. ESCA has not been applied since ESCA analyzes a 4 mm diameter area and these insulating regions are microscopic in size.

These regions can significantly affect the breakdown initiation by holding charge from one shot to the next. Graphite electrodes, on the other hand, exhibit smoother surfaces so that no studies of protrusions are necessary. However, insulating regions have been observed on graphite electrodes also. Since carbon does not form solid oxides the surfaces were investigated for more complex molecules using fluorescence techniques. Measurements on one graphite electrode, using a UV spectrofluorimeter, indicated the presence of a polymer which we cannot identify unambiguously. The same sample showed a high concentration of nitrogen on the surface when analyzed using ESCA. It is possible that a CN compound formed on the surface or that material from the polymer dielectric (Lexan) used as an insulator in the gap deposited on the electrode. We know of no analysis technique capable of resolving this problem. Evidence that the polymer insulator material does contaminate the electrodes is indirect. However, all electrode samples investigated exhibit hydrocarbon surface layers which could be decomposition products of the polymers used in these experiments.

## 2. Insulators

Surface studies of dielectrics used in the Mark I and II spark gaps and the surface discharge switch have played an impor-

tant role in the evolution of these projects. When  $\text{AlF}_3$  was identified on the surface of a blue nylon insulator, used in Mark I with  $\text{SF}_6$  gas, it was discovered that the aluminum electrode holders were arcing and modifications were made immediately. Another example of the importance of the surface studies comes from analysis of dielectrics used in the surface discharge switch. No deposited metal coatings were found on these dielectrics except right at the electrode-dielectric interface. However, the operating characteristics of the switch did change with the number of shots across the dielectric, and all materials gave approximately the same performance characteristics. ESCA showed that all the materials used became coated with a hydrocarbon which is most likely the result of plasma chemistry induced by the arcs in the compressed air jet ("dirty" laboratory supply) used to keep the surface from charging to the point where the switch would no longer multichannel [12]. The switch was then changed to include a chamber in which pure  $\text{N}_2$  (or clean air) and an  $\text{N}_2$  gas (or clean air) jet could be used instead of laboratory air [13]. Samples of dielectrics used with these clean gases do not show the hydrocarbon coating, and different dielectric materials do give different switch performance characteristics. See the Project 6 report for details of switch performance.

In almost all cases, the cylindrical insulator sleeves used in the Mark II gap accumulated a coating of evaporated electrode material. The one exception occurred when graphite electrodes were used in one atm. of air. Figure 5 is an SEM micrograph of the region on the Lucite cylinder where the heaviest coating should be expected. No coating of graphite occurred, only a low





Fig. 5 Lucite insulator used in the Mark II spark gap with graphite electrodes and air



Fig. 6 Lucite insulator used in the Mark II spark gap with copper-graphite electrodes and air

density of graphite microparticles with a maximum size of 10 microns is seen. When graphite electrodes were used with pure N<sub>2</sub> gas a heavy coating of carbon, some tenths of a mm thick, accumulated. The only reasonable explanation is that the oxygen in the air combines with the carbon from the electrodes to form CO and/or CO<sub>2</sub> which is carried out of the gap by the flowing air. The same test, run with copper-graphite composite electrodes in air and N<sub>2</sub> gas, produced heavy coatings on the Lucite insulator (Fig. 6) in both cases. This coating, using ESCA, appears to be carbon, no copper was detected. Most likely, copper is present but is covered by carbon so that ESCA which analyzes only to a depth of about 50 Å does not reveal the copper.

Two unusual results were obtained using blue nylon insulators. When blue nylon was used with graphite electrodes in N<sub>2</sub> gas a nodule containing silicon was found on one of the electrode samples. As discussed above, such protrusions can cause field enhancement on the surface, and if they are insulators (as the silicon nodules are) may also increase the emissivity of the surface. Silicon was found on the blue nylon and turned out to be a residue from the mold release used during the manufacturing process [14]. In another case, a blue nylon insulator used with K-33 electrodes in N<sub>2</sub> gas was analyzed with ESCA. Compared with a virgin sample, the surface carbon content had decreased by 50%, oxygen increased by about 30%, and silicon increased by about 20%. No copper or tungsten from the electrodes was detected. The surface changes can be attributed to damage by U-V radiation from the arc, but the lack of deposited metal film is difficult to understand. Perhaps the silicon on the surface inhibits the for-

mation of such films. The significance of this discussion is that with the silicon in the blue nylon there is a trade-off. Inhibition of metal films is beneficial, since these can lead to surface failure by promoting flashover. Nodules growing on the electrode surface are not desirable because they lead to erratic changes in the breakdown voltage as they appear and burn off.

Samples of Delrin, Lucite, and G-10 used in the surface discharge switch, in a pure  $N_2$  atmosphere, were analyzed with ESCA. Neither Lucite nor G-10 showed any surface structure changes. The surfaces were eroded and large surface charges appeared on all three after 500 shots in the switch [15]. The Delrin sample exhibited large changes in surface structure. Compared to a virgin Delrin sample, the sample subjected to 500 shots had 40% less surface carbon and 70% more oxygen. The ESCA spectrum also shows a large increase in the number of C-O double bonds at the expense of single bonds. Since the Delrin polymer contains C-O single bonds and the monomer contains a double bond, the conclusion is that the Delrin has decomposed into the monomer. This is known to happen when Delrin is exposed to U-V radiation or high temperatures, both of which are available as a result of the arcs near the surface. There are two reasons why this makes Delrin unsuitable as a dielectric switching surface. Decomposition to the monomer is an extremely efficient erosion process and the monomer has a high vapor pressure resulting in contamination of the switch chamber.

The surface resistivities of G-10 and Lucite, virgin and used samples are listed in Table IV.

Table IV  
 Surface Resistivities of Dielectrics  
 Used in the Surface Discharge Switch

G-10	Virgin	$5.8 \times 10^{12}$ ohms
G-10	After 4000 shots	$1.6 \times 10^9$ ohms
Lucite	Virgin	$2.8 \times 10^{13}$ ohms
Lucite	After 4000 shots	$4.3 \times 10^{10}$ ohms

In each case there is a large decrease in surface resistivity after use in the switch. Since no changes in surface structure and no signs of metal films were observed it is difficult to account for this large change. It is possible that some change has taken place at a depth in the material greater than the analysis depth of ESCA (50 to 100 Å in these materials). There is a contribution of the volume resistivity to the surface resistivity which is unavoidable. If the resistivity of the material at a depth of more than 100 Å has decreased dramatically, the surface resistivity indicated by our technique would also decrease.

## D. REFERENCES

1. G.L. Jackson, L.L. Hatfield, M. Kristiansen, J. Marx, and A. Bowling, "Pulse Flashover of Solid Dielectrics in Vacuum", IEEE Transactions on Electrical Insulation, EI-18, 310 (1982).  
  
G. Jackson, L. Hatfield, G. Leiker, M. Kristiansen, and J. Marx, "Pulsed Flashover of Solid Dielectrics in Gases", Proceeding of the 4th IEEE Pulsed Power Conference, Albuquerque, NM, June 6, 1983.
2. G. Jackson, L. Hatfield, M. Kristiansen, M. Hagler, J. Marx, A.L. Donaldson, G. Leiker, R. Curry, R. Ness, Lloyd Gordon, and D. Johnson, "Surface Studies of Dielectric Materials Used in Spark Gaps", Journal of Applied Physics, 55, 262 (1984).  
  
G. Jackson, L. Hatfield, M. Kristiansen, M. Hagler, A.L. Donaldson, R. Ness, and J. Marx, "Surface Studies of Electrodes Used in Spark Gaps", Proceedings of the 4th IEEE Pulsed Power Conference, Albuquerque, NM, June, 1983.
3. George L. Jackson, "Pulsed Flashover of Solid Dielectrics in Vacuum and Gases", Ph.D. Dissertation, Texas Tech University, 1983.
4. S. Berger, "Onset or Breakdown Voltage Reduction by Electrode Surface Roughness in Air and SF<sub>6</sub>", IEEE Trans. Power Appar. and Sys., PAS-95, 1073 (1976).
5. A. Pillai and R. Hackam, "Surface Flashover of Solid Dielectric in Vacuum", Journal of Applied Physics, 53, 2983 (1982).
6. R.A. Anderson and J.B. Brainard, "Mechanism of Pulsed Surface Flashover Involving Electron-Stimulated Desorption", Journal of Applied Physics, 51, 1414 (1980).
7. C.M. Cook, "Charging of Insulator Surfaces by Ionization and Transport in Gases", IEEE Trans. Elect. Insul., EI-17, 172 (1982).
8. S.C. Brown, "Basic Data of Plasma Physics", Massachusetts: MIT Press, p. 207, 1966.
9. T.S. Sudarshan and J.D. Cross, "The Effect of Cuprous Oxide Coatings on Surface Flashover of Dielectric Spacers in Vacuum", IEEE Transactions on Electrical Insulation, EI-9, 146 (1974).
10. See ref. 1

11. Dr. Paul Predecki has analyzed some of the stainless steel samples using facilities at the Denver Research Institute. His results explain the difference in erosion rate for stainless steel in air and nitrogen.
12. D. Johnson, M. Kristiansen, and L. Hatfield, "Multichannel Surface Discharge Switch", Annual Report of the Conference on Electrical Insulation and Dielectric Phenomena, Amherst, MA, October 17, 1982.
13. R. Curry, D. Johnson, M. Kristiansen, L. Hatfield, and A.H. Guenther, "Triggering of Surface Discharge Switches", Proc. of the 4th IEEE Pulsed Power Conference, Albuquerque, NM, June 6, 1983.
14. Private communication with technical personnel at Polypenco Corporation.
15. R.D. Curry, M. Kristiansen, L.L. Hatfield, V.K. Agarwal, and G.L. Jackson, "Surface Charging of Insulators in a Surface Discharge Switch", Annual Report of the Conference on Electrical Insulation and Dielectric Phenomena, Buck Hill Falls, PA, October 16, 1983.

## Project No. 5

Excited State Spectroscopy of Electrically Excited Gases

(S. K. Dhali, and P.F. Williams)

## A. SUMMARY

Work during the contract period on this project centered around developing and using numerical techniques based on flux-corrected-transport ideas for solving the standard transport equations in the space-charge-dominated regime. As a result of this work, we are now able for the first time to simulate numerically the propagation of streamers without the numerical difficulties that have limited previous work in the field. This work has important consequences for understanding, not only laser-triggered and other types of triggered spark gaps, but also more general questions of over-volted breakdown. At the end of the contract period the work had already shed new light on long-standing questions concerning polarity effects in laser-triggered breakdown, and work is continuing to understand better the roles of photoionization and of the laser-streamer interaction.

## B. ACCOMPLISHMENTS

Work under this project has centered around the study of streamer propagation and space-charge-dominated transport in general in gases. In this effort, we have developed numerical techniques which for the first time allow the numerical simulation of the propagation of a streamer under realistic conditions.

The primary motivation for this study is to improve quantitative understanding of laser-triggered breakdown in support of the more experimentally-oriented work discussed under Project No. 2 of this report. Our efforts to date have been quite successful in this regard in that the results we have obtained have provided us with new insight into the operation of laser-triggered switches. Additionally, because the numerical techniques we have developed allow us to investigate problems important to streamer propagation which can not be addressed with older techniques, our results also have an important impact on more general, long-standing questions regarding the electrical breakdown of over-volted gaps.

## 1. Introduction

Since the streamer mechanism was first suggested by Raether, a large volume of evidence has been accumulated showing the importance of streamers to many aspects of electrical breakdown of gases. Because a streamer is a stable propagating mode under space-charge-dominated transport, this is an important area of study for the proper understanding of electrical breakdown in gases. Unfortunately, the mathematical description of transport under conditions for which space-charge fields play an important role proves very difficult to deal with in general. Several workers [1-4] have described the results of one-dimensional (both analytical and numerical) approaches to the problem, and there have been a few reports of numerical calculations based on an approximate two-dimensional approach [5,6]. We describe here



fully two-dimensional (three-dimensional with cylindrical symmetry) numerical calculations based on the flux-corrected transport technique. The technique has proved stable and capable of dealing with the steep density gradients which appear in streamer calculations. To our knowledge, this work represents the first application of this technique to the problem of space-charge-dominated transport in a fully two-dimensional model.

For a pure gas, where only one species of positive ions is present, the charge conservation equations may be written as

$$\frac{\partial n_e}{\partial t} = \alpha n_e |\vec{W}_e| - \vec{\nabla} \cdot (n_e \vec{W}_e) + \vec{\nabla} \cdot (D_e \vec{\nabla} n_e) + P \quad (1a)$$

$$\frac{\partial n_p}{\partial t} = \alpha n_e |\vec{W}_e| + \vec{\nabla} \cdot (n_p \vec{W}_p) + P, \quad (1b)$$

where  $n_e$  is the electron density,  $n_p$  is the positive ion density,  $W_e$  is the electron drift velocity,  $W_p$  is the ion drift velocity,  $\alpha$  is the electron impact ionization coefficient,  $D_e$  is the electron diffusion coefficient, and  $P$  is the source term due to photoionization and other secondary mechanisms.

The electric field is determined by the Poisson equation

$$\nabla^2 \phi = -q_e(n_p - n_e)/\epsilon_0 \quad (2)$$

where  $\phi$  is the electrostatic potential. To close our system of equations we assume a first order hydrodynamic model, for which the electrons come to instantaneous equilibrium with the local value of the ratio of electric field to gas pressure ( $E/P$ ). The various ionization and drift processes are then represented by microscopic, empirically determined parameters.

If the gap voltage remains constant and the charge densities are small then the electric field will be constant in time and space and it is then possible to obtain analytical solutions to the above set of equations. A discharge soon reaches a stage where the space-charge due to charged particles will no longer be negligible. The conservation equations now become non-linear and cannot be solved analytically so that numerical techniques must be used. One dimensional numerical models of discharges between plane-parallel electrodes have been described by Davies et. al. [4], Kline [3], and Yoshida et. al. [1], who numerically solved the above set of equations in one dimension using the method of characteristics. Three dimensional models of discharges between plane-parallel electrodes, assuming axial symmetry, have been solved by Davies et. al. [5] and Yoshida et. al. [6] by extending the method of characteristics to two dimensions. Here we describe the application of flux-corrected transport to solve the above set of equations in three dimensions assuming axial symmetry.

## 2. Computational Method

In the process of formation and propagation of streamers the electron and ion densities attain very steep gradients. An algorithm used to solve the transport equation should be able to maintain these gradients without becoming unstable. An algorithm which has been successfully used to model the shock front in fluids is the flux-corrected transport (FCT) algorithm developed

by Boris and Book [7]. Zalesak has extended the one dimensional method to a multi-dimensional flux corrector for fluid problems [8]. We have extended the two-dimensional flux correction technique to solve the continuity equation for an axially symmetric discharge.

Higher order (2nd and above) schemes for numerically integrating the continuity equations produce ripples near steep gradients. Lower order schemes, such as donor cells, do not produce ripples but suffer from excessive numerical diffusion. The flux-corrected transport constructs the net transportive flux point by point as a weighted average of a flux computed by a low order scheme and a flux computed by a high order scheme. The weighting is done so that the high order flux is used to the greatest extent possible without introducing false ripples. A detailed description and analysis of FCT may be found in Ref. 8.

The convective part of Equation (1a) can be written as

$$\frac{\partial n}{\partial t} + \vec{\nabla} \cdot (n\vec{W}) = 0.$$

For axially symmetric geometry

$$\frac{\partial (rn)}{\partial t} + \frac{\partial (rnW_r)}{\partial r} + \frac{\partial (rnW_z)}{\partial z} = 0 \quad (3)$$

Treating  $rn$  as the dependent variable we have

$$(rn)_t + f_r + g_z = 0$$

where  $f = rnW_r$  and  $g = rnW_z$ .

We used the modified Euler finite difference approximation to Equation (3) to carry out the time integration [11]. The low order flux was calculated using a donor cell scheme and the high order was calculated using an eighth order difference scheme [8]. The source term was computed for one time step and simply added to the convection term at the end of the time step. The source term due to electron impact ionization was

$$S = n_e \alpha |\vec{W}_e| ,$$

where  $\alpha$  is the ionization coefficient. The electric field was obtained by solving the Poisson equation,

$$\nabla^2 \phi = -q_e(n_p - n_e)/\epsilon_0 = -\rho/\epsilon_0 ,$$

using a numerical algorithm based on Fourier transforming in the z-direction and using cubic spline functions for integrating in the r-direction.

The basic Courant-Friedrichs-Lewy conditions must be obeyed for stability, i.e.

$$\epsilon = \frac{\Delta t W}{\Delta x} < \frac{1}{2} ,$$

where  $\Delta t$  is the time step,  $\Delta x$  is the grid spacing, and  $W$  is the drift velocity. For a pure convection problem,  $\epsilon$  ranging from 0.1 to 0.5 gives stable results. We found it necessary to use a lower value ( $\sim 0.01$ ) due to the strong space-charge effects caused

by the motion of the electrons. If the electrons are transported using a large  $\Delta t$  too many ions may be uncovered causing an abrupt change in the electric field.

For small  $\epsilon$  and in the region where the density from one grid point to the next changes by a factor of two or more there was an instability in the flux corrector. Using the notation of Zalesak [8], in the standard FCT the coefficient  $(C_{i,j})$  is limited in such a way that the antidiffusive flux  $(A_{i,j+1/2})$  acting in concert with other fluxes into and out of grid point  $(i,j)$  does not produce a false maximum or minimum at  $(i,j)$  in one time step. In the modifications we made, the coefficient  $(C_{i,j+1/2})$  is limited in such a way that no false maximum or minimum is produced at  $(i,j)$  in  $1/\epsilon$  time steps instead of just one time step. This is physically more realistic because it takes  $1/\epsilon$  time steps to transport an electron from one grid point to the next. This algorithm was tested with a constant velocity convection problem, with known analytic solution and was found to perform well with no evidence of the instability which occurred in the standard FCT algorithm.

### 3. Results

Simulations have been carried out using values for the transport parameters appropriate for nitrogen at 760 Torr [2], and applied fields ranging from 130% to 200% of static breakdown voltage. Infinite, plane-parallel electrodes separated by 0.5 cm were assumed. The initial conditions in these simulations were

chosen to approximate those present in laser-triggered breakdown experiments and to provide insight in the most straight-forward way into the basic physics of streamer propagation. Specifically, three cases have been considered to date, all involving spherically shaped neutral plasmas of Gaussian profile and a diameter of 0.4 mm: 1) the peak density was  $10^{14} \text{ cm}^{-3}$  and the sphere was located in the center of the gap; 2) the peak density was the same and the sphere was located on one electrode; and 3) the peak density was  $10^3 \text{ cm}^{-3}$  with the sphere placed on the electrode.

Several authors have described the results of numerical calculations of the early stages of conventional over-volted breakdown where the process is initiated by one or a few free electrons [1,6]. In this case the charge densities are sufficiently low that space-charge fields are not important initially, and the initial electrons are amplified through simple Townsend avalanching until these fields become important. Numerical studies carried out previously have been able to follow this process into the space-charge-dominated region until the density gradients became too steep, whereupon the numerical algorithm becomes inaccurate due either to excessive numerical diffusion or to numerically-induced ripples. The purpose of considering the third type of initial condition was to compare the results of our program with those of others in a mutually compatible region. With the same input parameters, our results agreed very well with published results.

For the remainder of the simulations that we had carried out at the end of the contract period, the density of charged particles in the initial plasma sphere was high enough that substantial field enhancement was produced by space-charge effects, and streamer propagation could start immediately without the need for an initial avalanche stage. This situation is similar to that expected in laser-triggered breakdown, and the results we have obtained lend insight into not only the operation of laser-triggered spark gaps, but also into the more general question of the propagation of streamers in general.

Particularly for cathode-directed streamers, it is necessary to include photoionization effects into these calculations. Experimental data exist relating the photoionization magnitude to the ionization rate in the streamer head [12], and one approach for including these effects involves the use of these data to determine the degree of photoionization produced ahead of the streamer. Although this approach would be expected to provide the most realistic simulation of streamer propagation, the physical interpretation of the numerical results is clouded by the complex photoionization process. Another approach which eases this interpretation is one in which a tenuous uniform background density of neutral plasma is artificially placed throughout the spark gap as part of the initial condition. The streamer then propagates into a known ionization density which is independent of the internal streamer conditions, and which can be varied by the "experimenter". We have carried out simulations using both photoionization "mechanisms", although at the end of the contract

period most simulations had been carried out using the "artificial" mechanism. In these calculations the initial density was either  $10^5$  or  $10^8 \text{ cm}^{-3}$ .

Figures 1 and 2 show the electron density and axial component of the electron drift velocity for an anode- and cathode-directed streamer, respectively, for several times. Since the drift velocity is directly proportional to the electric field strength, the drift velocity curves also show the axial electric field. In these figures, the initial condition consisted of a plasma sphere of density  $10^{14} \text{ cm}^{-3}$  placed on one electrode, the applied voltage corresponded to approximately 200% of the self breakdown voltage, and photoionization was artificially simulated by placing a uniform background plasma density of  $10^8 \text{ cm}^{-3}$  in the gap initially. Several features of streamer propagation are evident in these figures. First, note the very steep density gradients which build up, particularly for the cathode-directed streamer. The ability to handle these steep gradients without numerical instability or diffusion is the feature of the flux-corrected transport technique which allows us to carry out these calculations in a regime inaccessible to previous workers.

As the initial plasma sphere begins to shield itself, a region of enhanced field builds up just outside it and a streamer starts to propagate outwards, into the gap. At first, the streamer propagates readily in the Gaussian tail of the initial plasma sphere. As the streamer enters the region where only the tenuous background electron density of  $10^8 \text{ cm}^{-3}$  is available, propagation slows and charge density builds up. Propagation is



so rapid that the streamer does not have time to completely shield itself. This charge density build-up has the effect of reducing the dielectric relaxation time, thus allowing more complete shielding and, therefore, greater field enhancement at the head of the propagating streamer. Streamer propagation then continues, but the electron density at the head of the streamer decreases slowly as the streamer head propagates across the gap. This feature appears to be primarily an artifact of the method used for introducing photoionization effects into the calculation. For this applied field the Townsend ionization is significant, even without field enhancement, and the artificially introduced background electron density slowly avalanches up in the applied field, so that as the streamer traverses the gap it encounters a steadily increasing free electron density. Calculations were made in which an attempt was made to correct for this unwanted charge multiplication by making the Townsend ionization term in Eqs. (1) proportional to  $n - n_0$  instead of  $n$ , where  $n_0$  is the artificial background density. Although it was possible to keep the background density constant by this means, the technique may have influenced streamer propagation by drastically reducing charge build up at the extreme front of the streamers. This effect was most important for cathode-directed streamers since charge drift may cause the electron density to actually decrease in front of the streamer in the absence of ionization. In these constant background calculations, we found that the density in the streamer head stayed nearly constant as the streamer traversed the gap.

Also shown in Figs, 1 and 2 are plots of the axial component of the electron drift velocity, which is directly proportional to the axial component of the electric field. These plots show that shielding partly depletes the field inside the body of the streamer, but that the shielding is by no means complete. Just outside the streamer head the field is strongly enhanced, rising to a value somewhat larger than three times the applied field. Note that the streamer velocities are considerably larger than electron drift velocities, even at the peak of the field.

Figure 3 shows plots of the electron density for a cathode-directed and an anode-directed streamer for the same time and under identical conditions. It is clear that the cathode-directed streamer propagates more slowly than the anode-directed streamer, and that the electron density in the streamer head is larger for the cathode-directed streamer. This observation may explain the long standing question about why better triggering is observed in laser-triggered spark gaps when the struck electrode is positive rather than negative. For the positive struck electrode, a cathode-directed streamer occurs and leaves behind it a trail of relatively high electron density. Since after the streamer has traversed the gap the streamer channel must still be ohmically heated to form the spark channel, the cathode-directed streamer provides a better initial condition for this heating than does the anode-directed streamer.

#### 4. Conclusions

Through the development and use of novel two-dimensional numerical techniques based on flux-corrected transport we have been able to simulate numerically streamer propagation under realistic conditions. This work has allowed us, for the first time, to determine the spatial dimensions, propagation velocity, and free electron density in a propagating streamer. Streamers play a crucial role in the operation of several types of triggered gas discharge switches, as well as in many other engineering aspects of electrical breakdown in gases. The availability of these numerical techniques, particularly when coupled with realistic numerical algorithms for handling the heating phase of spark formation, will have important consequences for triggered gas discharge switch designs. It will allow the engineer to test the initial stages of the design on a computer, instead of being forced to construct several prototype switches for testing. Further, the capability of running computer "experiments" will lend insight into the operation of the space-charge-dominated transport equations, and will lead to better approximate analytical methods for dealing with them.

REFERENCES

1. K. Yoshida and H. Tagashira, J. Phys. D. 9, 491 (1977).
2. I. Abbas and P. Bayle, J. Phys. D 13, 1055 (1980).
3. L.E. Kline, J. Appl. Phys. 45, 2046 (1974).
4. A.J. Davies, C.S. Davies, and C.J. Evans, Proc. IEE 122, 765 (1975).
5. A.J. Davies, C.J. Evans, P. Townsend, and P.M. Woodison, Proc. IEE 124, 179 (1977).
6. K. Yoshida and H. Tagashira, J. Phys. D 12, L3 (1979).
7. J.P. Boris and D.L. Book, J. Comput. Phys. 11, 38 (1973).
8. S.T. Zalesak, J. Comput. Phys. 31, 335 (1979).
9. E.E. Kunhardt and P.F. Williams, submitted to J. Comput. Phys.
10. N.W. Allbright and D.A. Tidman, Phys. Fluids 15, 86 (1972).
11. F.B. Hilderbrand, Introduction to Numerical Analysis, (McGraw-Hill, New York, 1956), p. 201.
12. G.W. Penney and G.T. Hummert, J. Appl. Phys. 41, 572 (1970).

FIGURE CAPTIONS

1. Plots of a) the electron density, and b) the axial electron drift velocity for an anode-directed streamer for times 0.5, 1.0, 1.5 and 2.0 ns. As discussed in the text, the drift velocity is directly proportional to the electric field strength.
2. Plots of a) the electron density, and b) the axial electron drift velocity for a cathode-directed streamer for times 0.5, 1.0, 1.5, 2.0 and 2.5 ns. As discussed in the text, the drift velocity is directly proportional to the electric field strength.
3. Plot showing the electron density at a specific time for an anode-directed and a cathode-directed streamer under otherwise identical conditions.

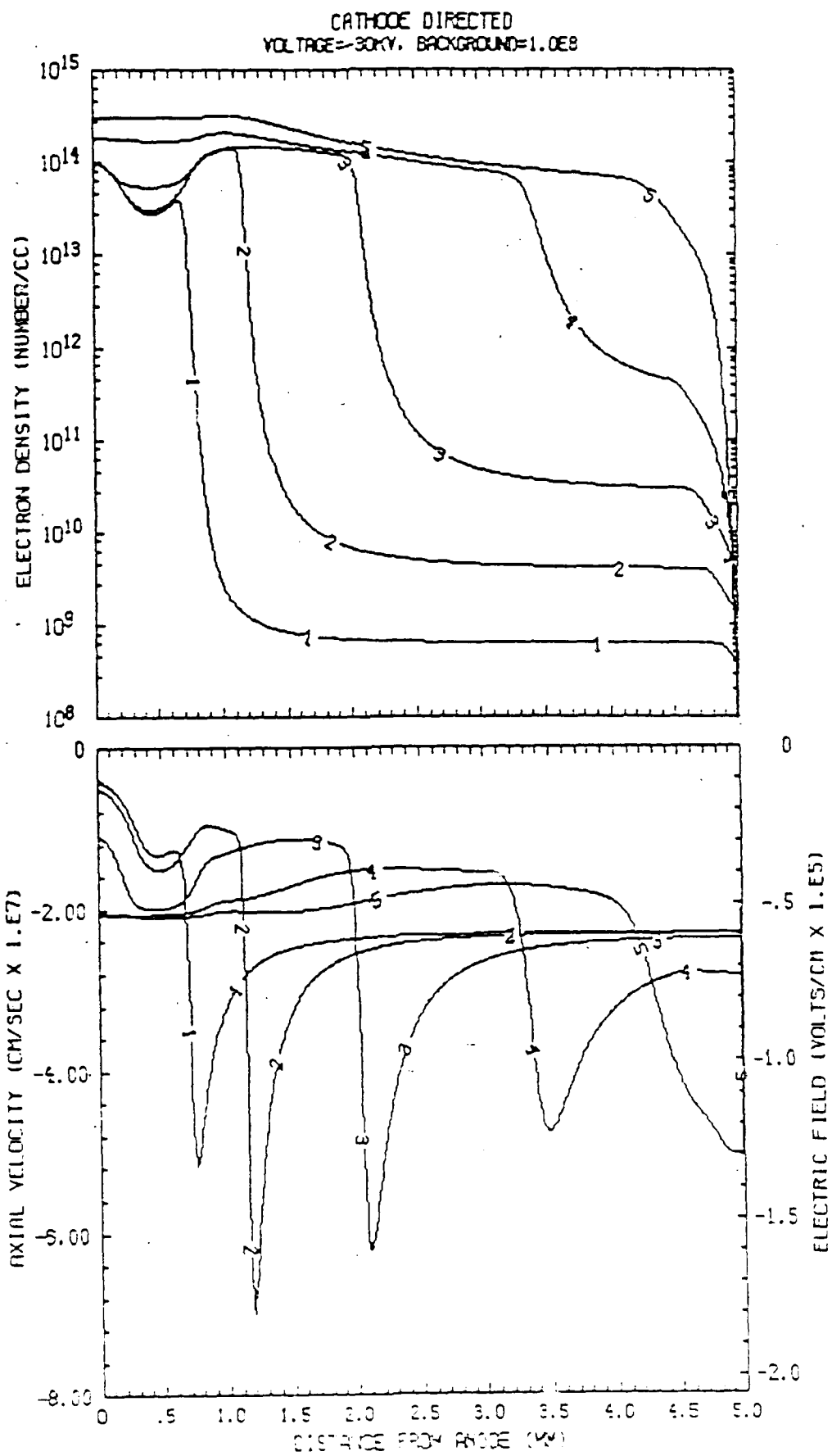


FIG. 1

ANODE DIRECTED  
VOLTAGE=30KV, BACKGROUND=1.0E8

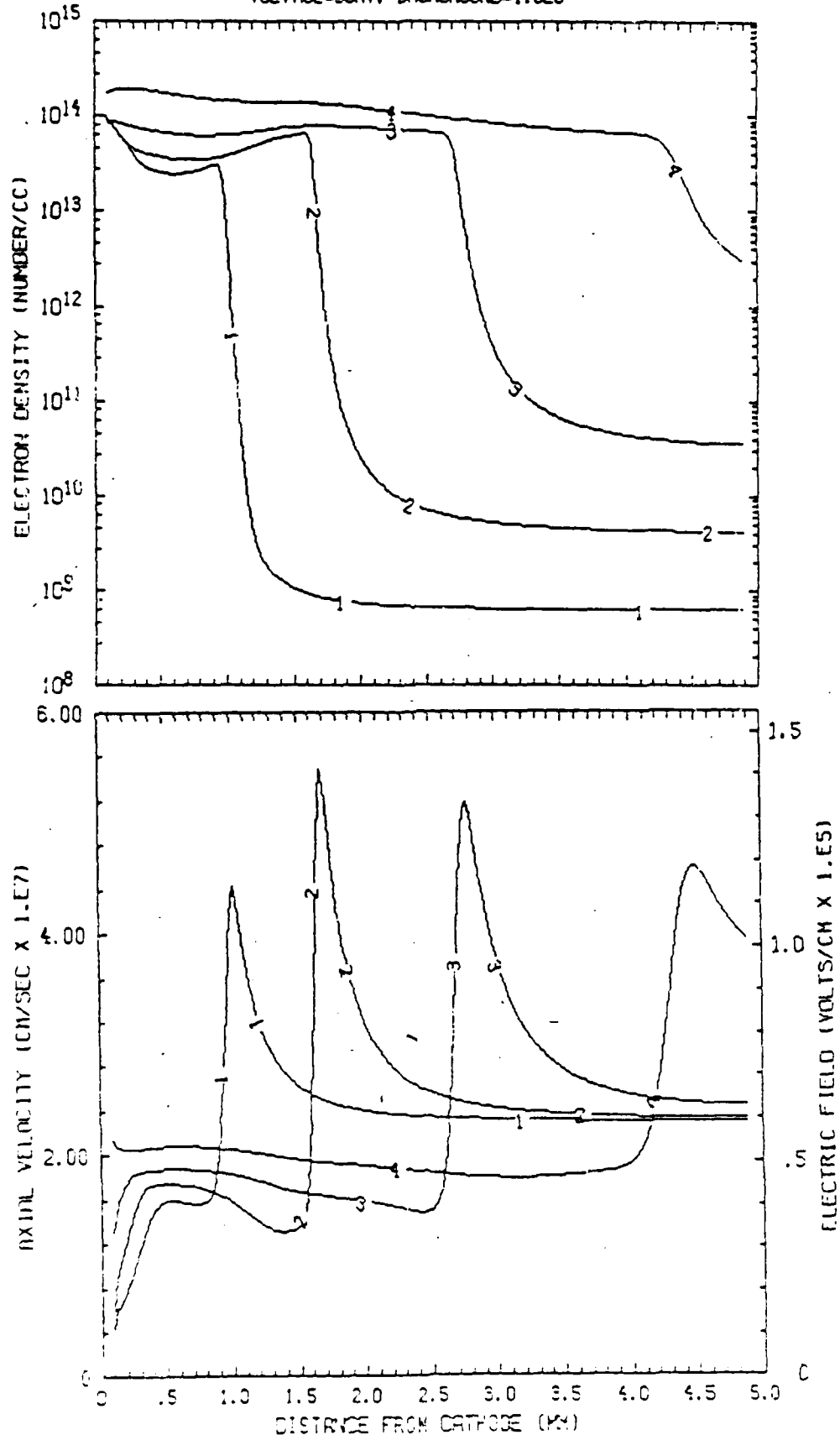


FIG. 2

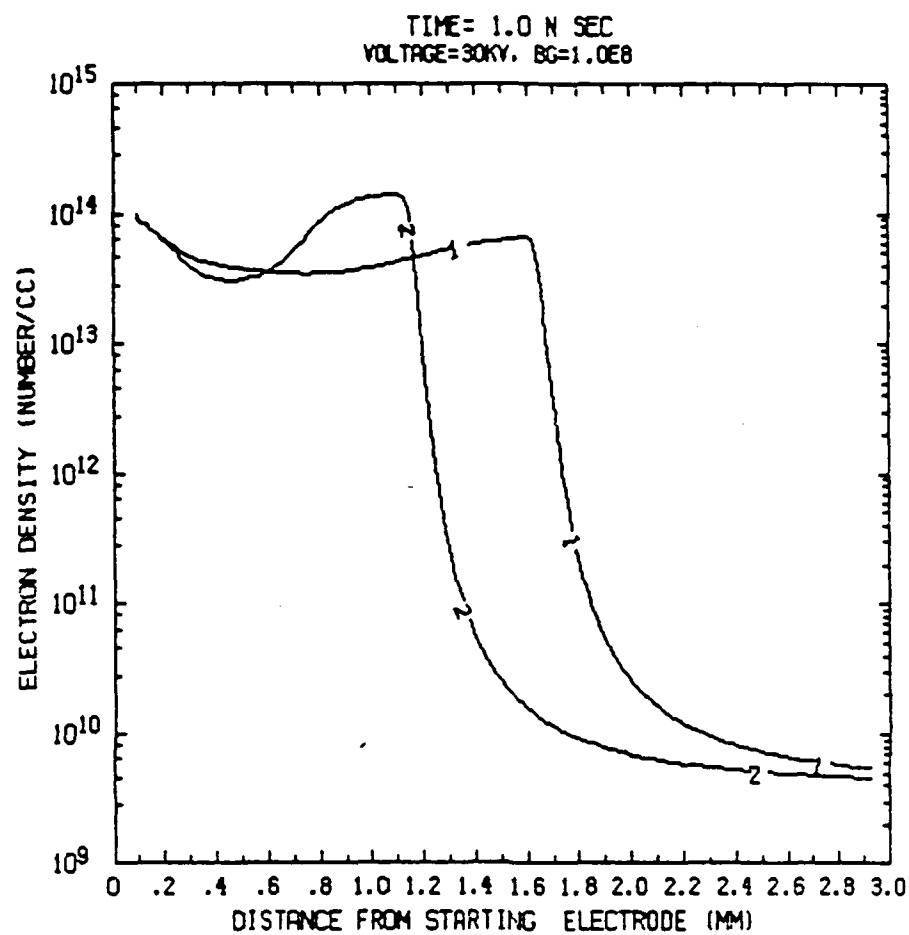


FIG. 3



## Project No. 6

Exploratory Concepts

(R. Curry, B. Maas, G. Schaefer, F. Williams, L. Hatfield,  
K. Schoenbach, M. Hagler, and M. Kristiansen)

## A. SUMMARY

This project involves several, smaller projects with the aim to determine their feasibility and promise for further development and increased emphasis. Some of the previous miniprojects have led to separate, major project inside or outside the Coordinated Program.

The main emphasis, this year has been on the triggering of surface discharge switches, on geometrical enhancement of field distortion triggering, on determining the time dependent resistance of a heavy duty (10's kA) pulsed arc, and on various novel opening switch concepts. The main parameters affecting surface discharge triggering have been investigated and certain optimum conditions have been determined. An experimental, computer interfaced, system for determining the resistance of a pulsed, large current ( $> 10$  kA) arc has been constructed, along with the required diagnostic equipment and computer software. Together with Project No. 9, we have also investigated several opening switch concepts. These include the Dense Plasma Focus (in cooperation with the University of Illinois), a magnetically controlled opening switch (in cooperation with GTE Research

Laboratories) and some novel solid state opening switches, such as an optically controlled opening switch and an e-beam and magnetically controlled on-off switch. Studies have also been initiated on methods for achieving multichanneling in spark gaps.

## B. SURFACE DISCHARGE SWITCH

(R. Curry, L. Hatfield, and M. Kristiansen)

### 1. Introduction

A D.C. charged, triggered surface discharge switch is being investigated. The performance evaluations, using three different insulators, include voltage and current measurements, jitter measurements, and surface analysis of the dielectric switching surfaces with SEM, ESCA and surface resistance measurements. The enclosed conference publications (Appendices I and II) summarize the results of tests run with G-10, Delrin, and Lucite, and all combinations of charging and trigger voltage polarities. The different dielectrics and polarity combinations have a dramatic effect on the switching, as can be seen from the results reported in these publications. Recently the investigations have emphasized photographic (streak, framing, and time integrated) diagnostic techniques to determine details about the streamer formation, as described later in this report, together with results from surface charge pattern measurements.

### 2. Triggering of a Surface Discharge Switch

A block diagram of the system and the diagnostics currently employed is shown in Fig. 1. The surface discharge switch

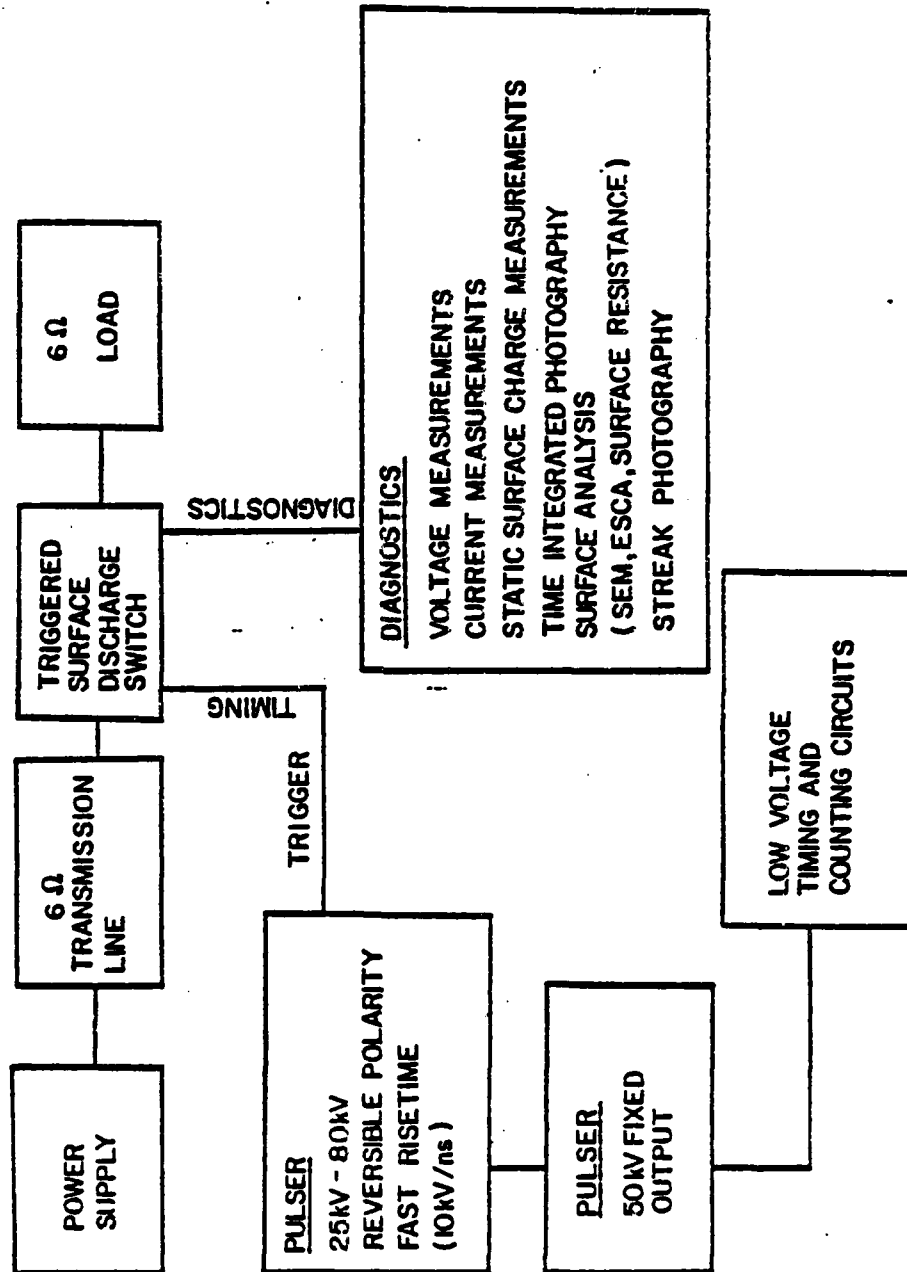


Fig. 1 Block Diagram of the System

consists of a modified version of the previously reported surface discharge switch used to study multichanneling and erosion [1]. The modifications include the addition of a Lucite chamber which allows different ambient gas mixtures to be evaluated and the addition of a trigger electrode and an auxiliary electrode. The capacitor (.18  $\mu$ f) of the previous study was replaced with four, 25  $\Omega$ , transmission lines in parallel, which provide an energy source of 13.9 joules when charged to 40 kV. Also, a new 6  $\Omega$  load has been constructed using ceramic resistors which allows the switch to be operated at various repetition rates [2].

Various triggering techniques have been evaluated. These include laser triggering and two methods of field distortion. When laser triggering was tried, single channel (shaped) electrodes with a spacing of 4 cm was used with one atmosphere of ambient air. A one megawatt pulse from a nitrogen laser was focused onto the surface of the switch from above. Even at 90% of selfbreak voltage, no triggering was achieved. When the laser beam was focused onto the electrodes (either cathode or anode) visible sparks off the electrode surfaces also failed to trigger the switch. These results indicated that higher energy levels would be needed for successful laser triggering or maybe that laser triggering is not practical for surface discharge switches. Two types of field distortion triggering were also investigated. The first method employed various geometries of trigger electrodes placed on the surface of the switch. Included among the electrode shapes were rods and metal strips placed at various positions (mid plane, 2/3 point, etc.) on the surface. Although the multichannel electrodes (parallel electrode surfaces) were

employed, multichanneling did not occur for any of the electrode-trigger polarity combinations. The last and most successful, trigger scheme also utilizes field distortion. The main trigger, however, is isolated from the main electrodes by a G-10 insert and by the dielectric sample, as shown in Fig. 2. In addition to the isolated trigger an auxiliary trigger was added which provides additional field distortion when a discharge occurs between it and the main switch electrodes. Three different dielectrics were tested under all possible polarity combinations. The results of these investigations are discussed in Appendix I.

### 3. Polarity and Dielectric Effects

The three dielectrics mentioned above (G-10, Delrin and Lucite) have been tested in dry air under all possible combinations of polarities. Dramatic differences in multichanneling, jitter, and voltage wave forms result for the different combinations. Under similar test conditions, different insulators affect the performance of the switch quite distinctly (see Appendix I). The overall best performance was obtained with G-10, using negative charging voltage and positive trigger voltage. It was also found that the switch performance improved (less jitter and more multichanneling) after the first few hundred shots when operated in a slow repetition mode (1-2 pulses/sec).

In order to investigate this conditioning phenomenon and the effect of the dielectrics on the switch characteristics, surface analysis techniques, including SEM, ESCA, and surface resistance measurements have been employed (results reported under Project

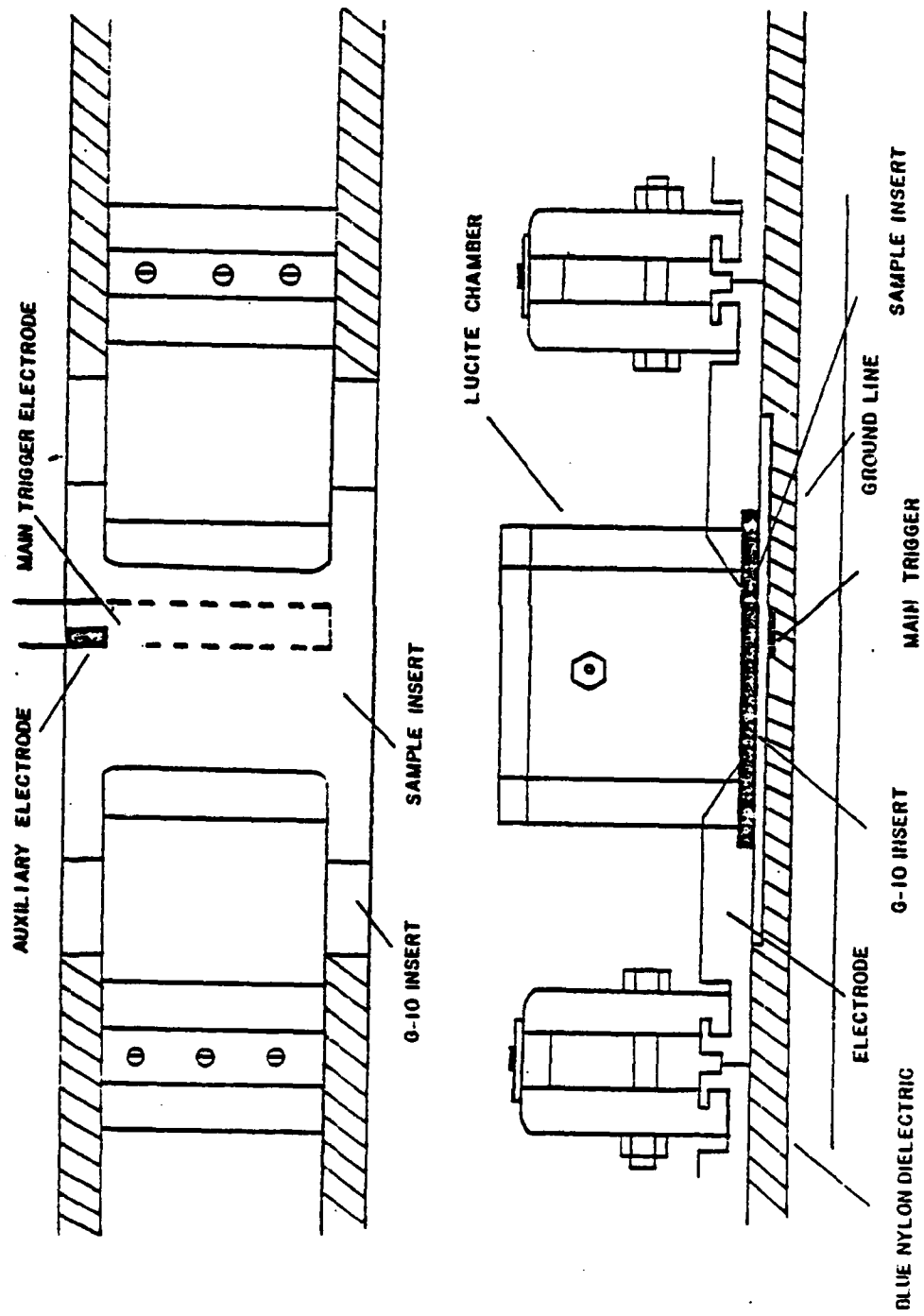


Fig. 2 Surface Discharge Switch

No. 4). The most interesting result is the lack of detectable chemical damage on G-10 and Lucite when compared to Delrin. Delrin exhibited considerable surface decomposition whereas Lucite and G-10 displayed no decomposition. The surface resistance did decrease on the G-10 and Lucite after 500 shots, although no surface damage was seen. Also, no deposited electrode material was found in the discharge region for these three insulators. To explore further the differences seen in the switching characteristics, surface charge measurements were made using an electrostatic field meter [3]. Differences in residual charge polarities and residual charge leak-off times were measured, as described in Appendix II. The G-10 retained positive charges with fields as high as 12 kV/cm for shorter times than either the Lucite or Delrin. The  $1/e$  decay time ranged between 3.85 and 7.37 hours for G-10. Delrin charged negative (-14 kV/cm) and had  $1/e$  decay times from 9.7 to 20 hours, whereas Lucite charged positive and showed no discernible decay in 24 hours after charging up to 18 kV/cm. From the investigations summarized in Appendices I and II, it is clear that the dielectric switch substrate has a profound effect on the switch performance and it is hypothesized that the difference in surface charging may be an important cause of this effect. The high residual fields, the reduced surfaced resistance, and the chemical composition changes of the surface probably all contribute to the characteristics of the switch, however.

In addition to the diagnostic techniques described above, streak photography and surface residual charge pattern photographs are also being applied. Streak photography measurements

performed to date indicate that the plasma channel originates on the surface and then lifts off. Single channel studies at  $\sim 3$  kA indicate that the channel may lift off about 0.3 mm from the surface. In high current switches ( $\geq 100$  kA/channel) the inductance of the switch could increase due to this lift-off and the discharge may even extinguish.

Simultaneity measurements using streak and time integrated photography show a spread in the closure times of the various channels. The simultaneity measurements are also being used to determine whether the discharge is anode or cathode directed. Preliminary measurements using the streak photography indicate that the discharge is cathode directed (luminosity appears first at the anode).

Residual charge patterns on insulators subjected to single channel discharges compared to those from insulators subjected to multichannel discharges are quite different. The insulators are dusted with a charged powder such as Xerox yellow tones (6500) and the patterns are then photographed.

Initial measurements on insulators subjected to multichannel discharges show that a large number of shots is required for the insulator to become uniformly charged. Studies of insulators subjected to 850 single channel arcs over a 2 hour period indicate that a time factor in the surface charging process may be involved in the previously described conditioning process. When G-10 insulators were used in the single channel studies definite patterns developed on the insulators which were run for several hours. On the insulators run for the same number of shots at 1 pps, on a continuous basis, the same patterns had also



started to develop but were not as distinct. This may indicate that the conditioning occurs from charging in the bulk or surface of the insulator and may require time for the charges to redistribute.

The research will continue to explore the charging and the effect of the residual charge on the performance of the switch. Also, further investigation is planned of the effect which different gases have on multichanneling characteristics. Further trigger studies which include different positionings of the isolated trigger and different widths of trigger strips is planned in order to further determine the mechanisms which affect the triggering of surface discharge switches.

### C. GEOMETRICALLY ENHANCED FIELD DISTORTION TRIGGERING

(G. Schaefer and P.F. Williams)

#### 1. Discussion of Trigger Concept

In field distortion triggering the gap is commonly designed to provide optimum performance without the trigger. A trigger electrode is then added, shaped and located on an equipotential surface in the gap. Triggering is accomplished by abruptly changing the potential of this electrode, thereby increasing the field at one of the gap electrodes. Only a limited field enhancement may be produced, however, because the enhancement is due solely to the change in relative potential of the trigger and gap electrode. It should be mentioned that a spark gap in which a spark crosses the gap

in two steps via the trigger electrode is not considered a pure field distortion trigger case. More efficient field distortion triggering could be produced if geometric field enhancement effects, such as occur at sharp edges, were included in such a way that they do not affect the hold-off voltage. In this case the trigger electrode would be used to shape the field distribution in the gap in both the hold-off state and the triggering state. In the hold-off state the trigger electrode would minimize the geometric field enhancement effects at the main gap electrode, thereby maximizing the hold-off voltage. In the triggering state, on the other hand, the trigger electrode would serve to enhance the field, providing improved triggering in two ways: moving the equipotential toward one gap electrode and simultaneously turning on the geometric field enhancement. An example is shown in Fig. 1. In the hold-off phase the trigger electrode is at the same potential as the electrode (1). For triggering, the potential of the trigger electrode is driven towards the potential of electrode (2). In this case the geometry of the trigger electrode is used for several purposes:

- (a) To produce a low field region on the surface of one electrode and to produce a field distribution in the gap as homogeneous as possible when no trigger pulse is applied. In this case the surface at the trigger electrode is responsible for the field distribution and the hold off voltage of the gap is not substantially reduced even though electrode (1) is shaped in such a way that a geometrically caused field enhancement is possible.

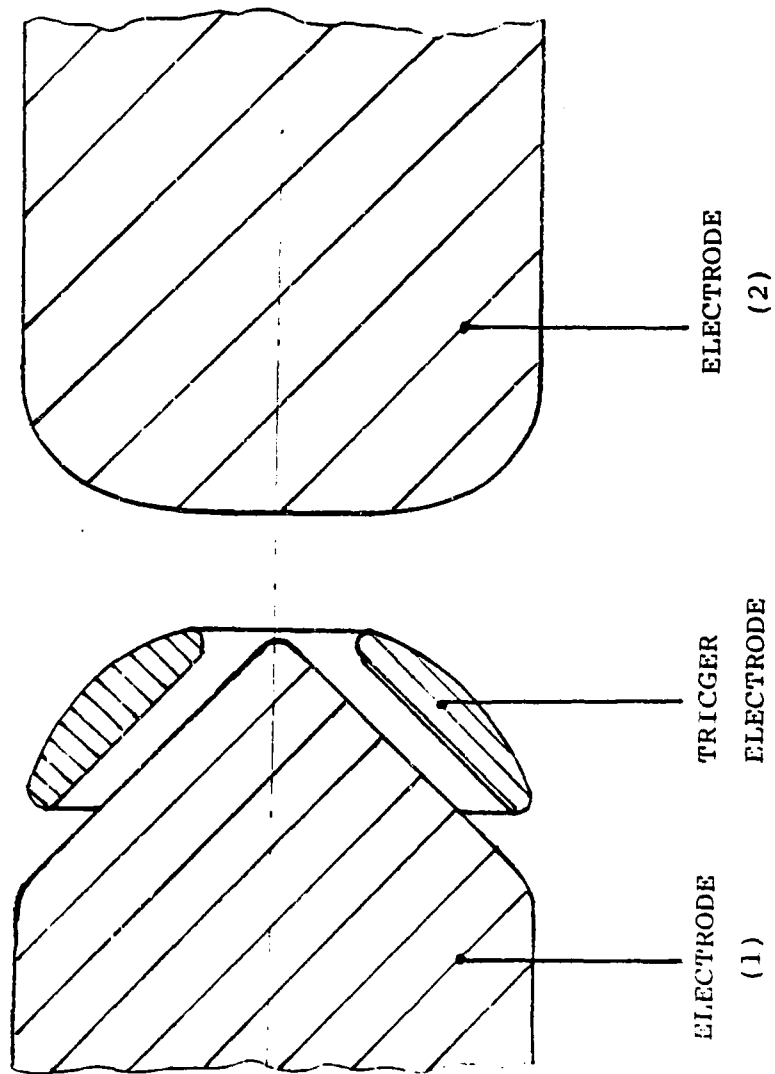


FIG. 1 Example for geometrically enhanced field distortion trigger

- (b) To produce a very high field close to the surface of electrode (1) if the potential of the trigger electrode is driven toward the potential of electrode (2).

Such a geometrically enhanced field distortion triggering would have several advantages:

1. The strongest field enhancement occurs at one of the main electrodes.
2. The shape and surface conditions of this electrode do not determine the hold-off performance of the gap and thus make the gap more independent of erosion.
3. Since this electrode can be shaped without changing the hold-off performance, the field enhancement can be much larger than in common field distortion triggering.
4. Electrode roughness produced by erosion on electrode (1) would actually enhance the switch performance since the electrode surface is only exposed to a strong field when the trigger pulse is applied.

## 2. Preliminary Experiments

An experimental setup with simplified geometry has been constructed and preliminary experiments have been performed. The geometry of the system is similar to that in Fig. 1, but without rotational symmetry. The trigger electrode consists of two rods on both sides of the main electrode. Eight gaps are operated in parallel, with the same rods acting as trigger electrodes for all gaps. This setup allows independent measurements of delay and jitter.

Preliminary experiments have demonstrated the feasibility of the proposed trigger concept. In trigger experiments in air at a selfbreakdown voltage of approximately 20 kV triggering was possible down to 60% of the selfbreakdown voltage. At 90% selfbreakdown a jitter of less than 2 ns was obtained and the delay was approximately 19 ns.

D. OPENING SWITCH INVESTIGATIONS  
AND ARC RESISTANCE MEASUREMENTS  
(K. Schoenbach and M. Kristiansen)

The investigations of arc resistance measurements have been carried out in close collaboration with Project No. 3 and the opening switch investigations in collaboration with Project No. 9 and they are, therefore, described in more detail under the description of those two projects rather than here.

E. REFERENCES

1. D. Johnson, M. Kristiansen, L. Hatfield, et.al., "Multi-channel Surface Discharge Switch," Proc. Conference on Electrical Insulation and Dielectric Phenomena, Amherst, MA, 1982.
2. R.D. Curry, D. Johnson, M. Kristiansen, et.al., "Triggering of Surface Discharge Switches", Proc. 4th IEEE Pulsed Power Conf., Albuquerque, NM, 1983.
3. R.D. Curry, "Surface Charging of Insulators in Surface Discharge Switches", Proc. Conference on Electrical Insulation and Dielectric Phenomena, Buck Hill Falls, PA, 1983.

## TRIGGERING OF SURFACE DISCHARGE SWITCHES\*

R. Curry, D. Johnson+, and M. Kristiansen  
Department of Electrical EngineeringL. Hatfield  
Department of Physics  
Texas Tech University  
Lubbock, Texas 79409 USAA.H. Guenther  
Air Force Weapons Laboratory  
Kirtland Air Force Base, New Mexico 87117 USAAbstract

The performance of a triggered 45 kV surface discharge switch operated in air, was investigated. Trigger performance evaluations include jitter measurements, channels per meter and the effects of charging voltage and trigger electrode polarity. Trigger electrode constraints, including positioning of the electrode and trigger pulse risetimes, are discussed. Multichannel performance of various dielectrics including G-10, Delrin, and Lucite are compared. Voltage and current measurements were the principle diagnostics used in the evaluation of the switch performance. The addition of an auxiliary electrode (which provides UV preillumination and added field distortion) is discussed.

Introduction

The multichannel characteristics of a surface discharge switch (SDS) makes it attractive to fast switching applications [1,2] which require low inductance switches. Commonly used surface discharge switches are over-voltaged by several hundred percent and allowed to self-break [3,4]. Overvoltageing the switch usually creates dense multichanneling when the switch closes. Likewise, triggered SDS's are usually pulse charged and triggered before self-break occurs. The pulse charging allows overvoltageing of the switch, thus causing dense-multichanneling and low jitter.

Little information is available about DC charged surface discharge switches, therefore they are generally not employed. Difficulties arise when the SDS is DC charged. Triggering of the switch is generally difficult if multichanneling and low jitter are required. A comparative study of the effects of different parameters on the characteristics of DC charged SDS's is underway and the preliminary results are reported here. The parameter studies include different dielectric substrates, charging voltage polarity, and trigger pulse polarity effects. The characteristics of the switch under these various conditions are discussed in the test of this paper.

Circuit Operation and Design

The surface discharge switch was constructed as part of a 1 m long, 6  $\Omega$  strip line. The electrodes are easily adjustable to various spacings and are presently constructed of brass. The electrodes shown in Fig. 1 are 20.3 cm long and 1.27 cm thick. A Blue Nylon dielectric, .63 cm thick and 30.5 cm wide, provides the insulation between the charged side of the transmission line and the ground return side. A .63 cm long and .63 cm deep, was milled into the Blue Nylon line in which a G-10 insert is placed. The main trigger electrode which consists of a .63 cm wide strip of 2 mil thick copper tape is placed

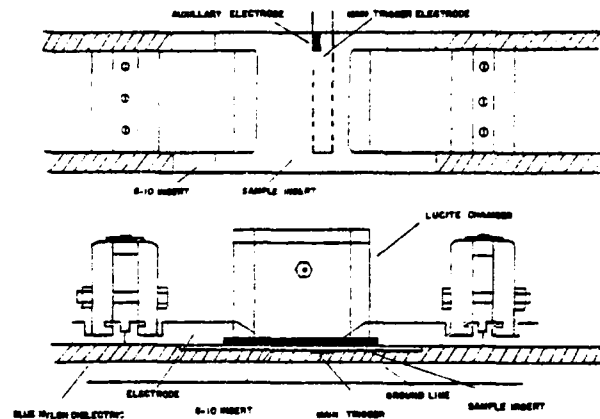


Fig. 1. Surface Discharge Switch

between the G-10 insert and the Blue Nylon, with the main trigger located 3 cm from the charged electrode. The G-10 insert isolates the trigger from the two main electrodes when the trigger pulse is applied. The electrode spacing is set at 0.3 cm to give self-break voltages between 45 and 55 kilovolts. For the 0.3 cm separation a surface discharge insulator sample with dimensions .16 cm x 30.5 cm x 12 cm is held in place by the electrodes. In addition to the main trigger, an auxiliary electrode is placed on the surface of the sample, at its edge. The auxiliary electrode provides additional field distortion and UV preillumination. The auxiliary electrode was a .63 cm wide 2.5 cm long strip of 2 mil copper tape. The auxiliary electrode is placed 5.2 cm from the edge of the sample and 2.54 cm from the grounded electrode so that an arc occurs between this electrode and the grounded electrode when the trigger pulse arrives. A Lucite chamber is placed over the electrodes and filled with dry air at atmospheric pressure.

The energy is stored in four parallel 25  $\Omega$  cables which are attached to the 6  $\Omega$  transmission line (Figure 2). The four cables are DC charged through a 2 M $\Omega$  resistor. The 20 m long lines provide a 200 ns wide pulse into the 6  $\Omega$  load. The distributed capacitance of the four cables is .0174  $\mu$ f, giving a 13.9 joule discharge when charged to 40 kilovolts. When a trigger pulse is applied to the trigger electrodes the switch breaks down, discharging into the 6  $\Omega$  load. The load consists of a 1  $\Omega$  ceramic disk resistor. The inductance of the load was measured and found to be about 22 nH. A 50 kV probe with a risetime on the order of 1 ns (10<sup>-9</sup> s) is applied to initiate breakdown (Figure 3). The voltage on the trigger strip and on the load were monitored with capacitive probes connected into the transmission line, while the current was monitored with a Pearson coil.

\* Supported by AFOSR  
+ IAP Research, Inc., Dayton, OH 45424

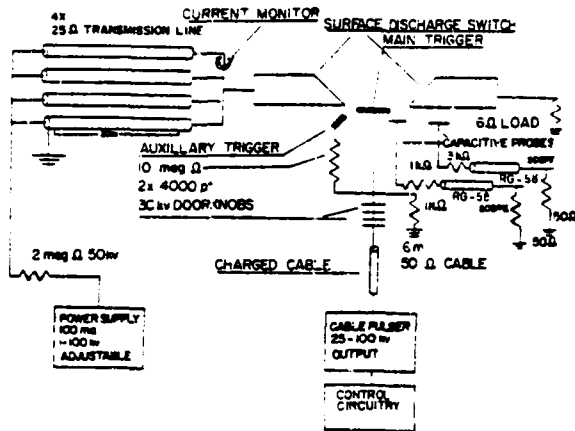


Fig. 1. Experimental Setup

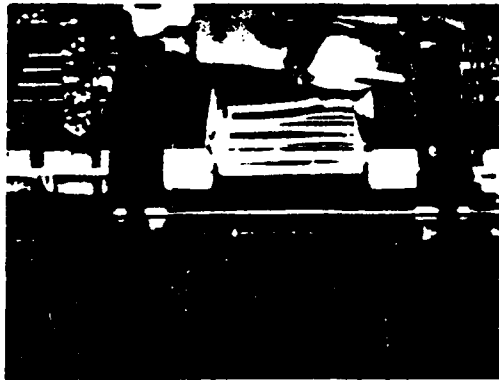
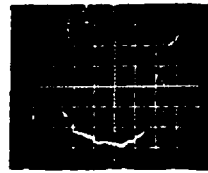


Fig. 3. Multichanneling of Surface Discharge Switch

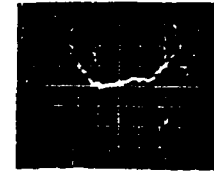
### Results

Three dielectrics (G-10, Delrin, Lucite) were tested in dry air under all possible charging and trigger polarities. Results are given in terms of the multichanneling characteristics, load voltage, current and jitter measurements. Throughout the tests a 50 kV trigger voltage was used, while the charging voltage was kept constant at 40 kilovolts. The repetition rate was 1.3 pulses per second.

G-10 had the best characteristics of the three materials tested (Table I). The first case tested was with negative charging voltage and positive trigger. The voltage fall time was 70 ns and the current fall time 70 ns (Figure 4). The jitter of five shots was 10 nanoseconds initially; however, after 500 shots it decreased to 5 nanoseconds (Figure 5). Multichanneling characteristics also changed as the material eroded away. Initially about 15 channels per meter were visible, however after 500 shots about 40 channels per meter were typical (Figure 6). All other electrode polarity combinations gave considerably worse performance. For the case of positive charging and trigger voltages the voltage risetime was 100 ns and the current risetime approximately 70 ns. Multichanneling was poor, resulting in only two channels per meter. The jitter dropped from 10 ns to approxi-

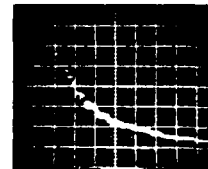


A. Voltage Measurement across a 6 Ω load, 3340 V/div; 50 ns/div.

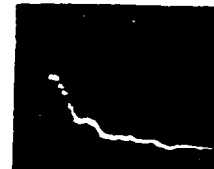


B. Current Measurement through a 6 Ω load, 1000 A/div; 50 ns/div.

Fig. 4. Voltage and Current Measurements on G-10 for a Negative, 40 kV, Charge Voltage and Positive, 50 kV, Trigger.

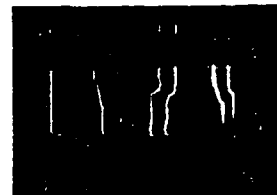


A. Jitter of first 5 shots. 3340 V/div; 20 ns/div.

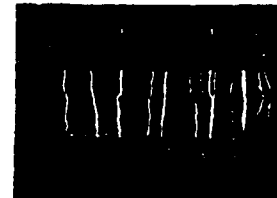


B. Jitter of 5 shots, after first 500 shots. 3340 V/div; 20 ns/div.

Fig. 5. Jitter of 5 Shots on G-10.



A. Multichannel Characteristics of First Shot



B. Multichannel Characteristics after 500 shots

Fig. 6. Multichannel Characteristics of G-10 over a 20.3 cm Length and 0.1 cm Electrode Separation.

mately 30 ns, during the first 500 shots. Likewise for the negative charging, negative trigger voltage, the voltage fall time remained about 120 ns and the current fall time 70 ns. The jitter, however, was too great to measure. Characteristics of this case included a large number of prefires and lower self-break voltages. The self-break voltage decreased from 45 to 20 kV after 500 shots. In the last case, of positive charging and negative trigger voltage, the voltage and current wave shapes varied from shot-to-shot. The voltage risetime on the average was about 100 ns and the current risetime was 70 to 100 ns. The jitter was approximately 10 ns. Multichanneling decreased from 15 channels per meter to 10 channels per meter during the first 500 shots. The number of prefires and jitter were better in this case.

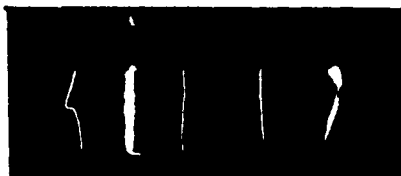
The performance of Delrin was similar to that of G-10 (Table 2). For the case of negative charging and positive trigger voltages, the voltage fall time was 80 ns and the current risetime 70 ns (Figure 7) with a jitter of approximately 15 ns. Multichanneling



A. Voltage Measurement across a 6  $\Omega$  load, 3340 V/div; 50 ns/div. B. Current Measurement through a 6  $\Omega$  load, 1000 A/div; 50 ns/div.

Fig. 7. Voltage and Current Characteristics of Delrin for a Negative, 40 kV, Charge Voltage and a Positive, 50 kV, Trigger Pulse.

remained stable at 25 channels per meter for the entire run (Fig. 8). When the voltage and current waveforms using Delrin are compared to the voltage and current characteristics using G-10 (Fig. 4), under the same conditions, a dramatic difference is seen in the voltage wave shapes and risetimes. Delrin gave significantly greater jitter and slower risetimes. The effect of different trigger and charging polarity combinations is also apparent when the two cases of positive trigger and positive charging voltage (Fig. 9) are compared with the most successful case of negative charging voltage and positive trigger (Fig. 7). The most significant change is in the risetime of the voltage across the load.



Multichanneling for a 6.2 cm Electrode Separation and 20.3 cm Electrode Length.

Fig. 8. Multichanneling Characteristics of Delrin For A Negative Charge Voltage of 40 kV and a Positive 50 kV Trigger Pulse.



A. Voltage Measurement across a 6  $\Omega$  load, 3340 V/div; 50 ns/div. B. Current through a 6  $\Omega$  load, 1000 A/div; 50 ns/div.

Fig. 9. Voltage and Current Measurements on Delrin for a Positive, 40 kV, Charge Voltage and a Positive, 50 kV, Trigger Pulse.

Results using lucite differed considerably from those using G-10 or Delrin (Table 3). Once again a negative charging voltage and a positive trigger pulse gave the best overall results. The 80 ns fall time of the voltage across the load and the 70 ns current risetime (Fig. 10) compared favorably with the similar cases for G-10 and Delrin. However, multichanneling decreased to only 2 channels when the switch was triggered. Unlike the G-10 results, the jitter was too great to measure for three of the charging-trigger voltage combinations, but no prefires or misfires were observed.



A. Voltage Measurement across a 6  $\Omega$  load, 3340 V/div; 50 ns/div. B. Current through a 6  $\Omega$  load, 3340 V/div; 50 ns/div.

Fig. 10. Voltage and Current Measurements on Lucite for a Negative, 40 kV, Charge Voltage and a Positive, 50 kV, Trigger.

In addition to voltage and current measurements static field measurements were made to check for residual charge. In the case of negative charging voltage and a positive trigger pulse, positive charging of the insulator was measured over the main trigger electrode. Near the cathode the insulator was charged negative. The charge decay directly above the trigger was checked and charges were found to decay only 10 percent in one hour. Charges on the insulator for the case of negative charge voltage and negative trigger polarity were also checked. Negative charging on the insulator, above the trigger and near the cathode was measured. The last case of positive charge voltage and negative trigger polarity was also checked and the insulator charge found to be positive.

### Conclusion

The auxiliary electrode was found to provide denser multichanneling in the case of the negative charging and positive trigger voltages, on G-10 and Delrin. The reason for the increased multichanneling due to the auxiliary electrode in this one case is not clear. This increase may be due to UV preillumination or to added field distortion. However, in the remaining cases the auxiliary electrode did not play a significant role in the multichanneling characteristics.

The data presented indicate that only certain dielectrics and a specific combination of charging voltage and trigger pulse polarities work well for the DC charged, triggered surface discharge switches. The voltage waveforms of G-10 (Figure 4) and Delrin (Figure 7) indicate that the dielectric plays a significant role in the discharge process. The multichanneling characteristics of G-10 (Figure 5) and Delrin (Figure 8) also show the dependence of the discharge process on the dielectric used. The basic physics of the trigger process and the dependence of the multichanneling process on the dielectric are not fully understood at this time. However, preliminary static charge measurements indicate that residual charges and surface resistivity influence the triggering. The charge measurements indicate significant charging of the insulators and a slow decay time of these charges. Future studies will



concentrate on isolating the basic trigger processes and understanding them.

#### Acknowledgements

This work was supported by AFOSR. The authors are also indebted to Mark Fowler, Mike Katsaras, H. Krompholz and Kim Zinsmeyer for their technical support and advice. Further thanks are extended to George Jackson, V.K. Aggarwal, Robert Druce and Lloyd Gordon for technical information.

#### References

1. H. M. von Bergmann, "Triggered Multichannel Surface Spark Gaps," Journal of Physics, Sect.E, 15, 243 (1982).
2. S. T. Pai and J.P. Marton, "A Preliminary Study of the Breakdown Mechanism of Surface of Discharge Switches," IEEE Fifteenth Modulator Symposium, p. 153, Baltimore, Md. (1982).
3. D. Johnson, et. al, "Multichannel Surface Discharge Switch," 1982 CEIDP, p. 573, 1982, Amherst, MA.
4. W. J. Sarjeant, "High Pressure Surface-Discharge Plasma Switches," IEEE Transactions on Plasma Science, PS-8, 216 (1980).

	CHARGE VOLTAGE POLARITY	TRIGGER PULSE POLARITY	VOLTAGE RISE TIME (or Fall Time)	CURRENT RISE TIME (or Fall Time)	JITTER TIMES (5 Shots)	CHANNELS PER METER	COMMENTS
1	-	+	70 ns	70 ns	5 ns	25	-
2	+	+	120 ns	70 ns	30 ns	2	-
3	-	-	120 ns	70 ns	-	1	PREFIRES
4	+	-	160 ns	100 ns	100 ns	15	PREFIRES AND REFIRES

Table 1. Characteristics of G-10

	CHARGE VOLTAGE POLARITY	TRIGGER PULSE POLARITY	VOLTAGE RISE TIME (or Fall Time)	CURRENT RISE TIME (or Fall Time)	JITTER TIMES (5 Shots)	CHANNELS PER METER	COMMENTS
1	-	+	80 ns	70 ns	15 ns	25	-
2	+	+	120 ns	70 ns	-	-	-
3	-	-	120 ns	70 ns	-	1	PREFIRES
4	+	-	120 ns	70 ns	-	1	SOME PREFIRES

Table 2. Characteristics of Delrin.

	CHARGE VOLTAGE POLARITY	TRIGGER PULSE POLARITY	VOLTAGE RISE TIME (or Fall Time)	CURRENT RISE TIME (or Fall Time)	JITTER TIMES (5 Shots)	CHANNELS PER METER	COMMENTS
1	-	+	80 ns	70 ns	40 ns	2	-
2	+	+	100 ns	70 ns	-	1	-
3	-	+	120 ns	70 ns	-	1	NO PREFIRES
4	+	-	110 ns	70 ns	-	1	" PREFIRE"

Table 3. Characteristics of Lucite.

## Appendix II

SURFACE CHARGING OF INSULATORS  
IN A  
SURFACE DISCHARGE SWITCH\*

R.D. Curry, M. Kristiansen  
Department of Electrical Engineering

and

L.L. Hatfield, V.K. Agarwal, and G.L. Jackson  
Department of Physics

Texas Tech University  
Lubbock, Texas 79409

## ABSTRACT

Surface charging of insulators in a 45 kV, triggered surface discharge switch has been studied after repeated discharges. Static electric field measurements on different insulators such as G-10, Delrin and Lucite are compared. Electric fields as high as 10 kV/cm have been measured after several hundred discharges. These measurements also indicate long surface charge decay times. Decay times ranging from one hour to several hours for the charge to decay 10 percent have been measured. Utilizing the field measurements the influence of multiple insulator interfaces and placement of the trigger electrode are discussed.

## INTRODUCTION

The multichanneling of surface discharge switches make them attractive for fast switching applications which require low inductance switches [1,2]. The usual mode of operation of a switch is to apply an over-voltage of several hundred percent and allow it to self break [3,4]. Triggered, DC-charged surface discharge switches are rarely employed for little information is available on their operating characteristics. A recent investigation

\*Supported by AFOSR.

into the parameters affecting the performance of triggered, DC-charged, surface discharge switches revealed that the dielectric used in the switch plays a key role in its operation [5]. A summary of the effect of each insulator (G-10, Delrin, Lucite) on the voltage, current, and jitter characteristics of the switch is shown in Tables, 1, 2, and 3. As shown by the data, the polarity of the charge voltage and trigger voltage were found to alter the performance of the switch dramatically. A preliminary investigation into the role of the dielectric is under way. Static field measurements have shown large differences in the residual charge on these dielectrics after operation of the switch for a relatively low number of shots.

### DESCRIPTION OF CIRCUIT PARAMETERS

The surface discharge switch was constructed as part of a 1 m long stripline with a characteristic impedance of  $6 \Omega$ . The blue nylon dielectric upon which the switch is constructed is .63 cm thick and 30.5 cm wide (Figure 1). A slot, 33 cm x .16 cm was milled into the stripline and the main trigger electrode ( $5.0 \times 10^{-3}$  cm x 2.54 cm) is placed in the slot 3 cm from the charged electrode. A .16 cm thick G-10 insert which isolates the trigger from the electrodes is placed over the trigger electrode in

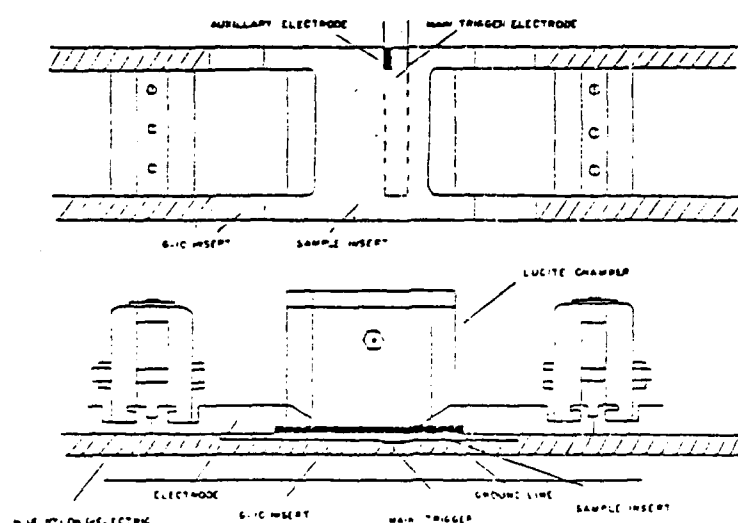


Figure 1. Surface Discharge Switch.

the slot. The dielectric sample is placed over the G-10 insert and held in place by brass electrodes which are 20.3 cm x 1.27 cm. The electrode spacing of 6.2 cm was set to provide self break voltages between 45 and 55 kV. An auxiliary electrode was placed at the edge of the dielectric sample to provide added UV preillumination on the surface and field distortion. The arc to the auxiliary electrode increased the multichanneling of the switch.

The primary energy storage element is four paralleled 25  $\Omega$  cables which are attached to the 6  $\Omega$  stripline. The total distributed capacitance of the four cables is .0174  $\mu$ f which stores 13.9 joules when charged to 40 kV. The four cables supply a 200 ns pulse into the 6  $\Omega$  load (Figure 2). To initiate the discharge a 50 kV pulse with a risetime of 10 ns (10%-90%) is applied to the trigger electrode.

← 5 ns

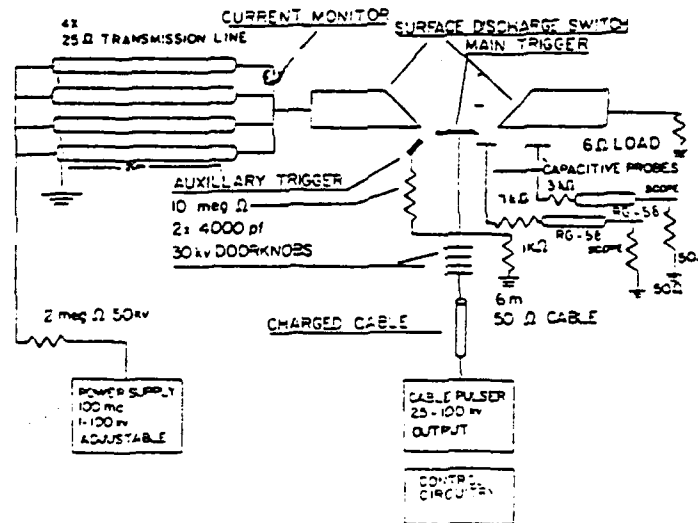


Figure 2. Experimental Setup.

## RESULTS

Since the preliminary voltage, current, and jitter measurements indicated a polarity dependence and an influence by the dielectric on the electrical characteristics of the switch, static electric field measurements

were made to determine the residual surface charge on the dielectric. The measurements utilized a commercially available field meter (Monroe, model 171) and probe (model 1019 B). The electric field above the dielectrics (G-10, Delrin, Lucite) was measured for the case which gave the best electrical characteristics, namely the negative 40 kV charge voltage and positive 50 kV trigger pulse case.

Preparation of the samples included cleaning with cyclohexane. The interface between the G-10 and Blue Nylon stripline dielectric was discharged after each experimental run by rubbing the Blue Nylon and G-10 insert with a commercial antistatic product known as "Bounce". The interface was then cleaned with cyclohexane and the stripline reassembled. All insulators tested were exposed to 500 shots at a repetition rate of 1.3 pps. After the 500 discharges the residual field above the trigger electrode was measured to determine the magnitude and decay time of the residual charge. In addition to the decay measurements, field measurements were made across the width of the dielectric and along the length of the dielectric to determine the uniformity of the residual fields.

#### G-10

On G-10, an epoxy laminate, the field remained uniform across the length of the dielectric but was non-uniform along the width of the sample. The residual field near the cathode ranged from 3.81 kV/cm to 5.71 kV/cm for three different samples. The positive field values indicate positive charging of the insulator although a negative charge voltage had been applied to the electrodes. The field above the trigger electrode ranged from 7.2 kV/cm to 14 kV/cm for the three different samples. The  $1/e$  decay times for the charge above the trigger electrode varied from 3.85 hours to 7.37 hours. Although the decay times differed the shape of the decay curve remained approximately the same. A typical decay curve for G-10 is shown in Figure 3. During the first 10-15 minutes a charging of the insulator occurs even though all external fields have been removed.

## DELIRIN

Measurements on Delrin (polyacetal) showed that the field near the cathode ranged from -8.6 kV/cm to -13.5 kV/cm. The negative fields observed indicate negative residual

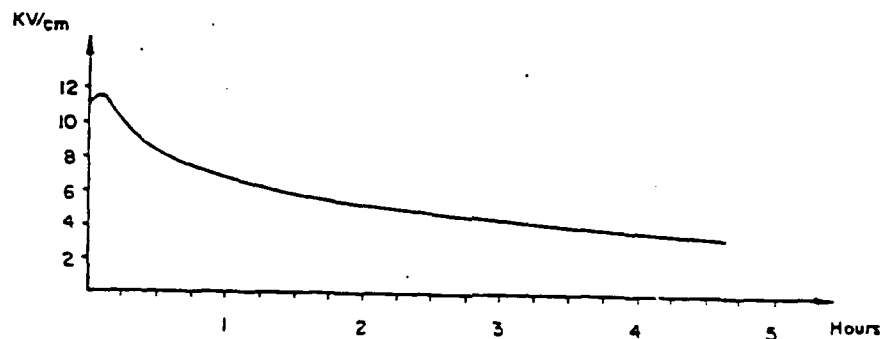


Figure 3. Charge Decay Curve of G-10.

charge on the insulator. The field along the length of the dielectric varied slightly ( $\ll 1$  kV/cm). The residual field over the trigger electrode ranged from -6.6 kV/cm to -8 kV/cm for 3 different samples. A typical decay shape for Delrin is displayed in Figure 4. Note that the field increased during the first 30-40 minutes of the static field measurements and then decreased with a  $1/e$  time constant ranging from 9.7 hours to over 20 hours.

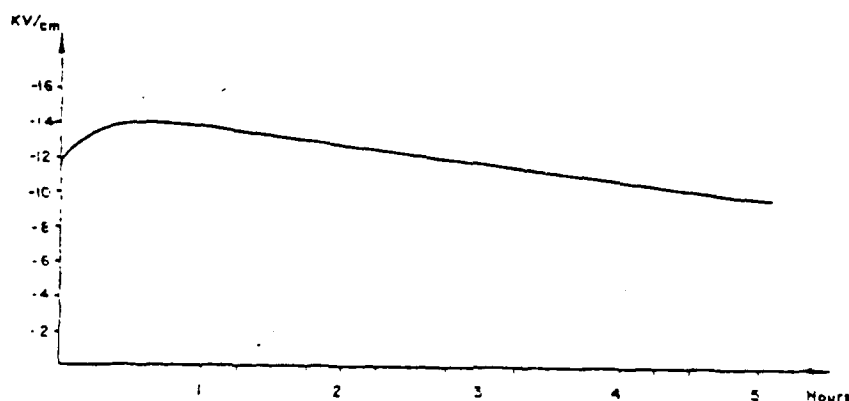


Figure 4. Charge Decay Curve of Delrin

## LUCITE

Lucite (PMMA) gave quite different results from the G-10 and the Delrin. The residual field near the cathode was found to range from -3.8 kV/cm to 1.9 kV/cm. The field over the length of the sample was found to vary by large amounts ( $\gg 1$  kV/cm). The initial field ranged from -3.2 kV/cm to 2.4 kV/cm above the trigger for the 3 samples measured. The lucite unlike the 2 previous insulators charged from the initial value to 17.4 kV/cm in 2 hours and showed no measurable decay over fifteen hours (Figure 5).

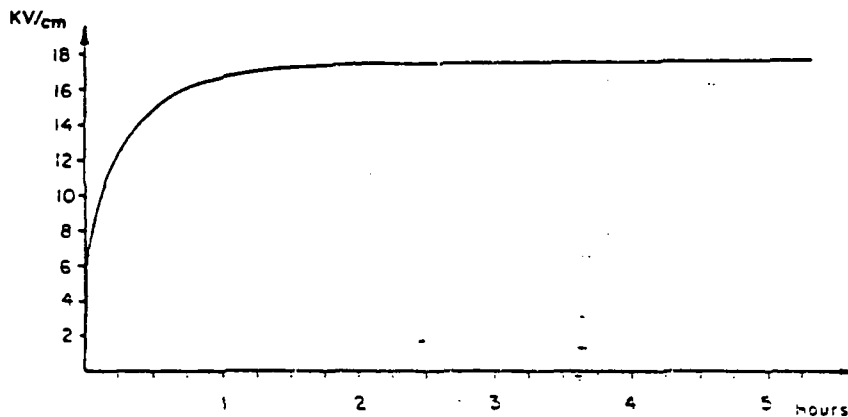


Figure 5. Charging Curve of Lucite.

## INTERFACIAL MEASUREMENTS

Additional measurements were performed to look for residual charge on the interface between G-10 and the Blue Nylon dielectric. A sample of G-10 was exposed to 500 discharges and then removed from the stripline. The field above the trigger electrode was measured and found to be -11.1 kV/cm indicating negative charge. The decay time of the residual charge was 10.5 minutes. Another sample of G-10 was exposed to 500 discharges and the residual field measured in the switch. Afterwards the sample was removed from the switch and the residual field on the sample measured. The residual field magnitude and decay rate for the sample remained approximately the same even though the sample had been removed.

These measurements indicated that the residual field on the samples is due to surface charging. As a first approximation a uniform sheet of charges across the surface of the dielectric was assumed thus giving  $\sigma = 2\epsilon_0 E$ , where  $E$  is the measured electric field in V/cm,  $\sigma$  the surface charge density in coul/cm<sup>2</sup> and  $\epsilon_0$  the permittivity of free space. For the case of G-10, the measured field of 14 kV/cm gave  $\sigma = 2.48 \times 10^{-9}$  coul/cm<sup>2</sup>. Similarly a value of -8 kV/cm for Delrin gives  $\sigma = -1.416 \times 10^{-9}$  coul/cm<sup>2</sup>. For Lucite a value of 17.4 kV/cm yields  $\sigma = 3.079 \times 10^{-9}$  coul/cm<sup>2</sup>.

### CONCLUSION

Even though these are preliminary measurements, several hypotheses can be proposed to explain the residual charge displayed by these three dielectrics. For instance, in this switch geometry, the dielectric samples are in contact with another dielectric surface of G-10 and this dielectric is in contact with the surface of the Blue Nylon stripline dielectric. This creates three interfaces where charging can occur. It seems likely that immediately after the external electric field is removed, some charge redistribution could occur thus accounting for the apparent charge buildup on the insulators after removal of the charge voltage. Moreover, for polymers subjected to such discharges the chemical impurities, specific surface defects caused by oxidation products, broken polymer chains, absorbed molecules etc., have been identified as being responsible for the capture of charges and the difference in charging displayed by different insulators [6]. Several other factors such as secondary electron emission, electric polarization of the dielectric, plasma interactions, UV radiation, and thermal effects have been found to cause differences in the charging of insulators. For example, electron energies in arcs are typically on the order of 1-2 eV, whereas an incident electron energy of 20-50 eV is needed to exceed the secondary electron emission coefficient of one for typical insulators. Thus, due to electron bombardment the charging of the insulator would be expected to be negative [7]. Another interaction that could cause charging of the insulator is UV illumination which, depending on the wavelength, has been found to break the polymer bonds which may perhaps result in either positive or negative residual charge. Future work



will concentrate on isolating the primary mechanisms responsible for the observed charging of insulators in surface discharge switches.

#### REFERENCES

- [1] H. M. Von Bergmann, "Triggered Multichannel Surface Spark Gaps," *Journal of Physics, E.*, 15, 243 (1982).
- [2] S. T. Pai and J. P. Marton, "A Preliminary Study of the Breakdown Mechanism of Surface Discharge Switches," *IEEE Fifteenth Modulator Symposium*, p. 153, Baltimore, Md. (1982).
- [3] D. Johnson, et. al., "Multichannel Surface Discharge Switch," 1982 CEIDP, p. 573, 1982, Amherst, MA.
- [4] W. J. Sarjeant, "High Pressure Surface-Discharge Plasma Switches," *IEEE Transactions on Plasma Science*, PS-8, 216 (1980).
- [5] R. Curry, et. al., "Triggering of Surface Discharge Switches," *IEEE Fourth Annual Pulse Power Conference*, 1983, Albuquerque, New Mexico.
- [6] G. M. Sessler, Topics in Applied Physics: Electrets, 33. Springer-Verlag Berlin Heidelberg, 1980.
- [7] R. F. Willis and D. K. Skinner, "Secondary Electron Emission Yield Behavior of Polymers," *Solid State Communications*, 13, p. 685, (1973).

	CHARGE VOLTAGE POLARITY	TRIGGER PULSE POLARITY	VOLTAGE RISETIME (or FallTime)	CURRENT RISETIME (or FallTime)	JITTER TIMES (5 Shots)	CHANNELS PER METER	COMMENTS
1	-	+	70 NS	70 NS	5 NS	35	-
2	+	+	120 NS	70 NS	30 NS	2	-
3	-	-	120 NS	70 NS	-	2	PREFIRES
4	+	-	100 NS	100 NS	100 NS	15	PREFIRES AND MISFIRES

Table 1. Characteristics of G-10.

	CHARGE VOLTAGE POLARITY	TRIGGER PULSE POLARITY	VOLTAGE RISETIME (or FallTime)	CURRENT RISETIME (or FallTime)	JITTER TIMES (5 Shots)	CHANNELS PER METER	COMMENTS
1	-	+	80 NS	70 NS	15 NS	25	-
2	+	+	120 NS	70 NS	-	1	-
3	-	-	120 NS	70	-	1	PREFIRES
4	+	-	120 NS	70	-	1	SOME PREFIRES

Table 2. Characteristics of Delrin.

	CHARGE VOLTAGE POLARITY	TRIG. P PULSE POLARITY	VOLTAGE RISETIME (or FallTime)	CURRENT RISETIME (or FallTime)	JITTER TIMES (5 Shots)	CHANNELS PER METER	COMMENTS
1	-	+	80 NS	70 NS	40 NS	2	-
2	+	-	100 NS	70 NS	-	1	-
3	-	+	120 NS	80 NS	-	1	NO PREFIRES
4	+	-	100 NS	70 NS	-	1	NO PREFIRES

Table 3. Characteristics of Lucite.

AD-A139 321

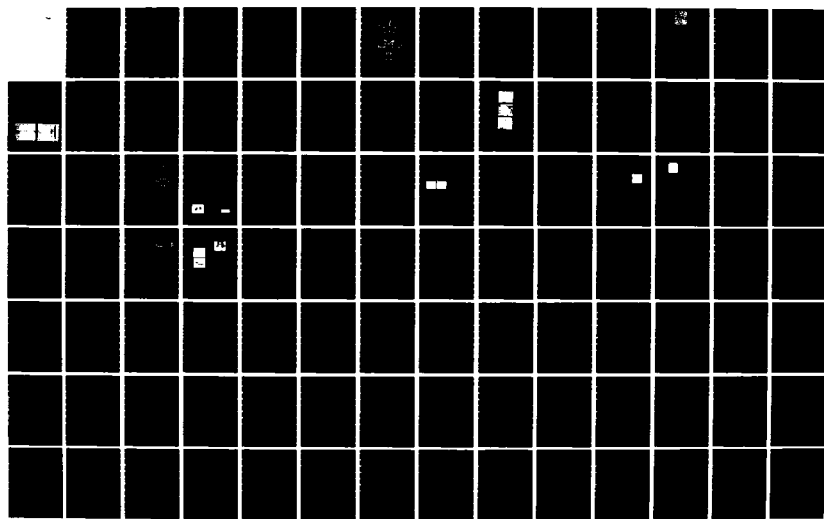
COORDINATED RESEARCH PROGRAM IN PULSED POWER PHYSICS  
(U) TEXAS TECH UNIV LUBBOCK DEPT OF ELECTRICAL  
ENGINEERING M KRISTIANSEN ET AL. 27 FEB 84  
AFOSR-TR-84-0174 F49620-79-C-0191

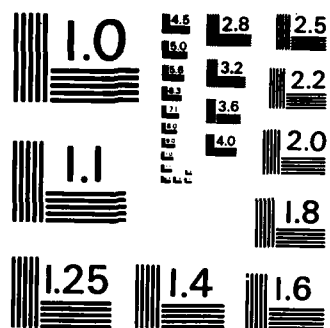
4/5

UNCLASSIFIED

F/G 10/2

NL





MICROCOPY RESOLUTION TEST CHART  
NATIONAL BUREAU OF STANDARDS-1963-A

## Project No. 8

Optically Controlled DischargesProject No. 9Opening Switches\*

(C. Harjes, G. Hutchinson, L. Thurmond, R. Cooper, K. Schoenbach,  
G. Schaefer, H. Krompholz, L. Hatfield, and M. Kristiansen)

## A. SUMMARY

These two Projects (8 and 9) are closely related in objective, theory, and diagnostic techniques. In both projects emphasis is on external discharge control (optical and electron beam), and the combination of both seems to offer new perspectives. In the continuing program they are integrated into one project "Opening Switches" and are also described here as one project. The primary objective of this work is to study control processes in externally sustained or controlled diffuse discharges, with respect to their application as opening switches. Concepts for diffuse discharge opening switches have been developed, experimental facilities have been assembled and experiments have been performed to investigate the applicability of these concepts. Computer codes have been developed and applied to different systems to allow optimization and scaling.

\*This project is funded by the Army Research Office.

The different groups of concepts discussed herein are:

- the electron-beam sustained diffuse discharge (Section B)
- the optically controlled diffuse discharge where optical control either means increased conductivity of the discharge by means of laser radiation or optical stimulation of loss processes in self-sustained discharges (Section C)
- the combination of these two concepts in one system.

For the investigation of the electron-beam sustained discharge an apparatus was designed which allows the investigations of repetitive opening in the time range of 100 ns at current levels of up to 10 kA.

The work done in the last year includes:

- 1) construction of an e-beam control system, which allows the generation of successive e-beam pulses with variable pulse width and pulse separation,
- 2) construction and testing of a high pressure discharge chamber with a transmission-line current source,
- 3) development of a novel e-beam current monitor,
- 4) initial opening switch investigations performed in  $N_2:O_2$  gas mixtures,
- 5) development of a computer program which allows modelling of an e-beam controlled diffuse discharge, and modelling of optically assisted e-beam sustained discharges.

For investigations of optically controlled discharges the following steps were taken to approach a feasible switch system:

- 1) Various optical control mechanisms of diffuse discharges have been considered for switching applications based on available data on basic photon-molecule interactions and results of optogalvanic experiments.
- 2) Small scale experiments have been performed to investigate the general feasibility of these concepts.
- 3) A high power discharge cell was constructed and operated.
- 4) Calculations on specific systems have been performed to evaluate the discharge characteristic and the time-dependent behavior of the discharge.

Several other exploratory opening switch concepts have also been examined for potential use as opening switches. Among these are the dense plasma focus (collaboration with University of Illinois), and a magnetically controlled switch (collaboration with GTE Laboratories, Inc.).

## B. E-BEAM CONTROLLED OPENING SWITCH SYSTEM

### 1. Introduction

An electron-beam controlled discharge circuit has been constructed to study the behavior of an e-beam sustained, attachment dominated discharge:

- a) at high discharge current densities,
- b) in gases which are suitable for low loss, fast opening operation,
- c) for rep-rated operation.

The objective of the investigation is to determine a set of criteria concerning electrical and gas parameters of an e-beam sustained discharge, which will guide the design of the rep-rated electron-beam controlled opening switch.

The switch concept is as follows: An e-beam is used to ionize the gas between two switch electrodes. An inductor can be charged through the then conducting gas. The switch voltage remains below the self breakdown voltage so there is no avalanche ionization. Thus, the discharge is completely sustained by the e-beam current. When the e-beam is turned off, electron attachment and recombination processes in the gas cause the conductivity to decrease and the switch opens.

## 2. Experimental Arrangement

### a. E-Beam Gun/Control System

The e-beam was designed to satisfy the following requirements:

- 1) high repetition rate,
- 2) fast turn on and turn off times,
- 3) variable beam energy and current density.

The e-beam gun is constructed as a triode to achieve the required repetitive, fast response control of the e-beam. It has a thermionic cathode which allows variation of e-beam current and voltage, independent of each other. The design and performance of the system was presented at the 4th IEEE Pulsed Power Conference [1] (see Appendix I).

A cross-section of the e-beam triode and the switch chamber is shown in Fig. 1. The e-beam cathode is located in an evacuated



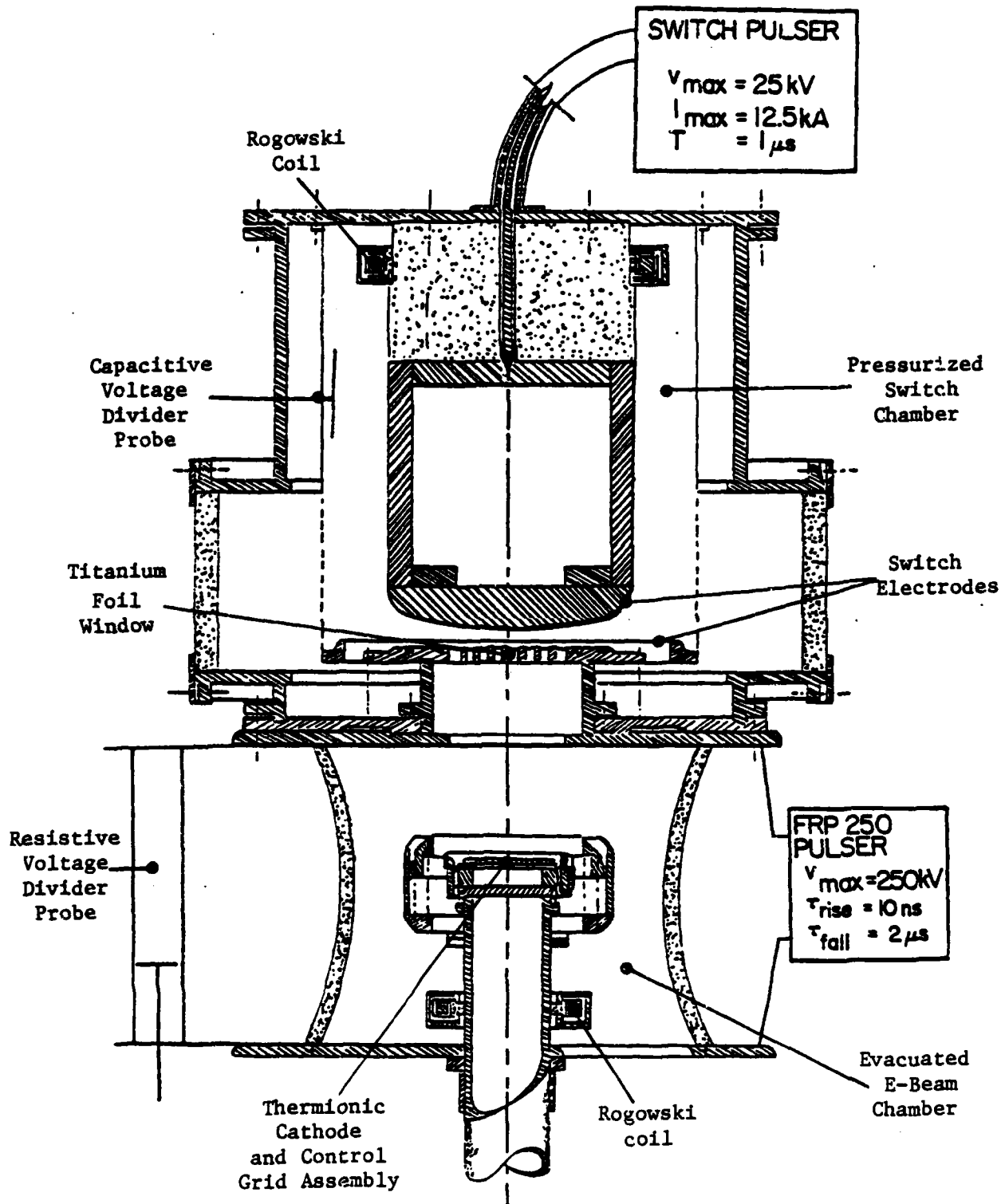


Fig. 1 Cross Section of Triode and Switch Chamber

pyrex cylinder between the two plates of a stripline. The bottom plate of the stripline is grounded and the e-beam accelerating voltage is applied to the top plate by a two stage Marx generator. This pulser (FRP-250) can deliver a maximum voltage of 250 kV with a 10 ns rise time and with an exponential decay time-constant of about 4  $\mu$ s. As the accelerating voltage decays, the transmission of the e-beam through the foil window (between the e-beam and switch chambers) decreases. Consequently, with this pulser the e-beam is only effective during the first two microseconds of operation.

The electron source is an electrically heated array of 15 mil diameter, thoriated tungsten filaments. When the filaments are heated to a temperature of about 2100 K, 800 W of heating power is required and the resulting e-beam current density is about 4 A/cm<sup>2</sup> over the 100 cm<sup>2</sup> cross-sectional area of the beam. With a thermionic cathode, the e-beam current density can easily be varied, independent of the accelerating voltage, by simply adjusting the filament temperature.

The control grid is located just above the filament array and is formed by an array of 10 mil diameter molybdenum wires stretched across a 7 inch diameter circular hole in the outer shell of the cathode assembly. These two arrays are connected to external power supplies through high vacuum electrical feed-throughs located in the aluminum base of the cathode. The base is water cooled and serves as a heat sink for the rest of the cathode.

The triode operates as follows. A negative bias voltage,  $V_B$ , is applied to the grid to hold the e-beam off even when the accelerating voltage is applied to the plate. The e-beam is then turned on by applying a positive voltage pulse to the grid. The pulser that drives the grid is depicted in Fig. 2. It consists of two, 75  $\Omega$ , coaxial cables separated by a triggerable coaxial spark gap. Cable 1 is connected to the grid, as shown, and is charged to  $V_B$  (typically about -6 kV). Cable 2 is charged through a 10 M $\Omega$  charging resistor to  $V_2$  (typically about 16 kV). When the gap is triggered, a positive voltage wave propagates from cable 2 along cable 1 to the grid. The grid is ideally an open circuit load to the cable, so the wave is totally reflected. The grid voltage at this time changes rapidly from  $V_B$  to  $V_2$  and the e-beam is turned on. The e-beam is later turned off again by the arrival of a negative voltage wave at the grid. This wave begins in cable 1, propagates along cable 2 to its essentially open end, is reflected, and then propagates to the grid. With the two open ends of this pulser, a train of positive and negative pulses is applied to the grid and the e-beam is repetitively turned on and off.

The primary advantage of this type of pulser is its overall simplicity. The pulse magnitudes are easily varied by changing the cable charging voltages and the pulse widths can be adjusted by simply changing the lengths of the cables. Obviously, this pulser cannot deliver a continuous train of unattenuated square pulses. Unavoidable losses present in the pulser (i.e. spark gap losses, capacitive loads at the ends of the pulser, etc.) will limit the useful length of the train to approximately 5 pulses.

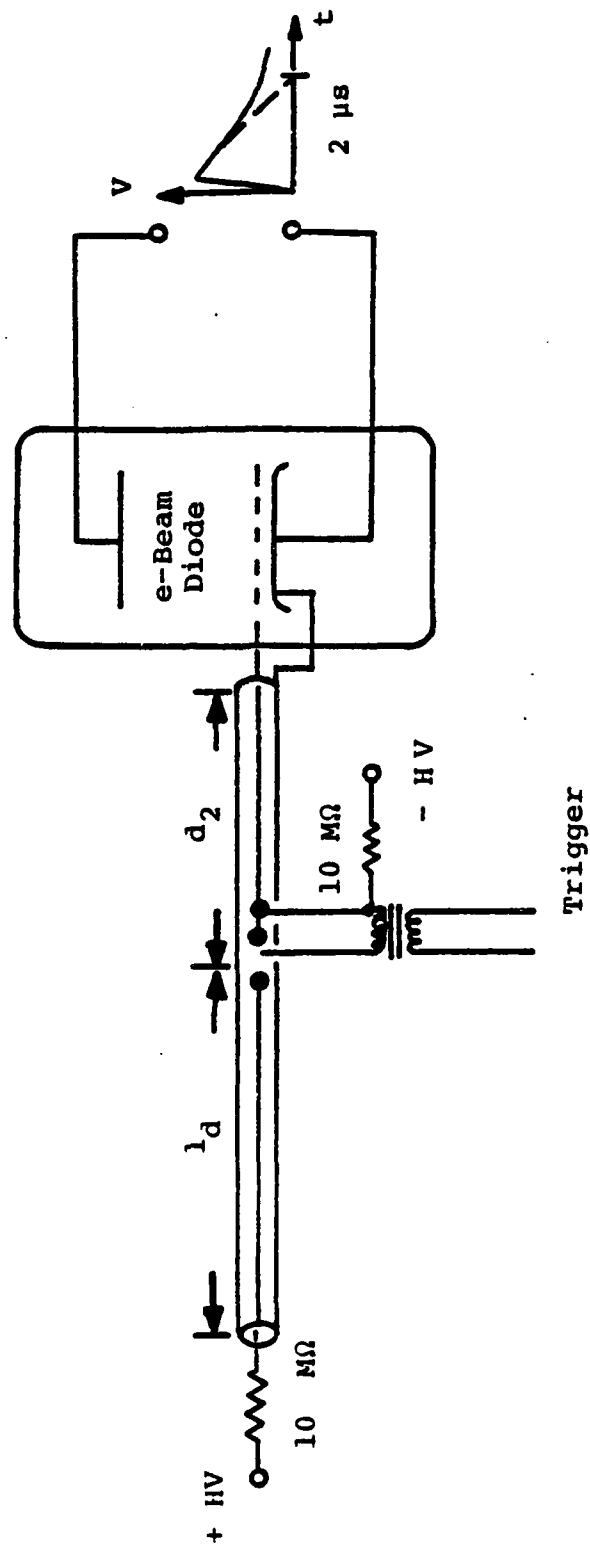


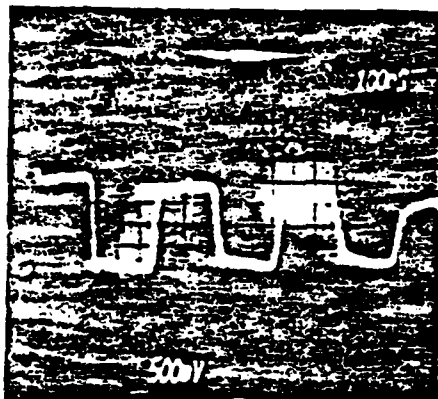
Fig. 2 Schematic Diagram of Grid Pulser

The output of the grid pulser when fired into a 100 k $\Omega$  load is shown in Fig. 3a. The rise and fall time of the first pulse is about 10 ns. There is significant degradation in the amplitude and in the rise/fall time of each subsequent pulse in the train due to the losses mentioned.

When the triode is connected in the simple circuit of Fig. 3b and the output of the grid pulser is applied to the grid, the e-beam current shown in Fig. 3c results. In this case the plate voltage was 30 kV, the filament temperature was about 2000 K, and the resulting peak current was 60 A. The output current follows the input grid voltage waveform (first pulse rise/ fall time ~ 10 ns), demonstrating the expected performance of the triode. The triode has been operated with plate voltages up to 240 kV, and filament temperatures up to 2100 K. The resulting beam current waveform is similar to the one of Fig. 3c with a peak value of about 400 A.

#### b. Switch/Diagnostic System

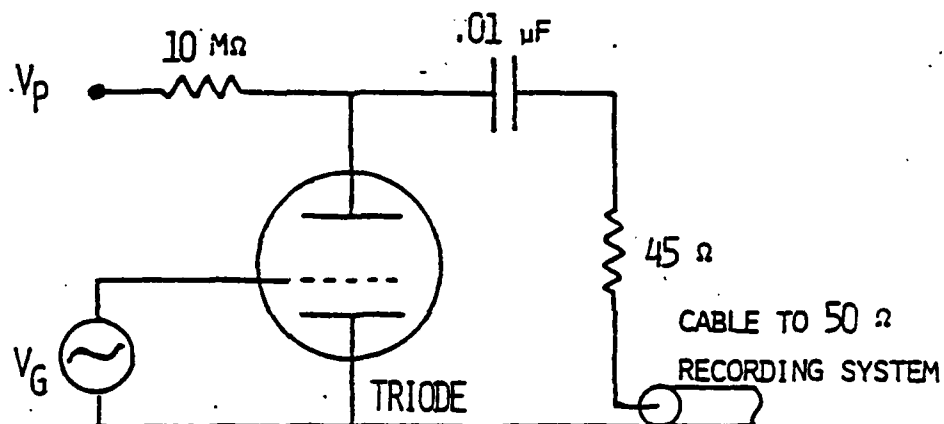
The switch is located in a pressurized stainless steel chamber just above the e-beam chamber, as shown in Fig. 1. The e-beam enters the switch chamber through a 1 mil thick Titanium foil window which separates the two chambers. After entering the switch chamber, the e-beam passes through the lower electrode of the switch which is a 1/2 mil thick aluminum foil and is incident on the stainless steel upper electrode. The e-beam ionizes the gas between the two switch electrodes and generates a diffuse discharge. The two electrodes are connected coaxially to the switch pulser, as shown. This pulser is a 2 $\Omega$  PFN that is able to



GRID PULSER OUTPUT  
INTO 100 k $\Omega$  LOAD

(100 ns/div)

(A)



(B)



E-BEAM CURRENT

$V_p = 30$  KV

$I_{peak} = 60$  A

200 ns/div

(C)

Fig.3 E-Beam Results

deliver a 25 kV, 12.5 kA, 1  $\mu$ s pulse to a matched load. The impedance of the PFN can easily be increased.

The e-beam is measured by a Rogowski coil located around the cathode feed tube, as shown in Fig. 1. The e-beam accelerating voltage is monitored by a resistive voltage divider between the two plates of the stripline. A Rogowski coil around the inner conductor of the short coaxial section in the switch chamber is used to measure the switch current. The switch voltage is monitored by a capacitive voltage divider probe, as also in Fig. 1. Since the switch diagnostics are floating at the switch chamber potential (i.e. the potential of the top plate of the stripline), it is necessary to decouple these diagnostics electrically from the recording system. Coupling is obtained through an analog optical link whose response time is better than 10 ns.

### c. Switch Current Monitor System

A current probe system has been designed, which allows the measurement of ns pulsed currents in high voltage environments, as, for instance, the e-beam controlled switch system. The design and performance of the current monitor was presented at the 4th IEEE Pulsed Power Conference in Albuquerque, New Mexico in June 1983 [2] and a paper has been accepted for publication in Rev. Sci. Instr. [3] (See Appendix II). The probe consists of a current transformer and an optical transducer. The transformer coil in a metallic torus is considered as a slow-wave transmission line and is terminated with its wave impedance. In this mode of operation current pulses shorter than twice the transit time of the transmission line are linearly transformed. The voltage gain of the transformer is considerably greater than

that of commonly used, self integrating Rogowski-coils. Sensitivities of up to 1 V/A can be obtained. The signal current drives a light emitting diode, with an impedance negligible compared to the wave impedance. The emitter is optically coupled to a photo diode, thus isolating the recording system from the pulsed power experiment. The probe, as used, has a linear response for pulses shorter than about 400 ns and currents of  $> 1$  A. The risetime is less than 5 ns.

The probe has been tested in a matched, 50  $\Omega$ , coaxial cavity by applying a rectangular input pulse of variable duration (Fig. 4a). The output signal of the probe is divided to show both the probe response directly and the output pulse transferred by the optical transducer. Figure 4b shows the leading pulse edges, Figure 4c shows the test results for an input pulse of 400 ns duration. This time is approximately 2/3 of the linearly transferred primary current duration of  $2T = 580$  ns. Probe responses to pulses with durations approaching twice the transit time show increasing oscillations, which are due to dispersive signal distortions in the slow wave transmission line.

### 3. Experimental Results

The results of preliminary switching experiments in  $N_2:O_2$  gas mixtures are shown in Fig. 5. These experiments were conducted to test the repetitive operation of the switch system, not to achieve optimum switch performance. In Fig. 5a, both the measured switch current waveform and the measured e-beam current waveform for one shot are shown. The experimental conditions for



# PROBE DATA

$N = 400$

$Z = 280 \Omega$

$R = 8.7 \text{ cm}$

$v = 1.9 \times 10^8 \text{ cm/s}$

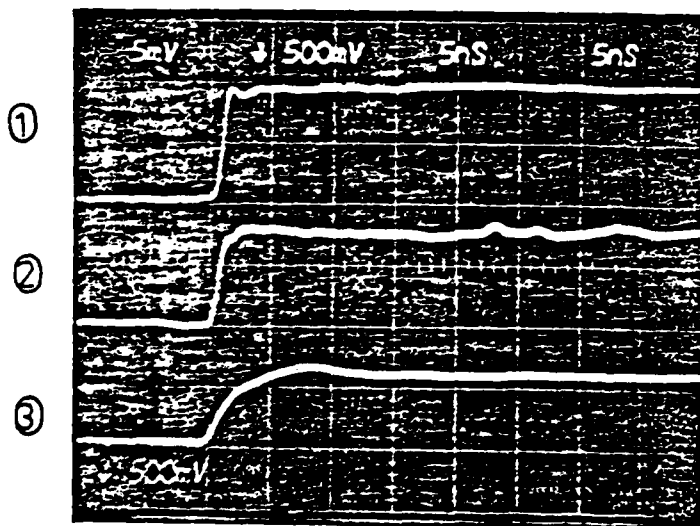
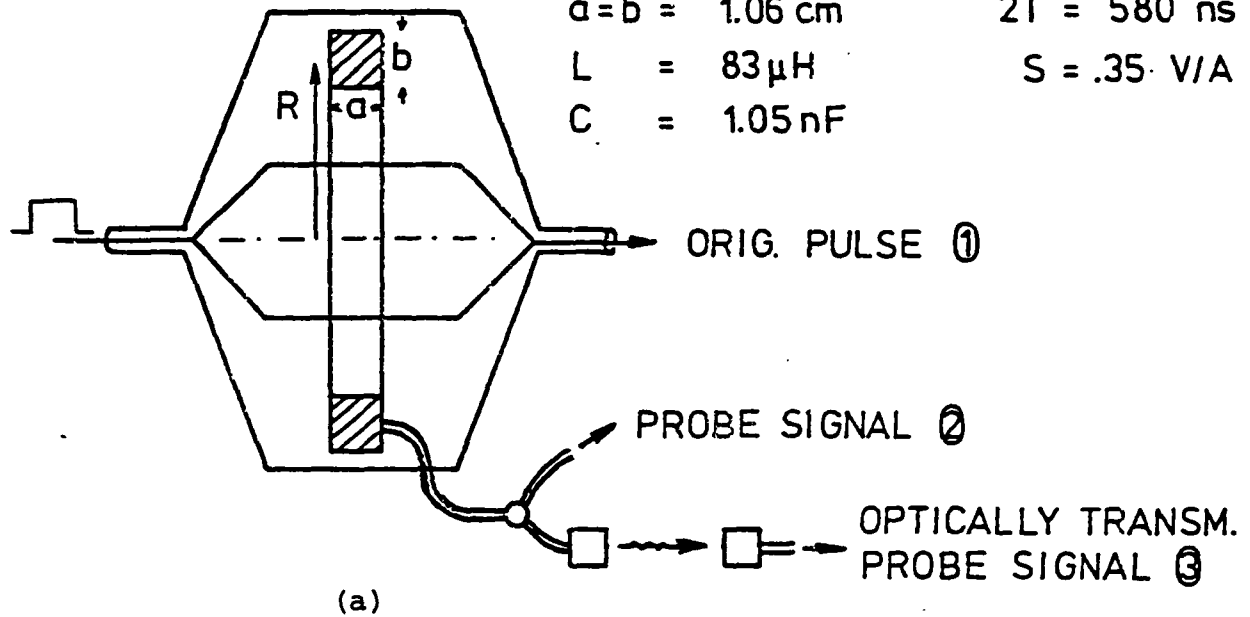
$a = b = 1.06 \text{ cm}$

$2T = 580 \text{ ns}$

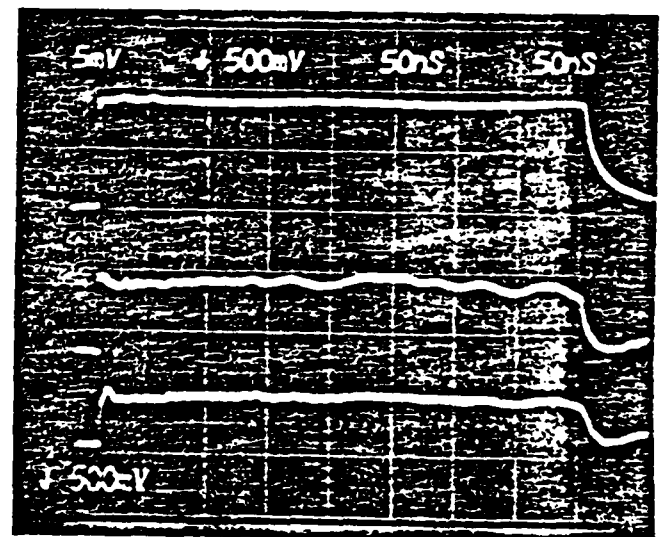
$L = 83 \mu\text{H}$

$S = .35 \text{ V/A}$

$C = 1.05 \text{ nF}$



(b)



(c)

Fig. 4 Test System and Test Results

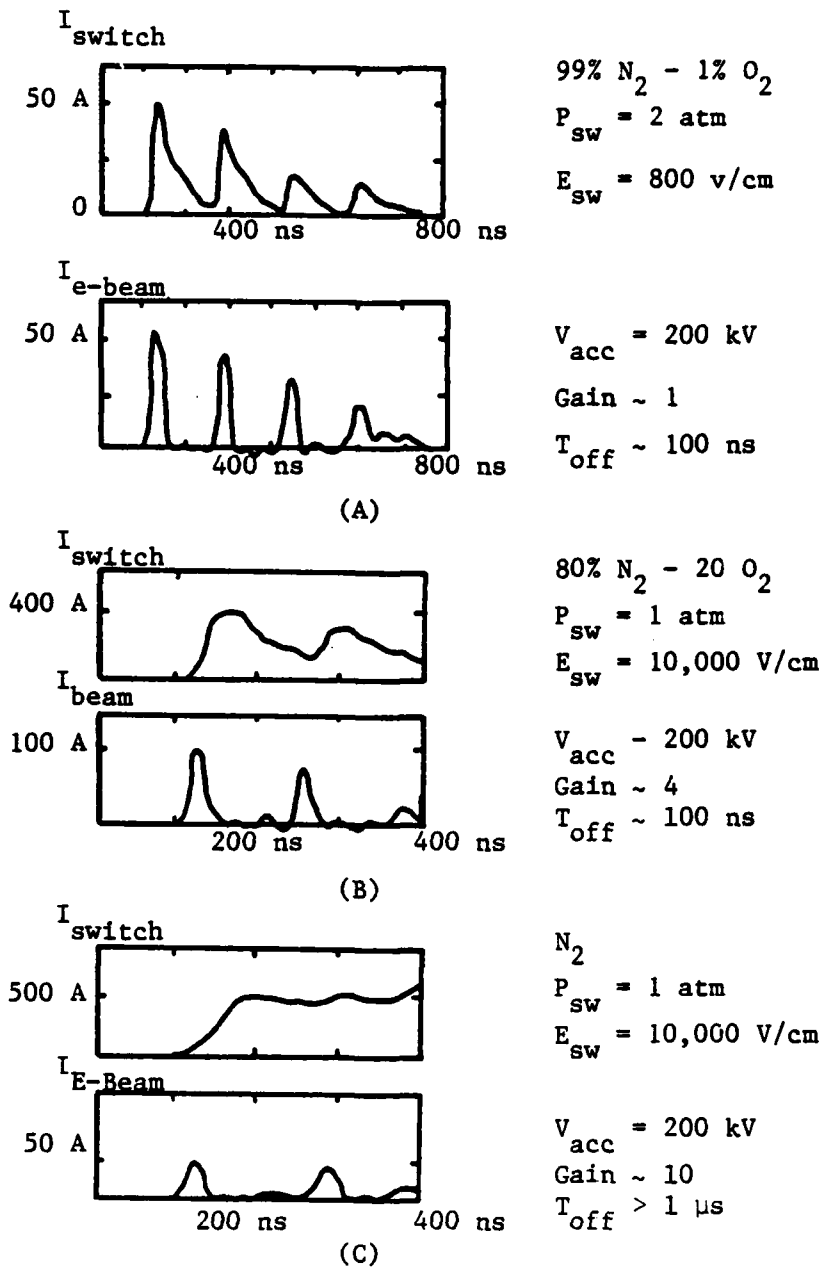


Fig. 5 Preliminary Switching Results

this shot are listed in the figure. Notice that the value of  $E/N$  is very small and there is no switch current gain in this case. In fact, the leading part of each switch current pulse is probably due to the collection of the corresponding incident e-beam current by the top electrode of the switch. The tail on each pulse is the component of the switch current caused by the ionization of the gas by the e-beam. This current is small because the electron drift velocity is small at low values of  $E/N$ . However, notice that the switch current turns off after each e-beam pulse (time constant  $\approx 100$  ns) due to electron attachment processes in the  $N_2:O_2$  gas mixture.

When the value of  $E/N$  is increased, the switch current waveform of Fig. 5b is observed. The experimental conditions are again listed in the figure. The e-beam input current waveform has the same shape as before but with a peak value this time of 100 A. In this case, a switch current gain of 4 is observed. The turn off time constant is, as before, about 100 ns.

In Fig. 5c, the effect of a slight change in the gas composition is demonstrated. In this case the concentration of the attacher,  $O_2$ , has been reduced to less than .1%. The other experimental parameters are essentially the same as before. The switch current waveform shows a slow decay with a turn off time constant in this case of greater than 1  $\mu$ s.

These results do not represent optimized switch performance. Experiments with gases which show the desired attachment characteristics (see Ref. 4) are underway.

#### 4. Theoretical Results

The code which was developed to describe the transient behavior of externally controlled discharges, is applicable as well for e-beam, as for optically controlled systems. The code and the results [10,11], which apply to e-beam control, are discussed in Section C.5.

### C. OPTICALLY CONTROLLED DISCHARGES

#### 1. Introduction

Optical discharge control means to make use of an optogalvanic effect. Here the conductivity of a discharge is changed by irradiation with light. Optogalvanic effects have been mainly applied to processes where the wavelength-specific response of the discharge is used, such as in spectroscopy, sensing of impurities, and frequency stabilization.

In these applications a detectable signal is required but its magnitude is of minor importance. For switching applications, however, only those processes can be considered that show a strong influence on the charge carrier balance of the discharge. In the beginning of this project the following four research areas were felt necessary for the solution of this problem:

- a. Concepts for optical control of diffuse discharge opening switches must be developed, based on known effects from optogalvanic experiments.

- b. Small scale optogalvanic experiments must be performed on promising systems where sufficient data are not yet available.
- c. High power discharge system experiments must be carried out to check the scaling laws for the optogalvanic processes and to investigate promising control systems.
- d. Detailed calculations on promising systems must be performed to predict the optimum parameter range for the experiments with respect to the suggested transient behaviors of the discharges.

It should be pointed out that all these research areas strongly interact with the work on electron beam controlled diffuse discharges, described in the previous section.

## 2. Concepts for Optical Control of Diffuse Discharge Opening Switches

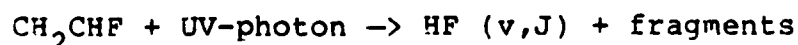
The aim of this work is to investigate several types of optogalvanic processes and to estimate the magnitude of the change of the discharge resistivity with regard to their possible application as a control mechanism for diffuse discharge switches. Some of the earlier results are summarized in a paper published in IEEE Trans. Plasma Sci. [4]. A more recent overview was given in an invited paper at the 4th IEEE Pulsed Power Conf. [5] (see Appendix III). In this report period the main emphasis was on processes related to the necessity of using attachers to achieve fast opening times. Processes such as photodetachment and photo-enhanced attachment also have strong relevance to electron beam sustained discharges. Model calculations on an electron beam sustained discharge with photodetachment as an addi-

tional control mechanism are discussed in detail in section C.5.

Photo-enhanced attachment through vibrational excitation of weak attachers seems to offer the possibility of strong external control. One obstacle to this mechanism is the competition of vibrational excitation by electrons in the discharge. Therefore, only those systems are considered that show a strong increase of the attachment rate in the E/N operation range of the discharge if higher vibrational states ( $v > 1$ ) are excited. Suitable excitation mechanisms seem to be transitions from electronically excited states to vibrationally and rotationally excited states ( $E \rightarrow V, R$ ) or photodissociation of larger molecules ( $ABC + \text{photon} \rightarrow A + BC(v > 1)$ ). There are very few data available on these processes with regard to their optogalvanic efficiency.

An example of a radiative ( $E \rightarrow V, R$ ) transition in  $I_2$  has been published by Beterov and Fatayev [6]. Radiation with a wavelength of  $\lambda = 532 \text{ nm}$  was used to excite the (B)-state. Intense Stokes fluorescence indicated a subsequent transition into highly vibrational excited states (see Fig. 10 in Appendix III). Vibrational relaxation had to provide the population of the optimum vibrational states, resulting in an increase of the attachment rate by three or four orders of magnitude.

Some informations on photo dissociation yielding vibrationally excited molecules can be found in the literature on lasers with transitions between vibrational states excited by photodissociation. An example is the reaction [7]:



which is used to operate HF lasers on rotational and vibrational transitions.

### 3. Small Scale Experiments

(in collaboration with Fraser Williams, Project No. 5)

Although the basic data available for several processes allow us to estimate the magnitude of certain optogalvanic effects, small scale experiments are necessary to prove the feasibility of these concepts. The reasons are that in a discharge the optogalvanic effect competes with a large number of processes and that a full set of rate constants is not available in most cases. Even if fairly complete sets of cross sections are available the necessary calculations are difficult and time consuming.

In the first study in 1982 in corporation with J. Mosely, Univ. Oregon, we looked at photodetachment of  $O^-$  in the flowing after-glow of a discharge containing  $O_2$  to show that the produced negative ions can be efficiently detached using a pulsed dye laser operating in the visible range. Photodetachment could be a possible control mechanism to overcome attachment during a special discharge phase, as discussed in detail in Section C.5. A paper describing the results of these experiment has been published in IEEE Trans. Plasma Sci. [8].

The characteristics of wall stabilized DC discharges in  $O_2$  exhibits bistabilities in a certain pressure and current range for a given discharge tube. The two branches of the discharge are called the T and the H form. The H form shows a much higher value of  $E/N$  than the T form. In optogalvanic experiments within the H form, close to the transition region, the photodetachment of  $O^-$  could cause gradient changes up to 65%, as shown in

Figure 6. These experiments show the advantage of operation conditions close to bistabilities. Bistabilities can also be expected in gas discharges containing attachers with a special  $E/N$  dependence on the attachment rate [11].

As discussed in Section C.2, processes such as  $E \rightarrow VR$  transitions or photodissociation could be used to produce vibrationally excited species to enhance the attachment rate of a gas mixture. It should be possible to investigate these processes with a flowing afterglow tube, such as used for photodetachment of  $O^-$ , however, UV light would be required in most cases. A new device with UV-transparent windows has been constructed and tested and modifications for UV operation of the laser systems used are underway. This new device will also allow us to look at photodetachment of  $SF_6$  which is considered to be an important process for laser triggering of  $SF_6$  filled spark gaps.

#### 4. High Power Discharge System

The design of an optically controlled high power discharge system was described in the last two Annual Reports. Two important changes have been made in this report period:

1. Transverse electrodes and appropriate windows have been incorporated to allow transverse illumination of the discharge with smaller beam cross sections and subsequently larger power densities.
2. A short pulse, low jitter preionization system has been incorporated. The design and performance of this system was presented at the 4th IEEE Pulsed Power Conference [9] (see Appendix IV).



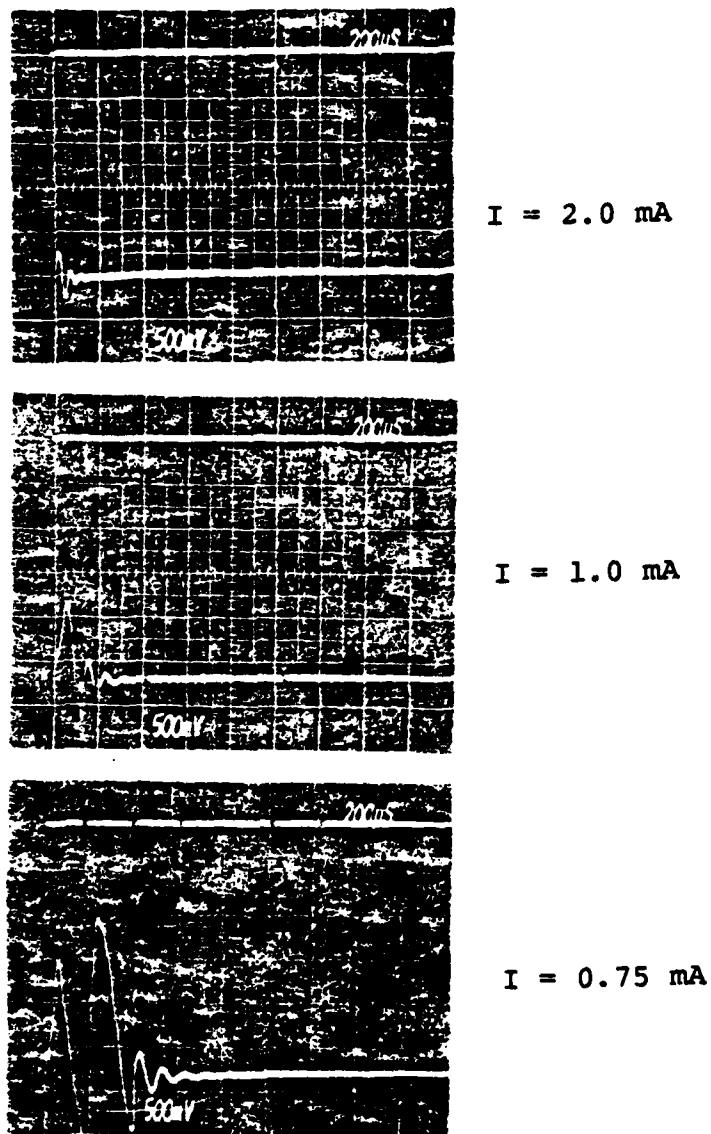


Fig. 6 Optogalvanic Signal (1:100) in an Oxygen Discharge (pressure 6 Torr, laser wavelength 560 nm, pulse energy 10 mJ) Parameter is the discharge current.

The high power discharge system is operational and was tested in rare gases and rare gas -  $N_2$  mixtures up to 1 atm and with admixtures of attachers. At this time experiments are under way to investigate the influence of photodetachment in these discharges.

#### 5. Calculations of the Time Dependent Behavior of Externally Controlled Discharges

A computer code has been developed to evaluate the time-dependent behavior of an externally controlled discharge in a given circuit. In order to allow fast calculations for different discharge and circuit parameters we used a code with two independent steps. In the first step, all rate constants necessary for the calculation of all rates of the significant processes are calculated, depending on  $E/N$ , for a representative gas mixture. These calculations require knowledge of the  $E/N$  dependent electron energy distribution function or the calculation of this distribution function. In the second step a system of time-dependent rate equations is solved using the  $E/N$  dependent rate constants and the circuit equation to incorporate the feedback of the circuit.

In a first approach (see 3rd Annual Report, Dec. 1982) the electron energy distribution was considered to be a Maxwellian distribution and calculations were performed on a system of  $N_2 + NO$ . In the recent research period a Monte Carlo code has been added to allow the calculation of the electron energy distribution function with  $E/N$  as the variable parameter. This code

has been used to calculate the characteristic and the transient behavior of an electron beam sustained discharge in  $N_2$  with admixtures of an attacher ( $N_2O$ ). Photodetachment of  $O^-$  is discussed as an additional optical control mechanism. The results of these calculations were presented in a paper at the 4th IEEE Pulsed Power Conference [10] and in a paper submitted to "Lasers and Particle Beams" [11], (See Appendix V).

#### D. EXPLORATORY OPENING SWITCH PROJECTS

Several other exploratory opening switch concepts have also been examined for potential use as opening switches. Among these are the dense plasma focus and a magnetically controlled switch. Cooperative efforts have been initiated with Dr. G. Gerdin of the Nuclear Engineering Laboratory at the University of Illinois at Urbana-Champaign and with Dr. Joe Proud of GTE Laboratories, Inc., Waltham, Mass. The work at the Univ. of Illinois is primarily funded by AFOSR under a separate grant and is concerned with the Dense Plasma Focus as an opening switch. The joint program with GTE Laboratories, Inc. (supervised by K. H. Schoenbach) has received funding from GTE and TTU to pay for a graduate student and fabrication services at GTE Lab. The work is concerned with a magnetically controlled low pressure switch. If the results of the project look promising then separate funding will be requested from DoD.

##### 1. Dense Plasma Focus

A cooperative research program has been initiated with the University of Illinois (Dr. G. Gerdin) on the use of the Dense

Plasma Focus as an opening switch. Conventional Plasma Focus devices can be considered as opening switches with no load attached. In such devices approximately 50% of the current flowing through the focus is interrupted. The interruption causes a strong voltage pulse across the focus plasma. At current levels of up to several MA, voltage spikes of several 100 kV were observed. Typical effective impedances of  $0.3 \Omega$  are generated in times of the order of  $10^{-8}$  to  $10^{-7}$  s. Repetitive operation (repetition frequency: several 100 kpps) was achieved in a burst mode lasting for 50  $\mu$ s. However, the opening effects were highly nonuniform and couldn't be controlled externally.

In order to use the Dense Plasma Focus as an efficient repetitive opening switch two main problems have to be solved first:

1. diverting the generated power into the load without disturbing the opening effect in the focus plasma,
2. external control of the repetitive switch events.

An experimental and theoretical research program in the Plasma Focus Group at the University of Illinois, is planned to determine whether the potential of a plasma focus repetitive opening switch can be realized.

The contribution of Texas Tech University consisted mainly of consulting (Drs. Schoenbach and Krompholz). Dr. Krompholz spent one month at the University of Illinois to consult on electrical and microwave measurement techniques. Preliminary results from this work were presented at the APS Plasma Physics Division meeting in 1983 [12].

## 2. Magnetically Controlled Opening Switch

A joint research program between TTU and GTE Laboratories, Inc. was initiated to explore the possibility of controlling the conductivity of low pressure plasmas, containing attachers, by means of externally applied magnetic fields. The concept is based on the change in the electron energy distribution towards lower energies, when external magnetic fields are applied. In a gas containing attachers with attachment cross sections which peak at low electron energies the attachment losses will thereby be increased. This effect, together with a change in electron mobility, can be utilized in an opening switch. One of our graduate students, R. Cooper, spent 2 months at GTE Laboratories to help design the experimental device which has been delivered to our laboratory.

Theoretical and experimental investigations presently funded by the Energy Center at TTU and GTE Laboratories, Inc. might provide background data to support a joint proposal to a DoD Agency.

## 3. Solid State Opening Switches

A very preliminary investigation of some novel, solid state, opening switch concepts was initiated in cooperation with Project No. 6. These investigations are based on the reported existence of deep levels (Cu-levels?) in n-type GaAs, approximately 1.1 eV below the conduction band. The switching concept is based on excitation by laser irradiation of electrons from these levels into the conduction band to provide switch turn-on. A subsequent laser pulse which creates holes in the valence band can then

provide a means for a direct recombination process which leads to fast switch opening.

The initial efforts were primarily aimed at fabricating the necessary material and we have also made arrangements with Sandia National Laboratory to obtain some possibly useful samples.

#### E. REFERENCES

1. H. Harjes, K. Schoenbach, G. Schaefer, H. Krompholz, M. Kristiansen, G. Leiker, and L. Hatfield, "E-Beam Triode for Multiple Submicrosecond Pulse Operation", Proc. 4th IEEE Pulsed Power Conf., Albuquerque, NM, June 1983.
2. H. Harjes, J. Doggett, J. Gahl, K. Zinsmeyer, H. Krompholz, K. Schoenbach, G. Schaefer, and M. Kristiansen, "Nanosecond-Current Probe for High Voltage Experiments", Proc. 4th IEEE Pulsed Power Conf., Albuquerque, NM, June 1983.
3. H. Krompholz, J. Doggett, K.H. Schoenbach, J. Gahl, C. Harjes, G. Schaefer, and M. Kristiansen, "Nanosecond Current Probe for High Voltage Experiments, Rev. Sci. Instrum., 55, 127, 1984.
4. K. H. Schoenbach, G. Schaefer, M. Kristiansen, L. L. Hatfield, and A. H. Guenter, "Concepts for Optical Control of Diffuse Discharge Opening Switches," IEEE Trans. Plasma Sci., PS-10, 246 (1982).
5. G. Schaefer, K. H. Schoenbach, A. H. Guenther, and W. K. Pendleton, "Some Recent Advances in Optically Controlled Discharges," Proc. 4th IEEE Pulsed Power Conf., Albuquerque, NM, June 1983. (Invited paper)
6. I. M. Beterov and N. V. Fatayev, "Optogalvanic demonstration of state-to-state dissociative electron capture rate in  $I_2$ ," Opt. Comm., 40, 425 (1982).
7. E. R. Sirkin and G. C. Pimentel, "HF rotational laser emission through photoelimination from vinyl fluoride and 1,1-difluoroethene," J. Chem. Phys., 75, 604-612, July 1981.
8. G. Schaefer, P. F. Williams, K. H. Schoenbach, and J. Moseley, "Photodetachment as a Control Mechanism for Diffuse Discharge Switches," IEEE Trans. Plasma Sci., PS-11, 263 (1983).

9. R. Cooper, G. Hutchenson, M. Kristiansen, G. Schaefer, K. H. Schoenbach and A. H. Guenther, "Multi-Spark Preionization Source for Diffuse Discharges Containing Attachers," Proc. 4th IEEE Pulsed Power Conf., Albuquerque, NM, June 1983.
10. G. Schaefer, K. H. Schoenbach, P. Tran, J.-S Wang, and A. H. Guenther, "Computer Calculations of the Time Dependent Behavior of Diffuse Discharge Switches," Proc. 4th IEEE Int. Pulsed Power Conf., Albuquerque, NM, June 1983.
11. G. Schaefer, K. H. Schoenbach, H. Krompholz, M. Kristiansen, and A. H. Guenther, "The Use of Attachers in Electron Beam Sustained Discharge Switches - Theoretical Considerations," submitted to Lasers and Particle Beams.
12. F. Venneri, J. Mandrekas, G. Gerdin, M. Tanis, and H. Krompholz, "Preliminary Results of the Plasma Focus as an Opening Switch", APS, 25th Annual Meeting of the Plasma Physics Division, Los Angeles, CA, 1983.

E-BEAM TRIODE FOR MULTIPLE SUBMICROSECOND  
PULSE OPERATION\*

H. Harjes, K. Schoenbach, G. Schaefer,  
H. Krompholz, and M. Kristiansen  
Department of Electrical Engineering  
G. Leiker and L. Hatfield  
Department of Physics  
Texas Tech University  
Lubbock, Texas 79409

ABSTRACT

Externally controlled diffuse discharge switches offer the potential of submicrosecond opening time and high repetition rate. For the investigation of an electron-beam controlled diffuse discharge, an e-beam gun was constructed which allows submicrosecond, multiple pulse operation. The 200 kV, 100 cm<sup>2</sup>, e-beam with thermionic cathode is designed as a triode. The control grid is pulsed to generate several successive e-beam pulses of ~ 100 ns duration and variable pulse-to-pulse interval. Electrical and optical diagnostics are used to monitor the triode performance. Preliminary switch experiments in N<sub>2</sub>-O<sub>2</sub> gas mixtures are discussed.

I. INTRODUCTION

In recent years there has been an increasing interest in the development of fast, repetitive, opening switches which would allow the use of inductive energy storage in repetitively operated pulsed power systems. An opening switch concept that shows promise for fast repetitive operation is the electron beam (e-beam) controlled switch (EBCS). Such a switch is depicted in the simple inductive energy storage circuit of Fig. 1. The switch electrodes are separated by a pressurized gaseous dielectric which conducts and charges the inductor when an ionizing e-beam is injected (usually through one of the electrodes which might be mesh or foil). The switch voltage remains below the self breakdown voltage so that there is negligible avalanche ionization in the switch gas. Thus, the discharge is completely sustained by the e-beam current. When the e-beam is turned off, electron attachment and recombination processes in the gas cause the discharge to die out and the switch opens. By commutating the repetitively operated EBCS with the second switch in the circuit of Fig. 1, a train of pulses can be delivered to the load until the inductor is discharged.

Obviously, the performance capability of such an inductive energy storage pulser is mainly dependent upon the performance capability of the EBCS. Consequently, one would like to have an EBCS that satisfies the following conditions:

- 1) high rep-rate capability
- 2) fast turn on and off capability
- 3) high current handling capability
- 4) high voltage standoff capability
- 5) high efficiency

Single shot EBCS's have been investigated by Hunter [1], Kovalchuk [2], Fernsler [3], Hallada [4], Kline [5], Comisso [6], and others. These investigations have demonstrated the promise of the EBCS in satisfying the above requirements. However, the only reported investigation into the repetitive operation of an EBCS has been theoretical [7]. These investigations also clearly indicate that the switch character-

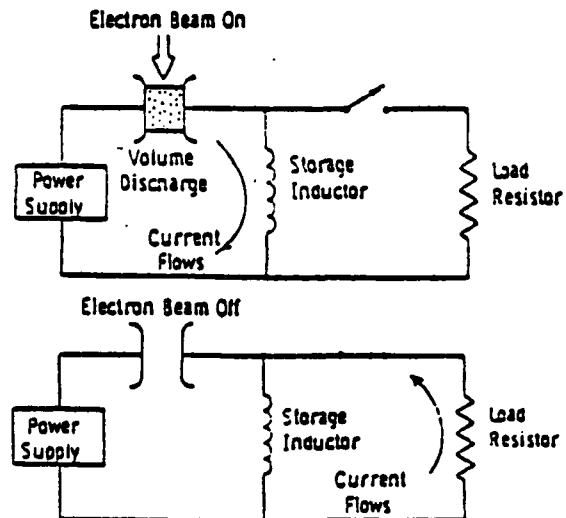


Figure 1. Schematic Diagram of Electron Beam Switch Operation [9].

istics mentioned in the above list depend primarily upon the parameters of the switch gas. The switch gas mixture should have a high mobility and a low attachment rate at low values of E/N when the switch is conducting. This reduces conduction losses and increases the switch efficiency. The gas mixture should then have a low mobility and a high attachment rate at high values of E/N when the switch is opened to decrease the switch opening time [8]. Since only a few gas mixtures have been tried in previous EBCS experiments, there are probably several more suitable gas mixtures. Consequently, experimental investigations into the repetitive operation of an EBCS with promising candidate gas mixtures are needed.

The e-beam triode that will be described in this paper was specifically designed to deliver a controllable e-beam for such an EBCS experiment. The purpose of the experiment is to study the repetitive operation of the switch under a wide range of gas and e-beam parameters. Consequently the e-beam has to satisfy the following requirements:

- 1) high repetition rate
- 2) fast turn on and turn off times
- 3) variable beam energy and current density.

The e-beam gun is constructed as a triode to achieve the required repetitive, fast response control of the e-beam and a thermionic cathode is used to satisfy the last condition. In the second section of this paper, the triode, the grid pulser, and the switch are described in detail. In the third section, the results of the triode operation and some preliminary switching results are presented. In the last section, a summary is given.

\* WORK supported by Army Research Office



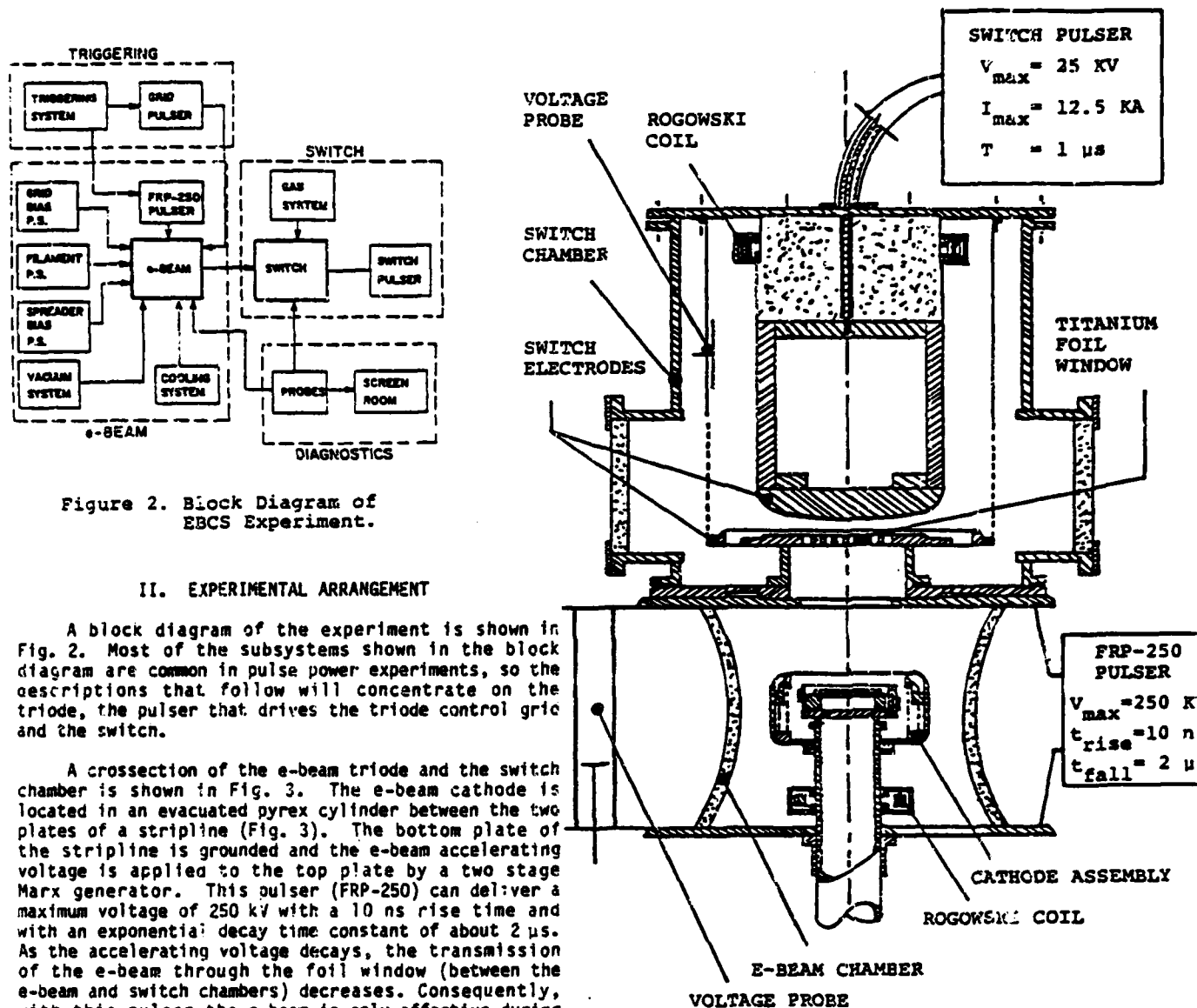


Figure 2. Block Diagram of EBCS Experiment.

## II. EXPERIMENTAL ARRANGEMENT

A block diagram of the experiment is shown in Fig. 2. Most of the subsystems shown in the block diagram are common in pulse power experiments, so the descriptions that follow will concentrate on the triode, the pulser that drives the triode control grid and the switch.

A cross-section of the e-beam triode and the switch chamber is shown in Fig. 3. The e-beam cathode is located in an evacuated pyrex cylinder between the two plates of a stripline (Fig. 3). The bottom plate of the stripline is grounded and the e-beam accelerating voltage is applied to the top plate by a two stage Marx generator. This pulser (FRP-250) can deliver a maximum voltage of 250 kV with a 10 ns rise time and with an exponential decay time constant of about 2  $\mu\text{s}$ . As the accelerating voltage decays, the transmission of the e-beam through the foil window (between the e-beam and switch chambers) decreases. Consequently, with this pulser the e-beam is only effective during the first microsecond of operation.

A more detailed cross-section of the cathode is shown in Fig. 4. The electron source is an electrically heated array of 15 mil diameter thoriated tungsten filaments. When the filaments are heated to a temperature of about 2100 K, 800 W of heating power is required and the resulting e-beam current density is about 4 A/cm<sup>2</sup> over the 100 cm<sup>2</sup> cross-sectional area of the beam. With a thermionic cathode, the e-beam current density can easily be varied independent of the accelerating voltage by simply adjusting the filament temperature.

The control grid is located just above the filament array and is formed by an array of 10 mil diameter molybdenum wires stretched across a 7 inch diameter circular hole in the outer shell of the cathode assembly. These two arrays are connected to external power supplies through high vacuum electrical feedthroughs located in the aluminum base of the cathode (Fig. 4). The base is water cooled and serves as a heat sink for the rest of the cathode.

The triode operates as follows. A sufficient negative bias voltage,  $V_g$ , is applied to the grid to hold the e-beam off even when the accelerating voltage is applied to the plate. Then, the e-beam is turned

Figure 3. Cross-section of Triode and Switch Chamber.

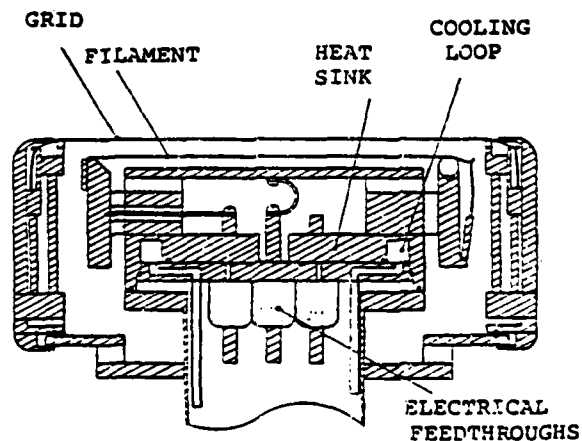


Figure 4. Cross-section of Cathode Assembly.

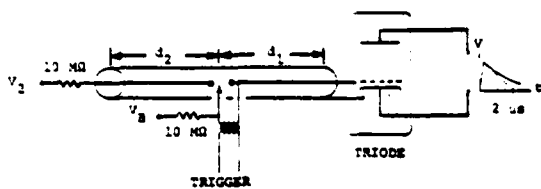


Figure 5. Schematic Diagram of Grid Pulser.

on by applying a positive voltage pulse to the grid. The pulser that drives the grid is depicted in Fig. 5. It consists of two, 75  $\Omega$ , coaxial cables separated by a triggerable coaxial spark gap. Cable 1 is connected to the grid as shown and is charged to  $V_B$  (typically about -6 kV). Cable 2 is charged through a 10 M $\Omega$  charging resistor to  $V_2$  (typically about 16 kV). When the gap is triggered, a positive voltage wave propagates from cable 2 along cable 1 to the grid. The grid is ideally an open circuit load to the cable so the wave is totally reflected. The grid voltage at this time changes rapidly from  $V_B$  to  $V_2$  and the e-beam is turned on. The e-beam is later turned off again by the arrival of a negative voltage wave at the grid. This wave begins in cable 1, propagates along cable 2 to its essentially open end, is reflected, and then propagates to the grid. With the two open ends of this pulser, a train of positive and negative pulses is applied to the grid and the e-beam is repetitively turned on and off.

The primary advantage of this type of pulser is its overall simplicity. The pulse magnitudes are easily variable by changing the cable charging voltages and the pulse widths can be adjusted by simply changing the lengths of the cables. Obviously, this pulser cannot deliver a continuous train of unattenuated square pulses. Unavoidable losses present in the pulser (i.e. spark gap losses, capacitive loads at the ends of the pulser, etc.) will limit the useful length of the train to a finite number of pulses.

The switch is located in a pressurized stainless steel chamber just above the e-beam chamber, as shown in Fig. 3. The e-beam enters the switch chamber through a 1 mil thick Titanium foil window which separates the two chambers. After entering the switch chamber, the e-beam passes through the lower electrode of the switch which is a 1/2 mil thick aluminum foil and is incident on the stainless steel upper electrode. The e-beam ionizes the gas between the two switch electrodes and generates a diffuse discharge. The two electrodes are connected coaxially to the switch pulser, as shown. This pulser is a 2  $\Omega$  PFN that is able to deliver a 25 kV, 12.5 kA, 1  $\mu$ s pulse to a matched load.

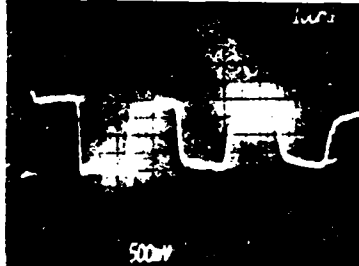
The e-beam current is measured by a Rogowski coil located around the cathode feed tube, as shown in Fig. 3. The e-beam accelerating voltage is monitored by a resistive voltage divider between the two plates of the stripline. A Rogowski coil around the inner conductor of the short coaxial section in the switch chamber is used to measure the switch current. The switch voltage is monitored by a capacitive voltage divider probe, as shown in Fig. 3. Since the switch diagnostics are floating at the switch chamber potential (i.e. the potential of the top plate of the stripline), it is necessary to electrically decouple these diagnostics from the recording system. Coupling is obtained through an analog optical link whose response time is better than 10 ns. Descriptions of this link and the Rogowski coils are given in Ref. 10

### III. RESULTS

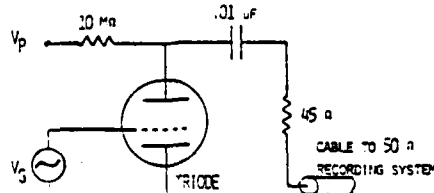
The output of the grid pulser when fired into a 100 K $\Omega$  load is shown in Fig. 6a. The rise and fall time on the first pulse is about 10 ns. There is significant degradation in the amplitude and in the rise/fall time of each subsequent pulse in the train due to the losses mentioned in the previous section.

When the triode is connected in the simple circuit of Fig 6b and the output of the grid pulser is applied to the grid, the e-beam current shown in Fig. 6c results. In this case the plate voltage was 30 kV, the filament temperature was about 2000 K, and the resulting peak current was 60 A. The output current follows the input grid voltage waveform (first pulse rise/fall time  $\sim$  10 ns) demonstrating the expected

GRID PULSER OUTPUT INTO  
100 K $\Omega$  LOAD (100 ns/div)

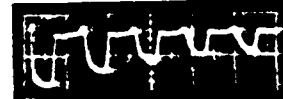


(A)



(B)

E-BEAM CURRENT  
 $V_p = 30$  KV,  $I_{peak} = 60$  A  
(200 ns/div)



(C)

Figure 6. E-beam Results.

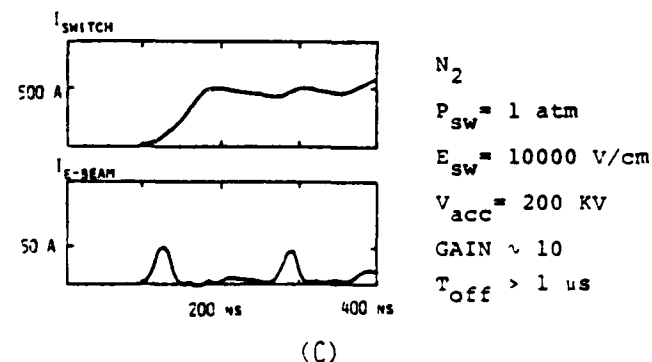
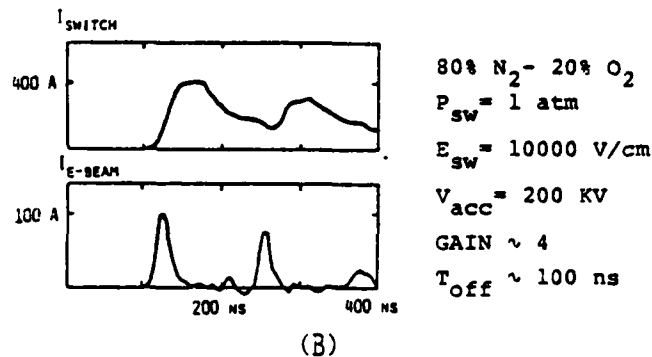
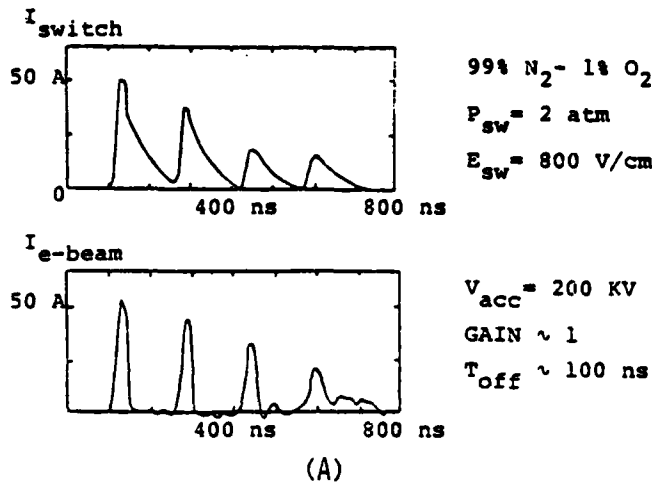
performance of the triode. The triode has been operated with plate voltages up to 240 kV, and filament temperatures up to 2100 K. The resulting beam current waveform is similar to the one of Fig. 6c with a peak value of about 400 A.

The results of some preliminary switching experiments in  $N_2:O_2$  gas mixtures are shown in Fig. 7. These experiments were conducted to test the repetitive operation of the switch system, not to achieve optimum switch performance. In Fig. 7a, both the measured switch current waveform and the measured e-beam current waveform for one shot are shown. The experimental conditions for this shot are listed in the figure. Notice that the value of  $E/N$  is very small and there is no switch current gain in this case. In fact, the leading part of each switch current pulse is probably due to the collection of the corresponding incident e-beam current by the top electrode of the switch. The tail on each pulse is the component of the switch current caused by the ionization of the gas by

the e-beam. This current is small because the electron drift velocity is small at low values of  $E/N$ . However, notice that the switch current turns off after each e-beam pulse (time constant  $\sim 100$  ns) due to electron attachment processes in the  $N_2:O_2$  gas mixture.

When the value of  $E/N$  is increased, the switch current waveform of Fig. 7b is observed. The experimental conditions are again listed in the figure. The e-beam input current waveform has the same shape as before but with a peak value this time of 100 A. In this case, a switch current gain of 4 is observed. The turn off time constant is, as before, about 100 ns.

In Fig. 7c, the effect of a slight change in the gas composition is demonstrated. In this case the concentration of the attachor,  $O_2$ , has been reduced to less than .1%. The other experimental parameters are essentially the same as before. The switch current waveform shows a slow decay with a turn off time constant in this case of greater than 1  $\mu$ s.



#### IV. SUMMARY

An e-beam triode that is able to deliver a controllable, 240 keV, 400 A, 100 cm<sup>2</sup>, e-beam for a EBCS experiment has been designed and tested. The triode is turned on and off with  $\sim 10$  ns response times at variable rep-rates up to  $\sim 25$  MHz in 1  $\mu$ s bursts by a simple pulser. A coaxial switch driven by a 2  $\Omega$  PFN, has also been constructed. The objective of the experiment is to study the behavior of an e-beam sustained attachment dominated discharge, suitable for fast, low loss, rep-rated operation, at high discharge current densities in various gas mixtures.

Preliminary repetitive switch experiments in  $N_2:O_2$  gas mixtures have been conducted. At a 5 MHz rep-rate, a switch current gain of 4 and a turn off time constant of  $\sim 100$  ns was observed. These results do not represent optimized switch performance but do demonstrate that the repetitive EBCS experiment is operational.

#### REFERENCES

- 1) R.O. Hunter, Proc. 1st IEEE Intl. Pulsed Power Conf., Lubbock, TX, 1976 IC8:pp 1-6.
- 2) B.M. Kovalchuck and G.A. Mesyats, Sov. Tech. Phys. Lett., 2, 252, (1976).
- 3) R.F. Fernsler, D. Conte, and I.M. Vitkovitsky, IEEE Trans. Plasma Sci., PS-8, 176, (1980).
- 4) M.R. Hallada, P. Bletzinger, and W.F. Bailey, IEEE Trans. Plasma Sci., PS-10, 218, (1982).
- 5) L.E. Kline, IEEE Trans. Plasma Sci., PS-10, 224, (1982).
- 6) R.J. Comisso, R.F. Fernsler, V.E. Scherrer, and I.M. Vitkovitsky, IEEE Trans. Plasma Sci., PS-10, 241, (1982).
- 7) R.J. Comisso, R.F. Fernsler, V.E. Scherrer, and I.M. Vitkovitsky, NRL Memorandum Report 4975, 1982.
- 8) K.H. Schoenbach, G. Schaefer, M. Kristiansen, L.L. Hatfield, and A.H. Guenther, IEEE Trans. Plasma Science, PS-10, 246, (1982).
- 9) L.E. Kline, Workshop on Repetitive Opening Switches, Tamarron, CO, p. 121, 1981.
- 10) H. Harjes, J. Dogget, J. Gahl, K. Zinsmeyer, H. Krompholz, K. Schoenbach, G. Schaefer, and M. Kristiansen, Proc. 4th IEEE Pulsed Power Conf., Albuquerque, NM, 1983.

Figure 7. Preliminary Switching Results.

# NANOSECOND-CURRENT PROBE FOR HIGH VOLTAGE EXPERIMENTS\*

H. Harjes, J. Doggett, J. Gahl, K. Zinsmeyer  
H. Krompholz, K. Schoenbach, G. Schaefer, and M. Kristiansen  
Department of Electrical Engineering  
Texas Tech University  
Lubbock, Texas 79409 USA

## Abstract

A current probe has been designed which allows measurement of ns-pulsed currents in high voltage environments. The probe consists of a current transformer and an optical transducer. The transformer coil in a metallic torus is considered as a slow-wave transmission line and is terminated with its wave impedance. In this mode of operation current pulses shorter than twice the transit time of the transmission line are linearly transformed. The voltage gain of the transformer is considerably greater than that of commonly used self integrating Rogowski-coils. The signal current drives a light emitting diode, with an impedance negligible compared to the wave impedance. The emitter is optically coupled to a photodiode, thus isolating the recording system from the pulsed power experiment. The probe, as used has a linear response for pulses shorter than about 400 ns and currents of  $> 1$  A. The risetime is less than 5 ns.

## Introduction

Rogowski coils are commonly used for current measurement in pulsed power experiments. For pulses in the ns range such coils have to be considered as slow wave transmission lines with distributed voltage sources due to flux changes  $\dot{\Phi}$  in the coil<sup>1,2,3</sup>. These transmission lines are usually operated in the so-called self-integrating mode, with a terminating resistor  $R$  which is small compared to the impedance of the line. The risetime, which can be achieved by using such a self-integrating current probe is in the order of ns. The response is linear for times short compared to the characteristic time  $L/R$  where  $L$  is the inductance of the coil<sup>2</sup>.

The sensitivity of the self-integrating Rogowski coil is approximately  $R/N$ , where  $N$  is the number of turns. Thus, increasing the characteristic time  $L/R$  lowers the sensitivity, which is generally in the order of several  $10^{-3}$  V/A<sup>4</sup>. The self-integrating coil, therefore is useful only for high current experiments. For currents less than 100 A, with 1 A resolution, characteristic signals are in the mV range and therefore susceptible to noise.

The sensitivity can be increased considerably by terminating the line with a resistor which equals the wave impedance. The response however, then only is linear for twice the transit time. With transit times which are usually in the order of 10 ns the matched probe was not seen as a competitor for the self integrating Rogowski coil. The transit time, however, can be increased drastically by taking a transmission line parameter into account which was not considered as being important so far: the distributed capacitance  $C'$ . By constructing the slow wave structure in a way that  $C'$  becomes very large (nF) it is possible to obtain a probe with almost optimum sensitivity and strictly linear response for pulse durations of up to several  $\mu$ s.

The high sensitivity of the probe allows use of a low cost optical transducer system for electrical

isolation against voltages of several 100 kV in pulsed power systems. The system, consisting of a slow wave structure current probe driving a light emitting diode, which is optically coupled to a photodiode, has a sensitivity of several mV/A and a risetime of 3 ns. It is suitable for measuring currents with amplitudes  $> 1$  A and a duration of up to several  $\mu$ s with reduced or eliminated influence of noise.

## Current Probe

The design of the current probe is shown in Fig. 1a. It consists of an  $N$ -turn coil with rectangular cross-section (sides  $a$  and  $b$ ), and major radius  $R$  in a metallic torus with a slit along the inner circumference. The coil and the surrounding electrostatic shield act as a slow wave structure with a characteristic impedance  $Z_0 = (L'/C')^{1/2}$  and propagation velocity  $v = (L'C')^{-1/2}$ , where  $L'$  and  $C'$  are the inductance and capacitance per unit length. The distance between the coil as an inner conductor and the housing as an outer conductor of the transmission line is minimized to provide a large value of  $C'$ . One end of the coil is shorted (coil connected to shield) and the output is matched with  $R = Z_0$ .

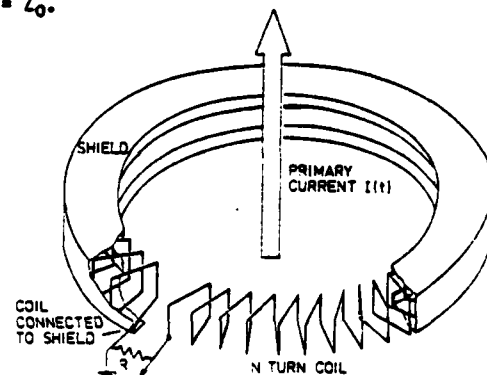


Fig 1a Geometry of the current probe

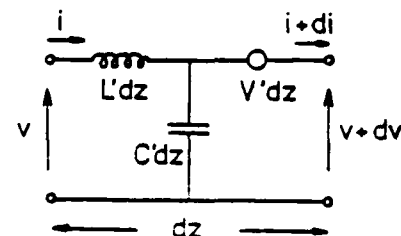


Fig 1b Equivalent circuit

\* This work was supported by ARO

The induced voltage per length  $dz$  of the circumference is given by Faraday's Law (for  $z \gg a, b$ ) as a function of the time derivative of the measured current  $I$ :

$$V_{ind,dz} = -N \frac{\mu_0}{(2\pi R)^2} (iab) \frac{dI}{dt} dz$$

and acts as a source voltage for an equivalent circuit element<sup>3</sup> of length  $dz$  (Fig 1b). The wave equation for the probe current  $i(z,t)$  in this case, using  $L' = \mu_0 N^2 / (2\pi R)^2 (ab)$ , is

$$\frac{\partial^2 i}{\partial z^2} = \frac{1}{L'C'} \frac{\partial^2 i}{\partial t^2} = \frac{i}{N} \frac{d^2 I}{dt^2}$$

with the solution for the output current

$$i_{out}(t) = i(z = 2\pi R, t) = \frac{1}{2N} (I(t) - I(t-2T))$$

where  $T$  denotes the coil transit time ( $T = 2\pi R/v$ ). Thus, for currents  $I(t)$  with a duration  $< 2T$ , the term  $I(t-2T)$  is zero and the output current is  $1/2N$  times the current to be measured.

#### Optical Transducer

Fig 2a shows the electrical circuits for the emitter, a laser diode (type LCW-10, M/A-Com Laser Diode Inc.) and the receiver (photodiode S1188, Hamamatsu). The emitting diode is biased with a forward current of 75 mA to the center of the approximately linear part of the power vs. current characteristics above threshold. This bias provides a linear transfer of negative and positive input signals up to a maximum amplitude of 10 mA (Fig 2b). The diode has been matched to 50  $\Omega$ , and limits the useful range of primary currents to  $-8A < I < 8A$  for test measurements. For higher currents, the probe output signal has to be attenuated to the linear transferred input current range of the laser diode. The emitted light is focused on the entrance of a quartz fiber (diameter 600  $\mu m$ , length 10 m) connected to the receiver. The amplitude transfer characteristic of the transducer system is shown in Fig. 2b. Its risetime of 3 ns is mainly determined by dispersion in the fiber.

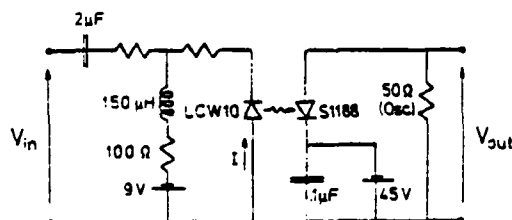


Fig 2a Optical transducer setup

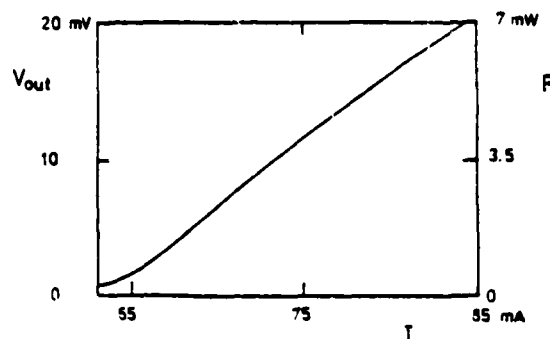


Fig 2b Transfer characteristics of the optical transducer

#### Results of Test Measurements

A probe with parameters given in Table 1 has been tested in a matched 50  $\Omega$  coaxial cavity with inner radius 4.4 cm, and outer radius 10.2 cm, by applying a rectangular input pulse of variable duration (Fig. 3a). The output signal of the probe is divided to show both the probe response directly and the output pulse transferred by the optical transducer. Fig. 3b shows the leading pulse edges, Fig. 3c shows the test results for an input pulse of 400 ns duration. This time is approximately 2/3 of the linearly transferred primary current duration of  $2T = 580$  ns. Probe responses to pulses with durations approaching twice the transit time show increasing oscillations, which are probably due to dispersive signal distortions in the slow wave transmission line. This dispersion, limiting the useful time range, is caused by the finite frequency dependent skin resistance of the coil and by the periodic variation of the line impedance due to the slit in the inner circumference of the shield.

N (number of turns)	: 400
R (major radius)	: 8.7 cm
a=b (sides of cross section)	: 1.06 cm
L' (inductance per unit length)	: 1.518 $\mu H/cm$
C' (capacitance per unit length)	: 19.2 pF/cm
Z <sub>0</sub> (characteristic impedance)	: 280 $\Omega$
v (propagation velocity)	: $1.9 \times 10^8$ cm/s
T (Transit time)	: 290 ns
R <sub>w</sub> (wire resistance)	: 1.8 $\Omega$
R/2N (sensitivity)	: .35 V/A

Table 1 Probe parameters

#### Summary

With transmission line type current sensors, matched with the line impedance, sensitivities of up to 1 V/A can be obtained. This is particularly important for low current e-beam devices or pulsed power experiments where sensor and recording system are coupled through optical links with current driven laser diodes as emitters. The measurement time range of these sensors is mainly determined by dispersion effects which limit the application to pulses with duration smaller than several microseconds.

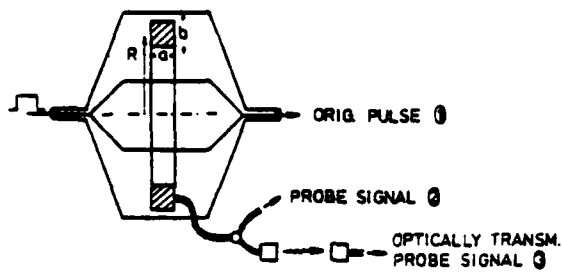


Fig 3a Test setup

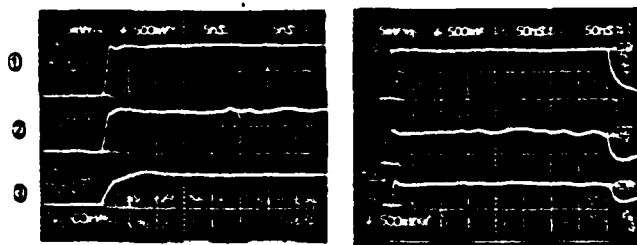


Fig 3b, c    upper trace: input pulse  
                  center trace: probe output  
                  lower trace: transducer output

#### References

1. J. Cooper, Plasma Physics (Journal of Nuclear Energy part C), 5, 285 (1963).
2. D.G. Pellinen, M.S. Di Capua, S.E. Sampayan, H. Gerbracht and M. Wing, Rev. Sci. Instrum. 51, 1535 (1980).
3. W. Stygar and G. Gerdin, IEEE Transactions on Plasma Science, PS-10, 40 (1982).
4. Marco S. Di Capua in Proceedings of the Workshop on "Measurements of Electrical Quantities in Pulse Power Systems" held at the National Bureau of Standards, Boulder, Colorado, March 2-4, 1981 p. 175.

SOME RECENT ADVANCES IN OPTICALLY CONTROLLED DISCHARGES

Gerhard Schaefer and Karl H. Schoenbach  
Texas Tech University  
Department of Electrical Engineering  
Lubbock, Texas 79409 USA

Arthur H. Guenther and Winston K. Perdleton  
Air Force Weapons Laboratory  
Kirtland Air Force Base, New Mexico 87185 USA

Abstract

The recent increase in modular pulsed power systems has amplified the potential of optically controlled discharges where stringent synchronization or precise timing is required. This interest had led to new switching applications and concepts as well as new understanding of the switching process from a fundamental standpoint. The increasing diversity of wavelengths available has necessitated a modification of the generally accepted laser-initiated breakdown mechanism. Advances in high time resolution diagnostics techniques have as well allowed a deeper insight into heretofore conjectured mechanisms.

New understanding in optically controlled discharges and new applications since the last review (1977) will be addressed. These include the impact of short wavelength lasers, their application in opening switches including the potential of optogalvanic effects which are of particular significance in controlling diffuse discharges. One additional area of considerable promise is photoconductive switching using intrinsic solid state materials. There is no question but that the potential of optically controlled discharges is only beginning to be realized, primarily as a result of improvements in laser versatility and reliability, efficiency of interaction of the optical control energy (particularly in a resonant mode), demonstrated precise timing and synchronization capability to below a picosecond and improved understanding of the total switching event. Possibilities of optically controlled discharges not yet demonstrated will also be discussed.

Laser-Triggered Switches

Since the first report of laser-triggered switching in 1964 [1], numerous investigations on laser-initiated discharges have been performed. Laser triggering of high voltage switches employing various dielectric media is well established as a precision technique for initiating conduction. The advantageous features inherent to the laser-triggered discharge are [2]:

- Electrically uncoupled
- Suitable for remote operation
- Short and variable delay with low jitter
- Simple structure
- Reproducible, reliable, low maintenance
- RFI insensitive
- Suitable for repetitive operation
- Triggering of low voltage long gaps
- Suitable for multigap or multichannel operation
- Suitable for all types of dielectric or semi-conductor media

The mechanism of laser triggering of spark gaps can take several forms:

1. The passage of the laser through the gas or its interaction at an electrode or in the dielectric can lead to a reduced pressure region tending to enhance breakdown.
2. Radiation causes the emission of charged particles from an electrode (plasma

production at an electrode), producing results similar to those active in a trigger or avalanche/streamer breakdown.

3. A laser causes localized optical breakdown in the switch medium.
4. A laser causes volume ionization along its total path (e.g., along the interelectrode axis of the spark gap).

Let us consider some specifics of the more important mechanisms leading to low delay, low jitter operation.

Laser-Electrode Interaction

The most commonly used method to laser-trigger spark gaps is to focus the laser light onto the surface of one of the electrodes, resulting in the formation of a plasma on the electrode surface or e.g. the emission of electrons at the cathode. The optical development of such an initial breakdown process in a configuration where the cathode was irradiated by a Nd:YAG-laser with a power of several MW is shown in the paper by Dougal, Williams and Guenther [3] (Fig. 4) in these Proceedings. A streamer develops rapidly from the electrode plasma which bridges the gap along the entrant path of the laser and finally causes thermalization and breakdown of the gas. This is the moment at which a rapid rise of current is observed.

The time between laser irradiation and current rise, the delay time, is dependent on a multitude of parameters such as the percentage of self-breakdown voltage, electrode material, fill gas and pressure, laser type and laser power, etc. Fig. 1 shows the

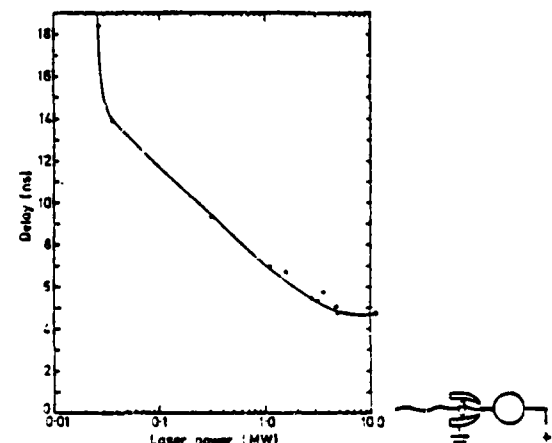


Fig. 1a. Delay vs laser power in 90% Ar-10% N<sub>2</sub>, stainless steel anode. Total laser duration 14-15 ns. The pulse width (FWHM) 5.6-6.3 ns.  $p=2925$  Torr.  $V_{SB}=42$  kV,  $V_{CH}=43.2$  kV [4].

delay versus laser power and, for the same experimental setup, jitter versus laser power. These experimental results obtained by Bettis and Guenther with a ruby laser in 1970 [4] demonstrate the excellent performance (jitter  $\sim 100$  psec) of laser triggering even at relatively low laser powers ( $\sim 40$  kW).

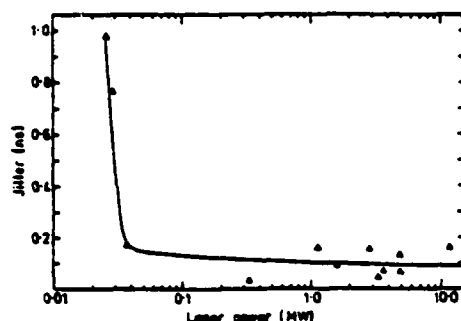


Fig. 1b. Jitter vs laser power in 90% Ar-10%  $N_2$ , stainless steel anode.  $p=2925$  Torr,  $V_{SB}=48$  kV,  $V_{CE}=43.2$  kV [4].

Subnanosecond jitter was observed employing laser powers of 10 kW by Schildbach and Basting [5] at a reduced voltage  $V/V_0$  close to unity. They obtained nanosecond delay and jitter at power levels as low as 2 kW. There, the corresponding energy of a 2 to 3 ns (FWHM) dye-laser pulse was 5  $\mu$ J. Triggering here was always initiated by plasma formation at the cathode.

Spark gap triggering was even obtained at power levels as low as 0.15 kW by Pinnekamp, Himmel, and Bergstedt [6]. Using frequency doubled Nd:YAG laser light, they investigated breakdown conditions in the sub-kW power range. As an initiation process, thermal emission of electrons was assumed. Yet, another model was proposed by Harsch, Salzmann, and Strohwald to explain the trigger effect at low power levels [7]. They performed measurements in the same power range as Pinnekamp et al. and concluded from their data that a two-photon process at the electrode was operative.

All the results discussed so far were obtained with visible, near-UV and near-IR lasers. A considerable amount of investigation has also been performed with  $CO_2$ -lasers at wavelengths of  $\sim 10$   $\mu$ m. Studies on the breakdown mechanism for  $CO_2$ -laser-triggered spark gaps where the laser is focused on an electrode seem to indicate that the ignition process is similar to that at shorter wavelengths. It is assumed that the electrode material is heated, evaporated, and partly ionized. Breakdown results from the development of an electron avalanche initiated in the products of surface evaporation [8]. Microscopic irregularities on the surface support this process [9].

In general, results of measurements with different lasers are not easily compared even though important parameters such as delay and jitter are usually determined in terms of output laser power. However, the important laser parameter seems to be the power density and caustic, a value which is due to different beam quality, the optics employed, and mode structure very difficult to measure.

#### Laser-Gas Interaction/Spark Discharge

The results of laser triggering which have been discussed so far were obtained with the laser radiation focused onto the electrodes. Another mode of spark triggering is based on generation of an optical breakdown in the gas, which initiates the spark breakdown. Investigations on laser midgap triggering were performed at Texas Tech University [3]. After the laser interaction in the center of the gap, a diffuse plasma is generated, which is stable for only a few tens of nanoseconds. After that time, instabilities occur at the electrodes and channels are formed which grow toward the center and bridge the gap. This trigger mechanism requires higher laser power than those previously discussed and is therefore not recommended.

#### Laser-Gas Interaction/Volume Discharge

A fundamentally different optically triggering mechanism has been used by Rapaport at Lawrence Livermore National Laboratory [10] and Woodworth, Frost, and Green at Sandia National Laboratories [11]. Instead of generating a point plasma at an electrode or in the gas, a volume ionization was achieved in the dielectric gas by use of an UV-laser. In the later case, a low divergence KrF excimer laser was used to trigger a 0.5 MV, pulse-charged switch in pure  $SF_6$ . The KrF beam was focused so that the focal point was between the switch electrodes along the interelectrode axis. With a total laser energy of 0.12 J, visible plasma channels stretching almost the entire length of the gap between the electrodes were generated. The dominant electron generation mechanism is obviously a multiphoton process. Four KrF photons are required to ionize  $SF_6$ .

The results as delay versus percentage of self-breakdown voltage are shown in Fig. 2. It is important to note that there is only a 0.5 ns difference in delay between 80 percent and 90 percent self-breakdown voltage, affording a low overall jitter in a multigap system where the % SBV or optically dimension and alignment may not be matched. The jitter for events above 70 percent of self-breakdown

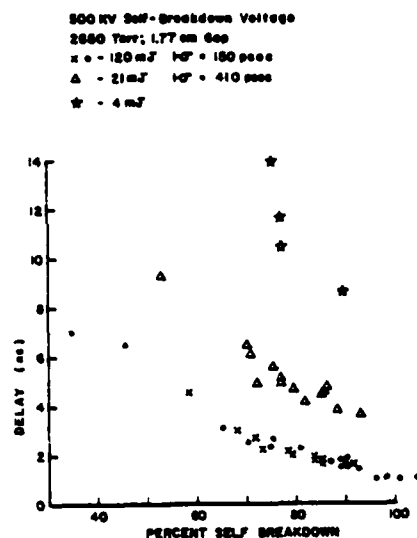


Fig. 2. Switch triggering results using uv laser-induced breakdown of pure  $SF_6$  with a low divergence KrF oscillator-amplifier used as the trigger source [11].

is  $\sim 150$  ps. The efficiency of the laser radiation can be enhanced by using a seed gas with low ionization potential [12] (trimethylamine [13], tripropylamine, fluorobenzene, triethylaniline), such that ionization involves at most a two-photon process compared to a four photon process in pure  $SF_6$ . In this case, much lower laser powers are required. These investigations were performed with the intention to trigger simultaneously 36 main gas switches, each of which must first hold off a pulsed voltage of  $\sim 2.7$  MV, then be triggered with a temporal jitter of less than a few nanoseconds.

The potential of laser triggered switching for repetitive multi switch operation was demonstrated in 1970 by Guenther et al [14]. With one laser four separate switches were triggered with subnanosecond synchronization. Guenther and Bettis [15] showed that it is even possible to generate two separate channels simultaneously in one spark gap system. In this experiment the laser beam was split geometrically



between two apertures and then focused on two opposite electrode elements. In experiments performed at Texas Tech University [16] similar results were obtained with the laser light fed through two optical fibers into the spark gap system, a method which allows a simple optical arrangement, eliminating many alignment considerations. Precise time delays may be added by introducing measured lengths of fiber.

#### Laser-Semiconductor Interaction

Laser triggering is not only used to generate breakdown in gas spark gaps, it has also been demonstrated in solid, liquid, and vacuum gaps [2]. One switch medium destined to become more important for pulsed power applications is the semiconductor. Ionization through carrier generation in the semiconductor is uniformly produced by single-photon photoionization; whereas in gases, volume ionization, even with UV lasers, generally is still a less efficient multiphoton process.

The advantages of optically controlled semiconductor switches compared to gas switches were recently summarized by Nunnally [17]:

- The energy required to produce a carrier pair is the band gap energy instead of the ionization energy.
- The total number of carriers required are produced simultaneously and uniformly between the electrodes, i.e., it follows the laser intensity.
- The spatial and temporal carrier density can be controlled externally during closure and conduction.
- Heat can be removed from the conducting medium in situ.
- Recovery or recombination of carrier pairs depends upon the photoconductive material and heat removal.
- The location of the conduction path can be distributed precisely to provide the minimum inductance.

Delay and jitter is expected to be in the ps regime, the achievable value being light-source limited. In addition, photoconductors are almost arbitrarily scalable.

The advantages of precisely controlled delay and low jitter were demonstrated by Austin [18] at Bell Telephone Laboratories. In his experiment employing mode-locked Nd-YAG lasers silicon devices were switched on and off on time scales of 10 ps. Several interesting experiments on laser-triggered semiconductor switches were performed recently by G. Mourou [19] and C. Lee [20]. Two experiments which demonstrate the advantages of optical semiconductor switching compared to gas spark gap switching will be discussed. The photoconductive switch consisted in both experiments [19] of a piece of high-resistivity semiconductor (usually GaAs or Si) inserted along the central conductor of a coaxial cable. The length of the crystal is typically a few mm.

In the first experiment switching was based only on the photogeneration of carriers in the semiconductor bulk by a picosecond laser pulse. Optical energy requirements are typically tens of microjoules to switch up to 10 kV into a 50  $\Omega$  load. The risetime is dictated by the laser pulse characteristics and the electrical circuit, while the maximum obtainable pulse length is dictated by the carrier recombination time, which ranges from ps to ns depending on the specific semiconductor material. A typical 1 kV output pulse is shown in Fig. 3. The observed risetime is 100 ps, and the pulse duration of 2 ns corresponds to the charge line length.

The switching efficiency of  $\sim 10$   $\mu\text{J}/\text{MW}$  in the experiment discussed can be increased by using avalanche effects in semiconductors. Laser triggering of avalanche transistors was studied at Lawrence Livermore National Laboratory by Thomas and Coleman [21]. By direct optical triggering of one avalanche

transistor in a series string of transistors nanosecond-rise kilovolt waveforms were generated, with time jitter being less than 100 ps. In a switch experiment performed by Mourou [19] the avalanche effect in the semiconductor bulk was utilized. The experimental setup is shown in Fig. 4. The GaAs sample was cooled down to 77 K, to reduce thermal breakdown at high electric fields. Switching was initiated by a deeply penetrating, 1.06  $\mu\text{m}$  light pulse. Through the creation of additionally charged carriers in the bulk of the sample, impact ionization was initiated which lead to an avalanche process. Light energies as low as 35 nJ were sufficient to trigger this process, corresponding to an efficiency of 0.5  $\mu\text{J}/\text{MW}$  at 77 K.

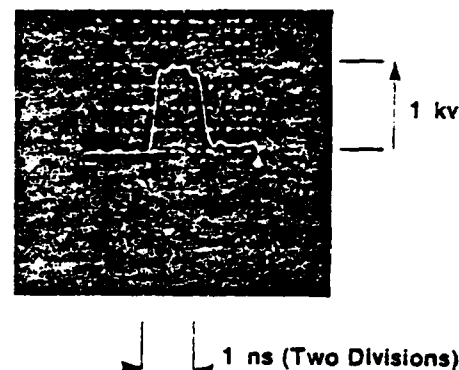


Fig. 3. A trace from a Thomson CSF TSN 660 oscilloscope. A DC bias voltage of 2 kV was used [19].

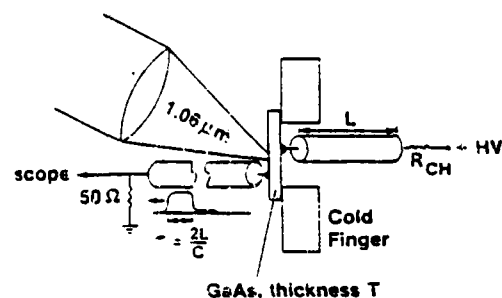


Fig. 4. Schematic of the arrangement. A cable of length  $L$ , charged through  $R_{CH}$ , is discharged through the cooled GaAs sample, which is triggered by the 1.06  $\mu\text{m}$  laser light. This produces a HV pulse of duration  $\tau = 2L/C$  [19].

In this experiment, the GaAs switch replaced the center conductor in a 50  $\Omega$  transmission line which also served as a charge line. Figure 5 exhibits the high voltage pulse switched from this device. The photoconductive contribution of the optical signal, triggering the avalanche, can be seen to the left of the pulse. Risetime of the pulse is  $\sim 1$  ns, with a delay of 1.5 ns and a jitter of 150 ps.

The two examples demonstrate the applicability of semiconductor switches in pulse power systems where high timing accuracy is required. The primary limitation of these switches is the burden placed on the laser and contact resistance, thermal heat sinking and low inductance connection. Critical research in this field is just beginning. Many semiconductor systems are increasing in the application to many pulse power systems.

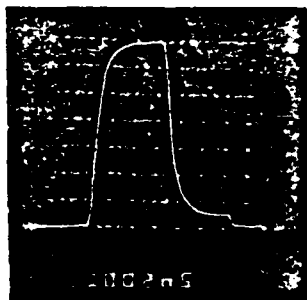


Fig. 5. A typical HV pulse switched through the GaAs spark gap. The photoconductive contribution is the small wiggle  $\sim 500$  ps before the foot of the main pulse [19].

#### LASER CONTROLLED DIFFUSE DISCHARGES

Diffuse discharges seem to offer a variety of advantages with respect to their applications in switching. One is that large area discharges offer an ease in impedance matching of a switch to a PFN, and through the low current density one will realize less erosion affording longer lifetime. On the other hand, large area diffuse discharges are unstable, and operation is generally possible for only short periods, depending, in the main, on the discharge parameters. Another aspect to be considered is that a diffuse discharge is a cold discharge, not in Local Thermodynamic Equilibrium, allowing one to influence individual transitions illuminating with a resonant frequency, thus controlling the subsequent density of states important in the generation or depletion of electrons.

As mentioned in the section on laser triggering, the increasing diversity, infact selectivity, of laser wavelengths has opened the possibilities of using other mechanisms for discharge control. For example, there are several processes that allow one to change the electrical properties along the total length of a path between the electrodes of a spark gap rather than just initiating the breakdown process in a limited volume element. Here the laser is acting on the gas in a spark gap clearly before LTE is reached; and, as such, the processes may be the same as employed in diffuse discharge switches. It is desirable to have the diffuse discharge remain relatively cold, so that the above mentioned possibility of influencing specific transitions is maintained, allowing one to control the closing and opening phase of discharge, i.e., to change the conductivity in either direction, as a closing or as an opening switch as first proposed by Guenther [12]. Normal or enhanced recovery of fast reprinted closing switches is an opening process and therefore will be discussed herein in that context.

The existence of optogalvanic effects has been known for a long time. Townsend [22] showed in 1902 that UV light emitted by a spark can initiate conductivity in gases when an applied voltage is present which is otherwise too low to maintain a discharge. Starting in the late twenties of this century, several very interesting papers appeared, showing that light at the wavelength corresponding to an optical transition will change the electric properties of the discharge. In an experiment by Pennings [23] for example, the light emitted by one Ne discharge was used to illuminate another Ne discharge.

It wasn't until the advent of lasers, particularly tunable lasers, that a veritable flood of papers on optogalvanic spectroscopy was seen (for an overview see [24]), principally initiated by those of Green et

al. [25] and Bridges [26]. In optogalvanic spectroscopy, a given laser wavelength can produce a specific response in a discharge; whereas for switching applications, the magnitude and direction of the response is the main objective. We will present an overview of these processes that have been considered as having potential as control mechanisms for switching and will also mention some recent results of research groups working in this area, either related to investigations of basic processes or to their application in switching devices or other related areas.

Before discussing the interaction of light with specific energy states, let us recall that the interaction of light with free electrons via Inverse Bremsstrahlung is considered to be the dominant process for IR optical breakdown in gases or the interaction of the laser with the propagating streamer in IR laser triggering. However, the total energy required makes it generally unsuitable for large volume discharges.

The interaction of light with specific energy states can be used to increase or to decrease the conductivity by controlling either the electron generation or depletion. Optically increased conductivity can be accomplished by photoionization or excitation with collisional assistance or by photodetachment, which may be considered as an electron generation process if negative ions are present or as an elimination of electron losses via attachment. Optically decreased conductivity can be accomplished by optical quenching of excited states or by optically enhanced attachment.

Let us discuss the following optically controlled processes which can be used to increase the conductivity:

(1) Single photon ionization does not in fact require any wavelength tuning above some energy threshold. Most TEA lasers employing UV preionization with spark radiation sources use this process [27]. The efficiency of UV ionization can be drastically increased using gas additives with low lying ionization levels [28]. Spark UV sources can also be used to operate a discharge below the glow voltage, sustained entirely by photoionization [29].

Considering that commonly available lasers produce photons up to energies of approximately 7 eV efficiently, only a few gases, like alkali vapors, are suitable for direct photoionization using lasers [30] but gases can be seeded with easily ionized impurities.

(2) Resonant two-step photoionization (Fig. 6a) appears to be a more efficient way to generate electron-ion pairs. Consider that UV excimer lasers have produced significant electron densities in several organic molecules [31]. For example, in trimethylamine, Lee and Bischel [13] produced an electron density of  $10^{15}/\text{cm}^3$  with a 10 ns, KrF laser at 248 nm over a 2  $\text{cm}^2$  cross section area. As previously noted, the UV laser triggering of gas filled gaps with organic additives at Sandia National Laboratories uses

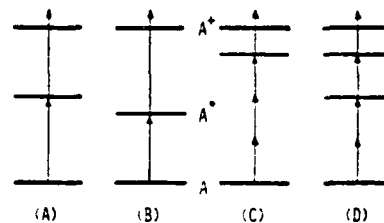


Fig. 6. Multiphoton ionization processes: (a) Resonant two-photon process (one wave-length); (b) Resonant two-photon process (two wave-lengths); (c) Resonant enhanced four-photon process; (d) Doubly enhanced four-photon process.

this process [11]. Also long plasma channels exceeding 1 m length have been generated with different organic additives in a buffer gas [32].

A diatomic molecule suggested for efficient resonant two step photoionization with narrow bandwidth lasers is NO [33]. John Moseley et al. at the University of Oregon [34] proposed to use the radiation from a KrF laser, Anti-Stokes Raman shifted in  $H_2$ , to operate in the spectral region of X-A transitions. The un-converted fraction of the KrF laser can then be used to provide the second photon to produce ionization from the A-state.

Resonant two step photoionization at different wavelengths in Cesium (Fig. 6b) is now being used at Sandia to provide large volume ionization in an ionization front accelerator [35].

(3) Multiphoton ionization will in general involve one or more nonresonant steps and the subsequent ionization rate will depend strongly on the intensity of the laser beam. Thus, it is not an efficient mechanism to produce large volume ionization. However, it may be a suitable mechanism for laser triggering acting either on the electrode or in the gas. Williams [36] used four-photon ionization in Xe involving one resonant step (Fig. 6c). With a pulse energy of approximately 300 nJ he could produce more than  $10^{10}$  electron-ion pairs in a volume of approximately  $10^{-5} \text{ cm}^3$ .

Some molecules allow a double enhancement of multiphoton ionization. In NO a transition from the ground state to the (A)-state requires twice the energy of the transition from the (A)-state to a higher lying Rydberg state, and this same energy is sufficient to ionize NO in a subsequent step. This is a doubly resonant enhanced four-photon transition with only one nonresonant step (s. Fig. 6d), requiring a wavelength of approximately 450 nm [37].

(4) Photoexcitation and subsequent collisional ionization has already been used by Green and co-workers in laser enhanced ionization spectroscopy [38]. Photoexcitation, in most cases starting from an excited state with subsequent collisional ionization is the key process in optogalvanic spectroscopy.

Another mechanism, laser resonance pumping [37] has been demonstrated in several alkali vapors. In this case if the absorption of a resonant transition is saturated, then the density of the resonance state is nearly the same as that of the ground state. Here the probability for an electron to collide with an excited atom is very high; and through super elastic collisions, the electrons can gain enough energy to ionize the gas. Ionization by laser resonance pumping is now being investigated at Sandia National Laboratories to produce large volume ionization for a high purity lithium ion source for one of their particle beam fusion accelerators [38].

(5) Photoionization from collisionally excited states can result in a large effect in systems with high densities of excited species or in systems where the rate into such an intermediate state is large. For example, in mercury high densities of metastables in the  $6^3P_0$  state can be produced.

(6) Photodetachment is one way to overcome attachment in a well defined switch period or in specific areas of a discharge. As such, photodetachment may be an important mechanism in UV laser triggering of SF<sub>6</sub> filled gaps [39].

In the case of diffuse discharge opening switches, attachers must be used to achieve fast opening [40]. However, during the conduction phase photodetachment may be used to eliminate electron losses via attachment. In experiments at Texas Tech University [41] in  $O_2$ -discharges and flowing afterglows, it was shown that strong optogalvanic signals can arise from photodetachment of  $O^-$ . For an energy flux of  $35 \text{ mJ/cm}^2$ , 30% of the  $O^-$  ions could be photodetached. An advantage of photodetachment is that it

is a nonresonant process and therefore it can easily be combined with other optical control mechanisms [42].

(7) Quenching of metastable atoms or molecules (Fig. 7) may also be a suitable mechanism to control the conduction of a discharge particularly if the electron generation, dominated by two-step ionization via metastables, can be controlled. In addition,

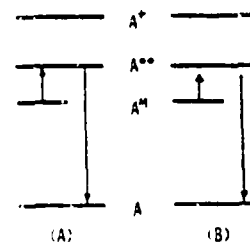


Fig. 7. Quenching of metastables: (a) Resonant and (b) Anti-Stokes Raman process.

the recovery of a gas, following a discharge pulse, can be affected if long living excited species dominate the recovery phase.

Quenching as used here describes the dissipation of energy deposited in metastables in the discharge by exciting a higher lying level which is optically connected to the ground state (Fig. 7). If this resonance radiation can escape the discharge vessel, the energy will not even contribute to heating of the ambient gas.

Lavler at the University of Wisconsin is studying the role of metastables in rare gas discharges and the effects caused by changing the metastable density [43]. A paper at this Conference [44] describes the specific role of metastables in the cathode fall region. It is shown that metastable atom bombardment is an important mechanism controlling electron emission from the surface of cold cathodes. Thus, a decrease of the metastable density in front of the cathode will decrease the electron emission rate. This effect is amplified by the fact that each electron, emitted from the cathode, gains enough energy in the cathode fall to produce several additional electrons through ionization.

Gundersen and his group at the University of Southern California are looking at the role of molecular metastable species in the operation of hydrogen thyristors and other applications [45], including the possibility of using Anti Stokes Raman Scattering as a quenching mechanism (Fig. 7b). Although this process has the disadvantage of being a non resonant process it has the advantage that the same frequency can be used when quenching different rotational states of a metastable molecule. An important aspect of their work is a determination of the dependence of the metastable lifetime on the intensity and frequency of the incident optical radiation.

The last group of processes to be discussed relates to optically enhanced attachment [46]. Certain attachers have an increased attachment cross section in their rotational and/or vibrational excited states. The mechanism can be understood by considering the potential energy curves of a diatomic molecular attacher and its negative ion. In Fig. 8, a general type of dissociative electron attachment process is illustrated. The potential energy curve of a neutral diatomic molecule AB is crossed at an energy  $E^*$  above the ground state by a repulsive branch of the negative ion  $AB^-$ . The probability of electron attachment and succeeding dissociation depends principally on the energetic state of the vibrationally excited molecule relative to the curve crossing. For the example shown, the attachment cross section

increases with vibrational excitation up to  $v = 4$ . On the other hand, the electron energy necessary to form the negative ion  $AB^-$  shifts to small values if the molecule  $AB$  is excited into a vibrational state closer to the curve crossing.

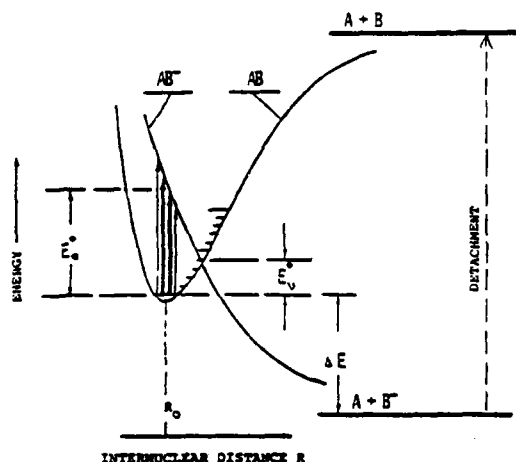


Fig. 8. Resonance associative electron attachment.

As yet, there are no known measurements of attachment cross sections for individual vibrational states. However, Bardsley et al. [47] have deduced the cross section for the vibrational states ( $v = 0 - 3$ ) of HCl (see Fig. 6 in the paper by Schoenbach and Kristiansen [49] in these Proceedings) from cross section measurements at different gas temperatures by Allan and Wong [48]. These data show that the attachment rate can drastically be increased using vibrational excitation, but this advantage disappears in HCl if the electron energy is larger 0.5 eV.

There are many ways to optically populate vibrational states. The first experiment performed using laser excitation to increase the attachment rate was done in  $SF_6$  by Chen and Chantry [50]. Figure 9 shows the cross section for dissociative electron attachment in producing  $SF_3$ ; (e) the curve without laser at 390°K, (d) with a CW  $CO_2$  laser (8W over 0.3 mm<sup>2</sup>), and (f) the laser produced change in the cross section. That this experiment was S-isotope specific, as seen from the laser wavelength dependence, indicates that the laser does not just result in a general gas heating. Recently, similar experiments have been performed in France by Barbe, Astruc, Lagreze, and Schermann using the valence electrons of Rydberg Ar-atoms instead of free electrons [51].

Another possibility for producing highly excited vibrational states is to employ transitions from electronically excited states, either radiative, or through collisions. Such a process has recently been used by Beterov and Fatayev [52] to show that vibrational excitation of  $I_2$  can increase the cross section for dissociative attachment. Figure 10 depicts the excitation mechanism. The radiation from a frequency doubled Nd:YAG ( $\lambda = 532$  nm) was used to excite the  $B^3\Pi(0_u^+)$  state. Intense Stokes fluorescence indicated a subsequent transition into highly vibrational excited states of the electronic ground state. Vibrational relaxation had to provide the population of the optimum vibrational states resulting in an increase of the attachment rate by three or four orders of magnitude.

It is appropriate to finish with some remarks concerning optically controlled discharge modeling. Assume a given device, and one wants to employ optical control processes to improve its performance, at first glance, one immediately notes a large number of transitions that will probably influence the discharge

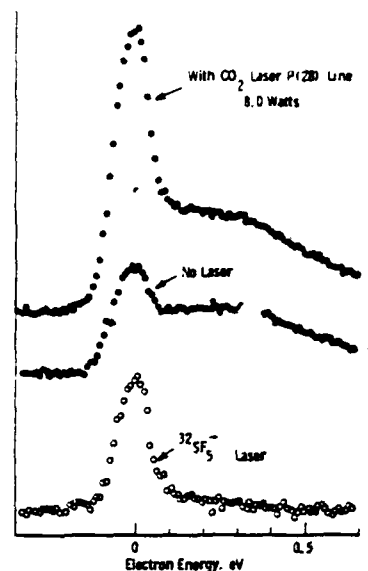


Fig. 9. An example of data showing photo-enhancement of the cross section for the production of  $SF_3$  from  $SF_6$  (From Chen and Chantry [20]).

to some degree in the direction you desire. To decide which transitions are the most effective, you must know the dynamics of the excited states, ions, and

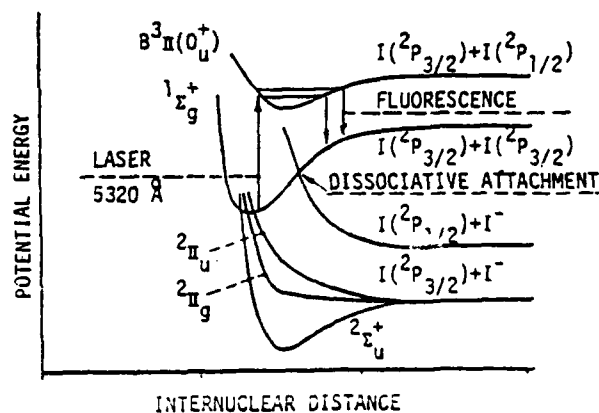


Fig. 10. Some potential curves for  $I_2$  and  $I_3$  and the scheme of excitation of vibrational levels (From Beterov and Fatayev [52]).

electrons involved in the gas discharge. In general, it is not difficult to design a computer code that allows such calculations; but you have to feed it, primarily, with the rate constants of all the processes that are important in determining the ultimate behavior of the discharge. Most of the rate constants are at least  $E/N$  dependent, and the applied field may be changing drastically in time. So one goes to those sources who provide us with the basic data we need.

Additionally, the field strength is strongly influenced by the circuit parameters. In this situation, the efficient use of the available photons requires a very basic understanding of all the processes in the gas discharge as well as an understanding of the interaction of discharge and the circuit. Unfortunately, in a different gas the discharge may be determined by a completely different set of processes, and one must, of necessity start all over again. So it is not surprising that every group

working on specific optogalvanic effects in certain gas mixtures does its own modeling.

But an incomplete or even worse an inapplicable model is not as good as an appropriate measurement. What we need are measurements on the requisite excited states, which are enhancing our ability to model with confidence difficult circuit features such as the time dependent behavior of gas discharge switches in real circuits.

In conclusion we would like to thank many of the cited researchers for providing us with their recent and frequently unpublished results, in most cases with much more detail than we could present here.

### References

- [1] A. H. Guenther, presented to the Am. Nuc. Soc. April 1964, and W. H. Pendleton and A. H. Guenther, *Rev. Sci. Instrum.* vol. 36, pp. 1546, 1965.
- [2] A. H. Guenther and J. R. Bettis, *J. Phys. D: Appl. Phys.*, vol. 11, pp. 1577, 1978.
- [3] R. A. Dougal, P. F. Williams and A. H. Guenther, *Proc. 4th IEEE Int. Pulsed Power Conf. Albuquerque, N.M.*, June 1983.
- [4] J. R. Bettis and A. H. Guenther, *IEEE J. Quantum Electron.*, vol. QE-6, pp. 483, 1970.
- [5] K. Schildbach and D. Basting, *Rev. Sci. Instrum.*, vol. 45, pp. 1015, 1974.
- [6] F. Pinnekamp, G. Himmel and K. Bergstedt, *Optics Comm.* vol. 11, pp. 225, 1974.
- [7] K. Harsch, H. Salzmann and H. Strohwal, *Phys. Lett.* vol. 55A, pp. 153, 1975.
- [8] E. V. Daschikov, V. A. Dymstakov, F. V. Lebedev and A. V. Ryazanov, *Sov. J. Quantum Electron.* vol. 12, pp. 62, 1982.
- [9] A. S. Kovalev and A. N. Popov, *Sov. Phys. Tech. Phys.*, vol. 25, pp. 196, 1980.
- [10] W. R. Rapaport, J. Goldhar, J. R. Murray, *IEEE Trans. Plasma Science*, vol. PS-8, pp. 167, 1980.
- [11] J. R. Woodworth, C. A. Frost and T. F. Green, *J. Appl. Phys.*, vol. 53, pp. 4734, 1982.
- [12] A. H. Guenther, *Proc. ARO Workshop on Repetitive Opening Switches*, pp. 48-64, Tamarron, CO. Jan. 1981. M. Kristiansen and K. H. Schoenbach, eds.
- [13] L. C. Lee and W. K. Bischel, *J. Appl. Phys.*, vol. 53, pp. 203, 1982.
- [14] A. H. Guenther, J. R. Bettis, R. E. Anderson, and R. V. Wick, *IEEE J. Quantum Electron.*, vol. QE-6, pp. 492-495, 1970.
- [15] A. H. Guenther and J. R. Bettis, *Laser Interaction and Related Plasma Phenomena* (New York: Plenum Press) pp. 131-171, 1971.
- [16] H. C. Harjes, E. E. Kunhardt, M. Kristiansen, L. L. Hatfield and A. H. Guenther, *IEEE Trans. Plasma Science*, vol. PS-10, pp. 261, 1982.
- [17] W. C. Nunnally, *Proc. 4th IEEE Int. Pulsed Power Conf. Albuquerque, N.M.*, June 1983.
- [18] D. H. Auston, *Appl. Phys. Lett.* vol. 2b, pp. 101, 1975.
- [19] G. Mourou, *Proc. ARO Workshop on Solid State Switches for Pulsed Power*, Tamarron, Co, 1983, pp. 114, W. M. Portnoy and M. Kristiansen, eds.
- [20] C. H. Lee, *Proc. ARO Workshop on Solid State Switches for Pulsed Power*, Tamarron, Co., 1983, pp. 160, W. M. Portnoy and M. Kristiansen, eds.
- [21] S. W. Thomas and L. W. Coleman, *Appl. Phys. Lett.*, vol. 20, pp. 83-84, 1972.
- [22] J. S. Townsend, *Phil. Mag.*, vol. 3, pp. 557-576, 1902.
- [23] F. M. Penning, *Physica*, vol. 8, pp. 137-140, 1938.
- [24] J. E. M. Goldsmith and V. E. Lawler, *Contemp. Phys.* vol. 22, pp. 235-243, 1981.
- [25] R. B. Green, R. A. Keller, G. G. Luther, P. K. Schenck, and V. C. Travis, *Appl. Phys. Lett.*, vol. 29, pp. 727-729, Dec. 1976.
- [26] W. B. Bridges, *V. Opt. Soc. Am.*, vol. 68, pp. 352-360, 1978.
- [27] H. Seguin and J. Tulip, *Appl. Phys. Lett.*, vol. 21, pp. 414-415, 1972.
- [28] J. S. Levine and A. Javan, *Appl. Phys. Lett.*, vol. 22, pp. 55-57, 1973.
- [29] A. Javan and J. S. Levine, *IEEE J. Quantum Electron.*, vol. QE-8, pp. 827-832, Nov. 1972.
- [30] F. L. Mohler, P. D. Foote, and R. L. Chenault, *Phys. Rev.*, vol. 27, pp. 37-50, 1926.
- [31] M. Seaver, J. W. Hudgens, and J. J. Decoro, *Int. J. Mass Spectrom. Ion Phys.*, vol. 34, pp. 159-173, 1980.
- [32] C. A. Frost, J. R. Woodworth, J. N. Olsen and T. A. Green, *Appl. Phys. Lett.*, vol. 41, pp. 813-815, 1982.
- [33] R. V. Hodges, L. C. Lee and J. T. Moseley, *Int. J. Mass Spectrom. Ion Phys.*, vol. 39, pp. 133-143, 1981.
- [34] J. T. Moseley, private communication.
- [35] C. L. Olson, J. R. Woodworth, C. A. Frost, and R. A. Gerger, *IEEE Trans. Nucl. Sci.*, vol. NS-28, pp. 3349-3351, 1981.
- [36] S. Dhall and P. F. Williams, *Proc. 3rd IEEE Int. Pulsed Power Conf.*, Albuquerque, NM, 1981, pp. 151-153.
- [37] R. M. Measures, *J. Quant. Spectrosc. Radiat. Transfer.*, vol. 10, pp. 107-125, 1970.
- [38] J. P. Vandevender, J. M. Hoffman, G. S. Mills, and E. W. Mendel, *Comments Plasma Phys. Controlled Fusion*, vol. 7, pp. 107-214, 1983.
- [39] A. Chutjan, *Boulder Meeting of the APS*, May 1983.
- [40] *Proc. ARO Workshop Repetitive Opening Switches*, Tamarron, CO., 1981. M. Kristiansen and K. H. Schoenbach, eds.
- [41] G. Schaefer, P. F. Williams, K. H. Schoenbach, and J. T. Moseley, *IEEE Trans. Plasma Sci.*, (accepted for publication).
- [42] G. Schaefer, K. H. Schoenbach, P. Tran, J. Wang, and A. H. Guenther, *Proc. 4th IEEE Int. Pulsed Power Conf. Albuquerque, NM*, 1983.
- [43] J. E. Lawler and A. H. Guenther, *Proc. 3rd IEEE Int. Pulsed Power Conf.*, Albuquerque, NM, 1981, pp. 147-150.
- [44] J. E. Lawler and D. Doughty, *Proc. 4th IEEE Int. Pulsed Power Conf. Albuquerque, NM*, 1983.
- [45] M. Gundersen, *Appl. Opt.*, vol. 21, no. 8, pp. 1486-1489, 1982.
- [46] K. H. Schoenbach, G. Schaefer, M. Kristiansen, L. L. Hatfield, and A. H. Guenther, *IEEE Trans. Plasma Sci.*, vol. PS-10, no. 4, pp. 246-251, 1982.
- [47] J. N. Bardsley and J. M. Wadehra, private communication.
- [48] M. Allan and S. F. Wong, *J. Chem. Phys.*, vol. 74, pp. 1687-1691, 1981.
- [49] K. H. Schoenbach and M. Kristiansen, *Proc. 4th IEEE Int. Pulsed Power Conf.*, Albuquerque, NM, 1983.
- [50] C. L. Chen and P. V. Chantry, *J. Chem. Phys.*, vol. 10, pp. 3897-3907, 1979.
- [51] R. Barbe, J.-P. Astruc, A. Lagreze, and J.-P. Schermann, *Laser Chem.*, vol. 1, pp. 17-36, 1982.
- [52] I. M. Beterov and N. V. Fateyev, *Opt. Comm.*, vol. 40, pp. 425-429, 1982.

This work was supported by AFOSR and ARO.

A MULTI-SPARK PREIONIZATION SOURCE FOR DIFFUSE DISCHARGES CONTAINING ATTACHERS\*

R. Cooper, G. Hutcheson,  
M. Kristiansen, G. Schaefer, K.H. Schoenbach  
Department of Electrical Engineering  
Texas Tech University  
Lubbock, Texas 79409 USA  
and  
A.H. Guenther  
Air Force Weapons Laboratory  
Kirtland Air Force Base, New Mexico 87117 USA

Abstract

Diffuse discharge opening switches usually operate with gas mixtures containing attachers when short opening times are desired. For arc free discharge initiation, a preionization source should produce a sufficient electron density at the time when the voltage rises across the discharge. Therefore, a preionizer must have 1) a short rise and fall time, 2) sufficient power, and 3) a sufficiently precise timing system to synchronize preionization and main discharge.

A device to generally fulfill these requirements is described. The energy for the preionization source is stored in eight individual coax cables and switched with one master gap into eight cables that are terminated by individual multi-spark gaps arrays. The gap for the main discharge and the master gap for the preionizer are triggered by a single laser using a beam splitter. The optical delay of the light pulse controls the synchronization. Experiments showing delay, preionization pulse length, and jitter are presented.

Introduction

Externally controlled diffuse discharges have been considered to be promising candidates for the realization of fast rep-rated opening switches [1,2]. Opening means a decrease in the switch conductivity and is in general only determined by a decrease in the electron density. Since recombination at electron densities of  $n_e \approx 10^{14} \text{ cm}^{-3}$  is too slow, an attacher can be used [2]. To avoid high losses in the switch the attacher should not be effective to any substantial degree in the conduction phase. One possibility would be to use attachment as a control mechanism e.g. optically induced attachment or photodetachment [2,3]. For all other control mechanisms however the attacher should exhibit the following conditions [1].

- (a) low attachment rate coefficient  $k_{\text{attach}}$  at low values of  $E/N$ .
- (b) high attachment rate coefficient  $k_{\text{attach}}$  at high values of  $E/N$ .

These requirements do not necessarily mean that the derivative  $d(k_{\text{attach}})/d(E/N)$  is positive under steady state operating conditions of a discharge. This situation has been known to cause instabilities [4]. However, any switching process and the initiation of the discharge itself will always cause a transition through such an unstable state. Therefore any gas discharge device used for this opening application has to permit very fast transitions through this state to avoid arcing [5]. For a self sustained discharge therefore the preionization has to be optimized with respect to several parameters:

- (1) preionization power
- (2) preionization pulse length
- (3) preionization rise and fall times
- (4) preionization timing with respect to the applied discharge voltage
- (5) proper illumination of the gap

This paper describes a UV preionizer capable of achieving the objectives aforementioned.

Requirements

The investigation and optimization of an efficient UV preionization system for gases containing attachers, requires one to consider the following processes and their time constants.

- (1) Photoionization  
In UV preionization, the dominant process will be one step photoionization and as such the electron generation rate will, to a first approximation, be proportional to the preionization intensity.
- (2) Attachment  
In attaching gases, electron depletion is dominated by attachment, thus for a constant electron generation rate the steady state electron density will depend solely on the attachment rate. For an attaching species with an attachment rate coefficient dependent on  $E/N$  as mentioned previously, the rate will be low before the voltage is applied, rise drastically when the voltage reaches its maximum value, and decrease again when the voltage drops as the conductivity increases.
- (3) Collisional Detachment  
It has been pointed out by several researchers that negative ions may serve as a reservoir of electrons for the initiation of diffuse discharges, since cross sections for collisional detachment have, in general, much lower threshold levels than those for ionization. This may only be effective if the negative ion density reaches a value nearly the same order of magnitude as the electron density in the steady state discharge.
- (4) Recombination  
Ion-ion recombination has relatively large cross sections. During the period of preionization in gases containing allading species the negative and positive ion density will increase and thus the negative ion lifetime will decrease and limit the negative ion density.

The effect of the above processes on the efficiency of the preionization system is demonstrated in Fig. 1. During a short preionization pulse (short compared to the time constant of attachment) the electron density rises nearly linearly with time while the negative ion density remain small compared to the electron density. After the preionization pulse, the electron

\* This work is supported by AFOSR

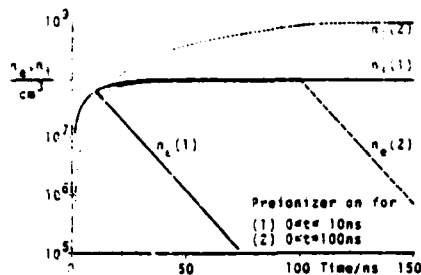


Fig. 1 Time dependent electron - and negative ion density, calculated for:

$$R_{\text{prei.}} = 10^4 \text{ cm}^{-3} \text{ S}^{-1}$$

$$N_{\text{attach}} k_{\text{attach}} = 10^8 \text{ S}^{-1}$$

$$k_{\text{ion rec.}} = 10^6 \text{ cm}^3 \text{ S}^{-1}$$

for two different preionization pulse length

density decrease while the negative ion density increases as long as attachment is significant.

For a long preionization pulse (long compared to the time constant for attachment) the electron density reaches a steady state value while the negative ion density increases still further. The maximum electron density will depend linearly on the power of the preionizer. Depending upon the value of the cross section for ion-ion recombination, the ion density may also reach a steady state value.

From these general considerations it becomes obvious that a preionization only be used efficiently for a time  $T_1$  (if only electron generation is considered) or for a time  $T_2$  if in addition the production of a reservoir of negative ions is thought to be beneficial. In general it is expected that the electron density is of principal import and, therefore the preionization pulse should not terminate before the voltage is applied across the discharge region.

The optimum preionization time ( $T_1$  or  $T_2$ ) depend strongly on the attaching species used and its concentration. A preionization system should therefore allow for adjustment of the following parameters

- (1) preionization power
- (2) preionization pulse length
- (3) rise and fall time to allow for the generation of short pulses
- (4) precise adjustable timing with respect to the main discharge
- (5) uniform preionization of the discharge volume

#### Design and Construction

It was decided to use a multi spark UV preionization source [6] since UV rich sparks are fairly easy to produce and gas degradation is of minor importance in these low rep rate systems with moderate gas exchange requirements. Coaxial cables were chosen as energy storage elements to drive the spark sources, thus allowing the device to produce rectangular pulses with fast rise and fall times. Eight multi-spark sources were connected to eight coaxial transmission lines. Eight similar lines act as charging lines and were switched by an impedance matched master spark gap (Fig. 2). The design of the laser pulses was 13.5 ns and charging line length of the preionizer was 2 m (see Fig. 4), thus the delay

between preionization and main system firing is 45 ns. Fig. 5 presents the traces of four consecutive events showing that the jitter in this case was of the order of 1 ns or less. The oscilloscope was

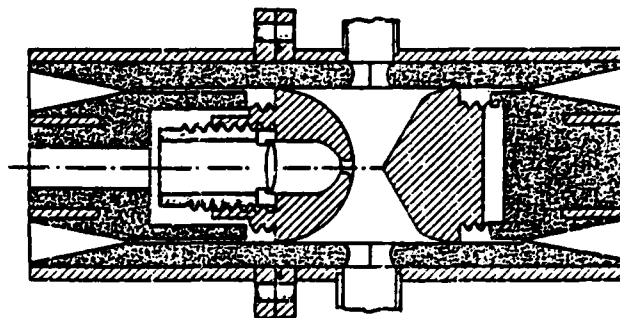


Fig. 2 Preionization Spark Gap Design

design of the switch allows one to change the charging lines and thus vary the pulse length of the preionization pulse. The cables used had an impedance of 75  $\Omega$  and were rated at 30 kV dc (Belden 8870). This made the total system impedance 9.3  $\Omega$ , with a capacitance of 240 pF per meter of charging line for eight cables. The energy stored was 0.05 Joules per meter at 20 kV or 0.8 Joules per meter at 30 kV. Both spark gaps, i.e. the gap used to switch the main discharge and the master gap for the preionizer, are laser-triggered gaps [7]. One laser and a beam splitter was used, and the delay between preionization and discharge initiation adjusted by changing the optical path length for the beam that triggers the main discharge.

The design of the two laser triggered gaps is in principle the same. The design of the master gap for the preionization source shown in Fig. 2. The laser beam is entrant into the gap axially through an aperture in one electrode. The other electrode in each gap is conical with a rounded tip. This shape ensures that the laser strikes the highest field point, and that laser triggered breakdown starts in the same region on the conical electrode where self breakdown occurs. This shape ensures that the gap can be laser triggered with minimum jitter in a voltage region close to self break.

The eight individual spark sources at the ends of the eight transmission lines allow for location of the preionization sources in the discharge chamber at different position. For our experiments we intend to investigate preionization through a screen electrode as well as using a side-on configuration. In the present device the discharge is cylindrical and the spark sources are arranged in a radially symmetric pattern to meet the requirement for a uniform illumination of the discharge region. The individual multi spark sources were designed as shown in Fig. 3.

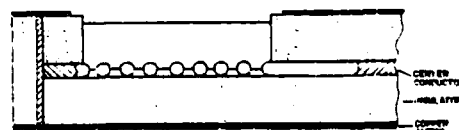


Fig. 3 UV Preionizer Design

The coaxial geometry was maintained through but as closely as possible. Eight sparks are distributed over a length of approximately 2 cm by using ball bearings as intermediate electrodes between the first and the last electrode. The individual gaps are highly overvolted so that they add little jitter to the system.

### Results

In the first series of test experiments the light emitted from the multi spark sources, when operated in air, was monitored with a vacuum photodiode (Hamamatsu #R1328U) shown schematically in Fig. 4. The upper trace indicates the time dependent

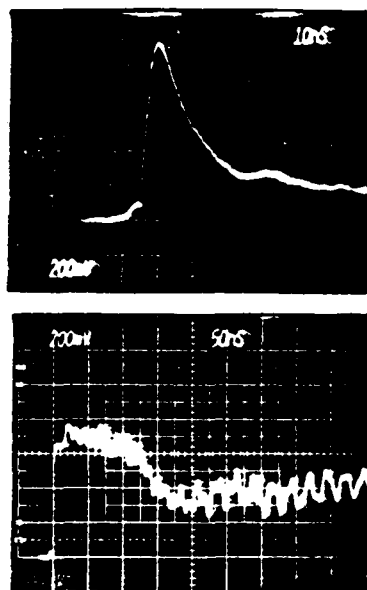


Fig. 4 Light Emission from UV Preionizer. Charging cable length 2 m (top), 10 m (bottom)

light emission for a charging line length of 2m while the lower trace is for a line length of 10m. The charging voltage in both cases was 20 kV. The light pulse has a risetime of less than 5 ns and the pulse length clearly is adjusted by using different length for the charging cables. The rise time was found to be relatively independent of the charging voltage as long as the spark arrays were overvolted by at least 10% however with the longer cables the effect of the reflected electrical waves became much more pronounced. It should be pointed out that illuminating the photodiode with all eight multi-spark sources simultaneously did not change the monitored pulse shape or length. If a fast falltime is desired, it is necessary to accurately terminate the cables.

In a second set of experiments the timing characteristics of the system were tested. Both preionization and main line gaps were laser triggered, the main line being terminated with a matching resistor. The light from the preionization source and the voltage across the matching resistor were monitored using the same oscilloscope (see Fig. 5). Here the optical delay length between the two laser pulses was 13.5 m and charging line length of the preionizer was 2 mm (see Fig. 4), thus the delay between preionization and main system firing is ~ 45 ns. Fig. 5 presents the traces of four consecutive events showing that the jitter in this case was of

the order of 1 ns or less. The oscilloscope was triggered by a current probe in the preionizer transmission line, showing the optimum timing of this system. It should be pointed out, however, that we used very high power laser pulses (Ruby laser, pulse energy = 0.1 J per gap, pulse length = 50 ns). Although the laser pulse was focused at a point

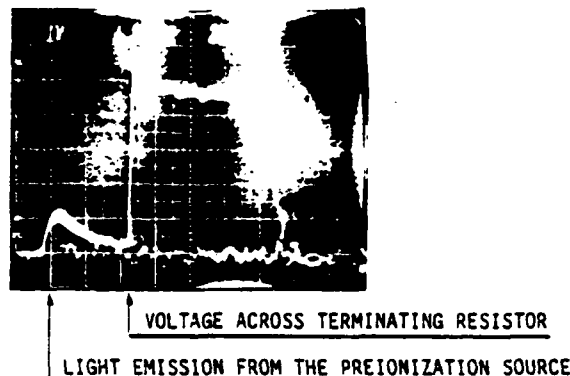


Fig. 5 UV Preionizer Timing (4 shots)

1-2 mm in front of the surface the opposite electrode, the laser tended to drill holes into the electrode surface. After several hundred shots without moving the focus on the electrode surface, the jitter increased markedly up to approximately 10-20 ns.

At the present time diffuse discharge experiments are being performed at atmosphere pressure in gas mixtures containing attaching species.

### Acknowledgments

The authors would like to thank George Ferguson and Leo Thurmond, without whose efforts and technical advice the work presented here would not have been possible.

### References

- [1] Proc. ARO Workshop on Repetitive Opening Switches, Tamarron, CO (1981).
- [2] Proc. ARO Workshop on Diffuse Discharge Opening Switches, Tamarron, CO (1982).
- [3] K. H. Schoenbach, G. Schaefer, M. Kristiansen, L.L. Hatfield, and A.H. Guenther, "Concepts for Optical Control of Diffuse Discharge Opening Switches, IEEE Trans. on Plasma Sci. vol. PS-10, 246, 1982.
- [4] D.H. Douglas-Hamilton and S.A. Mani, "Attachment Instability in a Externally Ionized Discharge", J. Appl. Phys., vol. 45, 4406, Oct. 1974.
- [5] G. Schaefer, K.H. Schoenbach, P. Tran, and J.-S. Wang, "Computer Calculations of the Time Dependent Behavior of Diffuse Discharge Switches", Proceedings of the 3rd IEEE Pulsed Power Conference, Albuquerque, NM, June 1983.
- [6] H. Sequin and J. Tulip, "Photoinitiated and photosustained laser," Appl. Phys. Lett., vol. 21, 414-415, 1972.
- [7] A.H. Guenther and J.R. Bettis, "The laser triggering of high voltage switches", J. Phys. D: Appl. Phys., vol. 11, 1577-1613, 1978.
- [8] C.L.M. Ireland, "A Multichannel Laser Triggered Spark Gap with Subnanosecond Risetime for Electro-optic Switching", J. Phys. E: Sci. Instr. vol. 8, 1007.



## Appendix V

The Use of Attachers in Electron Beam Sustained  
Discharge Switches - Theoretical Considerations

G. Schaefer, K.H. Schoenbach, H.Krompholz, M. Kristiansen  
Texas Tech University  
Lubbock, TX 79409

and

A.E. Guenther  
AFWL, Kirtland AFB  
Albuquerque, NM 87117

Abstract:

Electron-beam sustained discharges can be used in opening and closing switch applications for producing bursts of energy in pulsed power systems. The incorporations of admixtures of attachers with low attachment rate at low values of  $E/N$  and high attachment rate at high values of  $E/N$  in the gaseous switch dielectric has been proposed to achieve low forward voltage drop in the conduction phase as well as rapid opening when the sustaining e-beam is terminated. This paper presents model calculations on the characteristics and transient behavior of an electron-beam sustained discharge in the high current density regime in  $N_2$ . The influence of an attacher ( $N_2O$ ), with the property described above, and of the circuit parameters on the discharge is investigated as an illustrative example. The advantage of using such an attacher is demonstrated for the steady state conduction phases and for the opening phase, while the closing process is obstructed by the attacher. Additional possible control mechanisms, such as photodetachment to aid the closing process are discussed.

## I. INTRODUCTION

Inductive energy storage is attractive in pulsed power applications because of its intrinsic high energy density. The effective use of inductive storage, however, requires a rapid opening switch. Externally controlled diffuse discharges seem to offer the opportunity for fast as well as repetitive opening switching [1,2]. Diffuse discharges are advantageous for switching because of their low inductance [3], small electrode erosion and heating rates, and moderate energy density which offers the possibility of external control of the opening and closing processes by means of e-beams and/or lasers of reasonable powers.

The general feasibility of this concept has been demonstrated in earlier papers [3-6], and can be anticipated from numerous papers related to laser discharges. The practical knowledge of diffuse discharges has been drastically improved through the development of gas discharge lasers. However, the operating conditions, which the discharge must fulfill, are different for switching applications. Other discharge properties and mechanisms of importance in the discharge have to be considered and their collective influence on the coupling between discharge and circuit must be optimized in a different way.

Recently several papers [7-18] have appeared concerning e-beam controlled discharges. They specifically relate to switching applications, emphasizing different aspects of modes of operation, such as the influence of the gas mixture [7,8], the cathode sheath [11,12], the low e-beam current density and high current gain regime [13-15], as well as related optical control mechanisms [16,18].

The use of admixtures of attachers can be employed to achieve fast opening

of the switch but attachment will also increase the losses [7-10]. It has been proposed that these switch losses can still be kept low, if the gas mixture has the following properties, allowing both low forward voltage drop and fast opening [1,2]:

- a) at low values of  $E/N$ , i.e. during the conduction phase, the gas mixture should have a high drift velocity and a low attachment rate.
- b) at high values of  $E/N$ , i.e. during the opening phase, the gas mixture should have a low drift velocity and a high attachment rate.

Since attachers with a rate constant,  $k_{attach}$ , which increases with increasing  $E/N$  in a given  $E/N$  range are known to cause attachment instabilities if the discharge is operated in that  $E/N$  range [19,20], a third property is also desirable:

- c) the attachment rate should have a minimum at, or above the value of  $E/N$  at which the discharge is operated in the conduction phase, or the attacher should have an onset threshold above this value of  $E/N$ , below which attachment is not effective.

Along these considerations, several gas mixtures have been proposed for the use in diffuse discharge opening switches [21]. It seems that these gas properties will allow a low-loss, stable, steady state operation at low values of  $E/N$  and a sufficiently high hold off voltage, to assure the attainment of a zero current density if an external controlling e-beam is turned off. Any complete switching cycle, opening and closing, will, however, go through a lossy state and only the analysis of the time dependent behavior, including the losses during the switch transition period will allow one to determine the feasibility of this concept [18] and the optimum operating conditions.

There are two principal reasons to strive for a high  $dj/dt$  in the opening switch transition, (1) the efficient power extraction from the inductive energy storage system and (2) low energy loss in the switch (the later reason also

applies to the closing transition).

The main concern in achieving fast transitions in the discharge is the electron balance and hence the desirable properties of the attacher as described above in the gas properties a) and b), and the  $E/N$  dependence of the electron drift velocity. In this paper we concentrate on the consequences of the afore mentioned attachment properties.

The current density range will also affect the properties of the discharge to some degree. It was shown [5,11,13], that high current gains can only be achieved if the current density is kept low. On the other hand, device requirements may force one to operate at a high current density, if extremely high total currents are required.

With this as a background, this paper presents calculations to analyze the specific properties of an e-beam controlled discharge switch if an attacher with the suggested properties is present in the dielectric gas. The consequences of attacher properties on the steady state characteristics and the transient behavior in a specific circuit will be discussed. Photodetachment will also be considered as an additional opening switch control mechanism [22].

## II. CIRCUIT IMPLICATIONS IN AN INDUCTIVE ENERGY STORAGE SYSTEM

Fast, repetitive transfer of power from an inductive energy storage device to a load (e.g. a switch opening time of less than 100 ns) requires detailed consideration of the circuit elements (inductors, connectors) as transmission lines, i.e. effects due to finite transit times and reflections are not negligible. At high frequencies, the distributed capacitance,  $C'$ , of the energy storage device in concert with the high distributed inductance,  $L'$ , implies a high characteristic impedance  $(L'/C')^{1/2}$  on the order of several  $k\Omega$  and transit times,  $(LC)^{1/2}$ , of several 100 ns for a typical system [23]. Matching of this

impedance to the opening switch in parallel with the load is generally not possible, since for most applications the impedance of the load will be quite small compared to the generator impedance. Hence, power transfer from the generator to a low impedance load will be limited due to this mismatch in impedances.

In comparison with a lumped parameter description of the circuit, the reflections arising in the transmission line introduce an additional modulation of the power transfer with a time constant of twice the transit time of the inductive energy storage device, influencing both the load and switch behavior. Additionally, inductive storage devices can be considered as helical slow wave structures at high frequencies. The dispersion inherent in slow wave structures [24] presents further limitations on the efficiency of power transfer to the load for frequencies above 1 MHz.

A detailed consideration of transmission line effects in fast repetitive power transfer from inductive energy storage devices will be published in a separate paper [25]. For this paper, the crucial aspect is that for short switching times an inductive energy storage system has to be treated as a line with a relatively high impedance.

### III. DISCHARGE ANALYSIS

To evaluate the time dependent impedance of an externally controlled discharge in a given circuit, as well as to optimize the properties of the gas mixture together with circuit parameters, a computer model has been developed that enables fast calculations for a variety of conditions. The code does not, however, provide for spatial analysis, but it does allow one to evaluate the influence of general gas properties and of the circuit on the discharge, although not affording information about the sheaths and discharge

instabilities.

The code uses two independent programs. In a first computation all rate constants of significant processes are calculated as a function of  $E/N$  for a representative gas mixture. These calculations use the  $E/N$ -dependent electron energy distribution functions that have been previously compiled using a separate Monte Carlo code. In a second step a system of circuit equations and rate equations using the  $E/N$  dependent rate constants are solved. It is assumed that the  $E/N$  dependence of the rate constants does not change significantly for small variations of the gas mixture. Additionally the electron energy relaxation is considered to be faster than any significant change in  $E/N$ , thus allowing time dependent solutions.

It should be pointed out, that the set of processes considered in the Monte Carlo calculations and in the rate equation program are different. In the rate equation system, only those processes are considered which, according to the specific switching application, contribute to the electron density. Since the gas discharge is considered to stay relatively "cold" during one switch period, any  $V, R, T-E$  collisions (transfer of energy from vibrational, rotational, translational energy to electronic excitation) are neglected and transitions into rotational and vibrational states are considered only as loss mechanisms. On the other hand, in the Monte Carlo code a set of cross sections, as complete as possible, is employed. Such cross section sets, however, are only available for a few pure gases or rudimentary gas mixtures.

The calculations presented herein were performed for an e-beam sustained discharge in  $N_2$  with admixtures of  $N_2O$  as the attacher.  $N_2$  was used since a complete set of cross sections for inclusion in the Monte Carlo code was available [26], and the plasma chemistry in a mixture of  $N_2$  and  $N_2O$  appears to be relatively simple.  $N_2O$  in an  $N_2$  buffer gas exhibits an  $E/N$ -dependent electron decay rate, which increases more than a factor of 20 in the  $E/N$ -range from 3 Td

to 15 Td [27,28].

In calculations by Morgan and Pitchford [29], on the electron energy distribution function in weakly ionized plasmas created by an electron beam in  $N_2$ , it was demonstrated that the distribution function is different from just a superposition of the distribution function in a swarm and the distribution function of the electrons created in ionizing collisions of the fast electrons of the electron beam. Especially at low values of  $E/N$ , electrons produced at energies above the cross-sections for vibrational excitation create a side maximum in the distribution functions at  $E/N$  values where otherwise no electrons would be found. If admixtures of attachers are used with significant cross sections in this high energy range, a certain fraction of the created electrons will also be attached at low values of  $E/N$ . As a first approximation this effect could be considered when calculating the electron generation rate for a given electron beam, but according to the data available this effect will not change the electron density by more than a few percent.

Another objective was to investigate the feasibility of using photodetachment as an additional control mechanism. The  $N_2O$  undergoes dissociative attachment producing  $O^-$ . Photodetachment of  $O^-$  has already been proposed as a possible control mechanism for diffuse discharges [16,22].

It should be noted, however, that  $N_2$  has an electron mobility which increases with  $E/N$  and therefore is not an optimum candidate for a buffer gas in diffuse discharge opening switch applications.

For switching, an e-beam sustained discharge has to work well below the self-breakdown limit. Electron generation should, therefore, during the closed phase (at low values of  $E/N$ ), only depend on the direct ionization by the control e-beam electrons. The overall dynamic behavior, especially in the opening phase, however, may also depend on excitation and ionization processes through the discharge electrons. Thus, the  $E/N$  dependence of these processes

must also be considered [30].

The following processes are considered in the set of rate equations. The required cross sections or rate constants were obtained from the literature.

- (1) Direct ionization [31,32]
- (2) Excitation of the metastable A-state of  $N_2$ , direct or via other triplet states with subsequent optical transitions [33].
- (3) Ionization of  $N_2$  from the metastable A-state [34]
- (4)  $N_2$  metastable deactivation [35]
- (5) Electron-ion recombination [36]
- (6) Dissociative attachment of  $N_2O$  [27,28]
- (7) Collisional detachment of  $O^-$  [37]
- (8) Ion-ion recombination [38]
- (9) Photodetachment of  $O^-$  [39]
- (10) Electron drift velocity [40]

Experimentally derived rates as a function of  $E/N$  were used in the calculations, when ever available. If  $E/N$  dependent rates were not available, such as for processes (2), (3), and (7), or not known over the necessary  $E/N$  range, such as for (1), then the rate constants were calculated using the electron energy distribution function, evaluated through Monte Carlo calculations.

The electron energy distribution function, and subsequently the rate constants, change for a fixed value of  $E/N$  if the partial pressure of an attacher in a buffer gas is varied. This effect becomes very strong if a molecular attacher is added to an atomic buffer gas, since here the cross section of rotational and vibrational excitation and attachment are added in an energy range where the buffer gas does not have any appreciable inelastic cross section. Using  $N_2$  as a buffer gas with an admixture of an attacher, only the



attachment cross section of the attacher may cause a significant change of the electron energy distribution function [41]. We, therefore, performed the Monte Carlo calculations with the cross sections of  $N_2$  solely and for the cross sections of  $N_2$  plus the attachment cross section of  $N_2O$  considering a 1% admixture of  $N_2O$ . As expected, the electron energy distribution function was lowered in the energy range above the attachment threshold and raised below this threshold energy. In the high energy range ( $E > 6$  eV), at high values of  $E/N$ , this effect was not significant. All potential ionization processes (single and multi step) require a higher electron energy. The only process with a significant cross section in this range below 6 eV is collisional detachment of  $O^-$ . As will be seen later, the negative ion density will not reach values high enough to make collisional detachment a significant process if the discharge operation is optimized with respect to low losses.

For process (6), dissociative attachment of  $N_2O$ ; two reported experimental data ([27] and [28]) and the calculated values differ only slightly. The calculated values, using the cross sections for  $T = 300$  K [42], show a lower threshold at approximately 1.5 Td, while the experimental data [27] have a threshold at approximately 2.5 Td. For the calculations we used the experimental data [27] extended to high values of  $E/N$  according to our calculations (maximum rate constant of  $1.1 \times 10^{-9} \text{ cm}^3 \text{ s}^{-1}$  at 30 Td and nearly constant above this value). Note that this attachment rate constant is only an example of a specific attachment characteristic that can be found among several attachers. Its important features are:

- (a) a low attachment rate for low values of  $E/N$
- (b) a threshold value of  $E/N$  with a strong increase of the attachment rate above this value.
- (c) an attachment rate that saturates at some higher value of  $E/N$ .

#### IV. DISCHARGE CHARACTERISTICS

The steady state characteristics were computed assuming a constant voltage, calculating the current for which  $dj/dt = 0$ . These calculations were performed for various sets of parameters. Figure 1 shows the steady state characteristics for different  $N_2O$  concentrations in a  $N_2$  buffer gas. The total pressure is 1 atm and the e-beam electron generation rate is  $8 \times 10^{21} \text{ cm}^{-3}\text{s}^{-1}$ . As expected, the steady state characteristics are not affected by the attacher in an  $E/N$ -range of 0 - 4 Td; while in the range of approximately 5 - 30 Td high attacher concentrations cause the current density to decrease if the field strength increases and, therefore, produces a current density maximum. The threshold value of  $E/N$  at which the current density no longer rises strongly with  $E/N$  is determined by when attachment becomes the major loss mechanism. Thus the maximum of the current density shifts to higher  $E/N$  values when the attacher concentration decreases. It should be noted that attachers with a constant attachment rate coefficient result in steady state characteristics where the current density increases monotonically with  $E/N$ .

Figure 2 depicts the discharge characteristics for different values of the electron generation rate. (The attacher concentration is constant at 1%.) With increasing electron generation rates the electron density for a given value of  $E/N$  also increases. Since recombination depends quadratically on the electron density and only linearly on attachment, a higher value of  $E/N$  is required to cause attachment to become the major electron depletion mechanism. Therefore, the current density maximum shifts to higher values of  $E/N$  if the electron generation rate is increased. Figure 2 also demonstrates that the decrease of the current density with increasing  $E/N$ , caused by attachment, is more significant for lower electron generation rates.

These steady state characteristics give a strong hint as to which operating

point or region would be ideal with diffuse discharges switches. In order to operate in the low loss region, which is not attachment dominated, the operating point should be on the left side of the current density maximum. In order to achieve fast opening, with no long delay, the operating point should be close to the maximum.

As mentioned before, the system  $N_2 + N_2O$  has also been chosen to demonstrate the possibility of influencing the discharge properties by using photodetachment. If it is assumed that the dominant negative ion is  $O^-$ , then the dominant depletion mechanisms are  $O^-$ -ion recombination and/or photodetachment. Figure 3 shows the steady state characteristic for an  $N_2O$  fraction of 1% and an electron generation rate of  $8 \cdot 10^{21} \text{ cm}^{-3} \text{ s}^{-1}$ . The variable parameter is the power density of the illuminating laser operating in the photon energy range around 2 eV where the photodetachment cross section has a plateau. For comparison the steady state characteristics of a pure  $N_2$  discharge is also shown. The calculation shows that photodetachment can compensate attachment in a significant E/N range, especially if a power density of  $10^7 \text{ W/cm}^2$  or above is used.

## V. TRANSIENT DISCHARGE BEHAVIOR

As discussed in Section IV, it should be possible to operate an e-beam sustained, low loss discharge which is not strongly affected by an attacher, provided the attachment rate constant has a clear threshold at a certain value of E/N, below which the attachment is not efficient. How fast such a steady state operation is approached when the e-beam is turned on and how fast the discharge opens if the e-beam is turned off, will depend strongly on the circuit as well. To examine the circuit influence, let us discuss two different applications. In both cases we will discuss an inductive energy storage system

which has two separate loops, the charging loop and the discharge loop, having only the inductor in common (Fig. 4). In order to simplify our assessment let us assume that the load connected to the storage system is infinite during the inductor energizing phase, which can be achieved by an additional isolation spark gap in series with the load or if the load is a self-sustained gas discharge.

(a) Single pulse operation

In single pulse operation the switch has to close and open only once and it is thus possible to consider these two switching events in two different circuits. Let us assume that the discharge has to carry the total current after the inductor is already energized (Fig. 4). At this time the voltage drop across the inductor may be very small (i.e.  $di/dt \sim 0$ ). If the electron beam is turned on at the same time the slow switch begins to open then the e-beam sustained discharge may reach the steady state starting from  $j = 0$  and low  $E/N$ , without going through a range of high  $E/N$  values which would be in the attachment dominated range, i.e. high losses in the discharge. In addition, the slow switch does not experience a high voltage drop when it is opened. In this case, with appropriate circuit and discharge parameters, it can be shown, that the discharge approaches a steady state operation close to the maximum of the characteristics displayed in Figure 2. It should be pointed out that in using a fuse as the slow opening switch the e-beam sustained discharge can not take over the current until the fuse has started to open, therefore the time dependent characteristics of the fuse have to be considered as well.

For the next phase (opening) let us consider the open circuit, i.e. infinite load, case. As discussed in Section II the inductive energy storage system has to be considered as a transmission line with a high value of  $L'$  and a low value of  $C'$ , causing a very high impedance. The open circuit will produce the maximum value of  $E/N$  possible. Such a high impedance load line will

definitely move the discharge into the range of high  $E/N$  values causing attachment to become most effective and affording fast opening times. At high values of  $E/N$  ( $> 100 \text{ Td}$ ), however, ionization in the discharge becomes dominant. During switching operations, of course, the voltage drop across the discharge must stay well below that of a self-sustained discharge or self breakdown.

(b) Burst operation

In a burst operation the inductor is charged once and the energy is then deposited into a load, in a burst of pulses, using an e-beam sustained discharge as a repetitive opening switch. In this case the final voltage drop across the load at the end of the pulse (which is the same as across the discharge cell), will define the initial  $E/N$  value for the closing process of the switch, i.e. when the e-beam is reintroduced. The closing process will thus go through a lossy state, slowing down the closing process. This effect will be greater the higher the  $E/N$  starting value is. As a result, we performed calculations on this transient behavior. The experimental arrangement shown in Figure 5, will be used for validations of the general conclusions drawn from the model analysis.

It is obvious that a decreasing system impedance at a given impressed voltage will increase the current; the current density, however, can be kept constant if the discharge area is increased by a corresponding factor. Thus the quantity  $Z_t A$  acts as a similarity quantity, where  $Z_t = Z + R_E$  is the total system impedance and  $A$  is the discharge area.

For all calculation in this section the following parameters were kept constant: ( $A = 100 \text{ cm}^2$ ,  $d = 1 \text{ cm}$ ,  $p (\text{N}_2) = 1 \text{ atm}$ ,  $V_0 = 50 \text{ kV}$ , electron generation rate  $R_e = 8 \times 10^{21} \text{ cm}^{-3} \text{ s}^{-1}$  for  $0 \leq t \leq 100 \text{ ns}$ ). The values of the pressure  $p$ , voltage  $V_0$ , and discharge length  $d$  correspond to a maximum value of  $E/N = 185 \text{ Td}$ . In an initial set of calculations, the total system impedance was kept constant at  $Z_t = 20\Omega$ , giving a similarity quantity  $Z_t A = 2 \times 10^{32} \text{ cm}^2$ . Figure 6 depicts the discharge characteristics for these

parameters (see also Fig. 1) on a linear scale and, in addition, the load line for three system impedances,  $Z_t$ . The variable parameter is the %  $N_2O$ . This graph indicates that, for  $Z_t = 20\Omega$ , the system will approach the low range of  $E/N$  for  $N_2O$  concentrations of 0.75% and below, but not for an  $N_2$  concentration as high as 1%. For 0.75%  $N_2$ , the loadline ( $Z_t = 20\Omega$ ) comes very close to the steady state characteristics in an  $E/N$  range of  $\sim 40$  Td and below. It can be seen that  $E/N$  and the current density would change very slowly for  $E/N \leq 40$  Td.

Figure 7 shows the time dependent  $E/N$ , current density  $j$ , and power loss per volume behavior of the discharge. The curves for 0.1%, 0.5%, and 0.75% of  $N_2O$  approach the same steady state value for  $E/N$  and  $j$  in the conducting phase, demonstrating that under these conditions the discharge is not strongly influenced by attachment. Furthermore, after termination of the e-beam, the discharge properties change very slowly until an  $E/N$ -value is approached where attachment becomes effective. Such a time dependence has also been found by Chantry [43]. By contrast, for the case of 1%  $N_2O$ , the attachment is strong enough to prevent the discharge from ever reaching a low  $E/N$ -state and the steady state is therefore always attachment dominated. Thus, when the e-beam is turned off, the values for  $E/N$  and  $j$  change quite abruptly.

The power loss curve (Fig. 7, bottom) shows that, if the discharge is operating in a low  $E/N$  steady state, strong losses occur only in the transition region. The half width of the first loss peak (i.e. closing phase) increases as one increases the attachment concentration, while the half width of the second loss peak decreases. The values given in Table 1 show the energy input per unit volume for one switching cycle, or for 300 ns if the discharge is still on at that time.

Another set of calculations were performed for a constant admixture of  $N_2O$  (1%) with the total impedance  $Z_t$  as the parameter. Figure 6 shows the steady state characteristics for a 1%  $N_2O$  admixture and three loadlines, allowing

prediction of the steady state characteristics of such a diffuse discharge.

The time dependent behavior of the discharge for these parameters is shown in Figure 8. At a value of  $40\Omega$  for the total impedance, the discharge reaches the low E/N region where attachment does not dominate. In this state the system impedance only and not the switch discharge limits the current. For lower impedances the discharge does not approach low E/N values and, therefore, remains essentially attachment dominated during the closing phase. The loss curves also make it evident that only for high system impedances can the losses be kept small.

Thus both the system impedance,  $Z_t$ , and the  $N_2O$ -concentration can determine whether or not the discharge reaches the low E/N region where attachment is not dominant, i.e. where the switch operates in the conduction phase at low losses. On the other hand, the opening phase ( $t > 100$  ns) is controlled primarily by the attacher concentration. The consequences of the specific E/N dependence of the attachment rate will have an immediate effect if the E/N value is still high when the e-beam is turned off, and will become effective after some delay, if E/N is below  $3 Td$ .

From Figure 6 it would seem that the steady state operating point in the E/N-j diagram for some of the lower  $N_2O$  concentrations ( $<1\%$ ) can also offer possible operating points for  $N_2O$  levels as much as  $1\%$ . However, the circuit characteristics with a loadline which already crosses the steady state characteristics at a higher value of E/N, would prevent the transition of the system to the low E/N, steady-state operation. Lower E/N operation would have the advantage of low losses in the closed phase and fast opening time due to the higher attacher concentration.

There are several possibilities for combining these two features. One possibility for speeding up or enforcing this transition would be to use an e-beam current density with an additional peak at the beginning of the

controlling pulse, i.e. tailor the shape of the external control input. Such an e-beam shaping was already discussed for electron beam sustained excimer laser discharges; in that case, however, to enhance stability [44]. In Figure 2 it was seen how the steady state current density moves to higher values if the electron generation rate is increased. Another possibility would be to use laser induced photodetachment to compensate for attachment during the transition from the open phase to the conduction phase. Figure 3 depicted how different laser power densities influence the steady state characteristics. Figure 9 exhibits the time dependent behavior of such a laser augmented discharge. The total impedance is  $20 \Omega$ , the  $N_2O$  concentration is  $1\%$ , and the parameter is the laser power density. (The laser is on for the same duration as the e-beam.) With a laser power density of  $10^6 \text{ W cm}^{-2}$  the discharge can be switched into the low  $E/N$  region, however, it takes approximately 100 ns. With  $10^7 \text{ W cm}^{-2}$  the value of  $E/N$  drops very fast, and the total energy loss for one cycle is the lowest of all operating conditions for the same impedance (compare Table 1 and Table 2).

After a discharge has reached the low value of  $E/N$ , detachment will not strongly affect the electron balance and further laser irradiation to provide photodetachment is not warranted. Figure 10 depicts the time dependence of  $E/N$  for laser pulses of different length,  $t_L$ , starting simultaneously with the e-beam at  $t = 0$  ns. The laser power density here is  $10^7 \text{ W cm}^{-2}$ . For short laser pulses ( $t_L < 12.5$  ns) the discharge does not reach the region of low  $E/N$  values, while a laser pulse of  $t_L = 20$  ns has nearly the same effect as a laser pulse covering the full e-beam period ( $t_L = 100$  ns). The energy density loss for these calculations is listed in Table 2.

The efficiency of using photodetachment depends on the density of negative ions. At  $t = 0$  ns no negative ions have been produced, here laser irradiation in the first few ns is probably of little value. Figure 11 shows calculations of the time dependence of  $E/N$  for laser pulses of  $t_L = 10$  ns length, but



starting at different times. The power density again is  $10^7 \text{ W cm}^{-2}$ , so the beam fluence is  $100 \text{ mJ cm}^{-2}$ . For comparison, the curves without laser irradiation and for laser irradiation during the full e-beam period (0 to 100 ns) are also shown. The energy density loss for one switch cycle is listed in Table 2. For the early pulses, as expected, the discharge does not proceed into the low E/N region. The lowest losses of the examples shown are achieved for laser pulse starting after 7.5 ns. These calculations show that, on a high impedance load line, the transition from a high E/N, steady state operation to the low E/N, steady state operation can be induced with quite reasonable laser fluences.

## VI. SWITCH OPTIMIZATION

The calculations presented herein demonstrate the advantages of using e-beam controlled discharge switches with a gas mixture containing a buffer gas and admixtures of attachers with an attachment rate having a threshold at a given E/N value and then increasing with E/N. Such a gas mixture enables the optimization of the discharge conditions in the steady state conduction phase and the opening phase, but adds difficulties in achieving fast closing. For an attacher in a molecular, or at least partly molecular buffer gas, an attachment rate having a threshold at a desired value of E/N can be realized if the attachment cross section has a threshold at some reasonable electron energy value, i.e. well above that of the dominating cross sections for vibrational excitation. Such properties will allow optimization of the discharge properties nearly independently in two E/N ranges.

In the E/N range below the threshold value for attachment, the discharge character is determined mainly by the buffer gas. The optimum operating point for the conduction phase can therefore be selected, considering the steady state

characteristics for the pure buffer gas. For the selection of this steady state operating point, however, requirements which depend on the specific applications must be also considered, such as:

- (1) A practical consideration may be a limit on the size of the switch. If high total currents are required, one may be forced to operate at undesirable high current densities.
- (2) A high current density will limit the current gain. Kline's calculation shows that the current gain increases faster with decreasing e-beam current than the total current decreases, showing that the e-beam is used more efficiently at low current densities [13].
- (3) Stability requirements limit the total energy density dissipated in the discharge, and thus, for a given conduction time  $t_c$ , there are limits on the current density  $j$ .
- (4) Another consideration may be the necessity to optimize the ratio between the energy stored in the inductor, and the power dissipated in the switch. This is equivalent to a time constant  $T$  for the decrease of stored energy in the conduction phase, with disconnected power supply (Fig. 4) For a given system one obtains:

$$T = \frac{I^2 L}{I V} \propto \frac{I}{V} \quad \text{or} \quad T \propto \frac{j}{E/N}$$

This means that straight lines in the  $E/N$ - $j$  diagram:  $j = \alpha T * (E/N)$  where  $\alpha$  is a system constant, are lines for the different constants,  $T$ . Considering a given conduction time  $t_c$  then the efficiency of the system would increase with increasing  $T$ . This would be achieved for an increasing e-beam current or electron generation rate (Fig. 2). A

given electron generation rate will limit the current range as seen in Figure 6. This approximation does not include the fractional power input of the electron beam, which of course increases with increasing beam current.

As can be appreciated, optimizing a steady state switch operation is difficult since the choice of the optimum steady state operating point is not obvious unless the application and its operating characteristics are clearly specified. The application affects the decision whether a system with low current density and high current gain or vice versa should be employed.

Once the steady state operating point has been determined the attachment and its concentration can be selected. For short delay switch opening the attachment threshold should be as close as possible to the steady state operating value of  $E/N$ . The maximum attachment rate, determined also by the attachment concentration, will then be responsible for the maximum value of  $(dj/dt)$ . It of course is also responsible for the time the switch needs to close again. Here a compromise has to be made, unless additional control mechanisms such as lasers are used.

For most applications, the switching times, both closing and opening, will be short, compared to the conduction phase. In these cases an additional control mechanism would only be required for a short time, compared to the steady state e-beam control. Additional control mechanisms to overcome attachment during closing, while still having an attachment dominated discharge during opening, would be to use a tailored e-beam with a stiffer beam current peak at the front of the pulse.

An additional control would be to use optical means, which were discussed in an earlier paper [16]. Relevant to an attachment dominated discharge is optically induced attachment, initiated in the opening phase when the e-beam is

turned off, or, as discussed herein, photodetachment in the closing phase, during the beginning of the e-beam pulse.

It should be pointed out again that the gas mixture used for our calculations are not the optimum for all switching applications. For example,  $\text{CH}_4$  as a buffer gas [40], has a much higher drift velocity at low values of  $E/N$ , and  $\text{N}_2\text{O}$  as an attacher may not have the right threshold value of  $E/N$  for a desired steady state operating point. The calculations, however, show that the use of an attacher with a threshold  $E/N$ -value for attachment offers a unique combination of steady state and transient discharge properties, especially if additional control mechanisms are used.

#### ACKNOWLEDGMENT

Research sponsored by the Air Force Office of Scientific Research, Air Force Systems Command, USAF, under Grant Number AFOSR F49620-79-C-0191. The U.S. Government is authorized to reproduce and distribute reprints for Governmental purposes notwithstanding any copyright notation thereon.

# REFERENCES

- [ 1] Proc. ARO Workshop on Repetitive Opening Switches, Tamarron, CO, Jan. 1981, Texas Tech University, Dept. Elec. Eng., Lubbock, TX 79409.
- [ 2] Proc. ARO Workshop on Diffuse Discharge Opening Switches, Tamarron, CO, Jan. 1982, Texas Tech University, Dept. Elec. Eng., Lubbock, TX 79409.
- [ 3] B.M. Kovalchuk, V.V. Kremnev, and G.A. Mesyats, Sov. Phys.-Dokl., 15, 267 (1970).
- [ 4] B.M. Kovalchuk, Yu. D.Korolev, V.V. Kremnev, and G.A. Mesyats, Sov. Rad. Eng. Electron Phys., 21, 112 (1976).
- [ 5] B.M. Kovalchuk, and G.A. Mesyats, Proc. 1st IEEE Int. Pulsed Power Conf., Lubbock, TX, Paper IC7. (1975).
- [ 6] R.O. Hunter, Proc. 1st IEEE Int. Pulsed Power Conf., Lubbock, TX, Paper IC8, (1976).
- [ 7] R.F. Fernsler, D.Conte, and I.M. Vitkovitsky, IEEE Trans. Plasma Sci., PS-8, 176 (1980).
- [ 8] R.J. Commiso, R.F. Fernsler, V.E. Scherrer, and I.M. Vitkovitsky, IEEE Trans. Plasma Sci., PS-10, 241 (1982).
- [ 9] R.J. Commiso, R.F. Fernsler, V.E.Scherrer, and I.M. Vitkovitsky, Proc. 4th IEEE Pulsed Power Conf., Albuquerque, NM, (1983).
- [10] P. Bletzinger, Proc. 3rd IEEE Int. Pulsed Power Conf., Albuquerque, NM, 81 (1981).
- [11] M.R. Hallada, P. Bletzinger, and W.F. Bailey, IEEE Trans. Plasma Sci., PS-10, 224 (1982).
- [12] P. Bletzinger, Proc. 4th IEEE Pulsed Power Conf., Albuquerque, NM, (1983).
- [13] L.E. Kline, IEEE Trans. Plasma Sci., PS-10, 224 (1982).
- [14] J.W. Dzimianski and L.E. Kline, Final Report, Air Force Contract F33615-78-C-2010, Report AFWAL-TR-80-2041, (1980).
- [15] J.F. Lowry, L.E. Kline, and J.V.R. Heberlein, Proc. 4th IEEE Pulsed Power Conf., Albuquerque, NM (1983).
- [16] K.H. Schoenbach, G. Schaefer, M. Kristiansen, L.L. Hatfield, and A.H. Guenther, IEEE Trans. Plasma Sci., PS-10, 246 (1982).

- [17] H. Harjes, K. Schoenbach, G. Schaefer, H. Krompholz, M. Kristiansen, G. Leiker, and L. Hatfield, Proc. 4th IEEE Pulsed Power Conf., Albuquerque, NM, (1983).
- [18] G. Schaefer, K.H. Schoenbach, P. Tran, J.-S. Wang, and A.H. Guenther, Proc. 4th IEEE Pulsed Power Conf., Albuquerque, NM, (1983).
- [19] D.H. Douglas-Hamilton and S.A. Mani, J. Appl. Phys., 45, 4406 (1974).
- [20] W.H. Long, J. Appl. Phys., 50, 168 (1979).
- [21] L.G. Christophorou, S.R. Hunter, J.G. Carter, and R.A. Mathis, Appl. Phys. Let., 41, 147 (1982).
- [22] G. Schaefer, P.F. Williams, K.H. Schoenbach, J. Moseley, IEEE Trans. Plasma Sci., PS-11, (1983).
- [23] M. Kristiansen, Proc. ARO Workshop on Repetitive Opening Switches, Tamarron, CO, (1981).
- [24] D.A. Watkins, "Topics in Electromagnetic Theory", Wiley & Sons, New York, (1958).
- [25] H. Krompholz, G. Schaefer, and K. Schoenbach, to be published.
- [26] Provided by A.V. Phelps, JILA, Boulder, CO.
- [27] L.C. Lee, C.C. Chiang, K.Y. Tang, D.L. Huestis, and D.C. Lorents, Second Annual Report on AFOSR sponsored Coordinated Research Program in Pulsed Power Physics, Department of Electrical Engineering, Texas Tech University, Lubbock, TX. 189 (1981).
- [28] J.W. Gallagher, E.C. Beaty, J. Dutton, L.C. Pitchford, JILA Info. Center Report 22, Boulder, CO., (1982).
- [29] W.L. Morgan and L. Pitchford, private communication - to be published.
- [30] J.J. Lowke and D.K. Davis, J. Appl. Phys., 48, 4991 (1977).
- [31] D. Rapp and P. Erlander-Golden, J. Chem. Phys., 43, 1464 (1965).
- [32] C.S. Lakshminarasimha, J. Lucas, and R.A. Snelson, Proc. Inst. Electr. Eng., 122, 1162 (1975).
- [33] D.C. Cartwright, A. Chutjian, S. Trajuar, and W. Williams, Phys. Rev. A, 6, 1041 (1977).

- [34] V.I. Kukulin, A.P. Osipov, and Yu. M. Chuvillskii, Sov. Phys. Tech. Phys., 24, 883 (1979).
- [35] J.W. Dreye and D. Perner, J. Chem. Phys., 58, 1195 (1973).
- [36] D. H. Douglas-Hamilton, J. Chem. Phys., 58, 4820 (1973).
- [37] G.C. Tisone and L.M. Branscomb, Phys. Rev., 170, 169 (1968).
- [38] D. Lorents, private communication.
- [39] L.C. Lee and P.G. Smith, J. Chem. Phys., 70, 1727 (1979).
- [40] L.G. Christophorou, "Atomic and Molecular Radiation Physics", 247, Wiley-Interscience, (1971).
- [41] L.C. Pitchford and A.V. Phelps, 35th Gaseous Electronics Conf., Dallas, TX., (1982).
- [42] P.J. Chantry, J. Chem. Phys., 51, 3369 (1969).
- [43] P.J. Chantry, Presented at the Workshop on Optical Control of Diffuse Discharges, University of Oregon, (1982).
- [44] R.T. Brown and W.L. Nighan, Appl. Phys. Lett., 35, 142 (1979).

Table 1. Energy density loss per switch cycle (300 ns) in  $\text{mJ}/\text{cm}^3$ 

System Impedance	N <sub>2</sub> O-Concentration			
	0.1%	0.5%	0.75%	1.0%
10 $\Omega$	92.9 *	57.5	58.1	61.4
20 $\Omega$	37.1 *	15.8 *	13.0 *	22.0
40 $\Omega$	12.4 *	6.8 *	4.4 *	3.6 *

For 0.1% N<sub>2</sub>O and 0.5% N<sub>2</sub> the discharge was still on after 300 ns. At this time the power loss was still 70% of its maximum value for 0.1% N<sub>2</sub>O and 3% for 0.5% N<sub>2</sub>O, respectively.

\* In these calculations the discharge reaches the low values of E/N.

Table 2. Energy density loss per switch cycle for the curves shown in Figure 10 and Figure 11.

# in FIG 10.	1	2	3	4	5	6	7	8
laser on from-to (in ns)	no laser	0-5	0-7.5	0-10	0-12.5	0-15	0-20	0-100
Energy density loss in $\text{mJ}/\text{cm}^3$	22.0	28.9	21.65	20.7	13.2	10.5	9.4	9.0

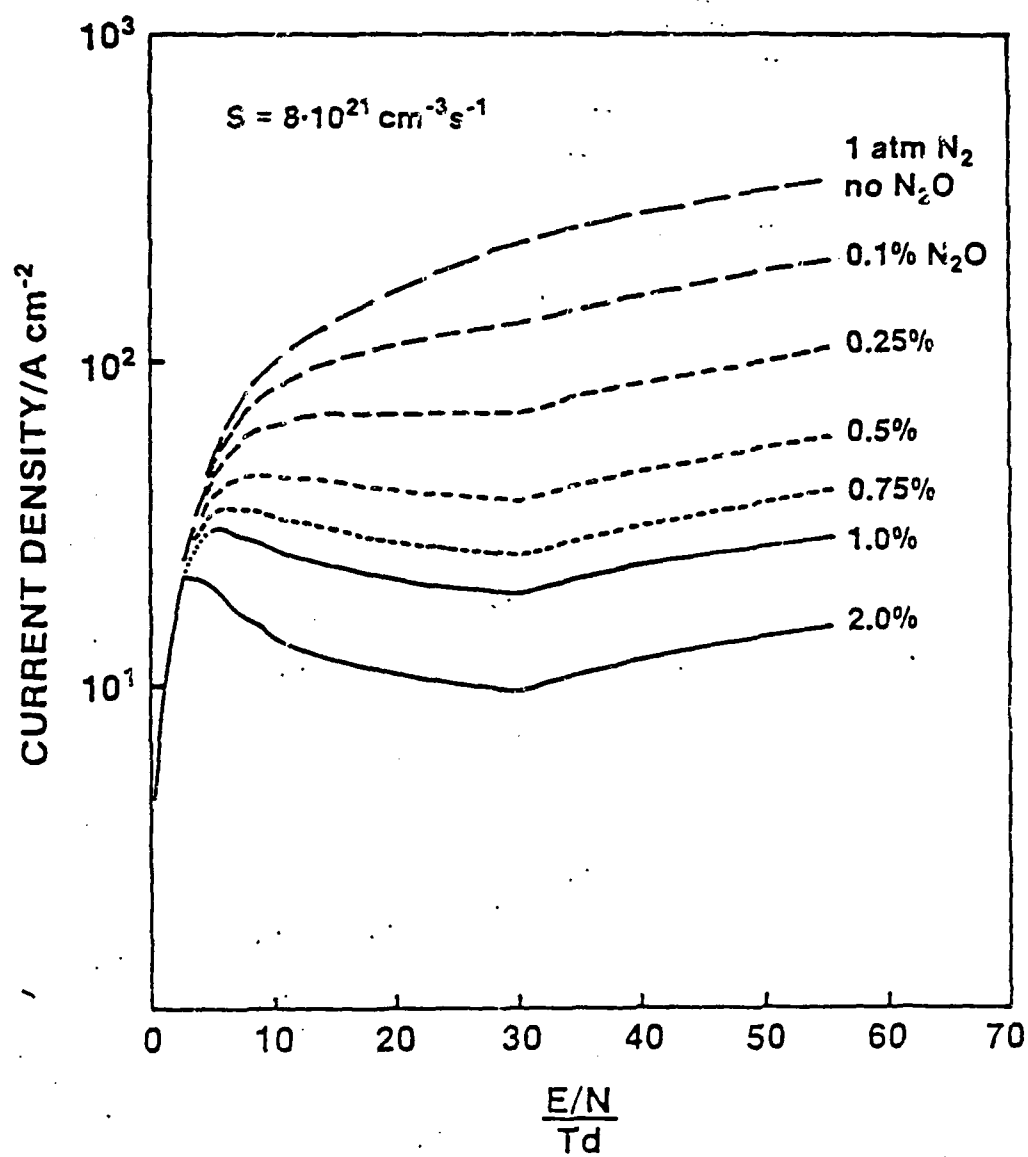
# in FIG. 11	1	2	3	4	5	6	7
Laser on from-to (in ns)	no laser	0-10	2.5-12.5	5-15	7.5-17.5	10-20	0-100
Energy density loss in $\text{mJ}/\text{cm}^3$	22.0	20.7	13.2	10.8	10.0	10.1	9.0

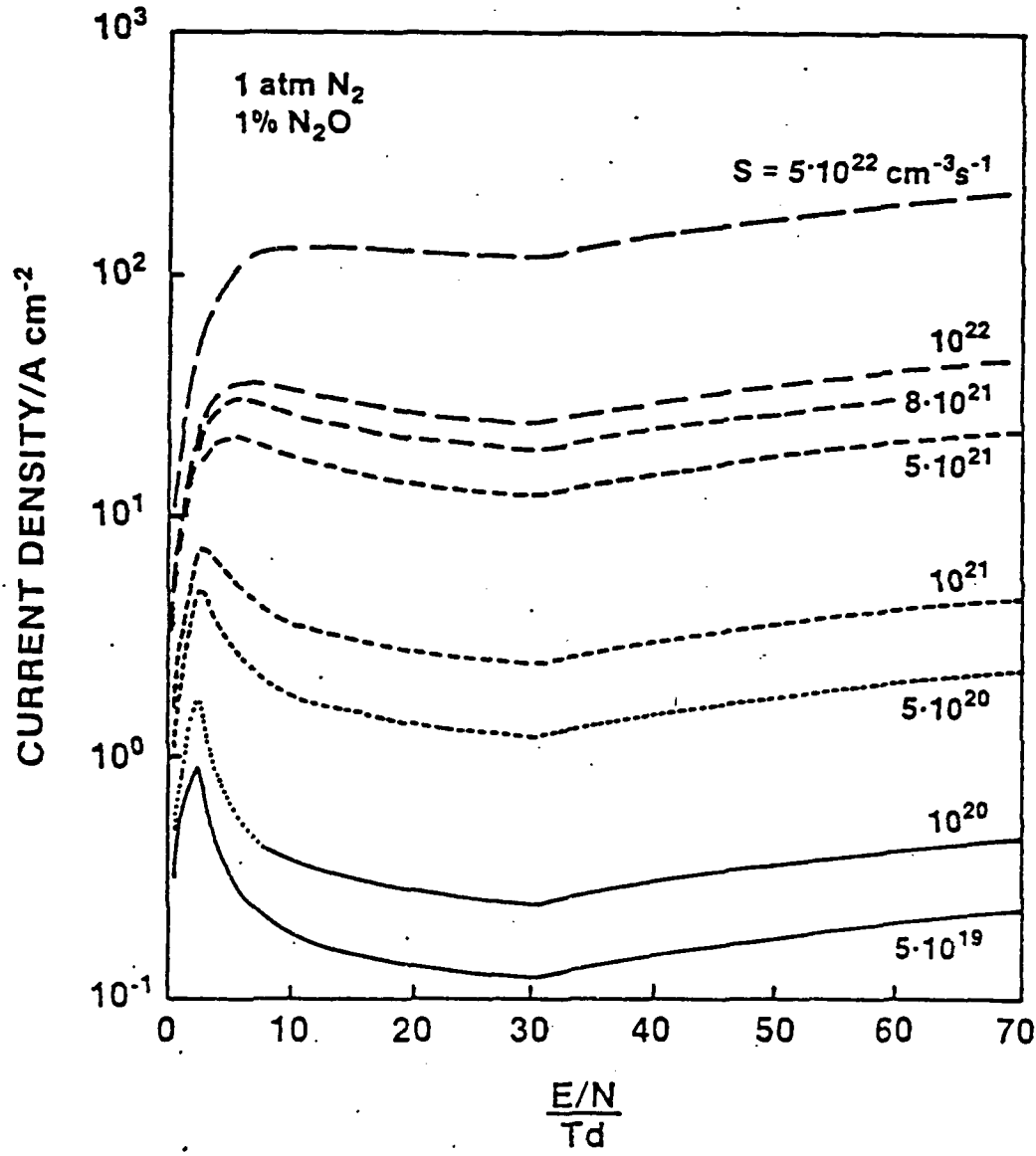


## FIGURES

- FIG. 1 Calculated steady state  $E/N$ - $j$  characteristics for an e-beam sustained discharge in  $N_2$  with admixtures of  $N_2O$ . The electron generation rate is  $8 \times 10^{21} \text{ cm}^{-3} \text{ s}^{-1}$ . The variable parameter is the  $N_2O$  fraction in %.
- FIG. 2 Calculated steady state  $E/N$ - $j$  characteristics for an e-beam sustained discharge in  $N_2$  with a  $N_2O$  fraction of 1%. The variable parameter is the electron generation rate.
- FIG. 3 Calculated steady state  $E/N$ - $j$  characteristics for an e-beam sustained discharge in  $N_2$  with a  $N_2O$  fraction of 1%, including photodetachment of  $O^-$ . The electron generation rate is  $8 \times 10^{21} \text{ cm}^{-3} \text{ s}^{-1}$ . The variable parameter is the laser power density.
- FIG. 4 Schematic circuit for an e-beam sustained discharge switch in an inductive energy storage system.
- FIG. 5 Schematic setup for an e-beam sustained discharge switch.
- FIG. 6 Calculated steady state  $E/N$ - $j$  characteristics for an e-beam sustained discharge in atmospheric pressure  $N_2$  with admixtures of  $N_2O$ . The electron generation rate is  $8 \times 10^{21} \text{ cm}^{-3} \text{ s}^{-1}$ . The parameters is the  $N_2O$  fraction in %. Also shown are three system load lines with the total system impedance,  $Z_t$ , as the variable parameter.
- FIG. 7 Time dependence of  $E/N$  (top), current density (middle), and power density loss (bottom) of an e-beam sustained discharge in 1 atm  $N_2$  with admixtures of  $N_2O$ . The system impedance is  $Z_t = 20 \Omega$ . The e-beam is on for  $0 \leq t \leq 100 \text{ ns}$ . The variable parameter is the  $N_2O$  fraction in %.

- FIG 8 Time dependence of  $E/N$  (top), current density (middle), and power density loss (bottom) of an e-beam sustained discharge in 1 atm  $N_2$  with a  $N_2O$  fraction of 1%. The e-beam is on for  $0 \leq t \leq 100$  ns. The variable parameter is the system impedance,  $Z_t$ .
- FIG 9 Time dependence of  $E/N$  (top), current density (middle), and power density loss (bottom) of an e-beam sustained, laser photodetachment assisted discharge in 1 atm  $N_2$  with a  $N_2O$  fraction of 1%. The system impedance is  $Z_t = 20 \Omega$ . The e-beam and laser are on for  $0 \leq t \leq 100$  ns. The variable parameter is the laser power density.
- FIG 10 Time dependence of  $E/N$  for an e-beam sustained, photodetachment assisted discharge in 1 atm  $N_2$  with a  $N_2O$  fraction of 1%. The system impedance is  $Z_t = 20 \Omega$ . The laser power density is  $10^7 \text{ W cm}^{-2}$ . The e-beam is on for  $0 \leq t \leq 100$  ns. The variable parameter is the laser pulse length (Table 2).
- FIG 11 Time dependence of  $E/N$  for an e-beam sustained, photodetachment assisted discharge in 1 atm  $N_2$  with a  $N_2O$  fraction of 1%. The system impedance is  $Z_t = 20 \Omega$ . The laser power density is  $10^7 \text{ W cm}^{-2}$ , and the pulse length is 10 ns. The e-beam is on for  $0 \leq t \leq 100$  ns. The variable parameter is the delay of the laser pulse with respect to the e-beam (Table 2).





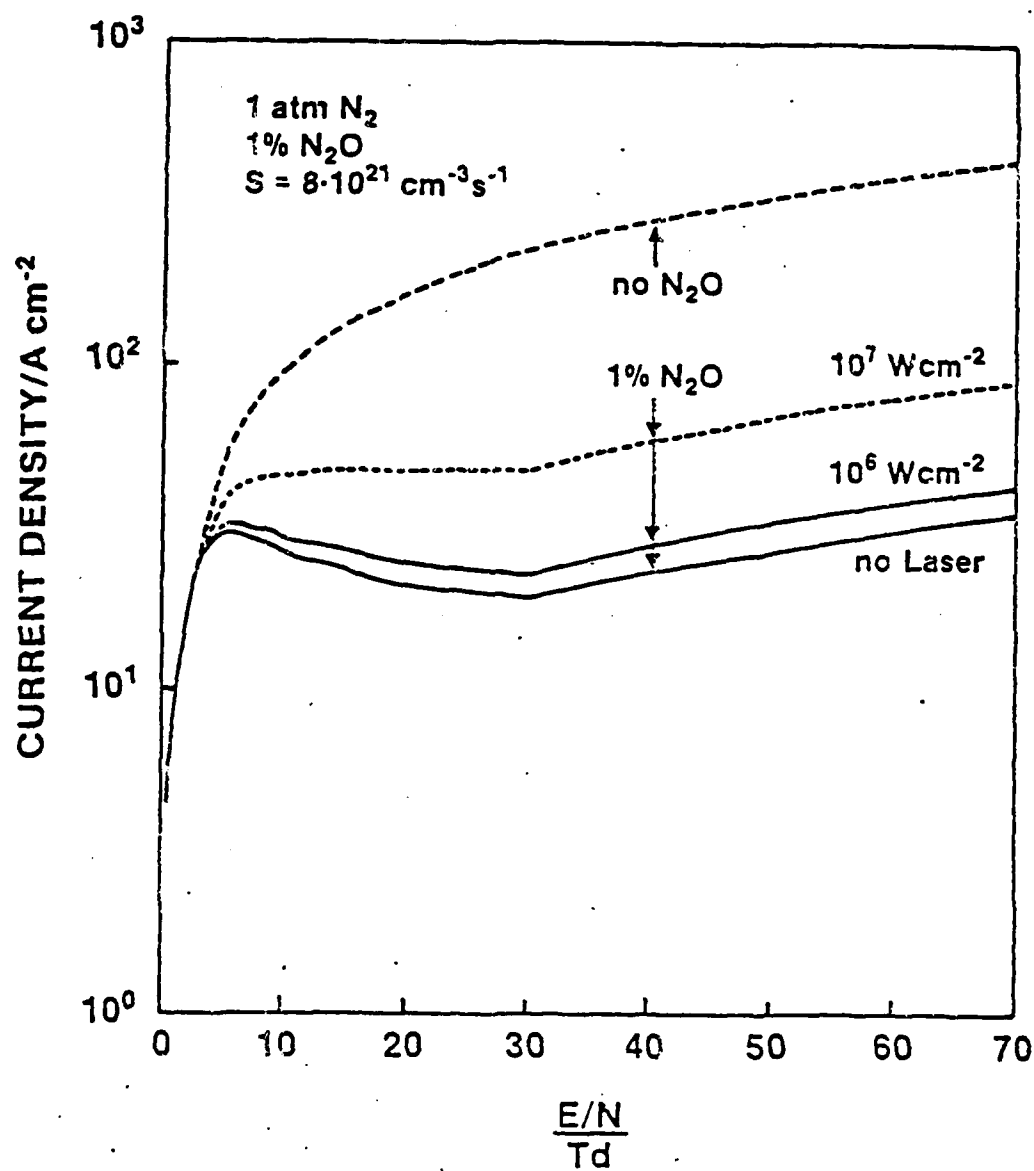


Fig. 3

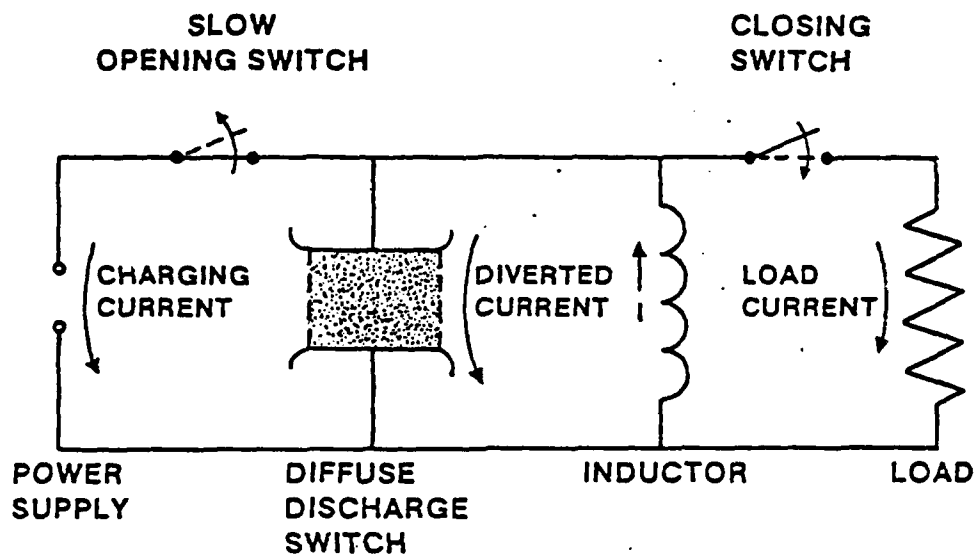


Fig. 4

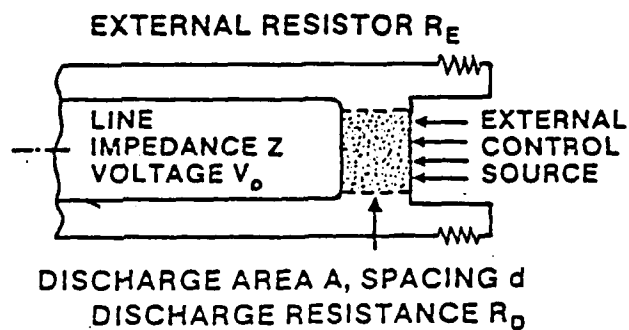
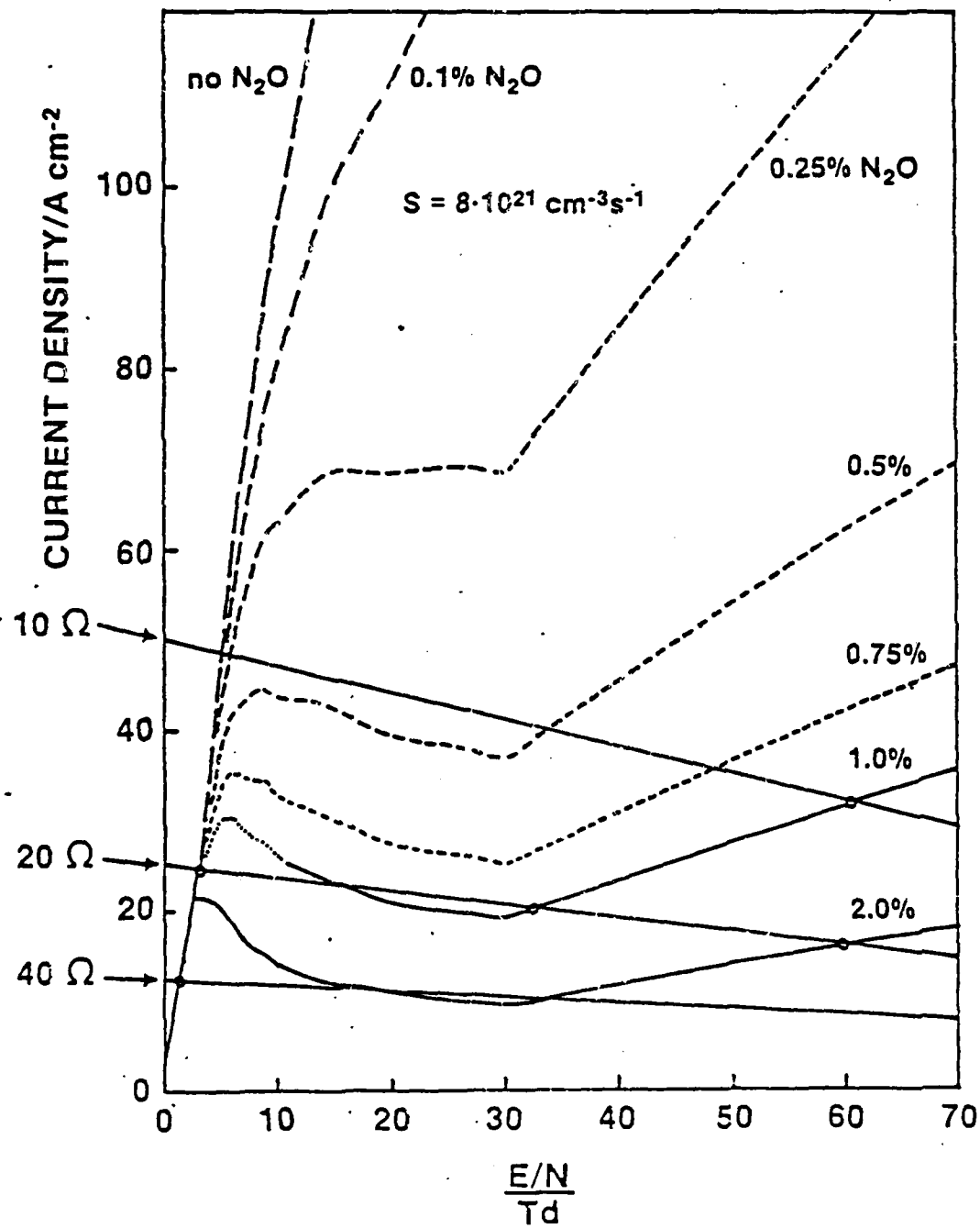
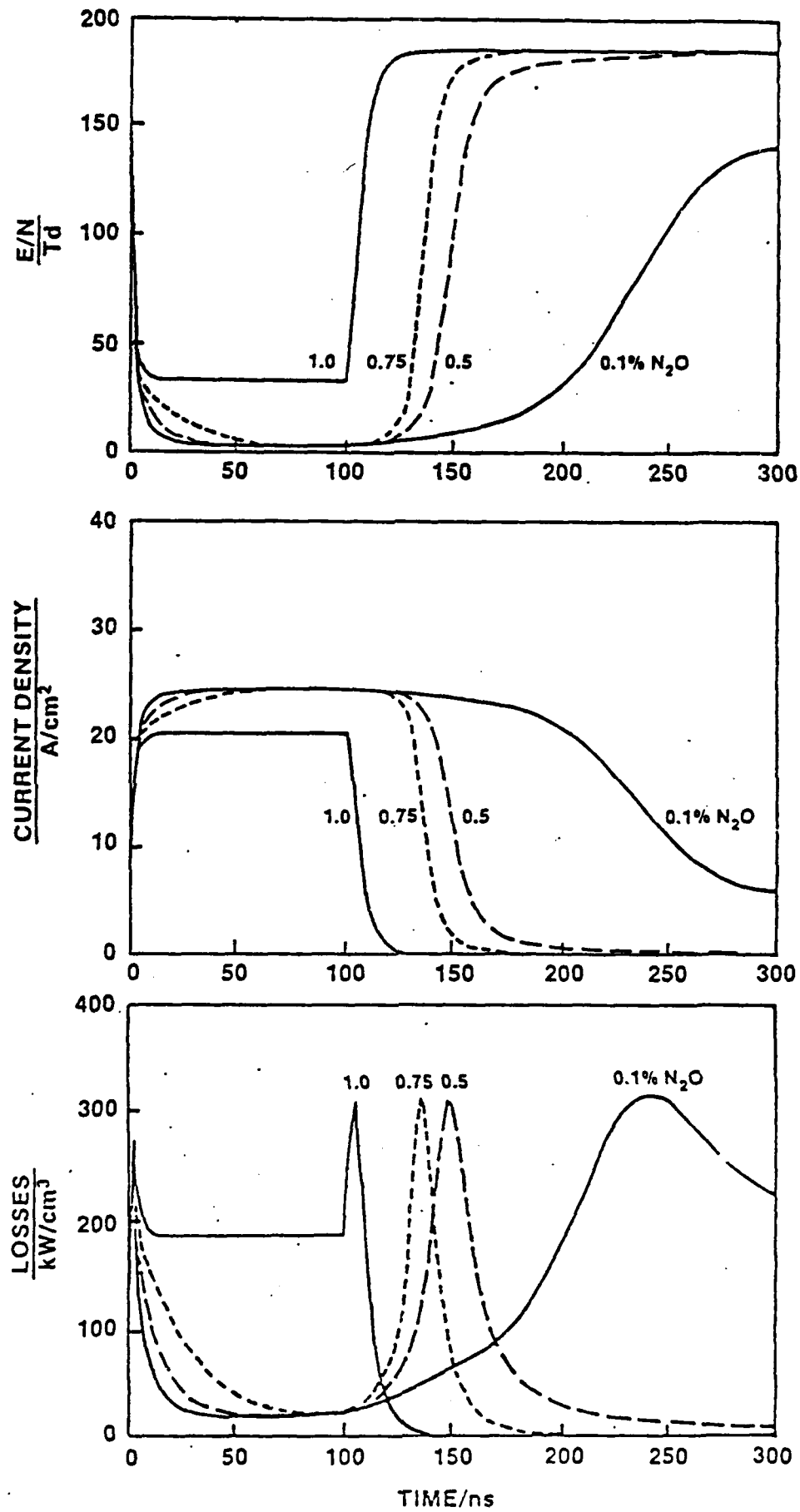
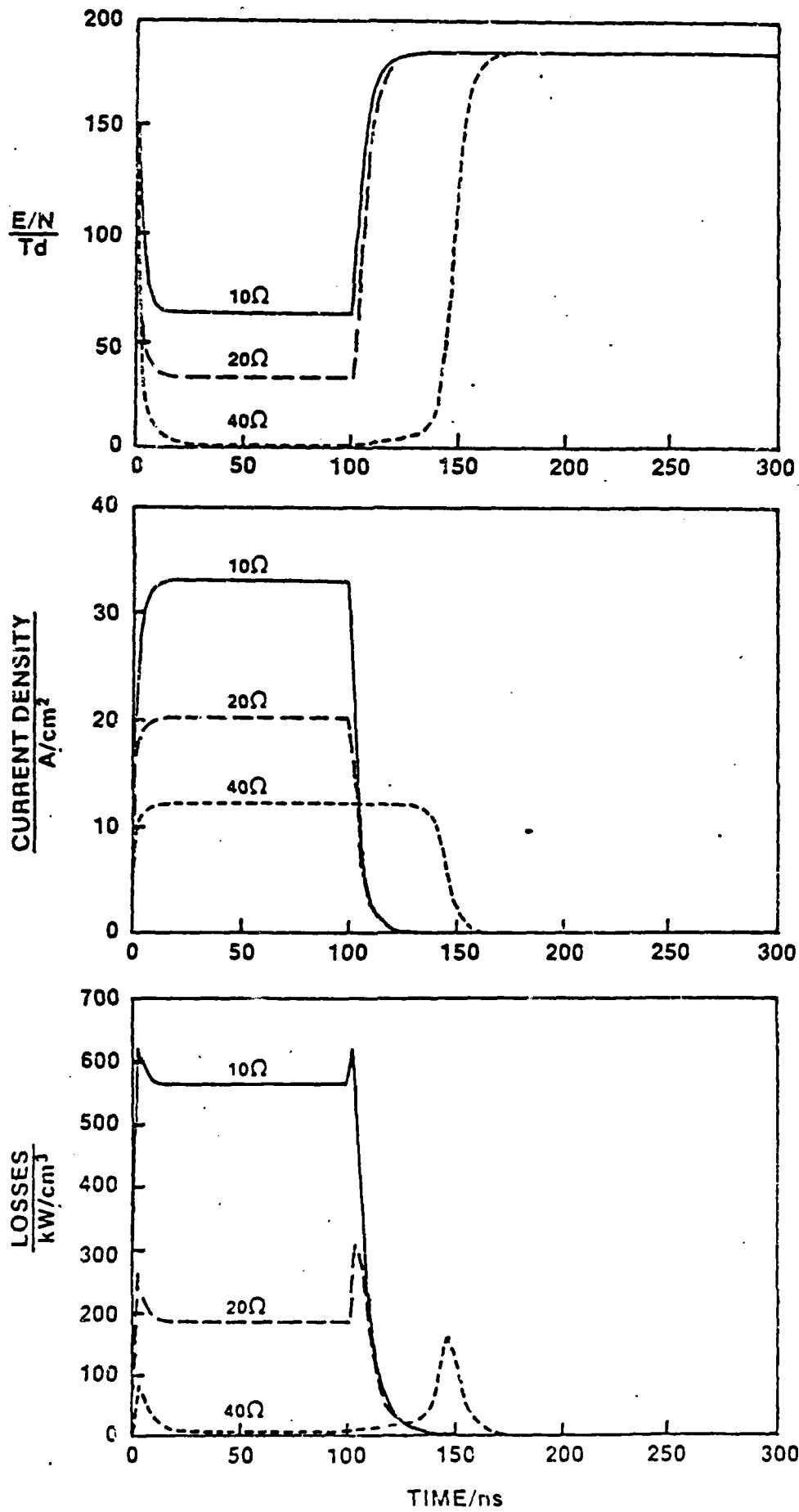


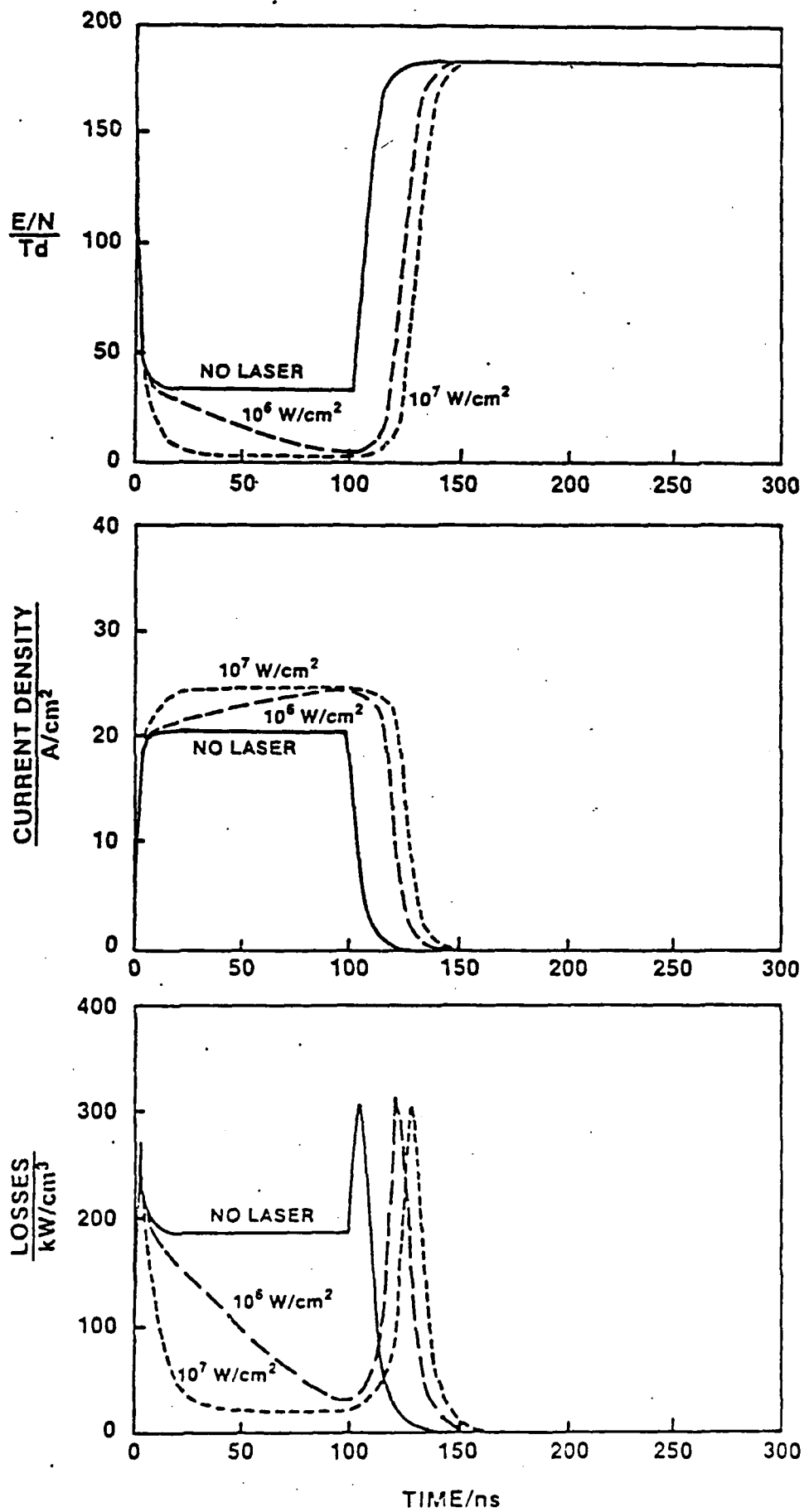
Fig. 5

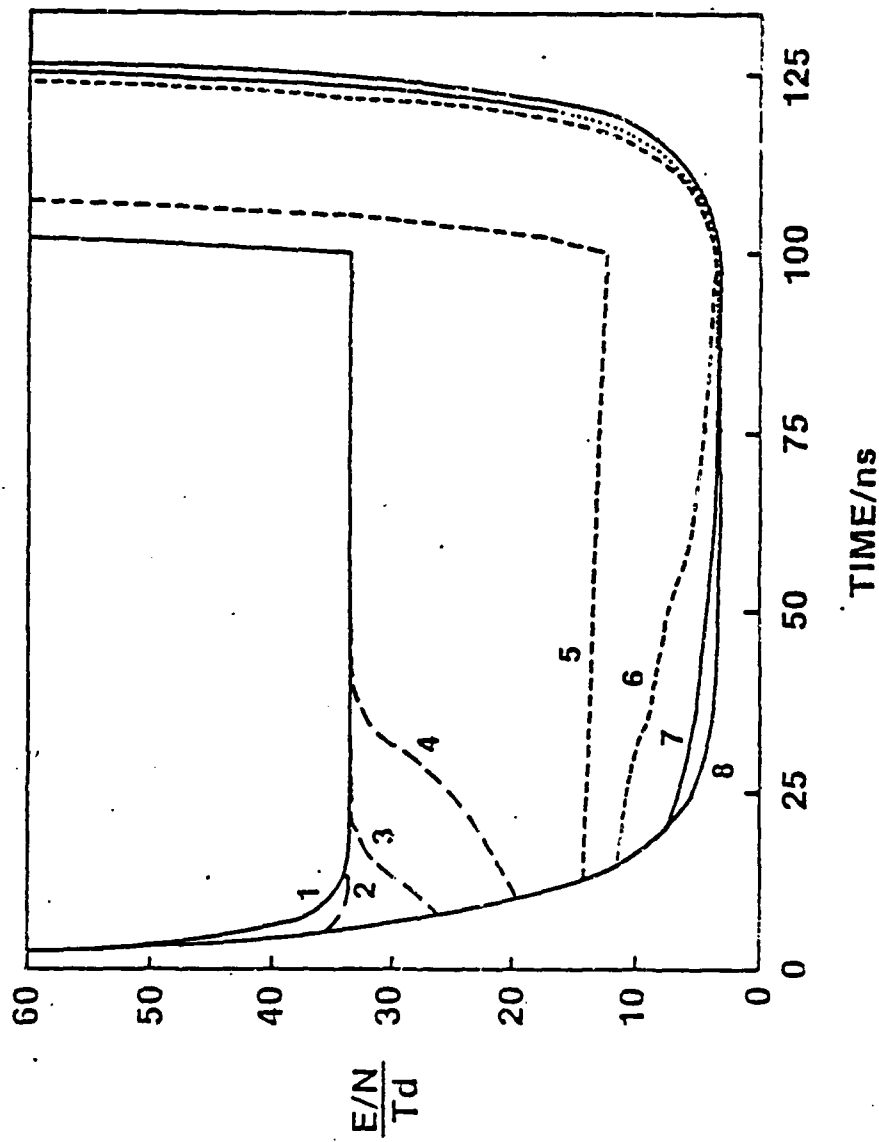


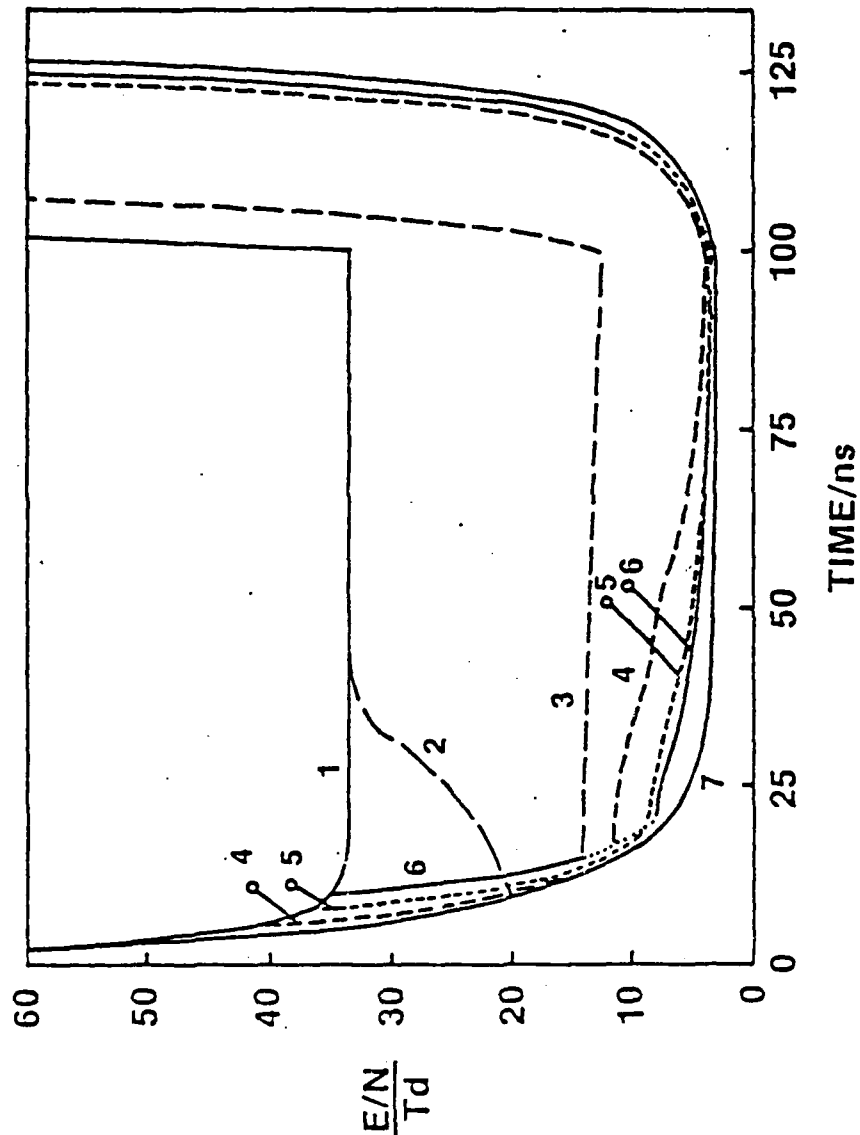












## FACULTY PUBLICATIONS, 1979-83

## Journal Papers and Conference Proceedings Papers

## Published with AFOSR-ARO Support

1. E. Chu, R. Druce, M. Kristiansen, M. Hagler, and R. Bengtson, "Beat Heating in Plasmas Using CO<sub>2</sub> Lasers," *Journal de Physique, Colloque C7, supplement No. 7, 40, C7-747 (1979).*
2. S. Levinson, E.E. Kunhardt, M. Kristiansen, and A.H. Guenther, "Simulation of Inductive and Electromagnetic Effects Associated with Single and Multichannel Triggered Spark Gaps," *Proc. 2nd IEEE International Pulsed Power Conference, Lubbock, Texas, 433 (1979).*
3. K. McDonald, M. Newton, E.E. Kunhardt, M. Kristiansen, and A.H. Guenther, "An Electron-Beam-Triggered Spark Gap," *Proc. 2nd IEEE International Pulsed Power Conference, Lubbock, Texas, 437 (1979).*
4. M. Newton, K. McDonald, E.E. Kunhardt, M. Kristiansen, and A.H. Guenther, "Applications of Electron Beams for Precise Switching of High Voltage," *Proc. 3rd International Topical Conference on High Power Electron and Ion Beam Research and Technology, Novosibirsk, USSR, 1979.*
5. M. Kristiansen and A.H. Guenther, "Digest of Technical Papers," *2nd IEEE International Pulsed Power Conference, Lubbock, Texas, 1979.*
6. M. Kristiansen and B. Miedzinski, "Investigations of Reed Switch Dynamics When Switching Heavy Loads," *Proc. 10th International Conf. Contact Phenomena, Bucharest, Hungary, Aug. 25-29, 1980.*
7. H.C. Harjes, K.H. Schoenbach, L.L. Hatfield, M. Kristiansen, and A.H. Guenther, "Laser Triggering, Through Fiber Optics, of a Low Jitter Spark Gap," *IEEE Transaction on Plasma Science, PS-8, 170 (1980).*
8. R.J. Crumley, P.F. Williams, and M. Gundersen, "Studies of the Basic Processes Responsible for Laser-Triggered Breakdown in Gases," *Journal de Physique Colloque C7, 40, 305 (1979).*
9. R.J. Crumley, P.F. Williams, M. Gundersen and A. Watson, "Electron Densities in Laser-Triggered Spark Gap Discharges," *Proc. 2nd IEEE International Pulsed Power Conference, 119 (1979).*

10. R.J. Crumley, P.F. Williams, and M. Gundersen, "Temporal Behavior of Electron Densities in Laser-Triggered Gaps", IEEE Trans. Plasma Sci, PS-9, 164 (1980).
11. \*E.E. Kunhardt and W.W. Byszewski, "Development of Over-voltage Breakdown in High Pressure Gases," Physical Review, A, 21, 2069 (1980).
12. J.P. Craig, "Multi-Megajoule Energy Storage and Conversion Device," Proc. Conf. on Electromagnetic Guns and Launchers, San Diego, CA, Nov., 1980.
13. IEEE Trans. Plasma Science, Special Issue on Plasma Switches, Sept. 1980, A.H. Guenther and M. Kristiansen, Guest Editors.
14. M. Kristiansen and A.H. Guenther, "Plasma Applications in Breakdown and Discharges in Gases", Pt B, pp 383-414, Plenum Publishing Co., 1983 (Edited by E. Kunhardt and L. Luessen).
15. K.H. Schoenbach, G. Schaefer, H.C. Harjes, G. Leiker, and M. Kristiansen, "Opening Switches", Proc. 3rd IEEE International Pulsed Power Conf., Albuquerque, N.M., June 1981.
16. K.H. Schoenbach, G. Schaefer, E.E. Kunhardt, M. Kristiansen and A.H. Guenther, "An Optically Controlled Diffuse Discharge Switch," Proc. 3rd IEEE International Pulsed Power Conf., Albuquerque, NM, June 1981.
17. S.K. Dhali and P.F. Williams, "Multiphoton Ionization - A Potential Trigger and/or Control for Electrical Breakdown," Proc. 3rd IEEE International Pulsed Power Conf., Albuquerque, NM, June 1981.
18. H.C. Harjes, E.E. Kunhardt, M. Kristiansen and L.L. Hatfield, "Space Charge Effects in a Laser-Fiber Optics Triggered Multichannel Spark Gap," 3rd IEEE International Pulse Power Conf., Albuquerque, NM, June 1981.
19. Y.H. Tzeng, E.E. Kunhardt, M. Kristiansen and A.H. Guenther, "The Effect of Electron Beam Induced Space Charge on Spark Gap Breakdown," Proc. 3rd IEEE International Pulsed Power Conf., Albuquerque, NM, June 1981.
20. B.H. Dunlap and J.P. Craig, "Time Varying Inductors for Electro-mechanical Pulsers," Proc. 3rd IEEE International Pulsed Power Conference, Albuquerque, NM, June 1981.
21. G.L. Jackson, Kai-Chin Yuan, L.L. Hatfield, and M. Kristiansen, "Surface Damage of Dielectrics in a Spark Gap," Proc. 3rd IEEE International Pulsed Power Conf., June 1981.

---

\*Partially supported by AFOSR and/ARO

22. L.B. Gordon, M.O. Hagler, M. Kristiansen and H.C. Harjes, "Investigations of a 60 kV, 5 cm Spark Gap for Several Electrodes, Insulator and Gas Types", Proc. 3rd IEEE International Pulsed Power Conf., Albuquerque, NM, June 1981.
23. M. Kristiansen, A.H. Guenther, John Ungvarsky, Fred Brockhurst, R.D. Franklin, A.K. Hyder, and R.L. Gullickson, "Modular Instructional Material in Pulsed Power Technology," Proc. 3rd IEEE International Pulsed Power Conf., Albuquerque, NM, June 1981.
24. S.K. Dhali, P.F. Williams, R.J. Crumley, and M.A. Gundersen, "Electron Densities in Laser-Triggered Hydrogen Sparks," IEEE Transactions on Plasma Science, PS-8, 164 (1980).
25. K. McDonald, M. Newton, E.E. Kunhardt, M. Kristiansen, and A.H. Guenther, "An Electron-Beam Triggered Spark Gap," IEEE Transactions on Plasma Science, PS-8, 181 (1980).
26. G.L. Jackson, L.L. Hatfield, M. Kristiansen, J. Marx, and A. Bowling, "Pulse Flashover of Solid Dielectrics in Vacuum," Proc. Xth Int. Sym. on Discharges and Elect. Insulation in Vacuum, Columbia, South Carolina, October 12, 1982.
27. K.H. Schoenbach, G. Schaefer, M. Kristiansen, L.L. Hatfield, and A.H. Guenther, "Optical Control of Diffuse Discharge Opening Switches", Proc. ARO Workshop on Diffuse Discharge Opening Switches, Tamarron, CO, p. 134, January, 1982.
28. Proceedings of ARO Workshop on "Diffuse Discharge Opening Switches," Tamarron, CO, January 1982 (M. Kristiansen and K.H. Schoenbach, Editors).
29. K. Schoenbach, G. Schaefer, M. Kristiansen, L.L. Hatfield, and A.H. Guenther, in "Diffuse Discharge Opening Switches," Electrical Breakdown and Discharges in Gases, Pt B, pp 415-427, Plenum Publishing Co., 1983 (Edited by E. Kunhardt and L. Luessen).
30. M. Kristiansen, et. al., "Report of Workshop on Repetitive Opening Switches", Proc. 3rd IEEE International Pulsed Power Conference, Albuquerque, NM, June 1981. (Invited Paper).
31. B. Miedzinski and M. Kristiansen, "Investigations of Reed Switch Dynamics and Discharge Phenomena When Switching Intermediate and Heavy Loads," IEEE Trans. on Components, Hybrids and Manf. Technology, CHMT-5, 231 (1981).
32. Proceeding of Workshop on "Repetitive Opening Switches," Tamarron, Colorado, January 1981, (M. Kristiansen and K.H. Schoenbach, Editors).

33. K.H. Schoenbach, M. Kristiansen, E.E. Kunhardt, L.L. Hatfield, and A.H. Guenther, "Exploratory Concepts of Opening Switches," Proc. ARO Workshop on Repetitive Opening Switches, Tamarron, Colorado, January 1981, p. 65.
34. K.H. Schoenbach, G. Schaefer, M. Kristiansen, L.L. Hatfield, and A.H. Guenther, "Optical Control of Diffuse Discharge Opening Switches," IEEE Trans. Plasma Science, PS-10, 246 (1982).
35. H.C. Harjes, E.E. Kunhardt, M. Kristiansen, L.L. Hatfield, and A.H. Guenther, "Space Charge Effects in a Laser-Fiber Optics Triggered Multichannel Spark Gap," IEEE Trans. Plasma Science, PS-10, 246 (1982).
36. Y.H. Tzeng, E.E. Kunhardt, M. Kristiansen, and A.H. Guenther, "The Effect of Space Charge Induced by an Electron Beam on Spark Gap Operation", IEEE Trans. Plasma Science, PS-10, 234 (1982).
37. L.B. Gordon, M. Kristiansen, M.O. Hagler, H.C. Kirbie, R.M. Ness, L.L. Hatfield and J. Marx, "Material Studies in a High Energy Spark Gap," IEEE Trans. Plasma Science, PS-10, 286, 1982.
38. D. Johnson and M. Kristiansen, "Multichannel Surface Discharge Switch," Proc. Conf. on Electrical Insulation and Dielectric Phenomena, Amhrest, Mass., Oct. 1982.
39. A. Donaldson, R. Ness, M.O. Hagler, and M. Kristiansen, "Electrode Erosion in High Power Spark Gaps," Proc. Fifteenth Power Modulator Symposium, Baltimore, Maryland, June 1982.
40. M. Kristiansen, "An Introduction to Gas Filled Spark Gaps," Proc. ARO Workshop on "Repetitive Spark Gap Operation," Tamarron, CO, January 1983.
41. I. Smith, T. Burkes, A. Guenther, M. Kristiansen, and G. Lauer, "Summary of the Capabilities of Repetitive Spark Gap Switches," Proc. ARO Workshop on Repetitive Spark Gap Operation, Tamarron, CO, January 1983.
42. H. Harjes, K. Schoenbach, G. Schaefer, H. Krompholz, and M. Kristiansen, "E-Beam Triode for Multiple Submicrosecond Pulse Operation", Proc. of 4th IEEE Pulsed Power Conference, June 1983.
43. H. Harjes, J. Doggett, J. Gahl, K. Zinsmeyer, H. Krompholz, K. Schoenbach, G. Schaefer, and M. Kristiansen, "Nanosecond Current Probe for High Voltage Experiments", Proc. 4th IEEE Pulsed Power Conference, June 1983.



44. G. Jackson, G. Leiker, L. Hatfield, M. Kristiansen, M. Hagler, A.L. Donaldson, R. Ness, and J. Marx, "Surface Studies of Electrodes Used in Spark Gaps", Proc. 4th IEEE Pulsed Power Conference, June 1983.
45. G. Jackson, L. Hatfield, M. Kristiansen, M. Hagler, J. Marx, A.L. Donaldson, G. Leiker, R. Curry, R. Ness, L. Gordon, and D. Johnson, "Surface Studies of Dielectric Materials Used in Spark Gaps", Proc. 4th IEEE Pulsed Power Conference, June 1983.
46. R. Cooper, G. Hutcheson, M. Kristiansen, G. Schaefer, K.H. Schoenbach, and A.H. Guenther, "A Multi-Spark Preionization Source For Diffuse Discharges Containing Attachments", Proc. 4th IEEE Pulsed Power Conference, June 1983.
47. R. Curry, D. Johnson, M. Kristiansen, L. Hatfield, and A.H. Guenther, "Triggering of Surface Discharge Switches", Proc. 4th Pulsed Power Conference, June 1983.
48. R.A. Dougal, P.F. Williams, and A.H. Guenther, "Breakdown Processes in Laser-Triggered Switching", Proc. 4th IEEE Pulsed Power Conference, June 1983.
49. M.O. Hagler and M. Kristiansen, "Repetitive Spark Gap Operation - A Review of the Tamarron Workshop", Proc. 4th IEEE Pulsed Power Conference, June 1983.
50. W.M. Portnoy and M. Kristiansen, "Solid State Pulse Power Switching - A Review of the Tamarron Workshop", Proc. 4th IEEE Pulse Power Conference, June 1983.
51. K.H. Schoenbach and M. Kristiansen, "Diffuse Discharges and Opening Switches - A Review of the Tamarron Workshop", Proc. 4th IEEE Pulsed Power Conference, June 1983. (Invited Paper)
52. S.K. Dhali and P.F. Williams, "Numerical Simulation of Space Charge Controlled Transport", Proc. 4th IEEE Pulsed Power Conference, June 1983.
53. R.A. Dougal, D.C. Pease, and P.F. Williams, "Laser-Induced-Fluorescence Imaging of Electrode Vapor in a Spark Gap Switch", Proc. 4th IEEE Pulsed Power Conference, June 1983.
54. G. Schaefer, K.H. Schoenbach, P. Tran, J.S. Wang, and A.H. Guenther, "Computer Calculations of the Time Dependent Behavior of Diffuse Discharge Switches", Proc. 4th IEEE Pulsed Power Conference, June 1983.
55. A.L. Donaldson, R. Ness, M. Hagler, M. Kristiansen, and L.L. Hatfield, "Modeling of Spark Gap Performance", Proc. 4th IEEE Pulsed Power Conference, June 1983. (Invited Paper)

56. A.L. Donaldson, M. Kristiansen, M. Hagler, G. Jackson, L. Hatfield, and J. Marx, "Electrode Erosion in a High Energy Spark Gap", Proc. 4th IEEE Pulsed Power Conference, June 1983.
57. G. Jackson, L. Hatfield, G. Leiker, M. Kristiansen, and J. Marx, "Pulsed Flashover of Solid Dielectrics in Gases", Proc. 4th IEEE Pulsed Power Conference, June 1983.
58. M. Kristiansen, A. Guenther, J. Ungvarsky, T. Skvarenina, A. Hyder, and H. Pugh, "Pulsed Power Education", Proc. 4th IEEE Pulsed Power Conference, June 1983.
59. C. Yeh, M. Hagler, and M. Kristiansen, "Voltage Recovery Measurements in a High Energy Spark Gap", Proc. 4th IEEE Pulsed Power Conference, June 1983.
60. R.A. Dougal and P.F. Williams, "Fundamental Processes in Laser-Triggered Breakdown", accepted, Journal of Physics D.
61. G. Schaefer, F. Williams, K. Schoenbach, and J. Moseley, "Photodetachment as a Control Mechanism for Diffuse Discharge Switches", IEEE Trans. Plasma Sci., PS-11, 263 (1983).
62. R.A. Dougal, P.F. Williams, and D.C. Pease, "Time Resolved Two-Dimensional Imaging of Ground State Species Using Laser-Induced Fluorescence", Rev. Sci. Instr., 54, 572, (1983).
63. A. Donaldson, M. Kristiansen, and M. Hagler, "Electrode Erosion Phenomena in a High Energy Pulsed Discharge", accepted for publication in IEEE Trans. Plasma Sci.
64. A. Donaldson, R. Ness, M. Kristiansen, M. Hagler, G. Jackson, and L. Hatfield, "Modeling of the Breakdown Voltage Stability in a High Energy Spark Gap", submitted to Journal of Appl. Phys.
65. G. Jackson, L. Hatfield, M. Kristiansen, M. Hagler, J. Marx, A. Donaldson, G. Leiker, R. Curry, R. Ness, L. Gordon, and D. Johnson, "Surface Studies of Dielectric Materials Used in Spark Gaps", Journal of Appl. Phys., 55, 262 (1984).
66. G. Jackson, L. Hatfield, M. Kristiansen, J. Marx, and A. Bowling, "Pulse Flashover of Solid Dielectrics in Vacuum", IEEE Trans. on Elect. Insul., EI-18, 310 (1983).
67. H. Krompholz, J. Doggett, K.H. Schoenbach, J. Gahl, C. Haries, G. Schaefer, and M. Kristiansen, "Nanosecond Current Probe for High-Voltage Experiments", Rev. Sci. Instrum., 55, 127 (1984).

68. E.E. Kunhardt and P.F. Williams, "A Fast Algorithm, for Numerically Integrating Poisson's Equation in Cylindrically-Symmetric Geometries", submitted to J. Comp. Phys.
69. R.D. Curry, M. Kristiansen, L.L. Hatfield, V.K. Agarwal, and G.L. Jackson, "Surface Charging of Insulators in a Surface Discharge Switch", Annual Report of the Conference on Electrical on Electrical Insulation and Dielectric Phenomena, Buck Hill Falls, PA, October (1983).
70. G. Schaefer, K.H. Schoenbach, H. Krompholz, M. Kristiansen, and A.H. Guenther, "The Use of Attachers in Electron Beam Sustained Discharge Switches - Theoretical Considerations", submitted to "Lasers and Particle Beams."
71. K.H. Schoenbach, M. Kristiansen, and G. Schaefer, "A Review of Opening Switch Technology for Inductive Energy Storage", submitted to the Proceedings of IEEE.
72. M. Kristiansen and M.F. Rose, "Pulsed Power Technology and Diffuse Discharges", Proc. of the US-FRG Workshop on Externally Controlled Diffuse Discharges, Bad Honnef, FRG (1983).
73. G.Schaefer, "Optically Controlled Diffuse Discharges, Proc. of the US-FRG Workshop on Externally Controlled Diffuse Discharges, Bad Honnef, FRG (1983).
74. K.H. Schoenbach, "Diagnostics for Diffuse Discharge", Proc. of the US-FRG Workshop on Externally Controlled Diffuse Discharges, Bad Honnef, FRG (1983).
75. Proceedings of Joint US-FRG Seminar on "Externally Controlled Diffuse Discharges" Bad Honnef, Germany, August 1983 (K.H. Schoenbach, Editor).
76. K. Schoenbach, H. Krompholz, and J. Doggett, "Transmission Line Geometry Current Sensors", to appear in Proc. of NATO Advanced Study Institute on Fast Electrical and Optical Diagnostic Principles, Castelvechio Pascoli, Italy, July 1983.
77. H. Krompholz, "100 ps Schlieren Diagnostics of Dense Plasma", to appear in Proc. of NATO Advanced Study Institute on Fast Electrical and Optical Diagnostic Principles, Castelvechio Pascoli, Italy, July 1983.
78. M. Kristiansen, F. Rose, and A. Hyder, "Overview of Applications and Needs", to appear in Proc. of NATO Advanced Study Institute on Fast Electrical and Optical Diagnostic Principles, Castelvechio Pascoli, Italy, July 1983.

Interactions

1982-83

a. Papers Presented

52 papers were presented (mostly at national and international conferences) by the faculty staff and students during the three first contract years and are listed in the first three annual reports. During the last contract period (October 1, 1982-September 30, 1983) the following papers were presented:

1. H. Krompholz, "100 ps Schlieren Diagnostics of Dense Plasma", NATO Advanced Study Institute on Fast Electrical and Optical Diagnostic Principles, Castelvechio Pascoli, Italy, July 1983.
2. K. Schoenbach, H. Krompholz, J. Doqqett, "Transmission Line Geometry Current Sensors", NATO Advanced Study Institute on Fast Electrical and Optical Diagnostic Principles, Castelvechio Pascoli, Italy, July 1983.
3. M. Kristiansen, F. Rose, and A. Hyder, "Overview of Applications and Needs", NATO Advanced Study Institute on Fast Electrical and Optical Diagnostic Principles, Castelvechio Pascoli, Italy, July 1983.
4. K. Schoenbach, "Diffuse Discharge Opening Switches", University of Illinois, Urbana, IL, February 1983.
5. K. Schoenbach, "Low Pressure Plasma Opening Switches", GTE Laboratories, Inc. Waltham, MA, April 1983.

6. G. Schaefer, "Optically Controlled Diffuse Discharges", Air Force/Texas Tech Pulsed Power Lecture Series, Sept. 29, 1983, Wright-Patterson AFB, OH; Sept. 30, 1983, Kirtland AFB, NM.
7. M. Kristiansen and F. Rose, "Pulsed Power Technology and Diffuse Discharges", NSF sponsored US-FRG Workshop on Externally Controlled Diffuse Discharges, Bad Honnef, FRG, August 1983.
8. K. Schoenbach, "Diagnostics of Diffuse Discharges", NSF sponsored US-FRG Workshop on Externally Controlled Diffuse Discharges, Bad Honnef, FRG, August 1983.
9. G. Schaefer, "Optically Controlled Diffuse Discharges", NSF sponsored US-FRG Workshop on Externally Controlled Diffuse Discharges, Bad Honnef, FRG, August 1983.
10. G. Jackson, L.L. Hatfield, J. Marx, A. Bowlin, and M. Kristiansen, "Pulse Flashover of Solid Dielectrics in Vacuum", Xth Int. Symp. on Discharges and Electric Insulation in Vacuum", Columbia, SC, October 1983.
11. M. Kristiansen, "An Introduction to Gas Filled Spark Gaps", DoD Workshop on Repetitive Spark Gap Operation, Tamarron, CO, January 1983.
12. D. Johnson, L. Hatfield, and M. Kristiansen, "Multi-channel Surface Discharge Switch", Conference on Electrical Insulation and Dielectric Phenomena, Amherst, MA, October 1982.

13. S.K. Dhali and P.F. Williams, "Multiphoton Ionization in Xenon and Xenon-Nitrogen Mixtures", 35th Gaseous Electronics Conference, Dallas, TX, October 1982.
14. P.F. Williams and K.H. Schoenbach, "Photodetachment as a Control Mechanism for Diffuse Discharge Switches", 35th Gaseous Electronics Conference, Dallas, TX, October 1982.
15. R.A. Dougal, P.F. Williams, and D.C. Pease, "Laser Induced Fluorescence Imaging of Electrode Vapor in a Spark Gap Switch", 35th Gaseous Electronics Conference, Dallas, TX, October 1982.
16. P.F. Williams and R.A. Dougal, "A Simple Model of Laser-Triggered Breakdown", 35th Gaseous Electronics Conference, Dallas, TX, October 1982.
17. H. Harjes, K. Schoenbach, G. Schaefer, H. Krompholz, and M. Kristiansen, "E-Beam Triode For Multiple Submicrosecond Pulse Operation", 4th IEEE Pulsed Power Conf., Albuquerque, NM, June 1983.
18. H. Harjes, J. Doggett, J. Gahl, K. Zinsmeyer, H. Krompholz, K. Schoenbach, G. Schaefer, and M. Kristiansen, "Nanosecond Current Probe for High Voltage Experiments", 4th IEEE Pulsed Power Conf., Albuquerque, NM, June 1983.
19. G. Jackson, G. Leiker, L. Hatfield, M. Kristiansen, M. Hagler, A. Donaldson, R. Ness, and J. Marx, "Surface Studies of Electrodes Used in Spark Gaps", 4th IEEE Pulsed Power Conference, Albuquerque, NM, June 1983.

20. G. Jackson, L. Hatfield, M. Hagler, J. Marx, A. Donaldson, G. Leiker, R. Curry, R. Ness, L. Gordon, and D. Johnson, "Surface Studies of Dielectric Materials Used in Spark Gaps", 4th IEEE Pulsed Power Conf., Albuquerque, NM, June 1983.
21. R. Cooper, G. Hutcheson, G. Schaefer, K.H. Schoenbach, and A.H. Guenther, "A Multi-Spark Preionization Source for Diffuse Discharge Containing Attachers", 4th IEEE Pulsed Power Conf., Albuquerque, NM, June 1983.
22. R. Curry, D. Johnson, M. Kristiansen, L. Hatfield, and A.H. Guenther, "Triggering of Surface Discharge Switches", 4th IEEE Pulsed Power Conf., Albuquerque, NM, June 1983.
23. M.O. Hagler and M. Kristiansen, "Repetitive Spark Gap Operation - A Review of the Tamatron Workshop", 4th IEEE Pulsed Power Conf., Albuquerque, NM, June 1983.
24. A.L. Donaldson, M. Kristiansen, M. Hagler, G. Jackson, L. Hatfield and J. Marx, "Electrode Erosion in a High Energy Spark Gap", 4th IEEE Pulsed Power Conf., June 1983.
25. G. Jackson, L. Hatfield, G. Leiker, M. Kristiansen, and J. Marx, "Pulsed Flashover of Solid Dielectrics in Gases", 4th IEEE Pulsed Power Conf., Albuquerque, NM, June 1983.
26. M. Kristiansen, A. Guenther, J. Ungvarsky, T. Skvarenina, A. Hyder and H. Pugh, "Pulsed Power Education", 4th IEEE Pulsed Power Conf., Albuquerque, NM, June 1983.

27. C. Yeh, M. Kristiansen, and M. Hagler, "Voltage Recovery Measurements in a High Energy Spark Gap", IEEE Pulsed Power Conf., Albuquerque, NM, June 1983.
28. K.H. Schoenbach and M. Kristiansen, "Diffuse Discharges and Opening Switches - A Review of the Tamarron Workshops", IEEE Pulsed Power Conf., Albuquerque, NM, June 1983. (Invited Paper)
29. S.K. Dhali and P.F. Williams, "Numerical Simulation of Space-Charge-Controlled Transport", 4th IEEE Pulsed Power Conf., Albuquerque, NM, June 1983.
30. R.A. Dougal, P.F. Williams, and A.H. Guenther, "Breakdown Processes in Laser-Triggered Switching", 4th IEEE Pulsed Power Conf., Albuquerque, NM, June 1983.
31. A.L. Donaldson, R. Ness, M. Hagler, M. Kristiansen, and L.L. Hatfield, "Modeling of Spark Gap Performance", 4th IEEE Pulsed Power Conf., Albuquerque, NM, June 1983. (Invited Paper).
32. G. Schaefer, K. Schoenbach, A.H. Guenther, and W.K. Pendleton, "Recent Advances in Optically Controlled Discharges", 4th IEEE Pulsed Power Conf., Albuquerque, NM, June 1983. (Invited Paper)
33. Gerhard Schaefer, Karl H. Schoenbach, Paul Tran, and Jia-Shinn Wang and Arthur H. Guenther, "Computer Calculations of the Time Dependent Behavior of Diffuse Discharge Switches", 4th IEEE Pulsed Power Conference, Albuquerque, NM, June 1983.



34. Prof. G. Schaefer presented a paper on "Control Mechanisms for Diffuse Discharge Switches", Report ARO Work-shop on Optical Control of Diffuse Discharges, Eugene OR, 1982 by G. Schaefer, K.H. Schoenbach, and P.F. Williams.

b. Consultative and Advisory Functions

Numerous consultative and advisory functions were carried out during the first three contract periods and are described in the first three annual reports. These functions included organizing DoD workshops and serving on DoD advisory boards. During the 1982-83 contract period the following functions were undertaken:

1. Prof. M. Kristiansen served on the Basic Science Panel of the AF Scientific Advisory Board and attended the Spring and Fall general meetings.
2. Prof. M. Kristiansen coordinated the AFOSR sponsored Pulsed Power Lecture Series together with Dr. A. Guenther of the AFWL.
3. Prof. M. Kristiansen served on the Air Force AD Hoc Committee on "Laser Weapons for Space Applications", 1983.
4. Prof. M. Kristiansen served as Co-organizer (with Prof. W. Portnoy) of the ARO sponsored workshop on "Solid State Switching for Pulsed Power" at Tamarron, CO on January 12-14, 1983.
5. Prof's. M. Hagler and M. Kristiansen organized the DoD sponsored Workshop on "Repetitive Spark Gap Operation" at Tamarron, CO on January 17-19, 1983.

6. Prof. M. Kristiansen served on the advisory committee for the NATO Advanced Study Institute on "Fast Optical and Electrical Diagnostic Techniques" in Castelvechio Pascoli, Italy, July 1983.
7. Prof. K. Schoenbach organized and Prof. M. Kristiansen served on the Advisory Committee for the NSF sponsored US-FRG Workshop on "Externally Controlled Diffuse Discharges", Bad Honnef, FRG, August 15-18, 1983.
8. Prof. M. Kristiansen served as a Visiting Staff Member (Collaborator) at Los Alamos National Laboratory and supervised a Ph.D. thesis project on repetitive opening switches conducted by one of their staff members.
9. Prof. M. Kristiansen served as a Consultant to Lawrence Livermore National Laboratory.
10. Prof. M. Kristiansen directed the Foreign Applied Sciences Assessment Center's study of Soviet Macro-electronics (Pulsed Power).
11. Prof.'s K. Schoenbach and H. Krompholz served as consultants to the AFOSR sponsored project (Prof. Gerdin, PI) on "Opening Switch Research on a Plasma Focus" at the University of Illinois and Prof. Krompholz spent the period of June 9 - July 2 in residence at the University of Illinois.

c. Other interactions

Numerous interactions with other universities, industry and government laboratories were carried out during the first three

contract periods. Our group effectively served as a coordination point for much of the ongoing work in high power gas discharges for switching applications in the U.S. These interactions are summarized in the first three annual reports. This effort was continued during the last contract period and is summarized below:

1. Professors Schoenbach and Krompholz visited Professor G. Gerdin at the University of Illinois, Urbana, in February 1983 to consult on his AFOSR sponsored Opening Switch Project (Plasma Focus).
2. Professor Schoenbach visited GTE Laboratories in Waltham, MA, in April 1983 to discuss a joint program on magnetically controlled low pressure gas discharges with Dr. J. Proud and Dr. W. Byszewski.
3. Professor Schoenbach visited Dr. W. Thompson, Director for International programs in the NSF, in Washington, D.C. in May 1983 to exchange information on research on e-beam controlled diffuse discharge opening switches.
4. Prof. Schoenbach visited Dr. B. Guenther at the Army Research Office, Research Triangle, N.C. in May 1983 to discuss planned research efforts on the E-Beam controlled opening switch project at TTU.
5. Prof. Schoenbach visited Prof. Herziger and Prof. Pfeiffer at the Technische Hochschule in Darmstadt, Germany, to discuss possible interaction in the field of fast plasma diagnostics and the exchange of students.

6. Prof. H. Krompholz attended the NATO-Advanced Study Institute on "Fast Electrical and Optical Diagnostic Principles and Techniques" in Castelveccchio Pascoli, Italy in July 1983. He gave a presentation on "100 ps - Schlieren diagnostics of dense plasma".
7. H. Krompholz visited Prof. Herziger at the Institute for Applied Physics, Technische Hochschule Darmstadt, FRG to discuss possible interactions in the field of plasma diagnostics.
8. Prof. Schoenbach served as session chairman at the 4th IEEE Pulsed Power Conference in Albuquerque, NM, June 1983.
9. Prof. Schoenbach served as session chairman at the NATO Advanced Study Institute on "Fast Electrical and Optical Diagnostic Principles" in Castelveccchio Pascoli, Italy in July 1983. He also organized a special session on "Diffuse Discharge Diagnostics".
10. Prof. Schoenbach visited Mr. I. Vitkovitsky at NRL, Washington, D.C., in May 1983 to exchange information about research on e-beam controlled diffuse discharge opening switches.
11. Prof's. H. Krompholz, G. Schaefer, D.F. Williams and R. Schoenbach attended the IEEE Pulsed Power Conference in Dallas, Texas, November 1983.

AD-A139 321

COORDINATED RESEARCH PROGRAM IN PULSED POWER PHYSICS

5/5

(U) TEXAS TECH UNIV LUBBOCK DEPT OF ELECTRICAL  
ENGINEERING M KRISTIANSEN ET AL, 27 FEB 84

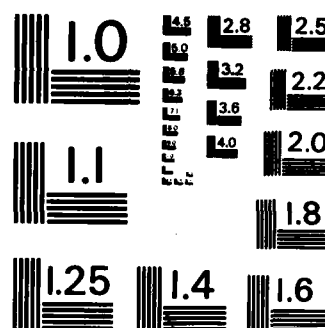
UNCLASSIFIED

AFOSR-TR-84-0174 F49620-79-C-0191

F/G 10/2

NL





MICROCOPY RESOLUTION TEST CHART  
NATIONAL BUREAU OF STANDARDS-1963-A

12. Prof's. G. Schaefer, K.H. Schoenbach and P.F. Williams attended the ARO/AFOSR Workshop on Optical Control of Diffuse Discharges, in December 1982 in Eugene, OR.
13. Prof. K.H. Schoenbach attended the Workshop on "Solid State Switches", in Tamarron, CO in January 1983.
14. Prof's. K.H. Schoenbach and G. Schaefer attended the Workshop on "Repetitive Spark Gap Operation" in Tamarron, CO, in January 1983.
15. Prof. G. Schaefer attended the "Conference on Laser and Electro Optics (CLEO)" in Baltimore in May 1983.
16. Prof. G. Schaefer visited AFOSR in Washington, D.C. (Contract Monitor Capt. Henry Pugh) and discussed ongoing research in AFOSR funded projects in May 1983.
17. Prof. G. Schaefer visited NSF in Washington, D.C. (James Aller - Electrical, Computer, and Systems Engineering, R. Rostenbach - Engineering Energetics and W. Thompson, International Programs) in May 1983.
18. Prof. H. Krompholz, M. Kristiansen, L. Hatfield, J. Marx, F. Williams, G. Schaefer and K.H. Schoenbach attended the 4th IEEE Pulsed Power Conference in Albuquerque, NM in June 1983. G. Schaefer and K.H. Schoenbach acted as Session chairmen. The group presented a total of 3 invited and 15 contributed papers.

19. Prof's. M. Kristiansen, G. Schaefer and K.H. Schoenbach attended the US-FRG Joint Seminar on Externally controlled Diffuse Discharges in Bad Honnef, FRG in August, 1983. K.H. Schoenbach acted as seminar chairman.
20. Prof. G. Schaefer visited the Institute of Applied Physics, Technical University of Darmstadt, FRG in August 1983. (Professors G. Herziger and W. Seelig).
21. Prof. G. Schaefer visited the Institute for Light Research, Technical University of Karlsruhe, FRG, in August 1983 (Professor H.P. Popp) and discussed possible cooperation in research on discharges with strong attachers.
22. Prof. Schaefer attended the XVI International Conference on Phenomena in Ionized Gases (ICPIG) in Duesseldorf, FRG, on August-September 1983.
23. Prof. G. Schaefer visited the Air Force Aeronautical Laboratory (P. Bletzinger and A. Garscadden) in September 1983 and discussed on-going Air Force sponsored research.
24. Prof. M. Kristiansen visited LLNL in November 1983 and consulted on pulsed power research problems.
25. Graduate students G. Jackson and G. Leiker visited the Center for Research in Surface Science and Submicron Analysis (CRISS) at Bozeman, MT on April 24, 1983 and August 19 1983 to use their surface analysis facilities.



## ADVANCED DEGREES AWARDED

1979-80

- R. Druce "An Experimental and Numerical Investigation of Laser-Plasma Interactions",  
Ph.D. Thesis
- H.C. Harjes "Laser Triggering Through Fiber Optics of  
a Low Jitter Spark Gap",  
M.S. Thesis
- R. Crumbly "Electron Densities in Laser-Triggered  
Spark Gap Discharge"  
M.S. Thesis
- M.A. Newton "An Investigation of Electron Beam  
Initiated Spark Gap Breakdown",  
M.S. Thesis

1980-81

- Alex K. Auyeung "A Computer Based Data Acquisition System  
for Fast Pulsed Power Experiments",  
M.S. Thesis
- S.K. Dhali "Multiphoton Ionization Spectroscopy in  
Xe",  
M.S. Thesis
- George Jackson "Ultraviolet Radiation Damage to  
Dielectrics in Spark Gaps",  
M.S. Thesis
- Kenneth McDonnald "An Electron Beam Triggered Spark Gap",  
M.S. Thesis
- Yonhua Tzenq "The Effect of Space Charge Induced by an  
Electron Beam on Spark Gap Operation",  
M.S. Thesis
- Kai-Chih Yuan "Ellipsometric Studies of Surface Damage  
on Dielectrics",  
M.S. Thesis

1981-82

- A. Donaldson "Electrode Erosion Measurements in a High Energy Spark Gap",  
M.S. Thesis
- D. Johnson "Multichannel Surface Discharge Switch",  
M.S. Thesis
- L. Gordon "Material Studies in a High Energy Spark Gap",  
Ph.D. Thesis
- H. Dunlap "Electromechanical Pulse Amplifier",  
M.S. Thesis

1982-83

- George Jackson "Pulsed Flashover of Solid Dielectrics in Vacuum and Gases",  
Ph.D. Thesis
- Roger Dougal "Breakdown Processes in Laser Triggered Switching",  
Ph.D. Thesis
- Richard Ness "A Computer System for the Acquisition and Analysis of Spark Gap Breakdown Voltage Data",  
M.S. Thesis
- George Hutcheson "Design and Construction of a Diffuse Discharge Experiment",  
M.S. Thesis
- Randy Cooper "A Fast Preionization Source for Diffuse Discharges Containing Attachers",  
M.S. Thesis

SEMINARS

1982-83

- Umberto Rossi "Fiber Optics Research at CSELT"  
October 11, 1982  
Centro Studi e Laboratori  
Telecomunicazioni  
Turin, Italy
- Wolfgang Pfeiffer "Optical Diagnostic Techniques for the  
Investigation of Breakdown Development"  
October 13, 1982  
Institut für Hochspannungs und  
Messtechnik,  
Technische Hochschule Darmstadt, FRG
- A.K. Jonscher "The Chelsea Dielectric Group - An  
Overview"  
October 14, 1982  
University of London  
England
- Reuben Shuker "Resonant Optogalvanic Effect"  
October 18, 1982  
Ben Gurion University  
Israel
- Ken Whitham "Pulsed Power Engineering for Inertial  
Confinement Fusion"  
November 3, 1982  
Lawrence Livermore National Laboratory  
Livermore, CA
- J.N. Bardsley "Dissociative Recombination and Its Role  
in Ionized Gases"  
December 9, 1982  
University of Pittsburgh  
Pittsburgh, PA
- R.V. Hodges "Spark Gap Research at Lockheed"  
March 4, 1983  
Lockheed Research and Development Lab  
Palo Alto, CA

- Gerard Mourou "Picosecond Optoelectronic Switching"  
March 7, 1983  
University of Rochester, NY
- Richard C. Powell "Laser Spectroscopy of Nd Laser  
Material"  
March 29, 1983  
Oklahoma State University  
Stillwell, Oklahoma
- Albert T. Fromhold, Jr "Charge and Mass Transport During Oxide  
Barrier Layer Growth on Metals"  
April 11, 1983  
Auburn University  
Auburn, AL
- Arthur H. Guenther "Pulsed Laser Induced Damage of Optical  
Thin Films"  
May 13, 1983  
Air Force Weapons Laboratory  
Albuquerque, NM
- A.V. Phelps "Solutions of the Boltzmann Equation for  
Electrons: The Determination of  
Electron-Molecule Cross Sections"  
September 22, 1983  
Joint Institute for Lab. Astrophysics  
National Bureau of Standards  
University of Colorado, Boulder, CO
- David T. Tuma "Modelling and Simulation of Thermal  
Plasmas"  
September 26, 1983  
Carnegie-Mellon University  
Pittsburgh, PA
- William Moeny "Computational Solutions of Electric  
Fields in Discharges"  
November 21, 1983  
Tetra Corporation  
Albuquerque, NM

Guests of Plasma and Switching Laboratory  
October 1, 1982 - September 30, 1983

October 11, 1982

Umberto Rossi

Centro Studi E Laboratori  
Telecomunicazioni, Turin, Italy

October 8, 1982

Wolfgang Pfeiffer

Technical University  
Darmstadt, FRG

October 13, 1982

Ronald Hodges  
Wolfgang Pfeiffer

Lockheed R&D, Palo Alto, CA  
Technical University  
Darmstadt, FRG

October 14, 1982

Andrew L. Jonscher

Chelsea College, London, UK

October 18, 1982

Reuben Shuker  
Wojciech Byszewski

Ben-Gurion University, Israel  
GTE Labs, Waltham, MA

November 3, 1982

Ken Whitham

Lawrence Livermore National  
Laboratory

November 4, 1982

Roger White  
M. Barton  
John Harris  
Jim Crissey  
Karl Freytag  
Dave Pehrson  
Ken Whitham

Maxwell Labs, San Diego, CA  
Maxwell Labs, San Diego, CA  
Maxwell Labs, San Diego, CA  
Air Force Weapons Laboratory, NM  
Lawrence Livermore Nat'l. Lab, CA  
Lawrence Livermore Nat'l. Lab, CA  
Lawrence Livermore Nat'l. Lab, CA

November 22, 1982

James C. Aller

National Science Foundation  
Washington, D.C.

December 9, 1982

J. Norman Bardsley

University of Pittsburg, PA

February 8, 1983

W. Pendleton

Air Force Weapons Laboratory, NM

A. Cole

Air Force Weapons Laboratory, NM

R. Reinovsky

Air Force Weapons Laboratory, NM

C. Enloe

Air Force Weapons Laboratory, NM

A. Guenther

Air Force Weapons Laboratory, NM

J. O'Loughlin

Air Force Weapons Laboratory, NM

February 18, 1983

Major General

Office of the Under Secretary  
of Defense

Donald L. Lamberson

Air Force Weapons Laboratory, NM

A.H. Guenther

Air Force Weapons Laboratory, NM

C.J. Head

Air Force Weapons Laboratory, NM

W. Tyler

Air Force Weapons Laboratory, NM

O. Spurlin

Air Force Weapons Laboratory, NM

A. Sobol

Air Force Weapons Laboratory, NM

D. Seegmiller

Air Force Weapons Laboratory, NM

March 3, 1983

J.F. Riley

Lockheed R&D, Palo Alto, CA

R.V. Hodges

Lockheed R&D, Palo Alto, CA

March 7, 1983

Gerard Mourou

University of Rochester, NY

March 24, 1983

A.W. Czanderna

Solar Energy Research Institute  
Denver, CO

March 29, 1983

Richard C. Powell

Oklahoma State University  
Stillwater, OKApril 8, 1983Billy Brock  
Jerry Holmes  
Jerry Edmonson  
Richard McCaskill  
W.C. Nunnally  
Rex E. Phillips  
John Ragland  
Louis Stevens  
J.E. Thompson  
Merle Whatley  
William GuionSandia National Laboratory  
Texas Instruments, Lewisville, TX  
Transok, Tulsa, OK  
Brazos Electrical Power  
Los Alamos National Laboratory  
Westinghouse Electrical Corp.,  
Hicks & Ragland Engr. Co., Inc.  
IBM, San Jose, CA  
Univ. of South Carolina  
Texas Instruments, Dallas, TX  
Southwest Research Institute,  
San Antonio, TX  
ELM Company, Houston, TX  
SPS Co., Amarillo, TXLynn Elliott  
Roger K. OwenApril 11, 1983

Al Fromhold

Auburn University, Alabama

June 13, 1983Gernot Decker  
Wolfgang PfeifferUniv. of Dusseldorf, Germany  
Technical University  
Darmstadt, GermanyJuly 6, 1983

William Streifer

Xerox PARC,  
Palo Alto, CAAugust 9, 1983

Chathan Cooke

Mass. Inst. of Tech, Cambridge, MA

September 22, 1983

A.V. Phelps

JILA, Bureau of Standards,  
University of Colorado  
Boulder, CO

September 26, 1983

David T. Tuma

Carnegie-Mellon University  
Pittsburg, PAOctober 15, 1983William Streifer  
Paul K. Predecki  
Rex E. Phillips  
Billy C. Brock  
John W. Welch  
W.C. Nunnally  
Merle Whatley  
H. Ray Kerby  
John Ragland  
Dick BrooksXerox PARC, Palo Alto, CA  
Univ. of Denver, Denver, CO  
Westinghouse Electrical Corp, Dallas  
Sandia National Laboratory  
IBM Corp, Austin, TX  
Los Alamos National Laboratory  
Texas Instruments, Dallas, TX  
IBM, Corp., San Jose, CA  
Hicks & Ragland Engr., Co, Lubbock  
Central Power & Light, CorpusNovember 29, 1983William M. Money  
John D. Jukes  
Trevor JamesTetra Corp, Albuquerque, NM  
Culham Laboratory, UK  
Culham Laboratory, UKDecember 16, 1983

Anthony K. Hyder

Auburn University, Auburn, AL

Tomoo Fujioka

Keio Univ., Yokohama, Japan



END

FILMED

4-84

DTIC